

# **Immunoaffinity-Based Mass Spectrometry – a Method for the Analysis of Combinatorial Pesticide Effects on Liver Proteins in HepaRG Cells**

**Dissertation**

an der Mathematisch-Naturwissenschaftlichen Fakultät  
der Eberhard Karls Universität Tübingen  
zur Erlangung des Grades eines  
Doktors der Naturwissenschaften  
(Dr. rer. nat.)

vorgelegt von  
**Felix Florian Schmidt**  
aus Miltenberg

Tübingen

**2019**

Gedruckt mit Genehmigung der Mathematisch-Naturwissenschaftlichen Fakultät  
der Eberhard Karls Universität Tübingen.

**Tag der mündlichen Qualifikation:**

**14.02.2020**

Dekan:

Prof. Dr. Wolfgang Rosenstiel

1. Berichterstatter:

Prof. Dr. Ulrich Rothbauer

2. Berichterstatter:

PD Dr. Albert Braeuning

The presented thesis was prepared at the Natural and Medical Sciences Institute at the University of Tübingen between October 2016 and July 2019.

**Supervisor at the Eberhard Karls University, Tübingen**

Prof. Dr. Ulrich Rothbauer

**Supervisor at the Natural and Medical Sciences Institute  
at the University of Tübingen**

Dr. Oliver Pötz

**Supervisor at the German Federal Institute for Risk Assessment  
(BfR), Berlin**

PD Dr. Albert Braeuning

**Parts of this work have been presented:**

F.F. Schmidt; A.E. Steinhilber; A. Mentz; J. Kalinowski; D. Lichtenstein; A. Braeuning; P. Marx-Stoelting; A. Lampen; T. Joos; O. Poetz; *Combinatorial Effects of Pesticides on Toxicologically Relevant Liver Proteins in HepaRG Cells*. Poster, Eurotox, Helsinki, **2019**.

A. Braeuning; D. Lichtenstein; A. Mentz; J. Kalinowski; F. Schmidt; O. Poetz; A. Lampen; *Analysis of hepatotoxic mixture effects of pesticides in vitro*. Poster, Eurotox, Helsinki, **2019**.

F.F. Schmidt; H.S. Hammer; D. Lichtenstein; A. Mentz; J. Kalinowski; A. Braeuning; A. Lampen; T.O. Joos; O. Poetz; *Determination of Additive, Synergistic and Antagonistic Effects by the Analyses of Protein Markers in Pesticide Mixture-treated HepaRG-Cells*. Poster, ISSX, Portland, **2019**.

A. Braeuning; D. Lichtenstein; A. Mentz; J. Kalinowski; F. F. Schmidt; O. Poetz; A. Lampen; *A targeted transcriptomic and proteomic approach to assess hepatotoxic mixture effects in vitro*. Poster, DGPT, Stuttgart, **2019**.

F.F. Schmidt; H.S. Hammer; D. Lichtenstein; A. Mentz; J. Kalinowski; A. Braeuning; A. Lampen; T.O. Joos; O. Poetz; *Effects of Combinatorial Pesticide Treatment on Tox Protein and mRNA Biomarker Profiles in HepaRG Cells*. Poster, SOT, Baltimore, **2019**.

F.F. Schmidt; A.E. Steinhilber; H.S. Hammer; A. Mentz; J. Kalinowski; D. Lichtenstein; A. Braeuning; P. Marx-Stoelting; A. Lampen; T. Joos; O. Poetz; *Analysis of Toxicologically Relevant Proteins in Pesticide-treated HepaRG Cells by MS-based Immunoassays*. Poster, HUPO, Orlando, **2018**.

F.F. Schmidt; A.E. Steinhilber; H.S. Hammer; A. Mentz; J. Kalinowski; D. Lichtenstein; A. Braeuning; P. Marx-Stoelting; A. Lampen; T. Joos; O. Poetz; *Analysis of Toxicologically Relevant Biomarkers in Pesticide-treated HepaRG Cells by MS based Immunoassays*. Poster, Eurotox, Brüssel, **2018**.



**Parts of this work have been published:**

A. Braeuning, A. Mentz, F.F. Schmidt, S.P. Albaum, H. Planatscher, J. Kalinowski, T.O. Joos, O. Poetz, D. Lichtenstein; *RNA-protein correlation of liver toxicity markers in HepaRG cells*. EXCLI Journal **2020**; 19:135-153)

F.F. Schmidt, A.E. Steinhilber, D. Lichtenstein, A. Mentz, J. Kalinowski, A. Braeuning, T.O. Joos, O. Poetz; *Analysis of pesticide mixture effects on toxicologically relevant liver proteins in HepaRG cells by immunoaffinity-based mass spectrometry*.  
(in preparation)

## **Acknowledgment**

First of all, I would like to thank Dr. Oliver Pötz for accepting me as a master's student in 2016 and subsequently allowing me to complete my doctoral thesis at the NMI, as well as for his continued support and trust in the past years.

Special thanks to Prof. Dr. Ulrich Rothbauer and PD Dr. Albert Braeuning for supervising the doctoral thesis, including the regular meetings in which valuable feedback was passed on during the entire doctoral phase.

Many thanks to the collaboration partners Dr. Dajana Lichtenstein from the BfR in Berlin and Dr. Almut Mentz from CeBiTec in Bielefeld for conducting the cell culture, providing the samples as well as the measurement and delivery of the mRNA data.

I particularly would like to thank my work colleagues: Dr. Helen Hammer for the supervision during the master thesis and the introduction to immunoaffinity-based mass spectrometric methods, Cornelia Sommersdorf for the introduction to antibody purification and the realization of this task, Dr. Andreas Steinhilber for the continuous exchange of knowledge and brainstorming, Dr. Hannes Planatscher for the support in bioinformatics and statistical questions, as well as Dr. Wael Naboulsi and Viktoria Anselm for their regular support during troubleshooting matters and the friendly working atmosphere.

I would like to thank all my colleagues at the NMI and Signatope GmbH for the pleasant working atmosphere, especially my doctoral colleagues Eugenia Salzmann, Marius Gramlich, Robin Kretz, and Dr. Bettina Keller, as well as my working group colleagues Sandra Maier, Sabrina Fenchel, and Anja Tausch.

I would also like to thank my family for mental and financial support, as well as my friends for motivation, encouragement, and energy during this time.

# Content

<b>1</b>	<b>Introduction</b>	<b>1</b>
<b>1.1</b>	<b>Pesticides</b>	<b>1</b>
1.1.1	Pesticide Types	3
1.1.2	The Regulatory Framework for Market Release of New Single Pesticides	5
<b>1.2</b>	<b>Metabolism of Pesticides &amp; Regulation of Metabolic Enzymes</b>	<b>7</b>
1.2.1	Xenobiotic Metabolism	7
1.2.2	Preliminary Study for the Determination of Toxicologically Relevant Markers at mRNA Level	8
<b>1.3</b>	<b>Proteomics</b>	<b>9</b>
1.3.1	Mass Spectrometry-Based Protein-Profilng Strategy	10
1.3.2	Targeted Proteomics	11
1.3.3	Immunoaffinity-Based Mass Spectrometry	12
1.3.4	Triple X Proteomics – an Example of an Immunoaffinity-Based Mass Spectrometry Approach	13
1.3.5	Mass Spectrometric Analysis Methods	15
1.3.5.1	Full-scan MS	15
1.3.5.2	Targeted selected ion monitoring	16
1.3.5.3	Parallel reaction monitoring	17
<b>2</b>	<b>Aim of this Thesis</b>	<b>19</b>
<b>3</b>	<b>Material and Methods</b>	<b>22</b>
<b>3.1</b>	<b>Buffer</b>	<b>22</b>
<b>3.2</b>	<b>Chemicals, Biochemicals, Reagents</b>	<b>23</b>
<b>3.3</b>	<b>Consumables</b>	<b>24</b>
<b>3.4</b>	<b>Laboratory Equipment</b>	<b>26</b>
<b>3.5</b>	<b>Databases and Software</b>	<b>27</b>

<b>3.6</b>	<b>Samples</b>	<b>28</b>
3.6.1	Pesticides	28
3.6.2	Pesticide Mixtures	30
3.6.3	Induction Controls	31
<b>3.7</b>	<b>Antibody Purification</b>	<b>31</b>
<b>3.8</b>	<b>Sample Preparation</b>	<b>32</b>
3.8.1	Peptide Standards	32
3.8.2	Cell Lysis and Protein Determination	33
3.8.3	Enzymatic Proteolysis and Immunoprecipitation	34
<b>3.9</b>	<b>Assay Development</b>	<b>36</b>
3.9.1	Database Search for Suitable Peptides	36
3.9.2	Peptide Detection Compatibility with Mass Spectrometry	38
3.9.3	Full-Scan Mass Spectrometry Measurement of In-Gel Digested HepaRG Cells	39
3.9.4	Comparison of Targeted Mass Spectrometry Methods for Better Suitability of Target Analyte Analysis	42
3.9.5	Testing the Antibody Functionality	43
3.9.6	Antibody-Protein Ratio Optimization	44
3.9.7	Examination of Proteolysis over Time	44
3.9.8	Conversion from Singleplex to Multiplex Assays	44
3.9.9	Optimization of Chromatographic Separation	45
3.9.10	Dynamic Ranges	45
3.9.11	Identification of Recovery Efficiency	46
3.9.12	Investigation of Repeatability	47
<b>4</b>	<b>Results</b>	<b>49</b>
<b>4.1</b>	<b>Assay Development for the Quantification of Toxicologically Relevant Proteins in HepaRG Cells</b>	<b>49</b>
4.1.1	Peptide Selection for the Detection and Quantification of Target Analytes	49
4.1.2	Detection Compatibility of Selected Peptides with Mass Spectrometry	49
4.1.3	Can Analytes be Detected in HepaRG Cells Directly after In-Gel Digestion and Full-Scan Mass Spectrometry Analysis?	51

4.1.4	Selection of Mass Spectrometry Detection Mode for Most Sensitive Detection of Target Analytes	52
4.1.5	Determination of Antibody Epitope Binding Motifs and Functionality in Complex Matrix	54
4.1.6	Least Optimal Antibody-Protein Extract Ratio for Reliable Target Analysis	56
4.1.7	Analysis of Optimal Proteolysis Time	58
4.1.8	Compiling of Multiplex Assay Panels	60
4.1.9	Effect of Chromatographic Separation on Signal Intensity and Repeatability	61
4.1.10	Determination of Assay Linearity and Accuracy to Discover Dynamic Ranges	63
4.1.11	Determination of the Target Analyte Yield – Recovery	67
4.1.12	Intra- and Interday Precision	68
<b>4.2</b>	<b>Analysis of Pesticide-Treated HepaRG Cells with Immunoaffinity-Based Mass Spectrometry</b>	<b>71</b>
4.2.1	Determination of the Fold Change's Significance Levels	71
4.2.2	Analysis of HepaRG Cells Treated with Single Pesticides – Screening	73
4.2.3	Time-Dependency of Effects after Varying Pesticide Incubations	75
4.2.4	HepaRG Cell Viability after Treatment with Single Pesticides and Mixtures thereof	78
4.2.5	Analysis of HepaRG Cells Treated with Pesticide Mixtures	85
4.2.6	Multiple Linear Regression Analysis for the Determination of Combinatorial Effects	92
<b>5</b>	<b>Discussion</b>	<b>104</b>
<b>5.1</b>	<b>Development of Immunoaffinity-Based Mass Spectrometry Assays</b>	<b>104</b>
<b>5.2</b>	<b>HepaRG Cells as a Suitable Model for the Analysis of Potential Mixture Effects after Pesticide Treatment</b>	<b>113</b>
<b>5.3</b>	<b>Comparison of mRNA and Protein Data</b>	<b>115</b>

<b>5.4</b>	<b>Combinatorial Effects of Pesticide Mixtures on Protein Profiles in HepaRG Cells</b>	<b>118</b>
<b>6</b>	<b>Summary</b>	<b>130</b>
<b>7</b>	<b>Zusammenfassung</b>	<b>132</b>
<b>8</b>	<b>References</b>	<b>134</b>
<b>9</b>	<b>Supplementary Data</b>	<b>143</b>
<b>10</b>	<b>Curriculum Vitae</b>	<b>180</b>

## List of figures

Figure 1.	Pesticide consumption of the world from 1990 to 2016 .....	2
Figure 2.	Rice, paddy production from 1990 to 2016 .....	2
Figure 3.	Schematic illustration of cumulative effects .....	6
Figure 4.	Top-down vs. Bottom-up approach.....	11
Figure 5.	Overview of a typical targeted bottom-up approach.....	12
Figure 6.	Anti-FSGR antibody with its respective targets.....	14
Figure 7.	Principle of Full-MS .....	16
Figure 8.	Principle of tSIM.....	17
Figure 9.	Principle of PRM .....	17
Figure 10.	Routes of pesticide intake .....	20
Figure 11.	Workflow tryptic proteolysis.....	35
Figure 12.	TXP-workflow.....	36
Figure 13.	Standard full-scan 45-min and standard 10-min PRM gradient.....	39
Figure 14.	Liquid chromatography gradient for full-scan measurement of in-gel digested samples.....	41
Figure 15.	Liquid chromatography gradient of the CYP 17-plex.....	42
Figure 16.	Normalized collision energy comparison .....	50
Figure 17.	Total ion current chromatogram of a prochloraz-treated HepaRG cell sample .....	51
Figure 18.	PRM and tSIM comparison for CYP2B6 and CYP2C9.....	53
Figure 19.	Epitope binding motifs of TXP antibodies .....	56
Figure 20.	Normalized target peptide release by enzymatic fragmentation from HepaRG protein extracts over time .....	58
Figure 21.	Normalized peptide release of CYP7A1 by enzymatic fragmentation from HepaRG protein extracts over time .....	59
Figure 22.	Mean normalized peptide release by enzymatic fragmentation from HepaRG protein extracts over time .....	60
Figure 23.	Chromatographic separation and area comparison .....	63
Figure 24.	Linearity of CYP1A1 in PBSC.....	64
Figure 25.	Accuracy plot of CYP1A1 in PBSC.....	65
Figure 26.	Histogram of randomly generated fold changes .....	72
Figure 27.	Heatmap of screening results .....	75

## List of figures

Figure 28.	Heatmap comparison of 24 h and 72 h treatment.....	77
Figure 29.	Relative potency factor matrix.....	80
Figure 30.	HepaRG cell viability after pesticide treatment.....	84
Figure 31.	Protein abundance analysis in HepaRG cells treated with the mixture of AOS/CC and AOS/DIF.....	87
Figure 32.	Protein abundance analysis in HepaRG cells treated with the mixture of AOS/THI and PPC/DIF.....	88
Figure 33.	Results of potential mixture effects on CYP3A4 protein abundance in HepaRG cells.....	90
Figure 34.	Results of potential mixture effects on LMNA protein abundance in HepaRG cells.....	91
Figure 35.	Dose-response plot of LMNA after 24-hour treatment with azoxystrobin.....	94
Figure 36.	Two different schematic cases for determining a combinatorial effect... .....	95
Figure 37.	Histogram of Model Deviation Ratios.....	98
Figure 38.	Matrix of Model Deviation Ratios.....	100
Figure 39.	Model Deviation Ratios for CYP3A4 and S100P .....	101
Figure 40.	Antibody-lysate amount optimization for ARG1 and UGT2B7 .....	108
Figure 41.	Comparison of cryopreserved human hepatocytes with HepaRG cells .. .....	114
Figure 42.	Comparison of mRNA and protein data from the screening .....	117
Figure 43.	Workflow multiple linear regression analysis .....	120
Figure 44.	Fold change of CYPs after prototypical inducer treatment.....	123
Figure 45.	Summary of normalized collision energy optimization .....	153
Figure 46.	Linearity results of multiplex assays in PBSC.....	161
Figure 47.	Accuracy plots for analytes in PBSC.....	166
Figure 48.	Results of potential mixture effects on ADH1B and ALDH3A1 .....	167
Figure 49.	Results of potential mixture effects on ARG1 (PFSK) and (YILK) .....	168
Figure 50.	Results of potential mixture effects on CYP1A1 and CYP1A2 .....	169
Figure 51.	Results of potential mixture effects on CYP2B6 and CYP2C8 .....	170
Figure 52.	Results of potential mixture effects on CYP2C9 and CYP2C19 .....	171
Figure 53.	Results of potential mixture effects on CYP2E1 and CYP7A1 .....	172
Figure 54.	Results of potential mixture effects on FASN and HSD11B2 .....	173



Figure 55.	Results of potential mixture effects on MDR1 and NCPR .....	174
Figure 56.	Results of potential mixture effects on NQO1 and PRKDC .....	175
Figure 57.	Results of potential mixture effects on S100P and SULT1B1 .....	176
Figure 58.	Results of potential mixture effects on TNFRSF12A and UGT1A1 .....	177
Figure 59.	Results of potential mixture effects on UGT1A3 and UGT2B7 .....	178
Figure 60.	Results of potential mixture effects on UGT2B15 .....	179

## List of tables

Table 1.	Classification of pesticides according to the WHO .....	4
Table 2.	Buffer and Eluents.....	22
Table 3.	Chemicals, Biochemicals, Reagents .....	23
Table 4.	Consumables .....	24
Table 5.	Laboratory Equipment.....	26
Table 6.	Databases and Software.....	27
Table 7.	Pesticides of the screening.....	28
Table 8.	Single pesticides for treatment kinetics .....	30
Table 9.	Single pesticides for comparison with mixtures.....	30
Table 10.	Mixtures with different treatment durations and concentrations.....	30
Table 11.	Prototypical Inducers .....	31
Table 12.	Dilution of the BSA standard curve for BCA assay .....	33
Table 13.	Overview of the target genes of the PCR array .....	36
Table 14.	Modified list of potential target analytes .....	37
Table 15.	Mass spectrometric parameters for the 45-min standard full-scan and standard 10-min PRM method.....	39
Table 16.	In-gel digestion protocol.....	40
Table 17.	Comparison of PRM and tSIM parameters for the CYP 17-plex .....	43
Table 18.	Tested gradients to optimize the chromatographic separation.....	45
Table 19.	Number of identified proteins and peptide groups after in-gel digestion .....	52
Table 20.	Least required antibody-protein ratio .....	57
Table 21.	Multiplex assays for proteins of interest.....	61
Table 22.	Linear equations of all analytes in PBSC .....	66
Table 23.	Recovery of analytes out of NIH3T3 cell samples.....	67
Table 24.	Intra- and interday precision of multiplex assays 1-6 .....	69
Table 25.	Pesticides of the screening.....	74
Table 26.	Selection of mixtures for the analysis of potential mixture effects.....	81
Table 27.	Slopes of regression lines and effects in the respective mixtures.....	97
Table 28.	Number of significant changes from the additive model.....	122
Table 29.	Comparison of cyproconazole protein data .....	125
Table 30.	Abbreviation of analytes covered in this work.....	143

Table 31.	Results of the database search for potential target peptides.....	145
Table 32.	Results of mass spectrometric detection compatibility .....	149
Table 33.	Results of Proteome Discoverer screening for analytes of interest...	154
Table 34.	Target EN <sub>s</sub> enrichment from a complex matrix.....	155

## List of abbreviations

A	Absorption
AB	Antibody
ABC	Ammonium bicarbonate (buffer)
ABCC	Ammonium bicarbonate (buffer) with CHAPS
ABC-transporter	ATP binding cassette-transporter
ACN	Acetonitrile
AGC	Automatic gain control
AhR	Aryl hydrocarbon receptor
AOP	Adverse outcome pathway
BCA	Bicinchoninic acid
BfR	German Federal Institute for Risk Assessment
BSA	Bovine serum albumin
BVL	Federal Office of Consumer Protection and Food Safety
C.V.	Coefficient of variation
CAG	Cumulative assessment group
CAR	Constitutive androstane receptor
CE	Collision energy
CeBiTec	Center for Biotechnology
CHAPS	3-[(3-Cholamidopropyl) dimethylammonio] -1-propanesulfonate
CIMS	Context-independent motif-specific
CITCO	6-(4-Chloro-phenyl) imidazo [2,1-b][1,3] thiazole-5-carbaldehyde O-(3,4-di-chlorobenzyl)oxime
d	Thickness
DAR	Draft assessment report
ddH <sub>2</sub> O	Deionized water
ddMS <sup>2</sup>	Data-dependent tandem mass spectrometry
DDT	Dichlorodiphenyltrichloroethane
DME	Drug metabolizing enzyme
DMSO	Dimethyl sulfoxide
EC	European Commission
EC <sub>x</sub>	Effect concentration causing an x% effect
EDTA	Ethylenediaminetetraacetic acid
EFSA	European Food Safety Authority
EN	Endogenous
EN <sub>s</sub>	Non-labeled synthetic standard peptide
ETD	Electron transfer dissociation
EU	European Union

FA	Formic acid
FAO	Food and Agriculture Organization of the United Nations
FAOSTAT	Data of the Food and Agriculture Organization of the United Nations
FDA	U.S. Food and Drug Administration
GST	Glutathione S-transferases
HCB	Hexachlorobenzene
HCD	Higher-energy collisional dissociation
HCT	Human colon tumor
HEK	Human embryonic kidney
HepG2	Hepatoma G2
HPLC	High-performance liquid chromatography
I.D.	Inner diameter
IAA	Iodoacetamide
IAC	Immunoaffinity chromatography
IgG	Immunoglobulin G
IMAC	Immobilized metal ion affinity chromatography
IP	Immunoprecipitation
IS	Isotopically labeled internal standard peptide
IT	Injection time
JKI	Julius Kühn Institute
LC	Liquid chromatography
LC-MS	Liquid chromatography coupled with mass spectrometry
LD	Lethal dose
LDS	Lithium dodecyl sulfate
LLOQ	Lower limit of quantification
LOD	Limit of detection
LOQ	Limit of quantification
MDR	Model Deviation Ratio
MOA	Mode of action
Mp	Multiplex
MRM	Multiple reaction monitoring
mRNA	Messenger ribonucleic acid
MRP	Multidrug resistance protein
MS	Mass spectrometry
ms	Millisecond
NCE	Normalized collision energy
NOAEL	No observed adverse effect level
NP-40	Nonyl Phenoxyethoxyethanol
OC	Organochlorines
OCP	Organochlorine pesticide

## List of abbreviations

OP	Organophosphates
pAB	Polyclonal antibody
PAGE	Polyacrylamide gel electrophoresis
PBS	Phosphate buffered saline
PBSC	Phosphate buffered saline with CHAPS
PCB	Polychlorinated biphenyl
PHH	Primary human hepatocytes
PMSF	Phenylmethanesulfonyl fluoride
POP	Persistent organic pollutant
PPP	Plant protection products
PRM	Parallel reaction monitoring
PXR	Pregnane X receptor
QC	Quality control
qPCR	Quantitative real-time polymerase chain reaction
rbt	Rabbit
RMS	Rapporteur member state
RPF	Relative potency factor
RT	Room temperature
SCoPAFF	Standing Committee on Plants, Animals, Food and Feed
SDS	Sodium dodecyl sulfate
SDS-PAGE	Sodium dodecyl sulfate polyacrylamide gel electrophoresis
SISCAPA	Stable isotope standards and capture by anti-peptide antibodies
SLC	Solute carrier transporter
SRM	Selected reaction monitoring
t	tonnes
TCEP	(Tris(2-carboxyethyl) phosphine
TEA	Triethanolamine
TFA	Trifluoroacetic acid
TIC	Total ion current chromatogram
tSIM	Targeted selected ion monitoring
TXP	Triple X proteomics
UBA	Federal Environment Agency
UHPLC	Ultra-high performance liquid chromatography
WHO	World Health Organization
$\epsilon$	Extinction coefficient

The abbreviations of the pesticides and analytes used can be found in Table 25 and Table 30, respectively.

# 1 Introduction

## 1.1 Pesticides

After the fipronil scandal became known to the public in 2017, in which the insecticide fipronil, which is used as a contact poison against ticks and mites, has been detected in chicken eggs and egg products, it could be assumed that the use of pesticides and the presence of residues in food is a relatively topical issue <sup>1</sup>. However, the history of pesticides goes back to the 19<sup>th</sup> century, where inorganic substances such as copper sulfate or lime sulfur were first used for pest control <sup>2</sup>. During the Second World War and the following years, synthetic organic substances were developed, which represented a breakthrough in pest control, and the introduction of insecticides greatly reduced diseases such as malaria and typhus <sup>3</sup>. Dichlorodiphenyltrichloroethane (DDT), first synthesized in 1874, was associated with insecticidal activity by Paul Hermann Müller in 1939, for which he was later awarded the Nobel Prize in physiology or medicine regarding the discovery of DDT's high efficiency as a contact poison against several arthropods <sup>2,4</sup>. Since then, new substances have been continuously developed, and a great variety of different pesticides have been introduced. The definition of a pesticide could be described as follows: The ideal function of a pesticide is that it is lethal to the target but not harmful to non-target species <sup>5</sup>. They are, for example, used for the protection of plants. This protection leads to higher crop yields and also better quality in cabbage <sup>5</sup>. Although many old pesticides with higher toxic potential were withdrawn, the global pesticide market is still growing <sup>2</sup>. Figure 1 shows the world's pesticide consumption in tonnes (t) from 1990 to 2016 <sup>6</sup>. The graph shows a steady increase in pesticide consumption from approximately 2.3 million tonnes up to 4.1 million tonnes in the last three decades.

## Introduction

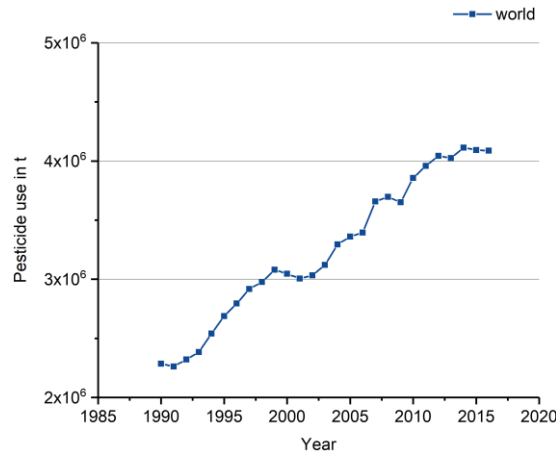


Figure 1. Pesticide consumption of the world from 1990 to 2016. The graph shows the pesticide consumption of the whole world in the specified period. A steady increase in pesticide use can be observed (from approximately 2.3 million t up to 4.1 million t). Data were obtained from the database FAOSTAT provided by the food and agriculture organization of the United Nations <sup>6</sup>.

According to data from the Food and Agriculture Organization of the United Nations (FAOSTAT), rice (paddy) is one of the most produced crops in the world. In the last three decades, the production increased globally from 519 million tonnes in 1990 up to 756 million tonnes in 2016, shown in Figure 2.<sup>6</sup>

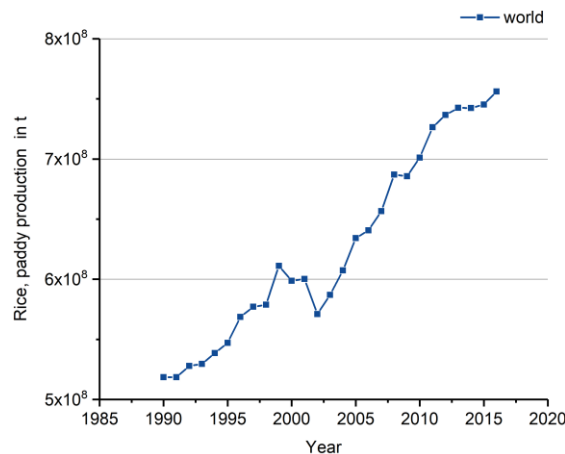


Figure 2. Rice, paddy production from 1990 to 2016. The production increased globally from 519 million t to 756 million t. Data was obtained from FAOSTAT <sup>6</sup>.

As the world population is expected to rise to about 9.8 billion people by 2050 and even up to 11.2 billion people by 2100, it is necessary to provide sufficient and safe food <sup>7</sup>. It is, therefore, hardly surprising that the number of pesticides used increases with the amount of food that needs to be provided. In 2016, the amount of pesticides used accounted for 2.6 kg ha<sup>-1</sup> (260 mg m<sup>-2</sup>) <sup>6</sup>. Although the definition of an ideal pesticide states that it should be lethal to the target and harmless to non-targets, for



most substances, this is not the case. Due to the high use, residues of these can get into the human body. Typical ways, how a pesticide can enter the body are via the skin, eyes, by oral uptake, or by inhalation <sup>8</sup>. Therefore, the exposure to certain pesticides can be associated with various diseases like cancer <sup>9</sup>, asthma <sup>10</sup>, leukemia <sup>11</sup>, and others <sup>12-14</sup>.

Furthermore, not all formerly or presently used pesticidal active compounds and additives, such as organochlorine pesticides <sup>15</sup> (OCPs) or polychlorinated biphenyls <sup>16</sup> (PCBs), are biodegradable, which makes them to so-called persistent organic pollutants <sup>17</sup> (POPs). These POPs are more stable to degradation, thus persisting in the environment for a long time, and bioaccumulation can occur after new application of the substance, which means that the initial concentration can even be exceeded many times over <sup>8</sup>. Therefore, the use of POPs like hexachlorobenzene (HCB) or endrin is nowadays forbidden. Since the use of pesticides has not only positive effects, such as increased crop yields but also adverse effects, such as health impairment, the production and use of new pesticides must be strictly controlled. The regulatory framework for the authorization of new pesticides is described in 1.1.2 (The Regulatory Framework for Market Release of New Single Pesticides). So far, however, only the influence of individual pesticides has been considered. In many cases, pesticides are already offered as mixtures, which means that different pesticides, as well as co-formulants and excipients, are used in these formulations, or farmers use several pesticides simultaneously in their fields to increase the spectrum of action. Since only the effect of the individual substance is examined when new substances are authorized, data on possible mixture effects are lacking, and the question arises as to whether the consumption of pesticides as residues and the additional mixing of these substances may lead to adverse health effects.

### 1.1.1 Pesticide Types

Pesticides are either chemical or biological substances that are used for the control of pests, mites, rodents, weeds, nematodes, and many more <sup>18</sup>. Depending on the vermin, pesticides can be classified as fungicides, herbicides, insecticides, nematocides, or rodenticides <sup>2,19</sup>. Besides that, the World Health Organization (WHO) recommended a classification system according to the toxicity of pesticides. Table 1 shows the classification of pesticides based on the WHO <sup>20</sup>.

## Introduction

Table 1. Classification of pesticides according to the WHO. The classification was based on the 50% lethal dose (LD<sub>50</sub>) of rat in mg kg<sup>-1</sup>, and the table was prepared based on the WHO.<sup>20</sup>

Class	Toxic effect based on the LD <sub>50</sub> in rat in mg kg <sup>-1</sup> body weight
Ia	Extremely hazardous
Ib	Highly hazardous
II	Moderately hazardous
III	Slightly hazardous
U	Unlikely to present acute hazard

Fungicides are used to eradicate fungi and prevent their growth. The Bordeaux mixture, which consisted of inorganic compounds such as copper sulfate, was one of the first fungicides <sup>2</sup>. Nowadays, mainly organic fungicides are used. Pathogens that can become resistant to a specific fungicide are problematic. Therefore, it is essential that not only substances with a specific mode of action are used, but that they are applied alternately with other substances that follow a different route of effect. Because of that, it is also recommended to use mixtures thereof, which comprise different modes of action. Most of the substances that were investigated in this work come from the fungicide group, as they are already frequently applied as mixtures.<sup>2</sup> These are azoxystrobin, boscalid, captan, carbendazim, cyproconazole, cyprodinil, difenoconazole, dimethomorph, epoxiconazole, fenhexamid, fludioxonil, flusilazole, fluxapyroxad, imazalil, iprodione, maneb, metalaxyl, myclobutanil, prochloraz, propiconazole, pyraclostrobin, tebuconazole, and thiram.

Within pesticides, herbicides are the most widely used substances in pest control. These chemical substances destroy weeds selectively in order to increase crop yield. The use of herbicides can increase crop yield by up to 10%. Among this group, there are many different chemical classes such as phenolic herbicides, phenoxy acids, dinitroanilines, carbamates, or amide herbicides.<sup>2,18</sup>

Insecticides are used in different fields like agriculture, medicine, or at home against insects. Also, eggs or larvae of insects are thereby addressed. They can be differentiated to inorganic and organic substances, whereby the organic insecticides can be further divided into organochlorines (OCs) and organophosphates (OPs). Both groups act as neurotoxins. Another group of insecticides is the neonicotinoids. These substances are used in particular where insects started to show resistance against

other types of insecticides. They are also distinguished by their high effectiveness, even at low doses, and rapid onset of action.<sup>2,18</sup>

Insecticides that were used in this study are chlorpyrifos, ethoprophos, fipronil, thiacloprid, and thiamethoxam.

Nematicides are used to kill nematodes. Many nematicides are too toxic to be used as sprays. These substances can be used as granules and are introduced directly into the soil, e.g., to protect potatoes. Substances, which can be used as nematicides and were investigated in this work are ethoprophos and iprodione.<sup>2</sup>

Other pesticides that were used in this study were acaricides, which are used against ticks and mites, like fenpyroximate, or plant growth regulators like chlormequat.

### 1.1.2 The Regulatory Framework for Market Release of New Single Pesticides

The approval procedure for a new active substance is based on the European Union (EU) Regulation 1107/2009/EC<sup>21</sup>. This achieves a homogenous and high level of safety for humans, animals, the environment, and groundwater in all member states<sup>21,22</sup>. The approval of a new active substance involves several steps. Firstly, an application for approval of this substance must be submitted by the manufacturer to a member state. This responsible member state is called rapporteur member state (RMS). The content of the application for authorization can be found in EU Regulation 1107/2009/EC and includes, among other things, the summary and the complete dossier of the active substance. Secondly, an initial risk assessment of the RMS takes place, and a draft assessment report (DAR) is prepared. The RMS can modify the application and add amendments. Thirdly, the Pesticides Unit of the European Food Safety Authority (EFSA) carries out a peer review of the RMS's dossier. A conclusion report is then written and published by EFSA. In the next step, the Standing Committee on Plants, Animals, Food and Feed (SCoPAFF) decides whether the new active substance will be approved or not. Upon approval, this is adopted by the Commission, and the regulation is published in the EU official journal (list of approved active substances). These steps must be taken to obtain authorization of a new active substance at the EU level. Once the EU approval has been granted, the individual member states decide separately on the approval of plant protection products (PPPs) at the national level. In Germany, for example, this is coordinated by the Fed-

eral Office of Consumer Protection and Food Safety (BVL) and carried out in cooperation with the Julius Kühn Institute (JKI), the Federal Environment Agency (UBA) and the German Federal Institute for Risk Assessment (BfR).<sup>22,23</sup>

While EU Regulation 1107/2009/EC sets the framework for the authorization of a new active substance, Regulation 283/2013/EU<sup>24</sup> (active substances) and Regulation 284/2013/EU<sup>25</sup> (plant protection products) set the necessary tests required for authorization. In addition to physical and chemical properties, toxicity and metabolism studies must also be carried out. These last-mentioned studies include many animal experiments. They comprise acute toxicity tests, short-term toxicity, long-term toxicity, and carcinogenicity, as well as many others. Regulation 1107/2009/EC describes that pesticide residues must not have harmful effects on humans or animals and that it is necessary to address potential cumulative and synergistic effects. These cumulative effects can be divided into additive, antagonistic, and synergistic effects. The following scheme (Figure 3) illustrates how these effects might look like.

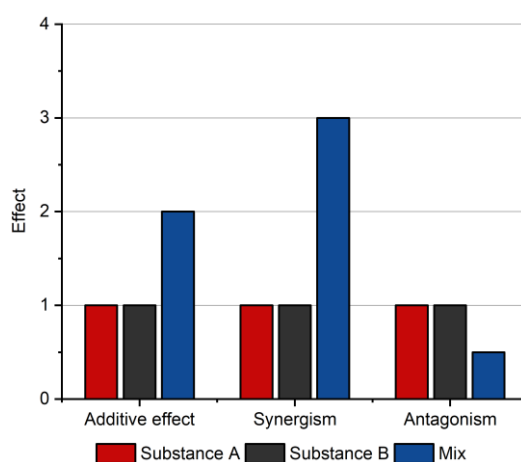


Figure 3. Schematic illustration of cumulative effects. Illustrated are cumulative effects of a binary mixture consisting of Substance A and Substance B as an example. In the first case (left), the substances are additive. The effects of the individual substances are added. The second case (mid) represents a synergism, whereby the effect in the mixture is stronger than the additive effect. In the third case (right), an antagonism is shown where the effects of the individual substances cancel each other out, and the resulting effect in the mixture is weaker than the additive effect.

An additive effect of substances A and B (left side) is schematically shown, where the effect of the binary mixture represents the sum of A and B. For a synergistic effect (mid), the effect in the mixture is even stronger than that of the additive. An antagonism (right) is defined as the effect in the mixture of substance A and B being weaker than the additive effect.

Due to the ever-increasing number of new active substances and the associated increase in potential mixtures, the number of animal experiments would increase dramatically if the examination of combinatorial effects in animals would become part of the authorization procedure. This fact calls for an alternative. With the development of suitable *in vitro* methods, this problem of the risk assessment of potential combinatorial effects can be addressed, and the number of animal experiments can be reduced to a minimum.

## 1.2 Metabolism of Pesticides & Regulation of Metabolic Enzymes

### 1.2.1 Xenobiotic Metabolism

The introduction to pesticides showed that an enormous amount thereof is used worldwide (1.1). However, pesticides are not the only substances to which organisms are exposed. Organisms can also be exposed to a great variety of different foreign substances, also termed xenobiotics, such as chemicals <sup>26,27</sup> or active pharmaceutical substances <sup>28</sup>. Due to this multitude of different influencing factors, which can also constantly change, organisms have developed defense mechanisms against these xenobiotics. In the so-called xenobiotic metabolism, which consists of several phases, endogenous or exogenous substances are processed and prepared for excretion from the body.<sup>29</sup>

In order to be metabolized intracellularly, the substances must first enter the cell. The uptake of these substances is mainly accomplished by transport proteins belonging to the solute carrier (SLC) transporter family <sup>30,31</sup>. In phase I, the often lipophilic xenobiotics are then converted by drug-metabolizing enzymes (DMEs). Activation is achieved by introducing a functional group to the substance by oxidation, reduction, or hydrolysis <sup>29</sup>. The majority of DMEs in Phase I are covered by the cytochrome P450 family (CYPs). This superfamily consists of many subfamilies, with mainly CYP1, CYP2, and CYP3 being responsible for the conversion of xenobiotics <sup>32</sup>. After the activation step, the substances are made even more water-soluble by conjugation reactions in phase II. This additionally improves the renal and biliary excretion. Phase II enzymes are transferases, like glutathione S-transferases (GSTs),

UDP-glucuronosyltransferases (UGTs), N-acetyltransferases (NATs), or sulfotransferases (SULTs).<sup>33</sup>

In phase III, metabolized, as well as unmetabolized substances, are excreted by multidrug resistance proteins (MRPs), which belong to the ATP-binding cassette (ABC) transporter family <sup>31,32</sup>.

In addition to these enzymes and transporters that play a role in the various phases of the xenobiotic metabolism, there are also receptors involved that are responsible for regulating these proteins. The mechanisms on which signal transduction is mainly based on include nuclear receptors <sup>34</sup>, such as the pregnane X receptor (PXR), the constitutive androstane receptor (CAR), the aryl hydrocarbon receptor <sup>35</sup> (AhR), as well as other important transcription factors <sup>32</sup>. The transcription regulation of genes related to xenobiotic metabolism takes place as soon as the nuclear receptors are activated. Activation is obtained through the binding of a ligand, for example, a pesticide. There are several ways to regulate transcription. For example, after activation, the receptors can translocate from the cytosol into the nucleus. Here, they can bind to specific response elements of the target genes and thus either activate or inhibit transcription. This binding leads to the induction or repression of protein synthesis.<sup>36,37</sup> PXR and CAR are mainly responsible for the transcriptional regulation of CYP3A and CYP2B isoforms, whereas CYP1A isoforms are primarily regulated by AhR <sup>38</sup>.

### 1.2.2 Preliminary Study for the Determination of Toxicologically Relevant Markers at mRNA Level

The metabolism of xenobiotics mainly takes place in the liver, the most important organ for detoxification. As already mentioned, many different enzymes are involved in these metabolic pathways. Foreign substances such as pesticides can alter the protein profile of these enzymes, which then could indicate liver toxicity. A pre-selection of these potential markers was identified in a first study conducted by the group of Dr. Philip Marx-Stoelting, in which potential combinatorial effects of azole fungicides were investigated using “omics” technologies (Table 13). They state that for the identification of common mode of actions (MOAs) or adverse outcome pathways (AOPs), not only mechanistic analyses but also the analysis of mixture toxic-

ties using relevant biomarkers are required to determine the assumed dose additions or concentration additions. The tested substances can then later be classified into cumulative assessment groups (CAGs). They also showed that species differences (between human and rat) were observed based on individual genes. In the case of pathway-level evaluation, the following five pathways were identified, which were affected across species by treatment with cyproconazole, epoxiconazole, and the mixture thereof: Chemical carcinogenesis, xenobiotic metabolism, drug metabolism, retinol metabolism, and steroid metabolism.<sup>39</sup>

This implies the need to perform analyses in a human model, such as HepaRG cells, when the analysis is performed at the individual gene level and not at the pathway level (differences could also occur on pathway level, but it was shown that the evaluation on pathway level led to higher accordances), since the analysis in an animal model may not reflect the situation in humans.

### 1.3 Proteomics

The era of "omics" began with genome analysis, known as genomics, and considerable progress has been made with these technologies<sup>40</sup>. In 1995 the term proteome was coined by Marc Wilkins, who defined it as the total protein equivalent of a genome<sup>41</sup>. Since then, the analyses of the proteome or transcriptome, which are generally referred to as proteomics or transcriptomics, came to the fore.

Genes are only the carriers of information, so expression analysis gives only indirect information on proteins and their functions. In the course of understanding how a biological system works, it is necessary to investigate proteins or protein functions directly.<sup>40</sup>

Comparing the genome with the proteome, one major difference is that the genome is a static source of information, which typically remains the same, while the proteome is of dynamic origin. That means that the proteome can not only vary quantitatively (changes in protein levels) but also qualitatively (presence of different proteins) depending on internal as well as external stimuli. This leads to the fact that different proteome data of the same genome can be obtained, depending on the time at which it is measured.<sup>40,42</sup>

In order to determine the function of a biological system, it is therefore essential to have a closer look at its proteome. One key aspect would be post-transcriptional protein regulation. Besides that, the protein synthesis, as well as the protein turnover rates, can be different for particular transcripts.<sup>40</sup>

A proteomic analysis typically involves several steps which consist of separation of complex sample mixtures, the identification of individual proteins as well as the quantification thereof<sup>40,43,44</sup>. Within the last two decades, the use of chromatographic methods such as high-performance liquid chromatography (HPLC) in combination with mass spectrometric (MS) detection methods has been the key technology of proteome analysis<sup>44-46</sup>. Regarding MS-based proteomics, it can be further subdivided into top-down or bottom-up approaches, which will be further explained in the following section.

### 1.3.1 Mass Spectrometry-Based Protein-Profiling Strategy

In general, there are two different MS-based protein-profiling strategies. These techniques are called top-down and bottom-up approach. Figure 4 (adapted from Gregorich et al.<sup>47</sup>) depicts both strategies. On the left side, the top-down, on the right side, the bottom-up approach is shown. The main difference between the two strategies is that the top-down approach aims to measure intact proteins, while the bottom-up approach measures peptides as surrogates for the proteins of interest. In the first step, proteins need to be extracted out of cells or tissues. A variety of different extraction methods already exist<sup>48</sup>, but it is crucial to choose an appropriate protocol regarding the MS analysis. Exemplarily, if buffers contain sodium, the formation of sodium adducts during the ionization process takes place, which changes the masses of analytes of interest<sup>49</sup>.

After the extraction of proteins, the workflow of the bottom-up approach comprises a proteolysis step. Proteolysis is either obtained by in-gel digestion or in-solution digestion (trypsin, endoprotease LysC, or endoprotease AspN are commonly used for MS-based proteomics approaches<sup>41,47</sup>). After proteolysis, peptides are separated, and MS profiling is done. In bottom-up approaches, separation is generally obtained with online liquid chromatography (LC). Compared to top-down, this approach offers a more robust way for protein identification<sup>47</sup>. Also, the production of internal standards is more convenient. On the other hand, it has to be taken into



account that an intensive and comprehensive database search has to be performed in advance to achieve reliable identification and quantification. Peptides as surrogates for the protein of interest should be unique and should not contain sequence variants or modifications within their sequence.

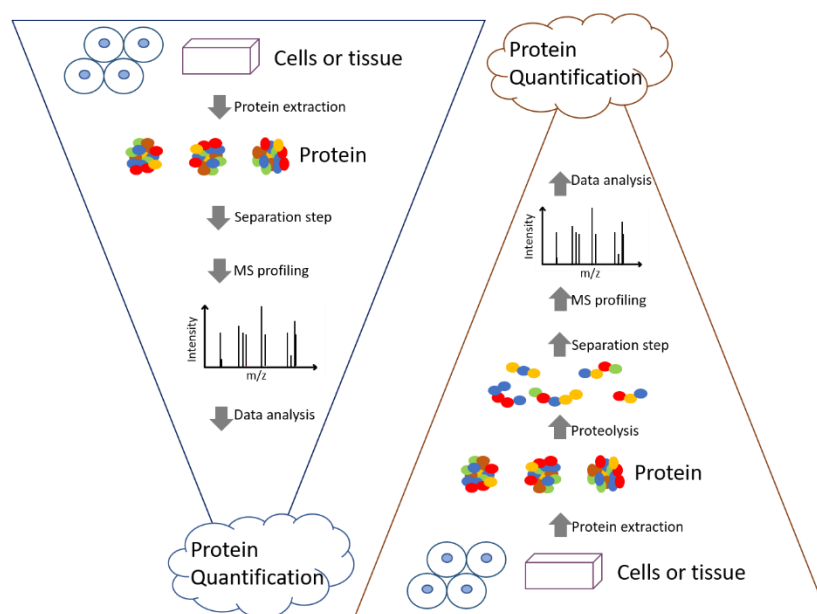


Figure 4. Top-down vs. Bottom-up approach. In the top-down approach (left), the protein is extracted from the cell or tissue, then chromatographically separated and directly analyzed by MS. In the bottom-up approach (right), the extraction is followed by a proteolysis step of the protein. The most common enzyme used for proteolysis is trypsin. The resulting peptides are then chromatographically separated and analyzed via MS (adapted from Gregorich et al. <sup>47</sup>).

### 1.3.2 Targeted Proteomics

The procedure in this thesis followed the targeted bottom-up approach, and Figure 5 (adapted from Uchida et al. <sup>50</sup>) gives an overview of a typical workflow. In the first step, the target proteins are selected. Since the analysis is performed at the peptide level, a target peptide has to be chosen as a representative for each protein. The next steps include the synthesis of non-labeled synthetic standard target peptides (EN<sub>s</sub>), the examination of their MS detection compatibility, and method development. After the successful generation of the assays, samples have to be prepared, i.e., tryptic proteolysis and immunoprecipitation (IP). Afterward, the analysis by liquid chromatography-mass spectrometry (LC-MS), as well as the data evaluation and quantification of target analytes, follows. Targeted proteomics applications are generally termed selected reaction monitoring (SRM) or multiple reaction monitoring

(MRM), as well as parallel reaction monitoring (PRM), depending on the mass spectrometer. Pre-filtration at MS1 level results in higher sensitivity. The isolated peptides are then fragmented, and the specificity is increased by the detection of the fragment ions at MS2 level, thus ensuring unambiguous identification.<sup>51-53</sup>

All steps are described in more detail in the following sections.

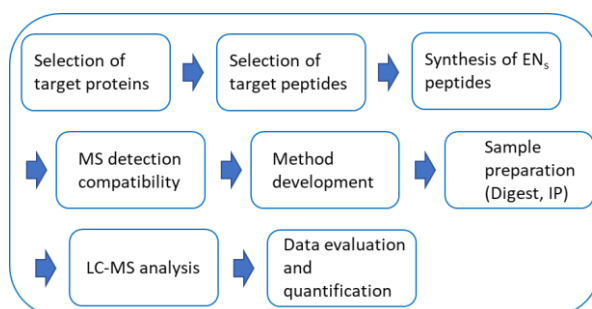


Figure 5. Overview of a typical targeted bottom-up approach. It comprises the selection of target proteins followed by the selection of respective target peptides. After target non-labeled standard synthetic peptides (EN<sub>s</sub>) are synthesized, their MS detection compatibility is checked, and the method development is performed. After digesting the samples, an immunoprecipitation (IP) is done, followed by the LC-MS analysis. The last step includes the data evaluation and quantification of target analytes (Scheme was adapted by Uchida et al.<sup>50</sup>).

### 1.3.3 Immunoaffinity-Based Mass Spectrometry

One challenge with bottom-up strategies is the concentration of low abundant proteins, which in most cases, cannot be detected. In order to detect these proteins, an additional sample preparation step has to be implemented. In this step, the analyte of interest is enriched, or the matrix complexity is reduced. This can be achieved, for example, by immunoaffinity chromatography<sup>54</sup> (IAC) or immunoprecipitation<sup>55</sup> (IP). For instance, Anderson et al. introduced a method in 2004, called stable isotope standards and capture by anti-peptide antibodies<sup>56</sup> (SISCAPA). Here, stable isotope standards and anti-peptide antibodies are added to the proteolyzed sample. By using anti-peptide antibodies, the peptides to be investigated, as well as the isotopically labeled standard peptides, are pulled out of the sample, which leads to a drastically reduced matrix complexity.

A reduced matrix complexity has several positive effects regarding LC-MS detection. First, ion suppression effects are reduced during the ionization at the ion source before the MS unit. Ion suppression affects the amount of charged ions and thus impairs the detection, identification, and quantification of target analytes.<sup>57</sup>

Second, typical LC-MS approaches that focus on identification use chromatographic gradients of several hours <sup>58</sup>. If the sample's complexity is reduced by immune enrichment or immune precipitation techniques, these gradients can be shortened exceedingly from 2-3-hour methods to 10-20-minute methods.<sup>59</sup>

Third, sensitivity can be improved, while the conditions of the detection system (such as scan range, scan speed, or injection time) remain unchanged. If parameters of the detection system are changed, background signals may also increase, or the resolution of the MS instrument may be reduced.<sup>60</sup>

Compared to ligand-binding assays, the immunoaffinity LC-MS application is able to differentiate interferences similar to the target, while the ability of the detection antibody in a ligand-binding assay may be limited <sup>61</sup>. In conclusion, immunoaffinity-based LC-MS approaches offer fast, specific, selective, and reproducible methods that allow multiplexing.<sup>62,63</sup>

Today, immunoaffinity enrichment or immunoprecipitation prior to mass spectrometric analyses is a widely used method for identifying and quantifying biomarkers such as peptide hormones <sup>64</sup>, important markers in cardiac diseases <sup>65</sup> or cancer-related research <sup>66</sup>.

#### 1.3.4 Triple X Proteomics – an Example of an Immunoaffinity-Based Mass Spectrometry Approach

As described in the previous section, immunoaffinity enrichment or precipitation of targets is performed, so low abundant proteins can also be detected. Although many capture approaches, such as hydrazide chemistry-based enrichment <sup>67</sup> or immobilized metal ion affinity chromatography <sup>68</sup> (IMAC), are available, polyclonal and monoclonal antibodies are the molecules of choice <sup>69</sup>. The SISCAPA method is an example of a one-target one-antibody approach, which means that one single target is enriched by a specific antibody. Therefore, a tremendous number of antibodies would have to be generated for the analysis of a whole proteome. Not only would that usher to enormous costs, but the number of animals immunized for the generation of antibodies would also increase dramatically. To address this issue, approaches that involve group-specific antibodies, such as context-independent motif-specific <sup>70</sup> (CIMS) or triple X proteomics <sup>71</sup> (TXP), came to the fore.

## Introduction

In the TXP strategy, specific antibodies are generated towards four amino acid antigens. Meaning, these particular antibodies do not bind to the whole sequence of the target peptide, but only the last four amino acids at the C-terminus. Since trypsin is used for proteolysis in this strategy, the TXP-antibodies enrich groups of tryptic peptides that share the same short C-terminal tag. Thus, one particular antibody is able to enrich many different peptides, resulting in cost, as well as workload reduction. Furthermore, the number of animals required for the generation of antibodies can be reduced significantly.<sup>71,72</sup>

The CYP450 superfamily already described in 1.2.1 consists of very homologous proteins. Therefore, the use of TXP antibodies is advantageous for the analysis of this family. Exemplarily, the anti-FSGR antibody, and the peptides, it can enrich, are shown in Figure 6. With this antibody it is possible to enrich at least five peptides simultaneously that are surrogates for CYP2B6, CYP2C8, CYP2C18, CYP2E1, and CYP2F1.



Figure 6. Anti-FSGR antibody with its respective targets. The anti-FSGR antibody is capable of enriching peptides derived from several metabolizing enzymes of the CYP450 family, like CYP2B6, 2C8, 2C18, 2E1, or 2F1.

Prior to the generation of TXP-antibodies, a bioinformatic approach is used to analyze theoretical fragments *in silico*. With this strategy, it is possible to further reduce the total number of group-specific antibodies recognizing the same C-terminal tag. In conclusion, the TXP approach, in combination with the bioinformatics strategy, is capable of reducing the total number of capture antibodies, thus minimizing the massive workload and costs of the one-target one-antibody approach.<sup>72</sup>

### 1.3.5 Mass Spectrometric Analysis Methods

In a typical mass spectrometric bottom-up approach, the proteolysis is performed after the extraction of proteins. As described before, this can either be done with in-gel digestion or in-solution protocols. Most extraction buffers contain detergents that are incompatible with the LC-MS application, such as sodium dodecyl sulfate (SDS) or Triton X-100<sup>73</sup>. To address this issue, in-gel digests are usually performed to shed interfering detergents. Afterward, proteolyzed samples can be directly injected to the LC-MS device, and with a full-scan approach (Full-MS / ddMS<sup>2</sup>; data-dependent tandem mass spectrometry), identification of proteins present in the sample can be performed. This procedure is commonly known as shotgun proteomics.<sup>74,75</sup>

For research projects, where not the identification of analytes but rather quantification of prior chosen analytes is in focus, targeted approaches are the application of choice. Since proteolyzed samples are much more complex than the corresponding protein sample (about 50 times more complex<sup>41</sup>), peptides of low abundance get lost in a non-targeted approach. Therefore, targeted approaches such as targeted selected ion monitoring (tSIM) or parallel reaction monitoring (PRM) methods are used. Besides the full-scan (Full-MS) method, these targeted approaches are available for the QExactive plus mass spectrometer (Thermo Fisher Scientific, Waltham, USA). Depending on the interrogation, one specific mode is chosen. In the following sections, the modes Full-MS / ddMS<sup>2</sup>, tSIM, and PRM will be explained in detail.

#### 1.3.5.1 Full-scan MS

For the analysis of complex samples, mass spectrometers are typically used, which combine different mass filters and mass analyzers. In the first unit (Q1), a pre-filtering can be performed according to different mass-to-charge ratios. In the second unit (commonly abbreviated with Q2), these precursor ions can be fragmented using different fragmentation methods such as higher-energy collisional dissociation<sup>76</sup> (HCD) or electron transfer dissociation<sup>77</sup> (ETD). In the last unit, the detection of either precursor or fragment ions is achieved by a mass detector like the Orbitrap mass analyzer. As described in the previous section (1.3.4), the full-scan (Full-MS) strategy is often used in identification projects (shotgun proteomics), to identify novel biomarkers<sup>78,79</sup>. In this mode, no prior knowledge of the analytes

within a sample is required, so no isolation list needs to be used. This means that in the quadrupoles of the mass spectrometer, no pre-filtering of the ions takes place. In the first step, all ionizable peptides reach the Orbitrap mass analyzer, and a scan is performed at the MS1 level (precursor ions). For each scan event, the most intense peptide ion mass-to-charge ratios (usually Top 10 or Top 15) are selected for fragmentation, and an MS2 level scan (fragment ions) is performed. Hence, the method is called Full-MS / ddMS<sup>2</sup>. The analytes are then identified by comparing the mass spectra obtained with databases. Figure 7 shows the principle of the Full-MS measurement mode.

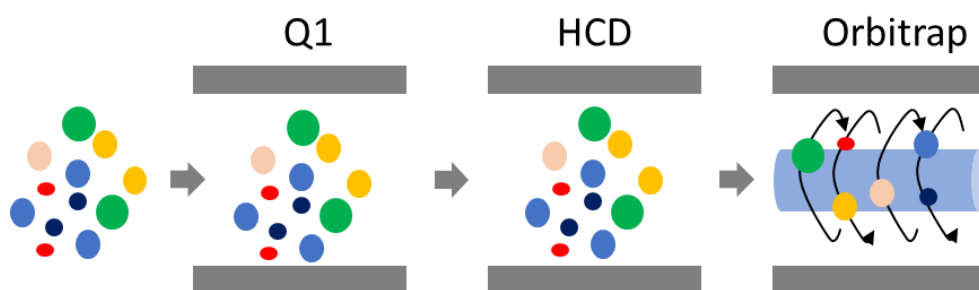


Figure 7. Principle of Full-MS. After chromatographic separation, all ionized peptides enter the first quadrupole (Q1) without filtering. Without being fragmented, these peptides enter the Orbitrap mass analyzer and are detected there.

### 1.3.5.2 Targeted selected ion monitoring

In targeted modes such as targeted selected ion monitoring (tSIM) shown in Figure 8, it is important to know that not all ionized analytes are detected by the Orbitrap mass analyzer because a pre-filtering is performed in the first quadrupole. This means that prior knowledge of the sample or the analytes is required, and this information is made available to the instrument via an isolation list. By using filters, the sensitivity of the measurement can be increased, since only specific masses are selected, which can pass the first quadrupole. The filtered ions that have passed the first quadrupole directly reach the Orbitrap mass analyzer where they are detected. An advantage compared to the Full-MS mode is that the sensitivity can be strongly increased. This mode is used for experiments, where the target and its mass are already known.<sup>80,81</sup>

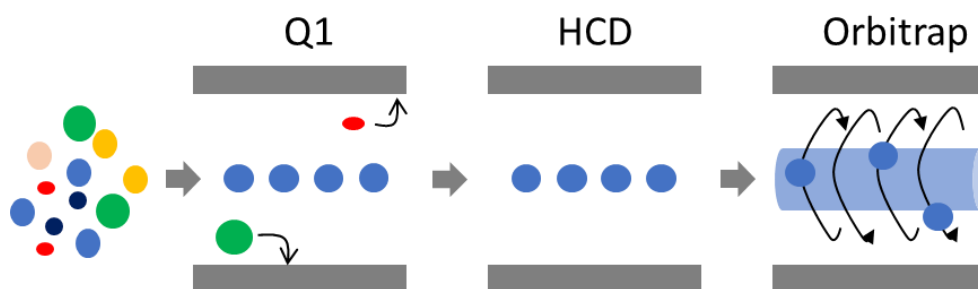


Figure 8. Principle of tSIM. All ions enter the first quadrupole (Q1), which serves as a filter. Only ions with a specific mass can pass it. Without fragmentation, the masses of interest enter the Orbitrap mass analyzer and are detected there.

### 1.3.5.3 Parallel reaction monitoring

Parallel reaction monitoring, also known as PRM, is also a targeted mass spectrometric approach available on a QExactive Plus mass spectrometer. After the pre-filtering step in Q1, these filtered ions are fragmented in the higher-energy collisional dissociation (HCD) cell. There, they collide with nitrogen atoms leading to fragmentation of the respective precursor ion. After fragmentation, all fragment ions enter the Orbitrap mass analyzer and can be detected in parallel. This approach offers excellent specificity by isolating specific masses and further fragmentation of the respective analyte<sup>52,82</sup>. Figure 9 shows the PRM principle. Since the measurement in tSIM is MS1 level-based and, therefore, prone to interferences, especially in complex matrices, PRM offers an excellent alternative with increased specificity<sup>82</sup>.

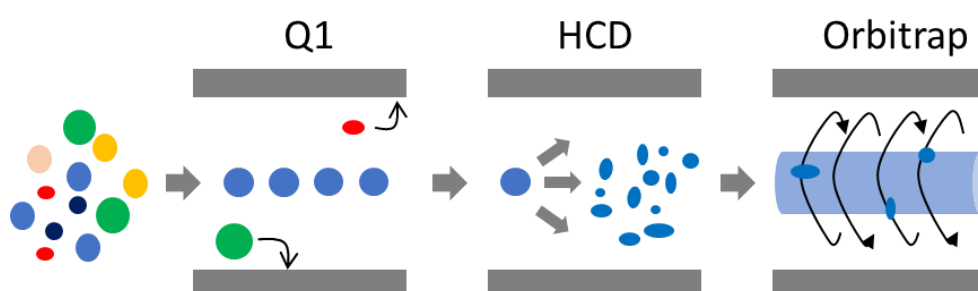


Figure 9. Principle of PRM. Ionized peptides enter the first quadrupole (Q1), where the filtering of specifically chosen masses is performed. Then, these precursor ions are fragmented in the higher-energy collisional dissociation (HCD) cell by colliding with nitrogen atoms. These fragments enter the Orbitrap mass analyzer, where they are detected.





## 2 Aim of this Thesis

People are exposed to various pesticide residues through the consumption of food. The possible intake routes are either directly through the consumption of crops and vegetables, or indirectly through the consumption of meat from animals that come into contact with pesticides in fields, soil, or drinking water (Figure 10). The toxicological properties of these substances are only investigated at the individual level during the authorization procedure. Therefore, only limited data on potential mixing effects are available so far. That means that the toxicological investigation of these mixing effects represents a central challenge for regulatory purposes and risk assessment. More than 450 active substances are approved in Europe, with many already being used as mixtures today. The investigation of toxicological properties during the authorization procedure includes a large number of animal experiments, such as short- and long-term toxicity or carcinogenicity. That means that the number of animal experiments would increase enormously if the mixing effects were investigated with the standard toxicological tests. This calls for an alternative that can be addressed by the development of *in vitro* methods.

Therefore, the first goal of this thesis was to develop immunoaffinity-based mass spectrometry assays to investigate potential mixing effects of pesticides on toxicologically relevant liver proteins. The development first included a comprehensive database search for suitable peptides, which had already been identified as possible representatives to indicate hepatotoxicity at the mRNA level. With these selected peptides and specifically generated antibodies against these peptides, various parameters should be investigated to ensure the reliability of these assays. These included the mass spectrometry (MS) detection compatibility of the peptides, the functionality of the antibodies, the optimization of the antibody-protein ratio, optimal digestion time, linearity studies, as well as recovery and intra-/ interday variation tests.

As a second goal, the influence of 30 pesticides on the protein profile in human cell culture samples should be investigated after successful method development. The cell line HepaRG was used as a test system, as it shows very similar characteristics to primary human hepatocytes, especially with regard to the protein profile of xenobiotic-metabolizing enzymes such as cytochrome P450 (CYP). The results of this

screening with the 30 pesticides should then be used to classify them according to their effect similarities. In addition, it should be investigated which mixtures were already available on the market.

The third goal was to prepare mixtures of pesticides from the screening in different concentrations to investigate the influence on the target proteins. As a final step, not only the regulation of the proteins but also potential combinatorial effects, such as synergism or antagonism, should be evaluated using statistical methods.

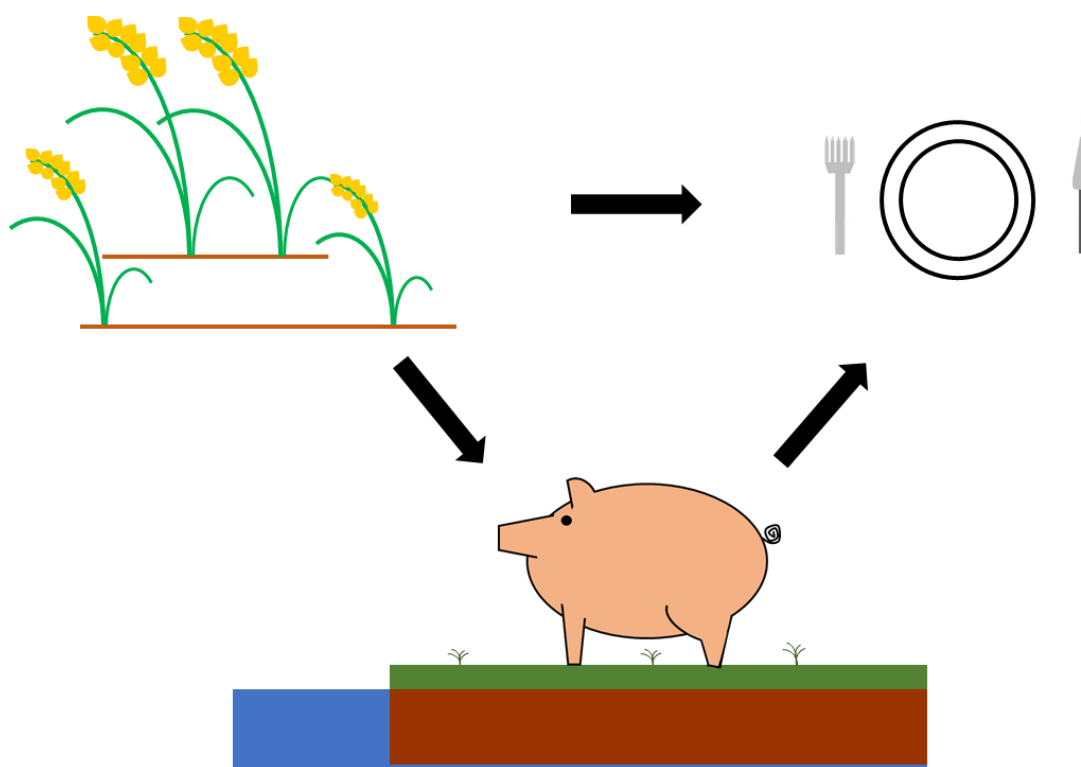


Figure 10. Routes of pesticide intake. Pesticides applied in agriculture can remain as residues in crops and thus enter the human body directly through consumption. In addition, these substances can enter animals from feed, drinking water, or soil and then indirectly enter the human organism through the consumption of meat.



### 3 Material and Methods

#### 3.1 Buffer

Table 2. Buffer and Eluents

Buffer/Eluents	Ingredients	Concentration/ Percentage share
ABCC Buffer	NH <sub>4</sub> HCO <sub>3</sub>	50 mmol L <sup>-1</sup>
	CHAPS	0.03%
Eluent A (LC)	FA	0.1%
	Water, LC-MS grade	
Eluent B (LC)	ACN	80%
	FA	0.1%
	Water, LC-MS grade	
Eluent C (LC)	IPA	10%
	Water, LC-MS grade	
Extraction Buffer (in-gel digest)	ACN	50%
	TFA	0.05%
Loading Buffer (LC)	ACN	2%
	TFA	0.05%
	Water, LC-MS grade	
Lysis Buffer	NP-40	1%
	SDS	0.01%
	NaCl	150 mmol L <sup>-1</sup>
	Na <sub>2</sub> HPO <sub>4</sub> x 2 H <sub>2</sub> O	10 mmol L <sup>-1</sup>
	EDTA	2 mmol L <sup>-1</sup>
PBSC Buffer	PBS 1x	
	CHAPS	0.03%
Triethanolamine	Triethanolamine	100 mmol L <sup>-1</sup>
Washing Buffer A (in-gel digest)	NH <sub>4</sub> HCO <sub>3</sub>	5 mmol L <sup>-1</sup>
	ddH <sub>2</sub> O	
Washing Buffer B (in-gel digest)	NH <sub>4</sub> HCO <sub>3</sub>	10 mmol L <sup>-1</sup>
	ACN	50%

### 3.2 Chemicals, Biochemicals, Reagents

Table 3. Chemicals, Biochemicals, Reagents

Substance	Manufacturer
3-[(3-Cholamidopropyl) dimethylammonio] -1-propanesulfonate (CHAPS)	Carl Roth, Karlsruhe, Germany
Acetic acid 100%	Carl Roth, Karlsruhe, Germany
Acetone, ACS grade	VWR, Darmstadt, Germany
Acetonitrile, ROTISOLV ≥99.98%, Ultra LC-MS (ACN)	Carl Roth, Karlsruhe, Germany
Ammonia solution 25%, Rotipuran	Carl Roth, Karlsruhe, Germany
Ammonium bicarbonate (ABC)	Sigma-Aldrich, St. Louis, USA
Bicinchoninic acid protein assay reagents (BCA)	Thermo Fisher Scientific, Waltham, USA
Blocking reagent for ELISA	Roche Diagnostics, Mannheim, Germany
Customized polyclonal antibody sera	Pineda GmbH, Berlin, Germany
Customized synthetic isotopically labeled peptides (IS)	Intavis AG, Tübingen, Germany
Customized synthetic non-labeled peptides (EN <sub>s</sub> )	Intavis AG, Tübingen, Germany
Dimethyl sulfoxide (DMSO)	Sigma-Aldrich, St. Louis, USA
Dionex Cytochrome C Digest	Thermo Fisher Scientific, Waltham, USA
Disodium phosphate (Na <sub>2</sub> HPO <sub>4</sub> x 2 H <sub>2</sub> O)	Carl Roth, Karlsruhe, Germany
Ethanol, >99.8%, p.a.	Carl Roth, Karlsruhe, Germany
Ethylenediaminetetraacetic acid (EDTA)	Carl Roth, Karlsruhe, Germany
Formic acid UHPLC-MS Optigrade (FA)	LGC Standards, Teddington, United Kingdom
Hydrochloric acid 37% fuming (HCl)	Carl Roth, Karlsruhe, Germany
InstantBlue Coomassie Protein Stain	Expedeon, San Diego, USA
Iodoacetamide (IAA)	Sigma-Aldrich, St. Louis, USA
Isopropyl alcohol, ROTISOLV ≥99.95%, Ultra LC-MS (IPA)	Carl Roth, Karlsruhe, Germany
LTQ Velos ESI Positive Ion Calibration Solution	Thermo Fisher Scientific, Waltham, USA
Methanol, ROTISOLV ≥99.98%, Ultra LC-MS	Carl Roth, Karlsruhe, Germany
NP40 Surfact Amps Detergent Solution	Thermo Fisher Scientific, Waltham, USA
NuPAGE Antioxidant	Thermo Fisher Scientific, Waltham, USA
NuPAGE LDS Sample Buffer (4X)	Thermo Fisher Scientific, Waltham, USA
NuPAGE MES SDS Running Buffer (20X)	Thermo Fisher Scientific, Waltham, USA
NuPAGE Sample Reducing Agent	Thermo Fisher Scientific, Waltham, USA
Phenylmethanesulfonyl fluoride (PMSF)	Roche Diagnostics, Mannheim, Germany
Phosphate buffered saline 10x (PBS)	Thermo Fisher Scientific, Waltham, USA
Pierce Bovine Serum Albumin Standard (BSA)	Thermo Fisher Scientific, Waltham, USA
Pierce Coomassie Plus Assay Kit	Thermo Fisher Scientific, Waltham, USA

## Material and Methods

Substance	Manufacturer
Pierce Trypsin Protease, MS-Grade	Thermo Fisher Scientific, Waltham, USA
SeeBlue Plus2 Prestained Standard	Thermo Fisher Scientific, Waltham, USA
Sodium azide (NaN <sub>3</sub> )	Merck, Darmstadt, Germany
Sodium chloride (NaCl)	Carl Roth, Karlsruhe, Germany
Sodium dodecyl sulfate (SDS)	Sigma-Aldrich, St. Louis, USA
Sodium hydroxide ≥99% (NaOH)	Carl Roth, Karlsruhe, Germany
Technical buffer solution pH 4.01	Mettler Toledo, Columbus, USA
Technical buffer solution pH 7.00	Mettler Toledo, Columbus, USA
Technical buffer solution pH 9.21	Mettler Toledo, Columbus, USA
Triethanolamine hydrochloride (TEA/TEA-HCl)	Carl Roth, Karlsruhe, Germany
Trifluoroacetic acid, ULC/MS Optigrade (TFA)	LGC Standards, Teddington, United Kingdom
Tris(2-carboxyethyl) phosphine (TCEP)	Carl Roth, Karlsruhe, Germany
Water, ROTISOLV Ultra LC-MS	Carl Roth, Karlsruhe, Germany

### 3.3 Consumables

Table 4. Consumables

Consumables	Manufacturer
96-Well robotic full-skirted plate, 0.2 mL	Thermo Fisher Scientific, Waltham, USA
Acclaim PepMap RSLC C18, 75 µm I.D. x 150 mm, 2 µm	Thermo Fisher Scientific, Waltham, USA
Acclaim PepMap RSLC C18, 75 µm I.D. x 500 mm, 2 µm	Thermo Fisher Scientific, Waltham, USA
Acclaim PepMap100 C18 µ-precolumn, 0.3 mm I.D. x 5 mm, 5 µm	Thermo Fisher Scientific, Waltham, USA
Axygen AxySeal sealing film	Corning Incorporated, Corning, USA
Cellstar tubes, 15 mL, PP, graduated, conical bottom	Greiner Bio-One, Frickenhausen, Germany
Cellstar tubes, 50 mL, PP, graduated, conical bottom	Greiner Bio-One, Frickenhausen, Germany
Cellstar tubes, 50 mL, PP, graduated, self-standing	Greiner Bio-One, Frickenhausen, Germany
DURAN Laboratory bottle with DIN thread, GL 45, 250 mL	Duran Group GmbH, Wertheim/Mainz, Germany
DURAN Laboratory bottle with DIN thread, GL 45, 500 mL	Duran Group GmbH, Wertheim/Mainz, Germany

Consumables	Manufacturer
DURAN Laboratory bottle with DIN thread, GL 45, 1000 mL	Duran Group GmbH, Wertheim/Mainz, Germany
Dynabeads Protein G	Thermo Fisher Scientific, Waltham, USA
Easy Peel Heat Sealing Foil	Thermo Fisher Scientific, Waltham, USA
Eppendorf Tubes 3810X, 1.5 mL	Eppendorf, Hamburg, Germany
Eppendorf Tubes, 5.0 mL	Eppendorf, Hamburg, Germany
epT.I.P.S. Standard 0.1-10 µL	Eppendorf, Hamburg, Germany
epT.I.P.S. Standard 100-5000 µL	Eppendorf, Hamburg, Germany
epT.I.P.S. Standard 2-200 µL	Eppendorf, Hamburg, Germany
epT.I.P.S. Standard 50-1000 µL	Eppendorf, Hamburg, Germany
HiTrap NHS-activated HP	GE Healthcare Life Sciences, Chicago, USA
KingFisher 96 tip comb	Thermo Fisher Scientific, Waltham, USA
Micro insert, 0.1 mL, clear glass 15 mm, top	VWR, Darmstadt, Germany
Micro inserts glass, 250 µL, conical	neoLab, Heidelberg, Germany
Microplate, 96 well, PS, F-Bottom, clear	Greiner Bio-One, Frickenhausen, Germany
Multi-safety microcentrifuge tubes, 0.65 mL	Carl Roth, Karlsruhe, Germany
Nitrile gloves	VWR, Darmstadt, Germany
Novex WedgeWell 4-20% Tris-Glycine Gel	Thermo Fisher Scientific, Waltham, USA
PCR Tube Strips 0.2 mL	Eppendorf, Hamburg, Germany
pH indicator paper range 1-14	Carl Roth, Karlsruhe, Germany
PipetteTips, SpaceSaver, LTS, 300 µL	Mettler Toledo, Columbus, USA
PipetteTips, StableRak, LTS, 10 µL	Mettler Toledo, Columbus, USA
PipetteTips, StableRak, LTS, 250 µL	Mettler Toledo, Columbus, USA
QUICKRACK Tip Transfer System, 1250 µL	Biozym Scientific, Oldendorf, Germany
Reaction tubes with screw thread, 1.5 mL, conical	neoLab, Heidelberg, Germany
Reaction tubes with screw thread, 1.5 mL, self-standing	neoLab, Heidelberg, Germany
Reaction tubes with screw thread, 2.0 mL, self-standing	neoLab, Heidelberg, Germany
Screw caps for reaction 1.5 mL and 2 mL tubes	neoLab, Heidelberg, Germany
Screw caps, 9 mm, natural rubber red-orange	VWR, Darmstadt, Germany
Vial short thread, 1.5 mL, amber glass with label	VWR, Darmstadt, Germany
Viper Inline Filter	Thermo Fisher Scientific, Waltham, USA

### 3.4 Laboratory Equipment

Table 5. Laboratory Equipment

Apparatus	Manufacturer
ABgene Combi Thermo-Sealer	Thermo Fisher Scientific, Waltham, USA
Absorbance microplate reader, BioTek ELx808	BioTek, Winooski, USA
Analytical balance CPA225D-OCE	Sartorius Stedim Biotech, Göttingen, Germany
Analytical balance XS205 DualRange	Mettler Toledo, Columbus, USA
Analytical balance, Explorer scale	OHAUS Waagen, Bad Hersfeld, Germany
Axyspin Mini Plate Spinner Centrifuge, Axygen	Corning Incorporated, Corning, USA
Ball mill, Micro-Dismembrator U	Sartorius Stedim Biotech, Göttingen, Germany
Centrifuge, Mini Star	VWR, Darmstadt, Germany
Chromatography system, ÄKTExpress	GE Healthcare Life Sciences, Chicago, USA
Chromatography system, UltiMate 3000 RSLCnano	Thermo Fisher Scientific, Waltham, USA
Electrophoresis Power Supply Power Ease 500	Thermo Fisher Scientific, Waltham, USA
Electrophoresis System XCell SureLock	Thermo Fisher Scientific, Waltham, USA
Ice machine Scotman AF40	Frimont S.p.A., Pogliano Milanese, Italy
Magnet Dynal MPF-96S	Thermo Fisher Scientific, Waltham, USA
Magnet DynaMag Spin	Thermo Fisher Scientific, Waltham, USA
Magnet KingFisher 96 PCR head	Thermo Fisher Scientific, Waltham, USA
Magnetic particle processor, KingFisher 96-purification system	Thermo Fisher Scientific, Waltham, USA
Magnetic particle processor, KingFisher Flex-purification system	Thermo Fisher Scientific, Waltham, USA
Mass spectrometer, QExactive	Thermo Fisher Scientific, Waltham, USA
Mass spectrometer, QExactive Plus	Thermo Fisher Scientific, Waltham, USA
Microcentrifuge 5415D	Eppendorf, Hamburg, Germany
Mixer, Vortex-Genie 2	Scientific Industries, Bohemia, USA
Multichannel Electronic Pipette, E4 XLS, 100–1200 µL	Mettler Toledo, Columbus, USA
Multichannel pipette 50–1200 µL, Eppendorf Research Pro	Eppendorf, Hamburg, Germany
Multichannel pipette, Pipet-Lite XLS, 2–20 µL	Mettler Toledo, Columbus, USA
Multichannel pipette, Pipet-Lite XLS, 20–300 µL	Mettler Toledo, Columbus, USA
Multichannel pipette, Pipet-Lite XLS, 5–50 µL	Mettler Toledo, Columbus, USA
Multi-syringe infusion pump SP220i	World Precision Instruments, Sarasota, USA
pH-meter, 766 Calimatic	Knick, Berlin, Germany
Pipette 0.1–2.5 µL, Eppendorf Research plus	Eppendorf, Hamburg, Germany
Pipette 10–100 µL, Eppendorf Research plus	Eppendorf, Hamburg, Germany



Apparatus	Manufacturer
Pipette 100–1000 µL, Eppendorf Research plus	Eppendorf, Hamburg, Germany
Pipette 2–20 µL, Eppendorf Research plus	Eppendorf, Hamburg, Germany
Pipette 20–200 µL, Eppendorf Research plus	Eppendorf, Hamburg, Germany
Pipette 50–5000 µL, Eppendorf Research plus	Eppendorf, Hamburg, Germany
Refrigerated microcentrifuge 5417R	Eppendorf, Hamburg, Germany
Sample mixer, HulaMixer	Thermo Fisher Scientific, Waltham, USA
Single Channel Electronic Pipette, E4 XLS, 20–300 µL	Mettler Toledo, Columbus, USA
Spectrophotometer, NanoDrop 2000c	Thermo Fisher Scientific, Waltham, USA
SWC Safety Weighing Cabinet	Sartorius Stedim, Biotech, Göttingen, Germany
Thermomixer C	Eppendorf, Hamburg, Germany
ThermoMixer, Comfort	Eppendorf, Hamburg, Germany
Ultrasonic bath, Sonorex	Bandelin electronic, GmbH, Berlin, Germany
Water purification system, Milli Q Plus	Sartorius Stedim, Biotech, Göttingen, Germany

### 3.5 Databases and Software

Table 6. Databases and Software

Software	Distributor
Gen 5.1.10.8	BioTek, Winooski, USA
Chromeleon 6.8	Thermo Fisher Scientific, Waltham, USA
Endnote x8	Thomson Reuters, Philadelphia, USA
Microsoft Office Home and Business 2016	Microsoft, Redmond, USA
Nanodrop 2000/2000c 1.5	Thermo Fisher Scientific, Waltham, USA
Origin 2017G	OriginLab, Northampton, USA
Proteome Discoverer 2.1	Thermo Fisher Scientific, Waltham, USA
ProteomicsDB	TUM, München, Germany
RStudio v.1.0.153	R Consortium, Boston, USA
Skyline 4.2.0.19072	MACOSS Lab, Department of genome sciences, University of Washington, Seattle, USA
Tune 2.8	Thermo Fisher Scientific, Waltham, USA
TXP-Tools	Dr. Hannes Planatscher, Signatope GmbH, Reutlingen, Germany
Unicorn 5.11	GE Healthcare Life Sciences, Chicago, USA
UniProtKB Protein knowledgebase	UniProt Consortium
Xcalibur 4.0	Thermo Fisher Scientific, Waltham, USA

### 3.6 Samples

The workgroup of Prof. Dr. Ulrich Rothbauer (University of Tübingen) kindly provided human cell culture (human blend: human embryonic kidney (HEK), human colon tumor (HCT), and hepatoma G2 (HepG2)), as well as mouse cell culture (NIH3T3) samples.

The German Federal Institute for Risk Assessment (BfR) in Berlin (Dr. Albert Braeuning) kindly provided treated and untreated HepaRG cells. For the screening, the pesticide concentrations used were chosen as high as possible without being toxic for the cells. The cells for the method development were treated with  $10 \mu\text{mol L}^{-1}$  prochloraz.

The samples to be analyzed after the method development were treated with different pesticides and pesticide mixtures (shown in 3.6.1 as well as in 3.6.2).

Dr. Almut Mentz (Center for Biotechnology (CeBiTec), Universität Bielefeld) kindly provided mRNA results measured with quantitative real-time polymerase chain reaction (qPCR).

Cryopreserved primary human hepatocytes (PHHs; donors 1, 2, and 3) were purchased from hepacult GmbH in Martinsried.

#### 3.6.1 Pesticides

Table 7. Pesticides of the screening

Substance	Chemical class <sup>83</sup>	Function <sup>84</sup>	WHO Category <sup>20</sup> (Table 1)	Concentration in $\mu\text{mol L}^{-1}$
Azoxystrobin	Strobilurin	Fungicide	U	100
Boscalid	Carboxamide	Fungicide	U	500
Captan	Phthalimide	Fungicide	U	50
Carbendazim	Benzimidazole	Fungicide	U	250
Chlormequat	Quarternary ammonium compound	Plant growth regulator	II	1000
Chlorpyrifos	Organophosphate	Acaricide, Insecticide	II	200
Cyproconazole	Triazole	Fungicide	II	80
Cyprodinil	Anilinopyrimidine	Fungicide	-	100
Difenoconazole	Triazole	Fungicide	II	25

Substance	Chemical class <sup>83</sup>	Function <sup>84</sup>	WHO Category <sup>20</sup> (Table 1)	Concentration in $\mu\text{mol L}^{-1}$
Dimethomorph	Morpholine	Fungicide	U	500
Epoxiconazole	Triazole	Fungicide	-	80
Ethoprophos	Organophosphate	Insecticide, Nematicide	Ia	500
Fenhexamid	Hydroxyanilide	Fungicide	U	250
Fenpyroximate	Pyrazolium	Acaricide	II	5
Fipronil	Phenylpyrazole	Insecticide	II	50
Fludioxonil	Phenylpyrrole	Fungicide	U	250
Flusilazole	Triazole	Fungicide	II	80
Fluxapyroxad	Pyrazolium	Fungicide	-	250
Imazalil	Imidazole	Fungicide	II	50
Iprodione	Dicarboximide	Fungicide, Nematicide	III	200
Maneb	Carbamate	Fungicide	U	200
Metalaxyl	Acylalanine	Fungicide	II	1000
Myclobutanil	Triazole	Fungicide	II	250
Prochloraz	Imidazole	Fungicide	II	80
Propiconazole	Triazole	Fungicide	II	80
Pyraclostrobin	Strobilurin	Fungicide, Plant growth regulator	-	25
Tebuconazole	Triazole	Fungicide	II	80
Thiacloprid	Neonicotinoid	Insecticide	II	500
Thiamethoxam	Neonicotinoid	Insecticide	-	1000
Thiram	Carbamate	Fungicide	II	100

## Material and Methods

Table 8. Single pesticides for treatment kinetics

Substance	Treatment duration in h	Concentration in $\mu\text{mol L}^{-1}$
Difenoconazole	24, 72	10 (72 h), 25 (24 h)
Fenpyroximate	24, 72	2.5 (72 h), 5 (24 h)
Flusilazole	24, 72	80
Imazalil	24, 72	50

Table 9. Single pesticides for comparison with mixtures

Substance	Treatment duration in h	Concentration in $\mu\text{mol L}^{-1}$
Azoxystrobin	24, 48, 72	10, 25, 35, 50, 70
Cyproconazole	24, 48, 72	35, 55, 70, 110, 140
Difenoconazole	24, 48, 72	4, 6, 8, 10, 12
Propiconazole	24, 48, 72	20, 30, 40, 60, 80
Thiacloprid	24, 48, 72	250, 375, 500, 750, 1000

### 3.6.2 Pesticide Mixtures

Table 10. Mixtures with different treatment durations and concentrations

Mixture #	Substances	Treatment time in h	Concentration in $\mu\text{mol L}^{-1}$	Total concentration in $\mu\text{mol L}^{-1}$	Product
1	Propiconazole, Difenoconazole	24, 48, 72	5, 1	6	TASPA
			10, 2	12	
			20, 4	24	
			30, 6	36	
			40, 8	48	
2	Azoxystrobin, Difenoconazole	24, 48, 72	5, 1	6	ASKON
			10, 2	12	
			15, 3	18	
			25, 5	30	
			35, 7	42	
3	Thiacloprid, Azoxystrobin	24, 48, 72	25, 2.5	27.5	-
			125, 12.5	137.5	
			250, 25	275	
			375, 37.5	412.5	
			500, 50	550	

Mixture #	Substances	Treatment time in h	Concentration in $\mu\text{mol L}^{-1}$	Total concentration in $\mu\text{mol L}^{-1}$	Product
4	Azoxystrobin, Cyproconazole	24, 48, 72	2.5, 5	7.5	Various
			10, 20	30	
			17.5, 35	52.5	
			27.5, 55	82.5	
			35, 70	105	

### 3.6.3 Induction Controls

Table 11. Prototypical Inducers

Substance	Chemical class	Function	Concentration in $\mu\text{mol L}^{-1}$
Benz[a]pyrene	Polycyclic aromatic hydrocarbon	AhR agonist	1.25, 2.5, 5
6-(4-Chlorophenyl)imidazo[2,1-b][1,3]thiazole-5-carbaldehyde O-(3,4-dichlorobenzyl)oxime (CITCO)	Imidazothiazole derivative	CAR agonist	2.5, 5, 10
Rifampicin	Ansamycin	PXR agonist	1.25, 2.5, 5

## 3.7 Antibody Purification

For the generation of polyclonal triple X proteomics (TXP) antibodies, rabbits were immunized with the respective antigens by Pineda GmbH (Berlin, Germany). The required KLH-peptide conjugate was generated according to Hoeppe et al.<sup>72</sup> The rabbit sera (approximately 10 mL each) containing the antibodies were purified with an affinity chromatography device (ÄKTApress™). The sera were first filtered through a 0.2  $\mu\text{m}$  sterile filter. Affinity columns with peptides as a stationary phase, which served as ligands for the antibodies, were prepared. The mobile phase consisted of a phosphate-buffered saline solution (PBS). The peptides immobilized on the column captured only the antibodies with the appropriate paratope, and other components were washed away. Elution was performed using 100  $\text{mmol L}^{-1}$

## Material and Methods

citric acid buffer at a pH of 2.5. The eluted sample was re-buffered in PBS and de-salted by using three consecutive 5 mL filtration columns. After the antibodies were purified, their concentration was determined. The Nanodrop 2000c spectrometer (Thermo Fisher Scientific, Waltham, USA) was used for this purpose. The absorption of the antibody solution was measured at 280 nm. Then, the concentration was calculated according to the law of Beer-Lambert:

$$A = \varepsilon \cdot c \cdot d \quad (41)$$

A= absorption

$\varepsilon$ = extinction coefficient of an immunoglobulin G antibody

c= concentration of the antibody to be determined

d= path length of the nanodrop device

The standard molecular mass of an immunoglobulin G antibody (IgG antibody) is  $\approx 1.5 \cdot 10^5 \text{ g mol}^{-1}$ , and the extinction coefficient  $\varepsilon$  is  $2.1 \cdot 10^5 \text{ L mol}^{-1} \text{ cm}^{-1}$ . The path length of the nanodrop device and the extinction coefficient could be regarded as constants so that the formula of the Beer-Lambert law can be adapted as follows:

$$A_{280 \text{ nm}}^{1 \text{ mg mL}^{-1}} = 1.4 \quad (85)$$

To preserve the antibody solution, 0.05% sodium azide ( $\text{NaN}_3$ ) was added, and the antibody solutions were stored in the refrigerator at  $4^\circ\text{C}$  until further use.

## 3.8 Sample Preparation

### 3.8.1 Peptide Standards

The synthetic peptide standards were synthesized by INTAVIS AG (Tübingen, Germany). Not only non-labeled synthetic standard peptides ( $\text{EN}_s$ ) but also isotopically labeled synthetic standard peptides (IS) were generated. The isotopically labeled synthetic peptides were used as internal standards for method development and analysis of samples. Both  $\text{EN}_s$  and IS have the same sequence, the only difference being the isotope-labeled ( $^{13}\text{C}/^{15}\text{N}$ ) C-terminal arginine or lysine. This label results in a mass shift of eight for lysine and ten for arginine when the analyte is singly

charged. Due to the same sequence of both peptides, they have the same physico-chemical properties and therefore elute at the same time during the chromatographic separation step. Before the peptides could be used, they had to be dissolved. About 1.5 mg of each peptide was weighed, pure dimethyl sulfoxide (DMSO) solution and ultrapure water (LC-MS grade) were added to obtain a final concentration of 5 mmol L<sup>-1</sup> DMSO. The peptide solutions were stored at -20°C until further use.

### 3.8.2 Cell Lysis and Protein Determination

The whole sample preparation included several steps. First, the samples were lysed, then digested, and before the mass spectrometry measurement, immune precipitation was performed. Lysis was done for one hour on ice with a lysis buffer containing Na<sub>2</sub>HPO<sub>4</sub> + 2 H<sub>2</sub>O (0.01 mol L<sup>-1</sup>), NaCl (0.15 mol L<sup>-1</sup>), NP-40 (1%), SDS (0.01%), and EDTA (0.002 mol L<sup>-1</sup>). After lysis, the samples were centrifuged for 10 minutes at 13 000 g and 4°C. To determine protein concentration, the bicinchoninic acid (BCA) protein assay kit (Thermo Fisher Scientific, Waltham, USA) was used. First, the dilution of the standard curve was performed (initial bovine serum albumin (BSA) concentration was:  $\beta=2$  mg mL<sup>-1</sup>). Table 12 shows the dilution steps of the standard curve.

Table 12. Dilution of the BSA standard curve for BCA assay. The initial concentration of bovine serum albumin (BSA) was  $\beta=2$  mg mL<sup>-1</sup>. The standard curve consisted of eight concentration levels and an additional blank.

Dilution	Concentration in $\mu\text{g mL}^{-1}$
A	2000
B	1500
C	1000
D	750
E	500
F	250
G	125
H	62.5
I (blank)	0

After preparing the standard curve, HepaRG samples were diluted with lysis buffer (1:5). To rule out measurement errors of the instrument, each dilution, including that of the dilution curve, was pipetted twice onto the sample plate (microplate, 96-well; Greiner Bio-One, Frickenhausen, Germany). In each well, 25  $\mu\text{L}$  sample and 200  $\mu\text{L}$  working solution (BCA protein assay reagents A and B in a ratio of 50:1) were pipetted. To check the accuracy of the measurement, four quality control (QC) samples (prepared and verified BSA dilutions) were also pipetted onto the plate. These QC samples had the following concentrations: 50  $\mu\text{g mL}^{-1}$ , 150  $\mu\text{g mL}^{-1}$ , 300  $\mu\text{g mL}^{-1}$ , and 800  $\mu\text{g mL}^{-1}$ . To consider the protein determination as valid, the measured concentration of the QC samples must not deviate by more than 20% from the theoretical concentration. After the samples and the working solution were pipetted onto the plate, the plate was sealed with a PlateMax-AxySeal Sealing Film (Corning Incorporated, Corning, USA) and the samples incubated at 37°C and 650 rpm for 30 minutes on a thermomixer (Eppendorf, Hamburg, Germany). After incubation, air bubbles formed during incubation were removed, and the plate cooled to room temperature. As a readout, the absorbance microplate reader BioTek ELx808 (Bio-Tek, Winooski, USA) was used, and the absorbance at 562 nm measured.

### 3.8.3 Enzymatic Proteolysis and Immunoprecipitation

The mass spectrometric measurement of proteins was performed indirectly at the peptide level. Therefore, the proteins had to be digested in order to obtain the peptides of interest (procedure shown in Figure 11). Triethanolamine (TEA; final concentration 0.05 mol L<sup>-1</sup>) and lysis buffer (3.1 Buffer) were added to the respective sample amounts. A subsequent denaturation step for five minutes at 99°C followed. Samples were then cooled down to room temperature, and 0.2 mol L<sup>-1</sup> tris(2-carboxyethyl) phosphine (TCEP) was added (final concentration 0.005 mol L<sup>-1</sup>). After shaking for 30 seconds, samples were alkylated with 0.4 mol L<sup>-1</sup> iodoacetamide (IAA; final concentration 0.01 mol L<sup>-1</sup>) for 30 minutes at room temperature in the dark. For initiating the digestion, trypsin was added (trypsin:protein ratio was 1:40), and the temperature set to 37°C. To stop digestion, 0.042 mol L<sup>-1</sup> phenylmethanesulfonyl fluoride (PMSF; final concentration 0.001 mol L<sup>-1</sup>) was used. After inactivation, the digested samples were centrifuged for 10 min at 13 000 g and then stored at -20°C until further use.



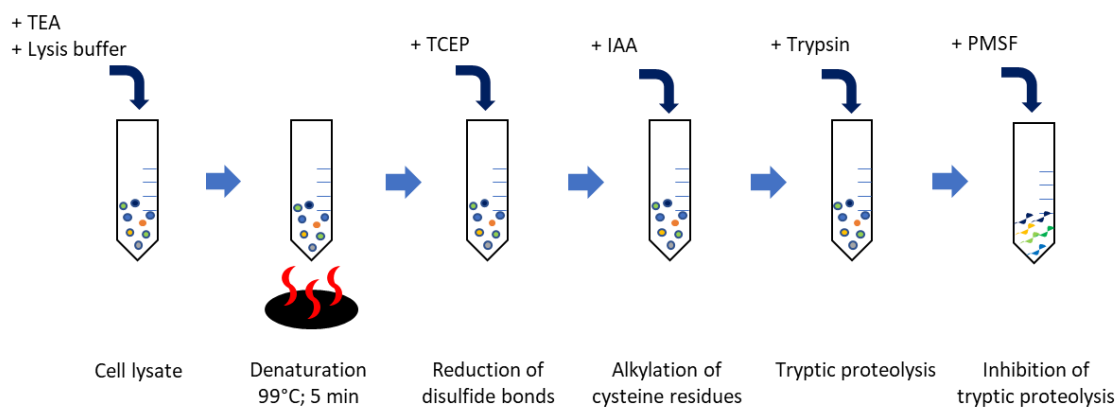


Figure 11. Workflow tryptic proteolysis. In the first step, TEA and lysis buffer were added to the samples, and then they were denatured at 99°C for five minutes. Reduction and alkylation of the sample were achieved by adding TCEP and IAA. With trypsin, proteins were fragmented down to peptides. Inactivation of trypsin was achieved by the use of PMSF.

For immunoprecipitation in 96-well format, PBS containing CHAPS (3-[(3-Cholamidopropyl) dimethylammonio] -1-propanesulfonate), sample, internal isotopically labeled standard peptide, and the corresponding amount of antibodies were mixed. An incubation step of one hour followed, during which the samples were mixed six times for two minutes with an eight-minute pause between the mixing steps. During this time, the antibody-peptide complex (both non-labeled synthetic standard or endogenous peptide and isotopically labeled standard peptide) was formed. The first incubation step was followed by a second incubation step in which magnetic microspheres coated with protein G (Dynabeads Protein G; Thermo Fisher Scientific, Waltham, USA) were added. The second incubation step was performed according to the first. Five washing steps followed, with the first two washing solutions consisting of PBSC and the last three solutions consisting of CHAPS-containing ammonium bicarbonate (ABCC). Finally, the peptides were eluted with formic acid (FA; 1%). To remove bead residues, the eluates were first transferred into a new 96-well microtiter plate and then into glass vials for liquid chromatography-mass spectrometry (LC-MS) measurement. The entire TXP workflow is shown in Figure 12.

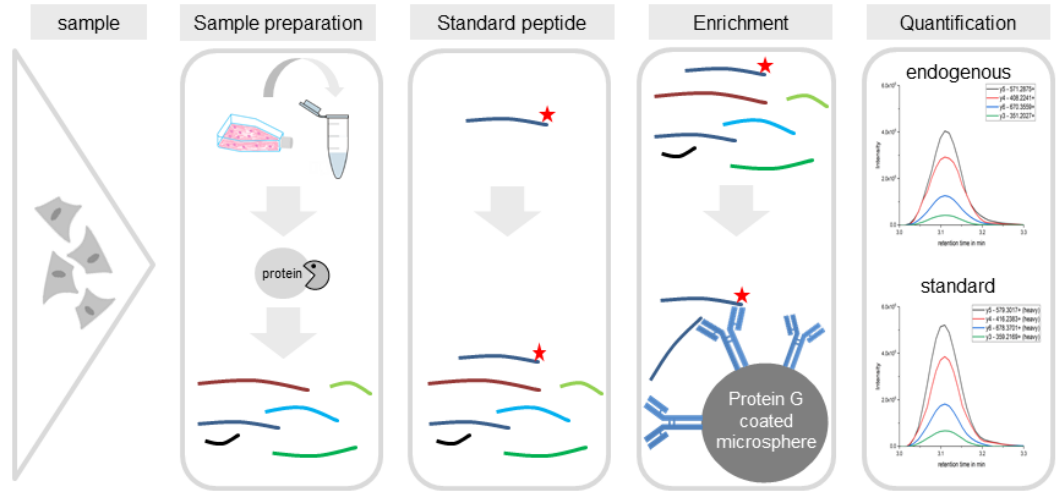


Figure 12. TXP-workflow. The TXP workflow consists of several steps. First, the sample preparation, where cells are lysed and then digested with trypsin. After that, isotopically labeled standard peptides and antibodies are added during the immunoprecipitation step. With protein G coated microspheres, the antibody-peptide complexes are pulled out of the matrix. The analysis is then performed with LC-MS.

### 3.9 Assay Development

#### 3.9.1 Database Search for Suitable Peptides

This project aimed to investigate several toxicologically relevant liver proteins. In a previous study by Seeger et al.<sup>39</sup>, potential toxicologically relevant target genes have already been identified at mRNA level by quantitative real-time polymerase chain reaction (qPCR). These targets were used as a basis for the selection of analytes at the protein level. Table 13 gives an overview of the 44 target genes from the optimized PCR array.

Table 13. Overview of the target genes of the PCR array. Here, the 44 target genes identified and measured by qPCR are shown.

#	Gene	#	Gene	#	Gene	#	Gene
1	<i>ABCC2</i>	12	<i>COX1</i>	23	<i>HRG</i>	34	<i>POR</i>
2	<i>ABCC3</i>	13	<i>CYP1A1</i>	24	<i>HSD11B2</i>	35	<i>PRKDC</i>
3	<i>ACOX2</i>	14	<i>CYP2A13</i>	25	<i>HULC</i>	36	<i>S100P</i>
4	<i>ADH1B</i>	15	<i>CYP2C9</i>	26	<i>IL6</i>	37	<i>SCARA3</i>
5	<i>ALDH3A1</i>	16	<i>CYP2D6</i>	27	<i>INSIG1</i>	38	<i>SCD</i>
6	<i>ANXA10</i>	17	<i>CYP2E1</i>	28	<i>LMNA</i>	39	<i>SLC01B1</i>

#	Gene	#	Gene	#	Gene	#	Gene
7	<i>ARG1</i>	18	<i>CYP3A5</i>	29	<i>LY6D</i>	40	<i>SREBF1</i>
8	<i>CCL20</i>	19	<i>CYP7A1</i>	30	<i>MLXIP</i>	41	<i>SULT1B1</i>
9	<i>CD36</i>	20	<i>FASN</i>	31	<i>NEAT1</i>	42	<i>SYT1</i>
10	<i>CES2</i>	21	<i>G6PC</i>	32	<i>NQO1</i>	43	<i>TNFRSF12A</i>
11	<i>CGA</i>	22	<i>GZMB</i>	33	<i>NR1I3</i>	44	<i>UGT2B7</i>

Before a database search was performed, the list was modified. For example, UGT1A1, UGT1A3, and UGT2B15 were added to this list. No database search was performed for targets such as CYP2C9 or CYP2D6 for which mass spectrometric immunoassays have already been established <sup>86</sup>. In total, the list of target analytes that should be analyzed at the protein level comprised 52 analytes. Table 14 shows all analytes to be investigated for possible combinatorial effects of pesticide mixtures.

Table 14. Modified list of potential target analytes. This list comprises 52 potential target markers for the analysis of pesticide mixtures in HepaRG cells and whether already assays existed.

Targets			Targets			Targets		
#	Analyte	Already developed	#	Analyte	Already developed	#	Analyte	Already developed
1	ACOX2	N	19	CYP2E1	Y	37	MLXIP	N
2	ADH1B	N	20	CYP2F1	Y	38	NCPR	Y
3	ALDH3A1	N	21	CYP3A4	Y	39	NQO1	N
4	ANXA10	N	22	CYP3A5	Y	40	NR1I3	N
5	ARG1	N	23	CYP3A7	Y	41	PRKDC	N
6	CCL20	N	24	CYP3A43	Y	42	S100P	N
7	CD36	N	25	CYP7A1	N	43	SCARA3	N
8	CES2	N	26	FASN	N	44	SCD	N
9	CGA	N	27	G6PC	N	45	SREBF1	N
10	COX1	N	28	GAPDH	N	46	SULT1B1	N
11	CYP1A1	Y	29	GZMB	N	47	SYT1	N
12	CYP1A2	Y	30	HRG	N	48	TNFRSF12A	N
13	CYP2B6	Y	31	HSD11B2	N	49	UGT1A1	N
14	CYP2C8	Y	32	IL6	N	50	UGT1A3	N
15	CYP2C9	Y	33	INSIG1	N	51	UGT2B7	N
16	CYP2C18	Y	34	LMNA	N	52	UGT2B15	N
17	CYP2C19	Y	35	LY6D	N			
18	CYP2D6	Y	36	MDR1	Y			

Y= Assays already developed; N= No existing assays

The selection of suitable peptides included a comprehensive database search, whereby first, the target protein was fragmented with trypsin *in silico*. Afterward, it was examined whether the peptides were proteotypic for the respective analyte, and only peptides with a sequence of 6-20 amino acids were selected. Then the amino acid composition was checked. Peptides containing methionine or an N-terminal glutamic acid were excluded. Peptides containing natural sequence variants and amino acid modifications such as glycosylation were also removed. Next, the hydrophobicity factor was investigated. Peptides with a factor of less than 2.8 were preferred. Finally, the Proteomics database (proteomicsDB<sup>87</sup>) was used to check whether the respective peptides were already detected by mass spectrometry. If possible, two synthetic non-labeled standard peptides (EN<sub>s</sub>) were ordered for each analyte.

### 3.9.2 Peptide Detection Compatibility with Mass Spectrometry

Once the synthetic non-labeled standard peptide solutions had been prepared (3.8.1 Peptide Standards), it was essential to investigate their detection compatibility by LC-MS. For this purpose, the charge state and the collision energy (CE), which should be used to achieve the optimal results, were determined. Peptides of each analyte were diluted with loading buffer from their initial concentration of 1 nmol  $\mu\text{L}^{-1}$  to the final concentration of 10 fmol  $\mu\text{L}^{-1}$  per peptide. The injection volume was 5  $\mu\text{L}$  meaning that 50 fmol of each peptide was applied to the chromatographic column. As an analytical column, an Acclaim PepMap RSLC C18 (75  $\mu\text{m}$  I.D. x 150 mm, 2  $\mu\text{m}$ , Thermo Fisher Scientific, Waltham, USA) and as a trapping column an Acclaim PepMap 100 C18  $\mu$ -precursor (0.3 mm I.D. x 5 mm, 5  $\mu\text{m}$ , Thermo Fisher Scientific, Waltham, USA) was used. Two different eluents for the LC gradient were prepared. Eluent A (aqueous phase) consisted of LC-MS-grade water containing 0.1% formic acid (FA). Eluent B (organic phase) consisted of 80% acetonitrile (ACN) and LC-MS-grade water with 0.1% FA. To load the samples onto the trapping column, a third buffer containing 2% ACN, LC-MS-grade water, and 0.05% trifluoroacetic acid (TFA) was used. The mass spectrometric analysis was performed by use of a QExactive Plus mass spectrometer (Thermo Fisher Scientific, Waltham, USA). In a first 45-minute full-scan (Full-MS / ddMS<sup>2</sup>) method run (Figure 13 (A)), it was determined which charge state led to higher peak intensities.

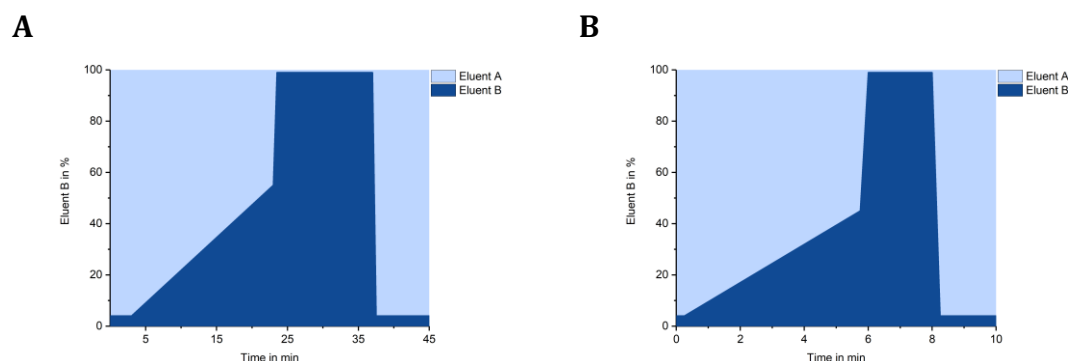


Figure 13. Standard full-scan 45-min and standard 10-min PRM gradient. In (A) the 45 min full-scan (Full-MS) and in (B), the standard PRM 10-min gradient is shown. In both cases, the column was equilibrated at 4% of eluent B and increased to 55% and 45%, respectively. The column was rinsed at 99% eluent B.

Once the ideal charge state had been identified, various CEs were tested. The standard PRM method (Figure 13 (B)) was used, and four different collision energies were examined for each analyte. The normalized collision energy (NCE) was set to either 15, 20, 25, or 30. The results were then compared, and the optimal NCE was selected for each analyte. The parameters that were set for the respective mass spectrometric detection are shown in Table 15 below.

Table 15. Mass spectrometric parameters for the 45-min standard full-scan and standard 10-min PRM method. The settings for the full-scan (Full-MS / ddMS<sup>2</sup>) are shown on the left, PRM settings on the right. Since PRM is an MS2 level-based method, ddMS<sup>2</sup> parameter setting is not applicable.

Parameter	Full-MS / ddMS <sup>2</sup>	PRM
Resolution	70 000	35 000
AGC target	3·10 <sup>6</sup>	2·10 <sup>5</sup>
Maximum IT in ms	100	60
Loop Count	10	1
MSX count	2	2
Isolation window in m/z	2.0	1.5
NCE	25	15, 20, 25, or 30
ddMS <sup>2</sup>	set	na

na= not applicable

### 3.9.3 Full-Scan Mass Spectrometry Measurement of In-Gel Digested HepaRG Cells

In this part, in-gel digestion of HepaRG cells and a full-scan (Full-MS) measurement was performed. An in-house revised protocol of the in-gel digestion described in Shevchenko et al. was used<sup>88</sup>. In-gel digestion was performed for three negative

## Material and Methods

controls (DMSO-treated) and three prochloraz-treated ( $10 \mu\text{mol L}^{-1}$ ) HepaRG cells. This was followed by a full-scan (Full-MS / ddMS<sup>2</sup>) measurement with a 130-minute gradient. The in-gel digestion procedure is shown in Table 16.

Table 16. In-gel digestion protocol. In the following table, the workflow of the in-house revised in-gel digestion protocol after Shevchenko et al. is shown <sup>88</sup>.

Step	Performance
1	Dilute samples with 2x LDS buffer (1:2)
2	Heat samples for 5 min at 90°C
3	Centrifugation for 5 min at 16 000 g
4	Gel electrophoresis for 15 min (4-20% Tris-Glycine SDS-PAGE gel)
5	Staining of protein bands with Coomassie brilliant blue for approx. 40 min at RT
6	Wash gel with ddH <sub>2</sub> O for approx. 2 h at RT
7	Cut the protein bands out of the gel
8	Destain the gel bands alternately for 15 min with buffer A and B (A: 5 mM L <sup>-1</sup> ABC in ddH <sub>2</sub> O; B: 10 mM L <sup>-1</sup> ABC in 50% ACN). Repeat four times
9	Remove liquid and dry gel bands in Speed Vac for approx 1 h
10	Add trypsin in a 1:15 (enzyme:protein) ratio
11	Incubate gel bands for 16 h at 37°C in trypsin solution
12	Add extraction buffer (100% ACN and 0.1% TFA in a 1:1 mixture) and sonicate for 15 min on ice. Repeat two times
13	Dry the samples using Speed Vac for approx. 1 h
14	Resuspend peptides in 1% FA

After in-gel digestion, the total protein and peptide concentration of each sample was determined by use of the Nanodrop 2000c spectrometer (Thermo Fisher Scientific, Waltham, USA). A volume of 2  $\mu\text{L}$  of each sample was applied to the sensor, and the absorption at 280 nm was measured. The concentration was calculated using the approximation  $1 \text{ Abs} \approx 1 \text{ mg mL}^{-1}$  <sup>89</sup>.

Samples were diluted to the same concentration of  $48 \text{ ng } \mu\text{L}^{-1}$ , then 15  $\mu\text{L}$  each, resulting in a total of 720 ng enzymatically proteolyzed sample, was injected for full-scan (Full-MS / ddMS<sup>2</sup>) analysis. The analytical column was an Acclaim PepMap RSLC C18 (75  $\mu\text{m}$  I.D. x 500 mm, 2  $\mu\text{m}$ , Thermo Fisher Scientific, Waltham, USA) and as a trapping column, an Acclaim PepMap 100 C18  $\mu$ -precolumn (0.3 mm I.D. x 5 mm, 5  $\mu\text{m}$ , Thermo Fisher Scientific, Waltham, USA) was used. A linear gradient from 2% to 30% of eluent B was used to separate peptides. The oven temperature

was set to 55°C, the flow to 0.25  $\mu\text{L min}^{-1}$ . The gradient for the full-scan (Full-MS / ddMS<sup>2</sup>) measurement of in-gel-digested samples is shown in Figure 14.

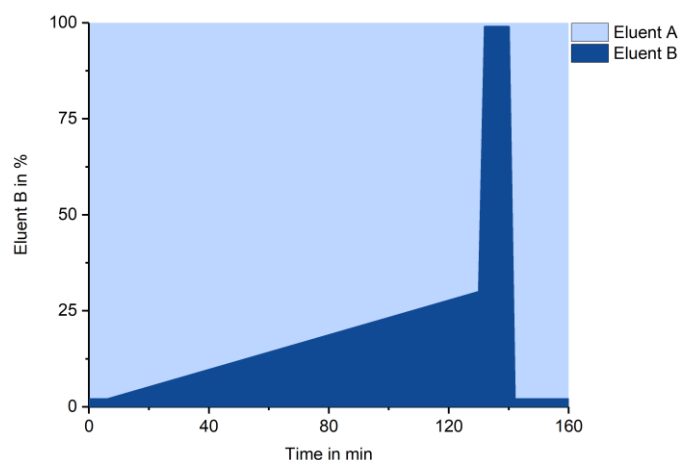


Figure 14. Liquid chromatography gradient for full-scan measurement of in-gel digested samples. Columns were equilibrated at 2% of eluent B. The separation of in-gel digested samples was performed by increasing eluent B from 2% to 30%. The total method duration was 162 min.

For this experiment, a full-scan (top 15 Full-MS / dd-MS<sup>2</sup>) data acquisition method was used. The resolution was set to 140 000 with an automatic gain control (AGC) target of  $3 \cdot 10^6$ , a maximum injection time (IT) of 40 milliseconds (ms), and the scan range was set to 200-2000 m/z. The dd-MS<sup>2</sup> resolution was set to 17 500 while the AGC target was set to  $1 \cdot 10^5$  and the maximum IT to 55 ms. The isolation window of dd-MS<sup>2</sup> was set to 4.0 m/z and the normalized collision energy (NCE) to 25. Additionally, unassigned, single charged, fivefold- up to eightfold-charged peptides were excluded. The dynamic exclusion time was 30.0 seconds.

Evaluation of results was performed with Proteome Discoverer 2.1 (Thermo Fisher Scientific, Waltham, USA) and Skyline 4.2.0.19072 (MACOSS Lab, Department of genome sciences, University of Washington, Seattle, USA). In order to identify the proteins and peptides, a search against the HumanRefUP201611 database using masquot and sequest was started via Proteome Discoverer. Trypsin was set as proteolysis enzyme, miss cleavage to one, and precursor mass tolerance to 10 ppm. In addition, a dynamic modification (oxidation of methionine) and a static modification (carbamidomethylation of cysteine) were specified. The confidence of the peptide identification was determined by the percolator validation node integrated into Proteome Discoverer. If the false detection rate of the identified peptides was above 1%, the results were discarded. This was determined by the q-value (q-value >0.01).

### 3.9.4 Comparison of Targeted Mass Spectrometry Methods for Better Suitability of Target Analyte Analysis

As described in 1.3.5, several measurement modes are available for the LC-MS device. To decide, whether targeted selected ion monitoring (tSIM) or parallel reaction monitoring (PRM) should be used for the method development and the analysis of pesticide-treated samples, test samples (prochloraz-treated HepaRG cells;  $20 \mu\text{mol L}^{-1}$ ) were measured with the existing CYP 17-plex assay in tSIM, as well as in PRM. The already developed and optimized LC gradient for the CYP 17-plex was used for the analysis. The separation was obtained by a two-step gradient starting at 4% to 10% and then continuing from 10% to 40% eluent B. The method duration was 18 minutes, and the flow rate was  $0.3 \mu\text{L min}^{-1}$  while the temperature was kept constant at  $40^\circ\text{C}$ . An Acclaim PepMap RSLC C18 ( $75 \mu\text{m I.D.} \times 150 \text{ mm}$ ,  $2 \mu\text{m}$ , Thermo Fisher Scientific, Waltham, USA) was used as the analytical column, and an Acclaim PepMap 100 C18  $\mu$ -precolumn ( $0.3 \text{ mm I.D.} \times 5 \text{ mm}$ ,  $5 \mu\text{m}$ , Thermo Fisher Scientific, Waltham, USA) was used as the trapping column. Figure 15 shows the chromatographic gradient of the CYP 17-plex.

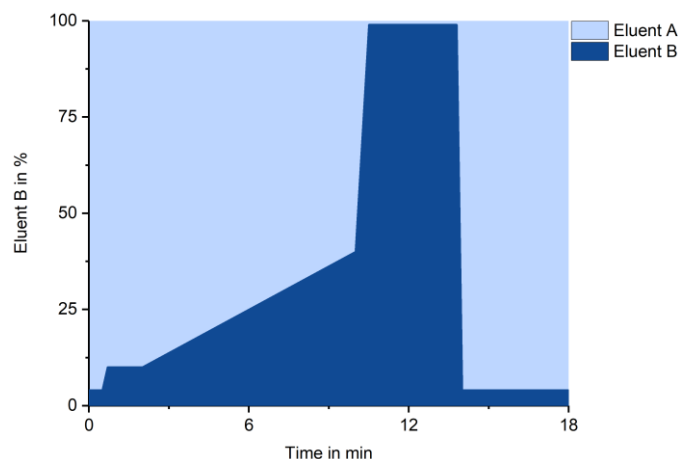


Figure 15. Liquid chromatography gradient of the CYP 17-plex. Columns were equilibrated at 4% of eluent B. The separation of the analytes was performed by a two-step gradient from 4% to 10% and then continuing from 10% to 40% of eluent B. The total method duration was 18 minutes.

The parameter for the analyte's detection in the Orbitrap with either tSIM / ddMS<sup>2</sup> or PRM is compared in Table 17. The NCE for the PRM measurement was optimized prior to this experiment for all analytes, according to 3.9.2. Since PRM is a method based on fragmentation, no ddMS<sup>2</sup> (data-dependent tandem mass spectrometry) parameters could be set. For the tSIM method, the ddMS<sup>2</sup> parameters were set as



follows: Resolution to 17 500, AGC target  $2 \cdot 10^5$ , maximum IT to 60 ms, isolation window to 2.0 m/z, and dynamic exclusion to 2.0 seconds.

Table 17. Comparison of PRM and tSIM parameters for the CYP 17-plex. Here, the parameters set for each data acquisition method are shown. NCE was optimized for each analyte in PRM mode. Data-dependent-MS<sup>2</sup> parameters are not applicable for PRM.

Parameter	PRM	tSIM / ddMS <sup>2</sup>
Resolution	35 000	35 000
AGC target	$2 \cdot 10^5$	$5 \cdot 10^6$
Maximum IT in ms	60	60
Loop Count	1	1
MSX count	2	2
Isolation window in m/z	1.5	2.0
NCE	various	30
ddMS <sup>2</sup>	na	set

na= not applicable

### 3.9.5 Testing the Antibody Functionality

In order to characterize the antibodies, their respective binding motif, and their ability to enrich target analytes from a complex matrix were tested. As a complex matrix, a mixture of three human cell lines (human embryonic kidney (HEK), human colon tumor (HCT), and hepatoma G2 (HepG2)) in the ratio of 1:1:1 was prepared (the cultivation of each cell line was performed by Dr. Bettina Keller; in the workgroup of Prof. Dr. Ulrich Rothbauer, University of Tübingen, Germany). For each TXP-tag, two rabbits were immunized with the respective antigen. For the determination of the epitope binding motif, three full-scan (Full-MS) runs (45 min) were performed for all antibodies (including both animals of each TXP-tag), and the results were evaluated using Proteome Discoverer 2.1 and the in-house developed TXP tool of Dr. Hannes Planatscher (Signatope GmbH, Reutlingen, Germany).

For the investigation of whether the antibody was able to enrich the target peptide sufficiently, immunoprecipitation of the human blend with spiked-in EN<sub>s</sub> peptides and the respective antibody was performed. The analysis was carried out in PRM mode.

### 3.9.6 Antibody-Protein Ratio Optimization

In this part, it was determined which minimum antibody-protein ratio was necessary to provide reliable and stable peptide signals. Several antibody-protein ratios were investigated for each analyte. Either 1  $\mu\text{g}$ , 2  $\mu\text{g}$ , or 5  $\mu\text{g}$  antibody were combined with 10  $\mu\text{g}$ , 20  $\mu\text{g}$ , or 40  $\mu\text{g}$  lysate. Immunoprecipitation was performed with these different combinations and subsequently measured with LC-MS. For the analysis, prochloraz-treated ( $10 \mu\text{mol L}^{-1}$ ) HepaRG cells were used. Each combination was examined in a single determination.

### 3.9.7 Examination of Proteolysis over Time

In order to investigate the ideal duration of tryptic proteolysis for each protein of interest, a time series experiment was performed. Prochloraz-treated ( $10 \mu\text{mol L}^{-1}$ ) HepaRG cells were proteolyzed for 2, 6, 16, 18, 24, 48, 72, or 96 hours with the tryptic proteolysis protocol (3.8.3). The digestions were performed in triplicates, followed by immunoprecipitation and LC-MS analysis. Not only the peptides of interest but also missed cleavage peptides (one miss cleavage on the N-terminal side) were analyzed. Therefore, the protein sequence was checked using the UniProt database<sup>90</sup>, and the mass (double and triple charge) of the peptide containing one miss cleavage site was included in the PRM method (data of miss cleavages not shown).

### 3.9.8 Conversion from Singleplex to Multiplex Assays

The availability of samples is often limited and therefore, it would be challenging to analyze each antibody and its peptide separately. For the compilation of multiplex assays, three criteria should be considered. First, the total antibody amount in an assay should not exceed 7  $\mu\text{g}$ . For each microgram antibody, it was necessary to use 5  $\mu\text{L}$  of the magnetic bead solution. The amount of microspheres per assay is limited by the transfer efficiency of the magnetic particle processor. Second, the minimum amount of lysate required to obtain reliable and stable results should be in line with the analytes to be compiled. Third, the duration of proteolysis should be the same for each analyte within a multiplex.

### 3.9.9 Optimization of Chromatographic Separation

After compiling multiplex assays, the chromatographic gradient was optimized for each assay. Standard peptides were diluted, and several gradients were tested in replicate measurements (n=3). Since only EN<sub>s</sub> peptides were used, no proteolysis and immunoprecipitation were performed prior to the LC-MS analysis. After measuring these different gradients, it was decided which gradient should be used for the investigation of further method development parameters. Not only the optimal separation but also the intensity of analytes for each gradient and the repeatability were considered. The gradients described in Table 18 were tested.

Table 18. Tested gradients to optimize the chromatographic separation. Five different gradients were tested for each multiplex. The respective percentage of eluent B is shown. The column was equilibrated at 4% and washed at 99% of eluent B.

Time in min	Tested gradients with eluent B in %				
	Standard	10-45	10-40	10-30	10-20
0	4	4	4	4	4
0.25	4	10	10	10	10
5.75	45	45	40	30	20
6	99	99	99	99	99
8	99	99	99	99	99
8.25	4	4	4	4	4
10	4	4	4	4	4

### 3.9.10 Dynamic Ranges

For the determination of the dynamic range, dilution series of EN<sub>s</sub> peptides in their respective IS peptide solution was performed while IS was kept constant. The linearity was investigated in the range from 0 to 1000 fmol EN<sub>s</sub> (for some high abundant analytes, the investigation of linearity was upscaled to 3000 fmol EN<sub>s</sub>). The dilution was done sequentially in 1:3 dilution steps. The dilution series was performed three times to cover the accuracy and precision for each dilution step. After the LC-MS measurement, linearity plots were prepared, and the limit of detection (LOD) for each analyte was calculated using the following, adapted formula, which was described and compared with other methods by Mani et al.<sup>91</sup>

$$LOD = \mu_B + z_{(1-\alpha)} \frac{(\sigma_B + \sigma_s)}{\sqrt{n}} \quad (91)$$

$\mu_B$ = estimated mean value of blank samples

$\sigma_B$ = standard deviation of blank samples

$\sigma_s$ = standard deviation of low concentration samples (where S/N > 3; own criterion)

$\sqrt{n}$ = square root of the number of replicates (n=3)

$z_{(1-\alpha)}$ = z-value with  $\alpha$  of 0.05; inserted value = 1.645

The linear equations obtained by evaluating the data with Origin 2017G (OriginLab, Northampton, USA) were used to calculate the accuracy of each analyte. The measured values should be within 80-120%, and the coefficient of variation (C.V.) within one replicate measurement  $\leq 20\%$ . The lower limit of quantification (LLOQ) was defined as the least concentration, where both described criteria were met.

### 3.9.11 Identification of Recovery Efficiency

The recovery experiment was performed using spike-in experiments. A complex matrix that preferably did not contain the peptide of interest was used. The mouse cell line NIH3T3 was selected. After cell harvesting and lysis, the lysates were digested and used as a matrix for immunoprecipitation. In addition, recovery experiments should be performed at three different concentrations. Hence, three different amounts of non-labeled standard synthetic peptides (15 fmol, 250 fmol, and 500 fmol) were spiked into the matrix, while the isotopically labeled peptide amount was kept constant. Each experiment was performed three times. Besides the spiked samples, also unspiked samples (blanks) were measured. The ratios of  $EN_s/IS$  were corrected with the linear equations obtained during the linearity experiment (3.9.10 Dynamic Ranges), and then the calculation of the recovery was performed using the following formula:

$$R'(\%) = \frac{(\bar{x}' - \bar{x})}{x_{spike}} \cdot 100 \quad (92)$$

$R'(\%)$ = relative spike recovery

$\bar{x}'$ = mean value of the spiked sample

$\bar{x}$ = mean value of the unspiked sample

$x_{spike}$ = the added amount of non-labeled synthetic peptide ( $EN_s$ )

### 3.9.12 Investigation of Repeatability

To perform the intra- and interday repeatability, three different samples were used: Non-treated HepaRG cells, prochloraz-treated ( $10 \mu\text{mol L}^{-1}$ ) HepaRG cells, and a cryopreserved primary human hepatocyte (PHH; donor 1) sample. For the determination of intraday repeatability, every sample type was digested five times each day. This was performed on three different days to determine the interday repeatability. For the evaluation, it was decided that the coefficient of variation should be  $\leq 20\%$  for intraday ( $n=5$ ) and interday ( $n=3$ ).



## 4 Results

### 4.1 Assay Development for the Quantification of Toxicologically Relevant Proteins in HepaRG Cells

#### 4.1.1 Peptide Selection for the Detection and Quantification of Target Analytes

As described in 3.9.1, database search was performed for 36 target proteins. For 16 analytes, mass spectrometric assays have already been developed previously<sup>86</sup>. It was checked whether all set criteria, like proteotypicity, absence of natural variants/modifications within the sequence, or low hydrophobicity factors were met. If possible, two potential peptides per analyte were chosen. For analytes from which only peptides that did not fulfill all criteria were found, it was decided that peptides should still be tested despite unfavorable properties such as cysteine occurrence or a high hydrophobicity factor. For example, only two proteotypic peptides with a hydrophobicity factor greater than 2.8 were found for glucose-6-phosphatase (G6PC). Despite that, both peptides were tested. The results for the database search are shown in Table 31 in the appendix (9 Supplementary Data). For those 36 proteins, standard non-labeled synthetic peptides (EN<sub>s</sub>) were synthesized, and the detection compatibility with mass spectrometry investigated.

#### 4.1.2 Detection Compatibility of Selected Peptides with Mass Spectrometry

With dilutions of each EN<sub>s</sub> peptide, ideal charge state and collision energy were determined. The charge state that led to higher signal intensities in a full-scan (Full-MS) experiment was chosen, and after that, the collision energy with these particular charge states was investigated by use of parallel reaction monitoring (PRM) mode. Several collision energies were tested. Therefore, the normalized collision energy (NCE) was set to either 15, 20, 25, or 30. Due to the different analyte charge states, it was possible that not only single but also double or triple charged fragment ions could arise. Therefore, they were also selected in Skyline 4.2.0.19072 (MACOSS Lab, Department of genome sciences, University of Washington, Seattle, USA) and evaluated. Depending on where the peptide was fragmented, different daughter ions were formed. Due to the use of isotopically labeled standard peptides at the

## Results

C-terminal arginine or lysine, it was decided that only y-ions should be evaluated to distinguish between the analyte and the standard. The most intense y-ion was considered as the quantifier. For the quantification, only the area of the quantifier ion was used. Figure 16 shows the collision energy optimization of cytochrome P450 1A1 (CYP1A1) and arginase-1 (ARG1 with C-terminus: YILK) exemplarily. Remaining data are shown in 9 Supplementary Data, Figure 45. For CYP1A1, a steady decrease in the peak area by increasing NCE could be observed. The peak area of ARG1 increased from 15 up to the highest area at NCE 25. By use of 30 NCE, the peak area decreased drastically.

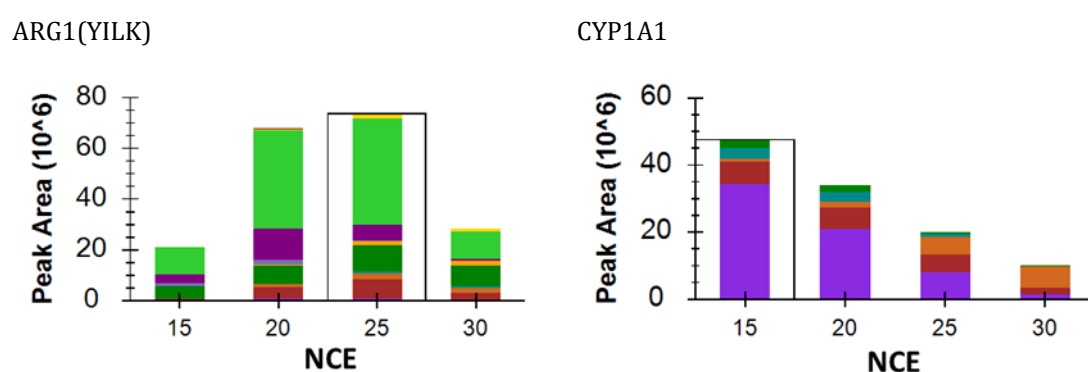


Figure 16. Normalized collision energy comparison. Results for arginase-1 (ARG1 with C-terminus: YILK) and cytochrome P450 1A1 (CYP1A1) are shown. The framed collision energy was selected, i.e., NCE of 25 for ARG1(YILK) and NCE 15 for CYP1A1.

In the case of proteins for which two EN<sub>s</sub> peptides were synthesized initially, one was selected based on the results with which the method development was further carried out. Table 32 (9 Supplementary Data) shows the results for all these analytes that have passed the compatibility test for mass spectrometric detection, as well as the CYP 17-plex, as this assay has only been established in targeted selected ion monitoring (tSIM) so far<sup>86</sup>. The table shows the analyte's particular peptide sequence, the determined precursor with charge state, the chosen quantifier ion with its mass, and the optimized NCE. For each analyte, at least one peptide was detected by mass spectrometry, so the method development was continued with each protein of interest (37 peptides representing 36 proteins of interest for which new assays should be developed).



### 4.1.3 Can Analytes be Detected in HepaRG Cells Directly after In-Gel Digestion and Full-Scan Mass Spectrometry Analysis?

Three negative controls (dimethyl sulfoxide (DMSO)-treated) and three prochloraz-treated ( $10 \mu\text{mol L}^{-1}$ ) HepaRG cell samples were prepared as described in 3.9.3. After proteolysis, the sample concentration was determined with the Nanodrop 2000c spectrometer (Thermo Fisher Scientific, Waltham, USA), diluted to the same concentration of  $48 \text{ ng } \mu\text{L}^{-1}$  and then measured by liquid chromatography-mass spectrometry (LC-MS). Full-scan analysis (Full-MS / ddMS<sup>2</sup>) was used as data acquisition method, whereby the separation of peptides was performed with a 130-minute gradient. Figure 17 shows the total ion current chromatogram (TIC) of one of the prochloraz-treated samples (PT3).

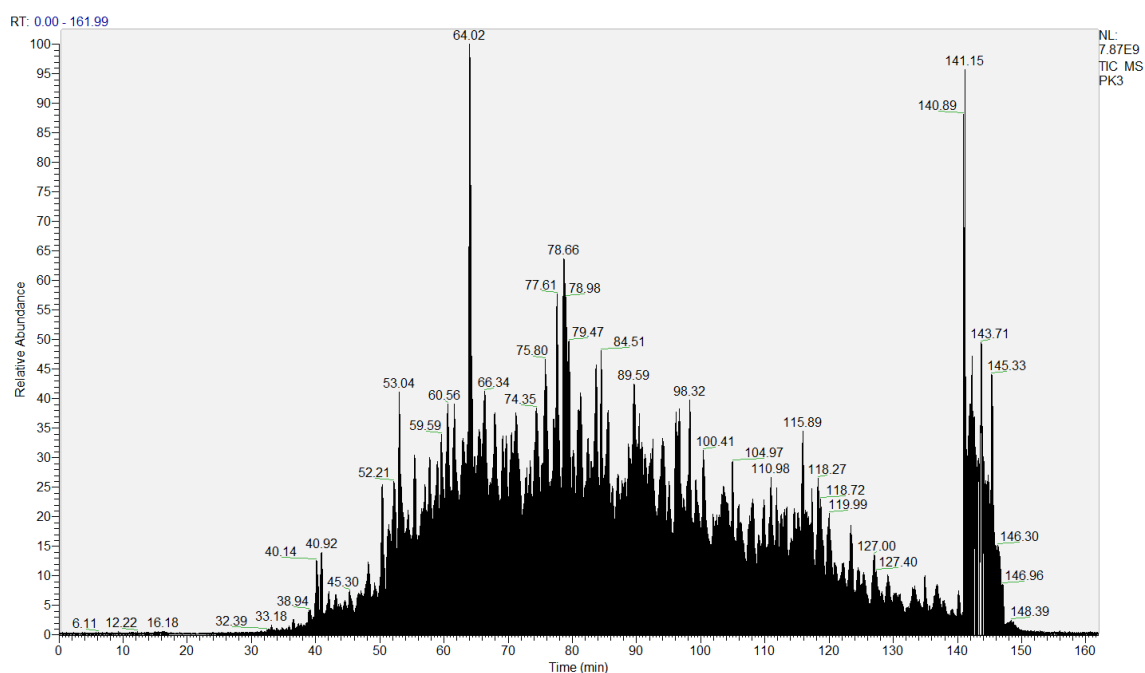


Figure 17. Total ion current chromatogram of a prochloraz-treated HepaRG cell sample. Shown is the third replicate of prochloraz-treated HepaRG cells (PT3). In this sample, 2907 proteins with 13125 peptide groups were identified by Proteome Discoverer. The analytes were separated by a 130-minute gradient.

At least 2570 proteins have been identified in all samples. The highest protein identification rate was observed in the third replicate of prochloraz-treated samples (PT3). Here, 2907 proteins and 13125 peptide groups were identified with Proteome Discoverer 2.1. A summary of identified proteins and peptide groups is shown in Table 19.

## Results

Table 19. Number of identified proteins and peptide groups after in-gel digestion.

Sample	Identified Proteins	Identified Peptide groups
SC1	2739	12074
SC2	2570	12175
SC3	2647	12665
PT1	2674	11705
PT2	2832	11952
PT3	2907	13125

After data processing with Proteome Discoverer 2.1 (settings and search criteria described in 3.9.3), the list of identified proteins and peptides was screened for the analytes of interest. The first step was to check whether the protein to be investigated was present. If the protein was found, it was further investigated whether the peptide, selected based on the database search and mass spectrometric detection compatibility (4.1.2), was observed, too. Table 33 in the appendix (9 Supplementary Data) shows the results for the screening. If both a protein and its desired peptide were found, the corresponding retention time was included in the table. Not all peptides were identified in all six samples. As an example, the peptide DVDPGEHYILK of ARG1 was identified in each sample in contrast to TIGIIGAPFSK of the same protein, which was only found in PT3. For some analytes such as glyceraldehyde-3-phosphate dehydrogenase (GAPDH), DNA-dependent protein kinase catalytic subunit (PRKDC) or UDP-glucuronosyltransferase 1-1 (UGT1A1), the protein, but not the peptide of interest was found. The analysis showed that 15/36 proteins were identified after in-gel digestion, while only 8/37 (for ARG1 two peptides were investigated) peptides of interest were found. In case of 16 proteins comprised in the CYP 17-plex assay, only 5 of 17 peptides (two peptides for CYP3A5) were identified by full-scan MS analysis.

### 4.1.4 Selection of Mass Spectrometry Detection Mode for Most Sensitive Detection of Target Analytes

Prochloraz-treated ( $20 \mu\text{mol L}^{-1}$ ) HepaRG cells were measured in targeted selected ion monitoring (tSIM), as well as in parallel reaction monitoring (PRM) mode. In Figure 18, the results for CYP2B6 and CYP2C9 in both measurement modes are

shown exemplarily. (A) and (B) show CYP2B6, measured in tSIM and PRM, respectively. (C) and (D) show the results for CYP2C9. The upper chromatogram in each case displays the signal of the endogenous peptide (EN); the lower chromatogram displays the internal isotopically labeled standard peptide (IS).

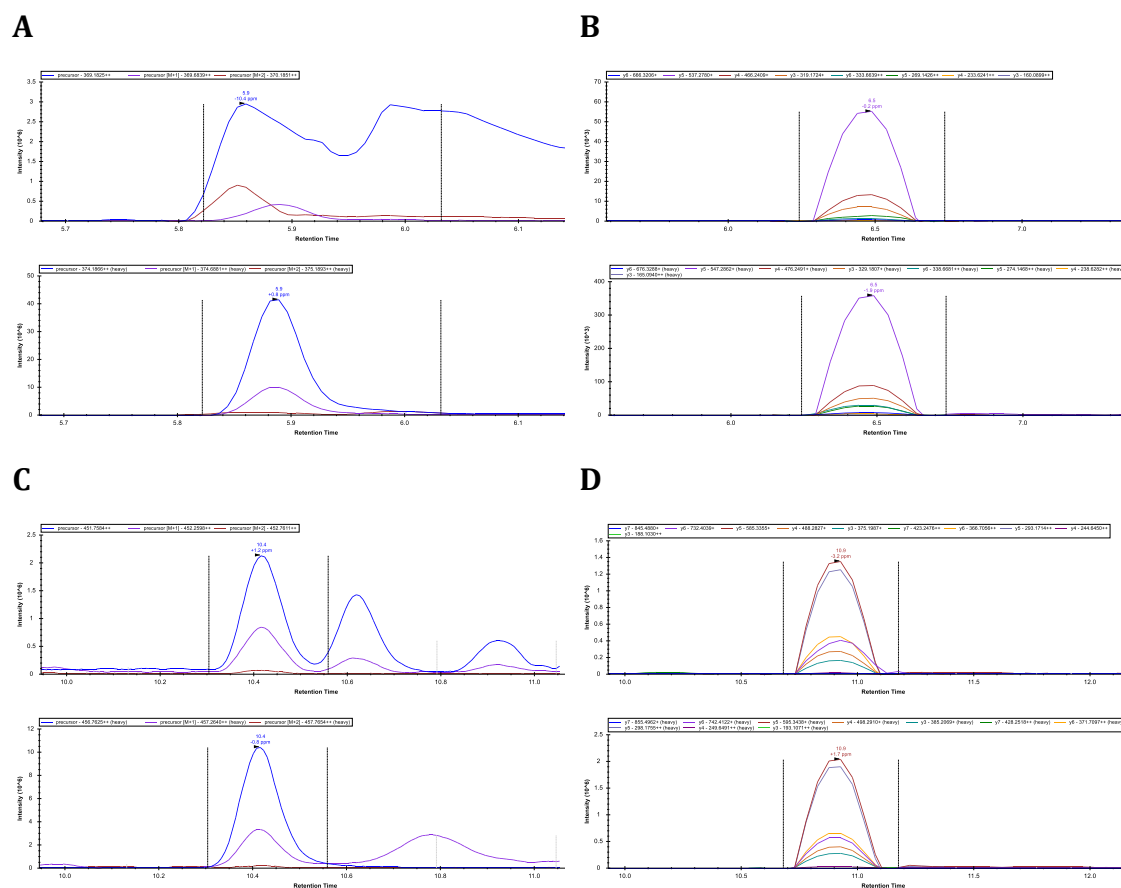


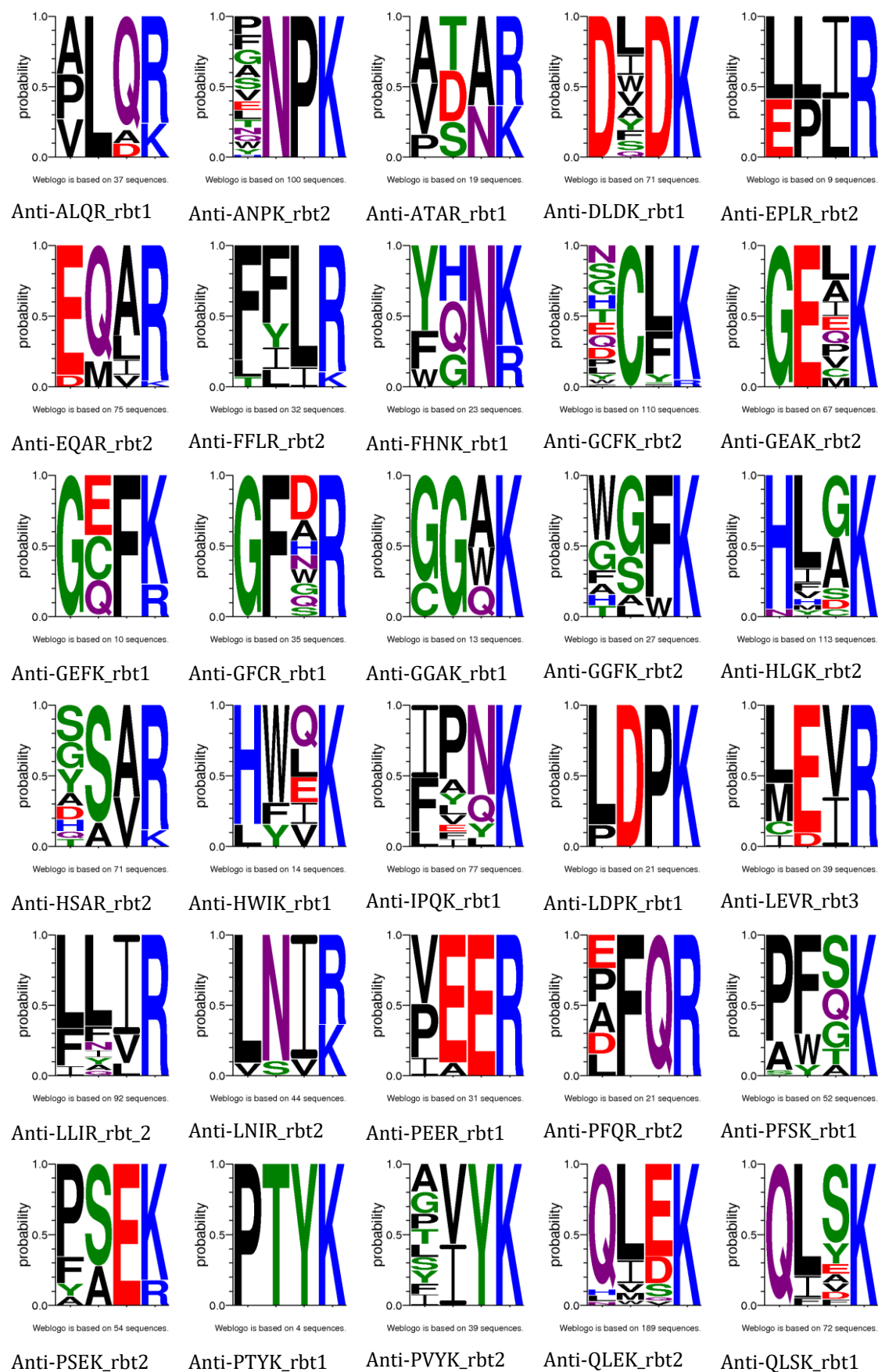
Figure 18. PRM and tSIM comparison for CYP2B6 and CYP2C9. (A) and (B) represent CYP2B6 in targeted selected ion monitoring (tSIM) and parallel reaction monitoring (PRM), respectively, and (C), (D) represent CYP2C9. In tSIM, the three most prominent precursor isotopes are shown, in PRM all detected transitions of the precursor ion. The upper chromatogram shows the endogenous peptide signal, the lower chromatogram the signal of the corresponding internal isotopically labeled standard peptide.

The tSIM results show the first (blue), second (violet), and third (red) isotopes of the precursor. In the PRM chromatograms, all detected transitions of the precursor mass are shown. For the results measured in tSIM, it can be clearly seen that interferences were present that made the evaluation for the CYP2B6 peptide in tSIM (A) impossible. The endogenous signal was influenced by other compounds with the same mass as the analyte under investigation. In (C; CYP2C9), several signals were obtained in the endogenous chromatogram. Without the use of the internal standard peptide, the assignment of the correct signal would not be possible. In addition, it can also be seen here that interferences were present in the IS chromatogram at MS1

level. The additional fragmentation in PRM (D) after the filtering of the precursor ion in the first quadrupole led to a clear chromatogram in which no interference was present. Based on these measurements, it was decided to use the PRM mode for further method development steps.

### 4.1.5 Determination of Antibody Epitope Binding Motifs and Functionality in Complex Matrix

A mixture of human embryonic kidney (HEK), human colon tumor (HCT), and hepatoma G2 (HepG2) cells in a ratio of 1:1:1 was used to test the antibody's functionality. In this experiment, the binding motif of the antibodies (AB) on the one hand, and on the other hand, the ability to enrich the target peptide from a complex matrix was investigated. Enzymatic proteolysis was performed for 16 hours, followed by immunoprecipitation (IP). In this case, no synthetic non-labeled standard (EN<sub>s</sub>) or isotopically labeled standard (IS) peptides were spiked into the proteolyzed samples before the IP. A 45-minute full-scan (Full-MS) mass spectrometry measurement was then performed to examine the epitope binding motif (n=3). The evaluation was done using Proteome Discoverer 2.1, and the in-house developed triple X proteomics (TXP)-tool (Dr. Hannes Planatscher, Signatope GmbH, Reutlingen, Germany). Both animals of each TXP-tag were analyzed. Only the results of the antibodies used for further method development are shown in Figure 19. Besides, epitope motifs were only generated for newly generated antibodies. For the antibodies of the CYP 17-plex, epitope motifs have already been generated in an earlier project<sup>86</sup>. Figure 19 shows that at least one epitope binding motif from two polyclonal antibodies could be generated for each analyte. For the tryptic fragment derived from histidine-rich glycoprotein (HRG), the TXP tag sequence is GFC(CAM)R. One antibody was capable of enriching peptides comprising amino acids matching the antigen at positions one, two, and four, but no cysteine was visible at position three in the graph. The second antibody enriched only peptides not related to the initially used antigen GFC(CAM)R. Hence, only the first antibody was used for further method development because the third position has a rather unspecific binding site, and it is highly probable that the analyte of interest is enriched.



## Results

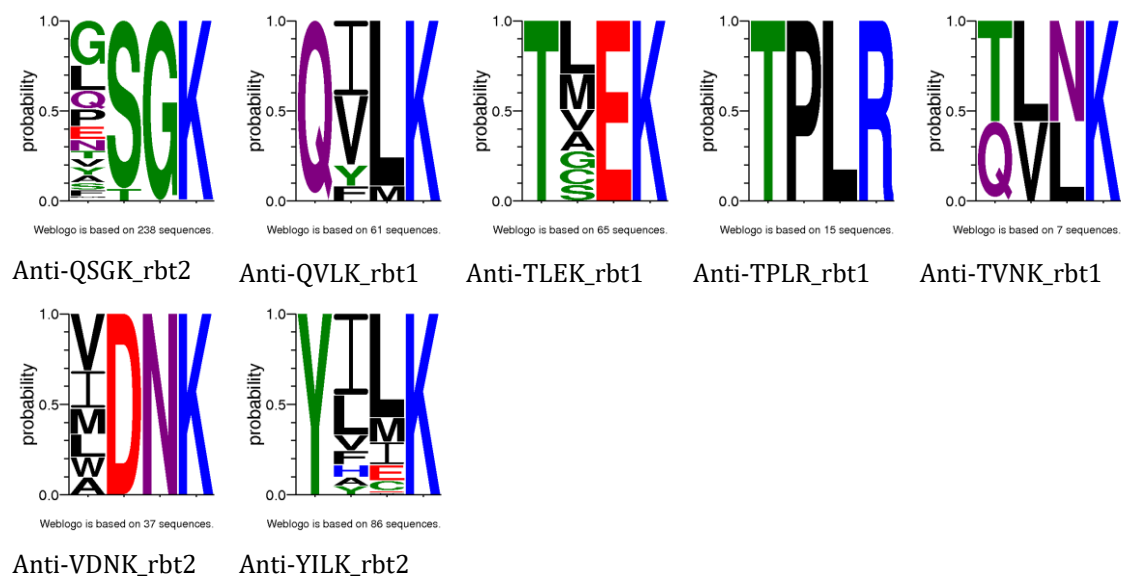


Figure 19. Epitope binding motifs of TXP antibodies. The in-house developed triple X proteomics (TXP) tool was used to generate epitope binding motifs. Only graphs of antibodies used for further method development are shown – one out of two. Furthermore, graphs were only generated for new analytes. For the CYP 17-plex assay, epitope binding motifs were already generated in a previous project <sup>86</sup>.

The second part was to investigate the antibody's ability to enrich the target peptides from a complex matrix. Here, the human blend sample was also used as the matrix. Target EN<sub>s</sub> peptides were spiked into the proteolyzed human blend sample, and the IP was performed. The results are shown in Table 34 in the appendix (9 Supplementary Data). The measurement was performed with a 10-minute PRM method (n=3). Antibodies that did not enrich the target peptide were not used further. The analysis was not performed for the CYP 17-plex. For all analytes, at least one antibody enriched the target from the complex matrix. Method development was continued for all 36 proteins.

### 4.1.6 Least Optimal Antibody-Protein Extract Ratio for Reliable Target Analysis

In chapter 4.1.5, it was described how suitable antibodies were for enriching the peptides of interest from a complex matrix. With these antibodies, a further analysis was performed to determine the least antibody amount in combination with the ideal sample protein amount. Different antibody-protein ratios were investigated, with either 1, 2, or 5 micrograms of each antibody combined with either 10, 20, or 40 micrograms protein extract. The analysis was performed using protein extracts from prochloraz-treated (10  $\mu\text{mol } \mu\text{L}^{-1}$ ) HepaRG cells. For all analytes, 50 fmol IS

peptide was used as an internal control. For those analytes, where 50 fmol IS peptide led to low signal intensities, the experiment was repeated, and either 100 fmol or 200 fmol of IS peptide was added. The results for the minimal antibody-protein ratio, leading to stable and reliable results, are shown in Table 20. For analytes, where both antibodies enriched the peptide of interest out of the complex matrix, both antibodies were tested. Only the antibody, which led to better results, in terms of fragmentation pattern and peak shape, is shown. In this experiment, 20 peptides had to be excluded from further method development, since no signals for endogenous peptide or even no internal standard signal were obtained. This means that 17/37 peptides were used for further analysis. The analysis was not performed for the CYP 17-plex.

Table 20. Least required antibody-protein ratio. Here, the analyte, its peptide sequence, the used antibody (AB), as well as the determined AB amount, lysate amount, and amount of substance of each internal isotopically labeled (IS) peptide are shown. Only the antibodies showed in this table will be used for further method development. The analysis was not performed for the CYP 17-plex.

Analyte	Peptide Sequence	Antibody #	AB amount in µg	Lysate amount in µg	n <sub>(IS)</sub> in fmol
ADH1B	GAVYGGFK	317_2	2	20	200
ALDH3A1	IQQLEALQR	318_1	2	20	100
ARG1	TIGIIGAPFSK	169_1	2	20	50
ARG1	DVDPGEHYILK	313_2	1	10	50
CYP7A1	LSSASLNIR	293_2	2	40	50
FASN	TGTVSLEVR	272_3	2	10	100
HSD11B2	VSHIQPGCFK	308_2	1	10	50
LMNA	LEAALGEAK	295_2	2	10	50
NQO1	FGLSVGHHLGK	297_2	1	10	50
PRKDC	LGLPGDEVNDK	311_2	1	20	50
S100P	ELPGFLQSGK	312_2	2	20	50
SULT1B1	TSGIEQLEK	300_2	2	20	50
TNFRSF12A	GSSWSADLDK	303_1	2	40	50
UGT1A1	TYPVPFQR	322_2	2	20	100
UGT1A3	YLSIPTVFFLR	323_2	2	20	50
UGT2B7	ANVIASALAIQPK	302_1	5	20	100
UGT2B15	SVINDPVYK	325_2	2	20	100

#### 4.1.7 Analysis of Optimal Proteolysis Time

Since the proteolysis time for the different analytes may vary, and multiplex assays should be generated, it was essential to investigate the respective optimal digestion times<sup>93</sup>. For this investigation, protein extracts from prochloraz-treated ( $10 \mu\text{mol L}^{-1}$ ) HepaRG cells were proteolyzed using trypsin for 2, 6, 16, 18, 24, 48, 72, or 96 hours ( $n=3$ ). After the analysis, mean values were calculated. To compare all analytes, the mean values for each analyte were normalized to the respective peak value. Figure 20 gives an overview of all analytes. It was observed that the peptide release for ARG1(PFSK), UGT1A1, and UGT1A3 differed considerably compared to all other analytes. In addition, no endogenous signals were obtained for CYP7A1. The analysis was not performed for the CYP 17-plex since this analysis was already conducted by Weiss et al.<sup>86</sup>

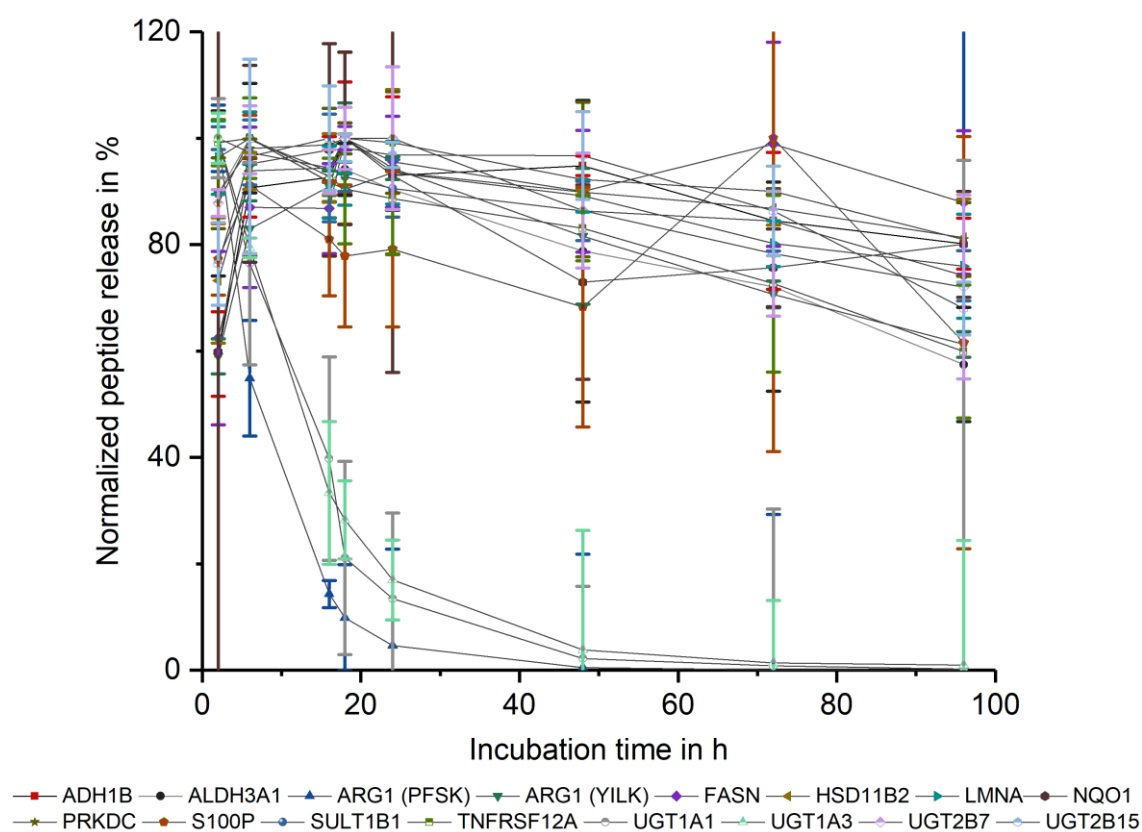


Figure 20. Normalized target peptide release by enzymatic fragmentation from HepaRG protein extracts over time. The normalized peptide release in percent (%) was plotted against the digestion time in hours (h). Peptide release for ARG1(PFSK), UGT1A1, and UGT1A3 differed significantly compared to the other analytes. No endogenous signals were obtained for CYP7A1. The analysis was not performed for the CYP 17-plex. Proteolysis was performed three times for each timepoint in prochloraz-treated ( $10 \mu\text{mol L}^{-1}$ ) HepaRG cells.



Since no endogenous signals were obtained for CYP7A1 during the determination of the ideal digestion time, it was decided to test another sample as a matrix. For this purpose, a mixture of DMSO-treated HepaRG cells and cyclosporin A-treated HepaRG cells was prepared and processed according to the enzymatic proteolysis protocol and the immunoprecipitation workflow (3.8.3).

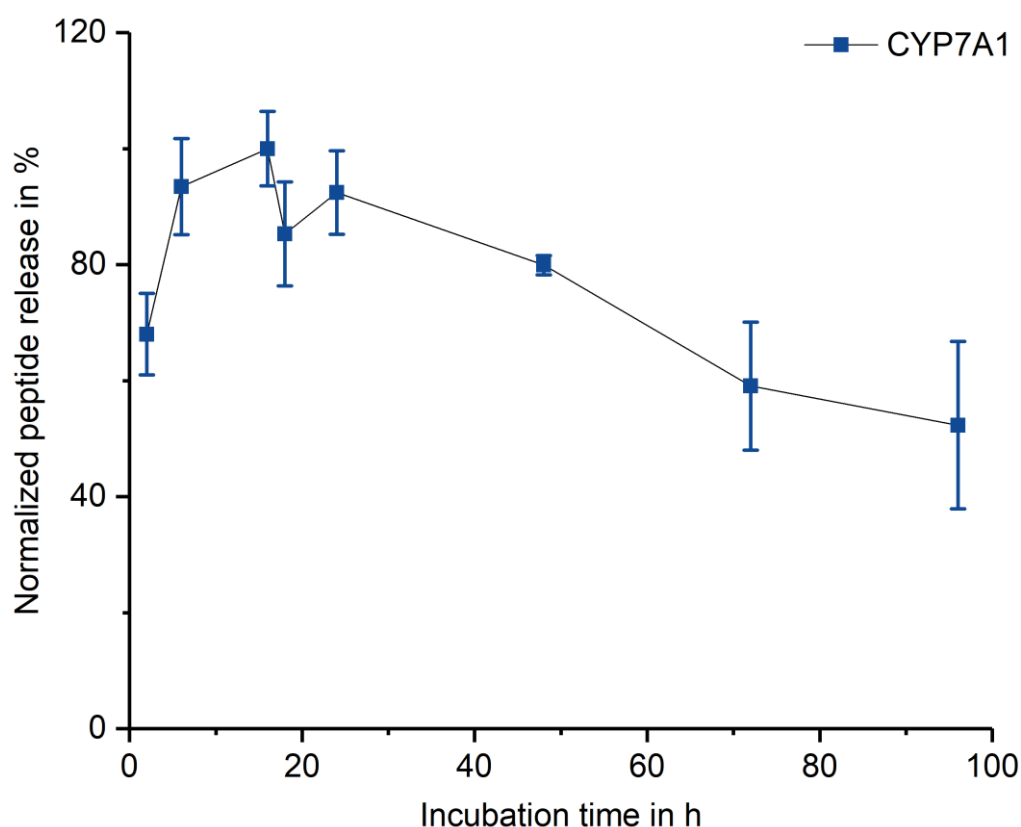


Figure 21. Normalized peptide release of CYP7A1 by enzymatic fragmentation from HepaRG protein extracts over time. The normalized peptide release in percent (%) was plotted against the digestion duration in hours (h). Proteolysis was performed three times in a mixture of DMSO-treated HepaRG cells and cyclosporin A-treated HepaRG cells.

In addition to Figure 20 and Figure 21, additional evaluation and visualization were carried out. Results are shown in Figure 22. In (A), mean values were calculated for each time point comprising all analytes (except ARG1(PFSK), CYP7A1, UGT1A1, and UGT1A3) to obtain a more unobstructed view. The same calculation was performed for ARG1(PFSK), UGT1A1, and UGT1A3, shown in (B).

## Results

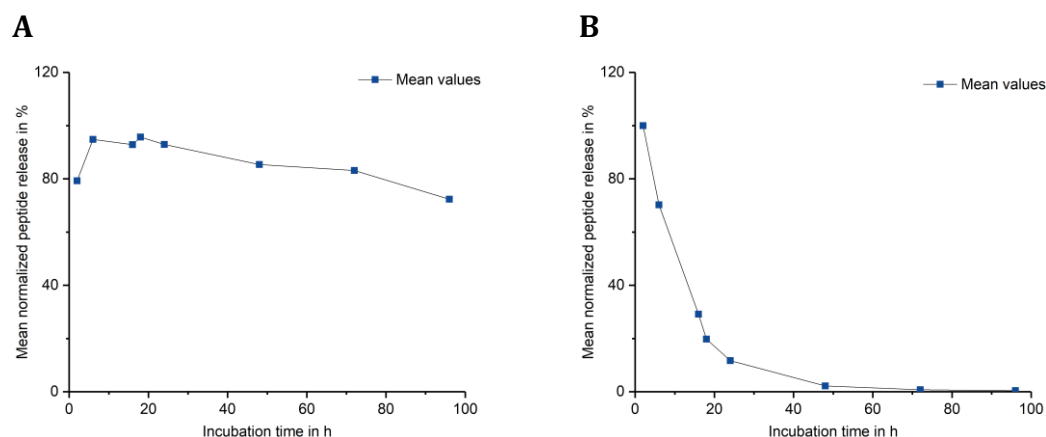


Figure 22. Mean normalized peptide release by enzymatic fragmentation from HepaRG protein extracts over time. In (A), the mean normalized peptide release in percent (%) over time in hours (h) is shown. For the calculation, all analytes except ARG1(PFSK), CYP7A1, UGT1A1, and UGT1A3 were used. (B) shows the mean normalized peptide release for ARG1(PFSK), UGT1A1, and UGT1A3.

Figure 20 shows that there is not one optimal incubation time for all analytes. However, Figure 22 (A) indicates that the best compromise is between 6 and 24 hours except for ARG1(PFSK), UGT1A1, and UGT1A3. The digestion time for the CYP 17-plex (16 h) was determined in an earlier project<sup>86</sup>, and thus, the digestion time was also set to 16 hours for all analytes (A) and to two hours for ARG1(PFSK), UGT1A1, and UGT1A3 (B). During this investigation of the optimal proteolysis time, no peptide was excluded from further method development (17 peptides representing 16 proteins were further used).

### 4.1.8 Compiling of Multiplex Assay Panels

Multiplex assays were compiled on the basis of the results obtained in sections 4.1.6 and 4.1.7. The minimum amount of proteolyzed sample required, the antibody amount required, and the optimal digestion time were taken into account. It was also considered that the total antibody amount within a multiplex should not exceed 7  $\mu$ g due to limitations with regard to magnetic microsphere transfer efficiency during the automated immunoprecipitation. As shown in Figure 22 (B), the digestion of ARG1(PFSK), UGT1A1, and UGT1A3 followed different kinetics. Therefore, these three analytes were combined into one multiplex. A total of six multiplex assays were compiled (Table 21). Digestion for multiplex 2-5 was set to 16 hours, for multiplex 1 to two hours. The lysate amount of all multiplexes except multiplex 5 was set to 20  $\mu$ g. Multiplex 5 required 40  $\mu$ g lysate.

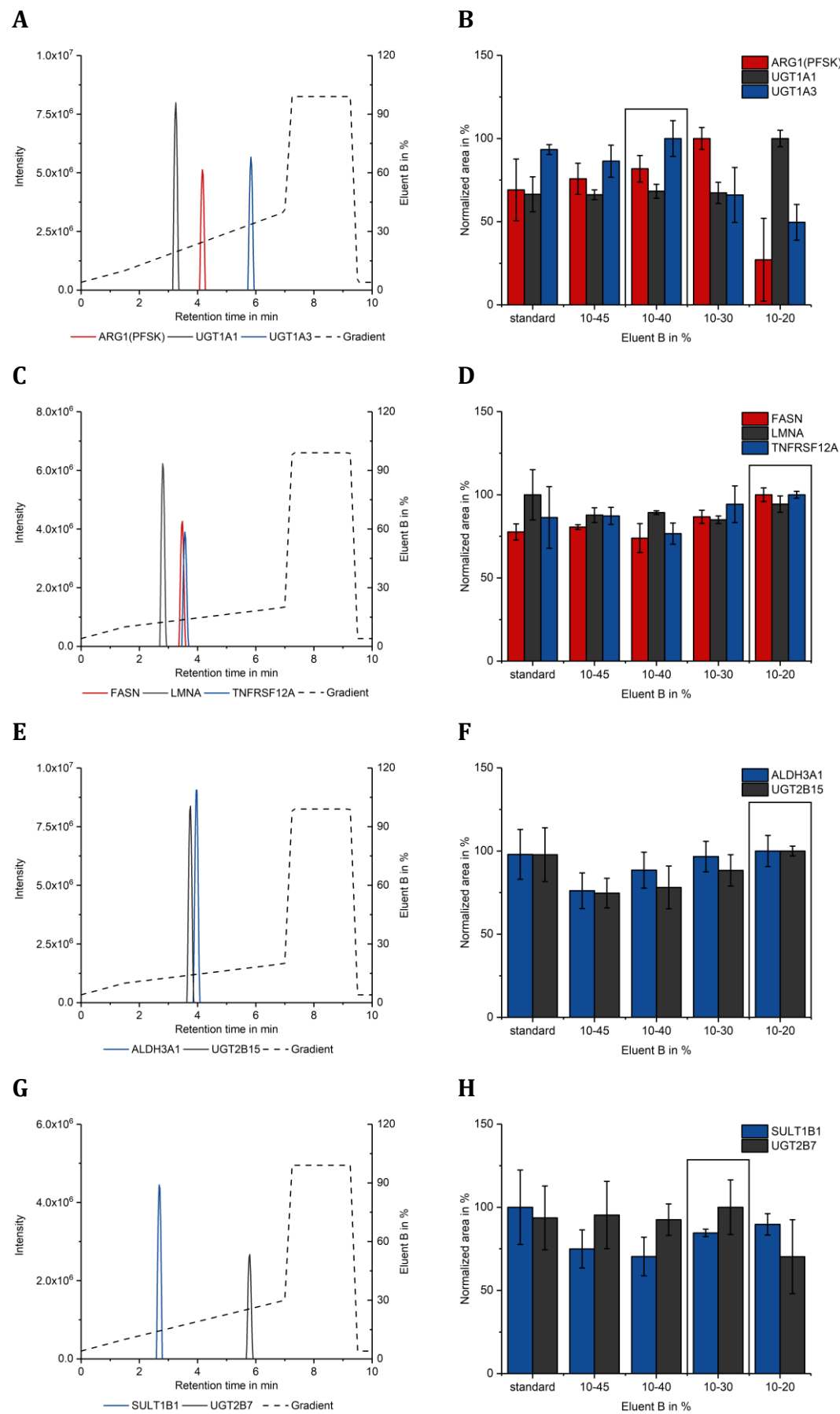
Table 21. Multiplex assays for proteins of interest. Six multiplex assays were generated. These are shown here with the respective total antibody (AB) amount in microgram ( $\mu\text{g}$ ), the minimal lysate amount needed ( $\mu\text{g}$ ), as well as the digestion duration.

Multiplex #	Analyte	Total AB amount in $\mu\text{g}$	Lysate amount in $\mu\text{g}$	Digestion duration in h
MpCombi1	ARG1(PFSK)	6	20	2
	UGT1A1			
	UGT1A3			
MpCombi2	FASN	6	20	16
	LMNA			
	TNFRSF12A			
MpCombi3	ALDH3A1	4	20	16
	UGT2B15			
MpCombi4	SULT1B1	7	20	16
	UGT2B7			
MpCombi5	ARG1(YILK)	5	40	16
	CYP7A1			
	S100P			
MpCombi6	ADH1B	5	20	16
	HSD11B2			
	NQO1			
	PRKDC			

#### 4.1.9 Effect of Chromatographic Separation on Signal Intensity and Repeatability

In Figure 23, the optimized chromatographic gradient, as well as the area comparison amongst the different gradients, are shown. The measurement was repeated three times for each gradient. The black boxes in (B), (D), (F), (H), (J), (L) indicate the gradient that was chosen for each multiplex, and these specific gradients are depicted in (A), (C), (E), (G), (I), and (K).

Results



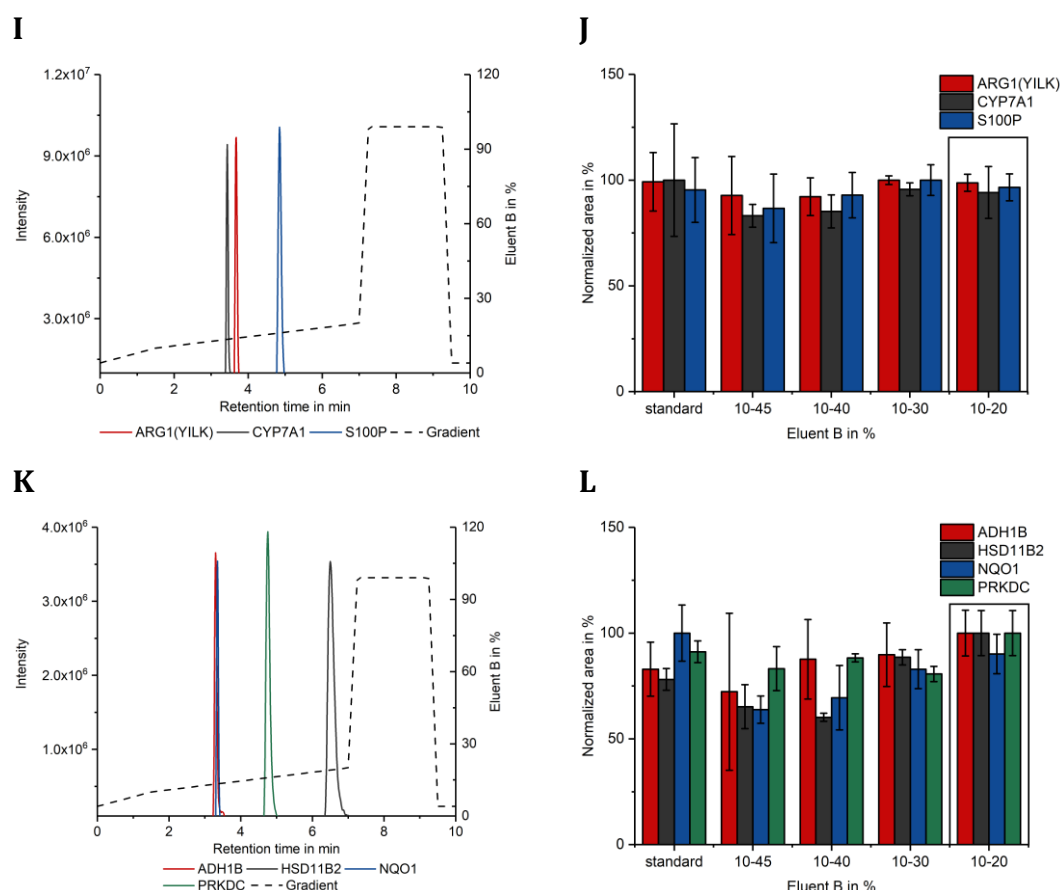


Figure 23. Chromatographic separation and area comparison of the different gradients. (A) shows the gradient of multiplex 1; (B) the area comparison of multiplex 1; (C) and (D) show multiplex 2; (E) and (F) multiplex 3; (G) and (H) multiplex 4; (I) and (J) multiplex 5; (K) and (L) multiplex 6. The black boxes in (B), (D), (F), (H), (J), and (L) indicate the selection for the individual multiplex. The chromatogram with the selected gradient is shown in (A), (C), (E), (G), (I), and (K).

#### 4.1.10 Determination of Assay Linearity and Accuracy to Discover Dynamic Ranges

The determination of linearity and accuracy was performed, as described in 3.9.10. As mentioned before, the dilution was performed sequentially in 1:3 dilution steps in phosphate-buffered saline (PBS) with CHAPS (3-[(3-Cholamidopropyl) dimethylammonio] -1-propanesulfonate), except values above 1000 fmol ENs. There, an additional dilution step of 2000 fmol ENs was integrated. The limit of detection (LOD) was calculated using the formula described by Mani et al.<sup>91</sup> Experiments were performed for all multiplex assays in PRM mode (MpCombi1-6, as well as the CYP 17-plex assay). In order to generate the linearity graphs, the ENs/IS area ratios were plotted against the theoretically expected ratios. Linear regression equations were calculated. Only data points, where also the range of the standard deviation was above the detection limit were taken into account. Using the obtained slope and

## Results

intercept from the determined linear equations, the respective accuracy was calculated, and accuracy plots were generated. Figure 24 shows the linearity plot for CYP1A1 as an example. The dashed horizontal line indicates the LOD. The graph shows that the analyte CYP1A1 was linear over a concentration range of five orders of magnitude. The coefficient of determination ( $R^2$ ) was 0.99935, and the LOD was 0.015 fmol. Graphs for all other analytes can be found in Figure 46 (9 Supplementary Data).

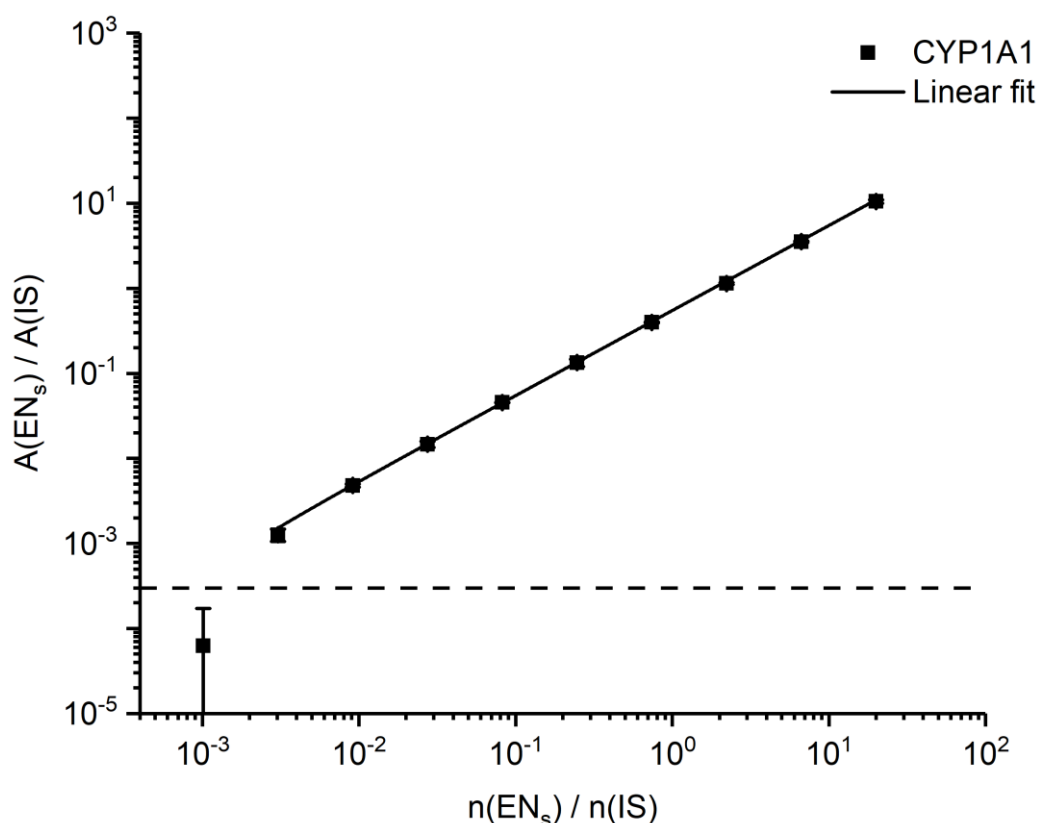


Figure 24. Linearity of CYP1A1 in PBSC. The ratio of the area (non-labeled synthetic standard/internal isotopically labeled standard;  $EN_s/IS$ ) was plotted against the expected ratio of  $EN_s/IS$ . The dashed horizontal line indicates the limit of detection (LOD). A logarithmic scale was used due to the broad concentration range investigated. Dilutions were done in triplicates.

Figure 25 shows the accuracy plot of CYP1A1, where the two horizontal lines indicate the limits of the acceptance criterion (accuracy 80-120%). The accuracy in percentage was plotted against the theoretical amount of  $EN_s$ . The linear range was defined where the accuracy was between 80-120%, and the coefficient of variation (C.V.) within one concentration level ( $n=3$ ) was  $\leq 20\%$  (these criteria were based on the U.S. Food and Drug Administration (FDA) guideline <sup>94</sup>). The lowest value meeting these criteria was determined as the lower limit of quantification (LLOQ). The

blue frame in Figure 25 indicates the linear range for CYP1A1, where the LLOQ is 0.15 fmol, and the upper limit of quantification (ULOQ) is 1000 fmol. Results for all other analytes can be found in Figure 47 (9 Supplementary Data).

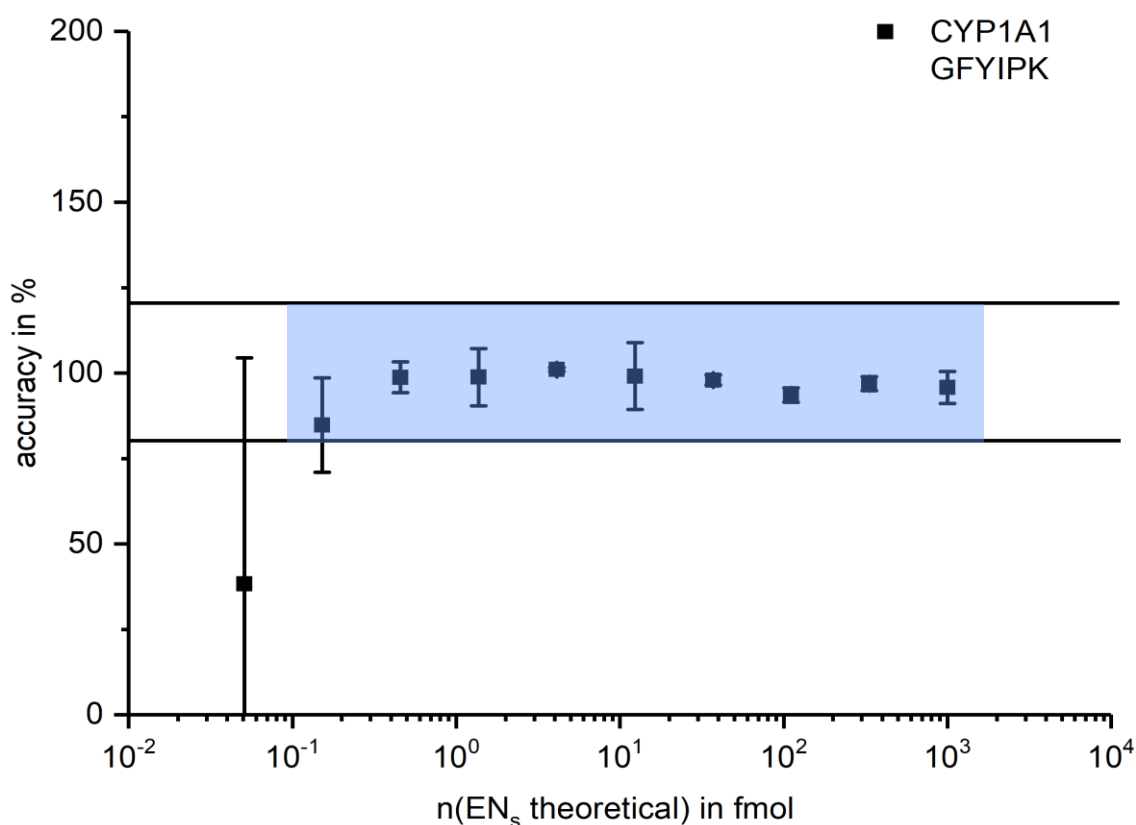


Figure 25. Accuracy plot of CYP1A1 in PBSC. The accuracy in percentage (%) was plotted against the theoretical EN<sub>s</sub> amount of substance in femtomole (fmol). Analyses were done in triplicates. Both horizontal lines mark the limit values of 80% and 120%. The blue frame indicates the linear range where all evaluation criteria were met (accuracy between 80-120%; coefficient of variation (C.V.) ≤ 20%).

All linear equations with the corresponding coefficients of determination ( $R^2$ ), the determined LODs, and LLOQs are shown in Table 22. Here, the analytes in the table were sorted by the multiplexes. All analytes showed a linear relationship between the EN<sub>s</sub>/IS area ratio and the theoretical amount of substance ratio of EN<sub>s</sub>/IS over several orders of magnitude. The coefficients of determination ranged from 0.97458 for protein S100-P (S100P) to 0.99999 for sulfotransferase family cytosolic 1B member 1 (SULT1B1). The lowest LLOQ was determined for CYP3A4 with 0.05 fmol, the highest for aldehyde dehydrogenase, dimeric NADP-preferring (ALDH3A1) with 12.35 fmol.

## Results

Table 22. Linear equations of all analytes in PBSC as well as the coefficient of determination ( $R^2$ ), the calculated limit of detections (LOD), and the determined lower limit of quantification (LLOQ).

Multiplex	Analyte	Linear equation	$R^2$	LOD in fmol	LLOQ in fmol
CYP 17-plex	CYP1A1	$y = 0.54665x - 0.000150$	0.99935	0.015	0.15
	CYP1A2	$y = 0.55626x - 0.00123$	0.99971	0.009	0.15
	CYP2B6	$y = 0.67992x + 0.00687$	0.99984	0.267	4.12
	CYP2C8	$y = 0.62282x - 0.0000917$	0.99986	0.024	0.46
	CYP2C9	$y = 0.66665x + 0.00674$	0.99957	0.314	4.12
	CYP2C18	$y = 0.55175x - 0.000216$	0.99597	0.018	1.37
	CYP2C19	$y = 1.10319x + 0.01086$	0.99515	0.586	0.46
	CYP2D6	$y = 0.17323x - 0.00395$	0.98589	0.025	4.12
	CYP2E1	$y = 0.67925x - 0.0012$	0.99886	0.027	0.46
	CYP2F1	$y = 0.78655x + 0.00597$	0.99913	0.155	4.12
	CYP3A4	$y = 0.74543x + 0.00227$	0.99916	0.126	0.05
	CYP3A5 (FIPK)	$y = 0.41002x + 0.01109$	0.99994	0.334	4.12
	CYP3A5 (LPNK)	$y = 0.55173x + 0.00233$	0.99987	0.237	4.12
	CYP3A7	$y = 0.62158x + 0.0039$	0.99959	0.452	4.12
	CYP3A43	$y = 0.57262x - 0.01326$	0.99928	0.274	4.12
	MDR1	$y = 0.5472x - 0.000151$	0.99986	0.030	1.37
	NCPR	$y = 0.49608x - 0.00148$	0.99982	0.033	0.46
MpCombi1	ARG1(PFSK)	$y = 0.57461x + 0.01076$	0.99952	4.553	1.37
	UGT1A1	$y = 0.998x - 0.00387$	0.99762	0.053	4.12
	UGT1A3	$y = 2.64329x + 0.01596$	0.99823	0.694	1.37
MpCombi2	FASN	$y = 1.59593x - 0.01567$	0.99342	1.127	4.12
	LMNA	$y = 1.5014x + 0.00355$	0.99973	0.948	1.37
	TNFRSF12A	$y = 1.19786x - 0.00604$	0.99625	0.079	1.37
MpCombi3	ALDH3A1	$y = 1.17059x - 0.03643$	0.99602	0.460	12.35
	UGT2B15	$y = 2.00952x - 0.06011$	0.99571	0.247	4.12
MpCombi4	SULT1B1	$y = 1.38987x - 0.00198$	0.99999	0.043	0.46
	UGT2B7	$y = 1.16501x - 0.01165$	0.99807	0.039	1.37
MpCombi5	ARG1(YILK)	$y = 1.89879x - 0.01273$	0.99322	0.088	1.37
	CYP7A1	$y = 1.01451x - 0.00937$	0.99803	0.103	1.37
	S100P	$y = 1.77549x - 0.00229$	0.97458	0.078	1.37
MpCombi6	ADH1B	$y = 1.29341x - 0.00701$	0.99975	0.316	4.12
	HSD11B2	$y = 1.24041x - 0.00435$	0.99829	0.048	0.46
	NQO1	$y = 1.54318x + 0.00258$	0.99923	0.125	1.37
	PRKDC	$y = 1.39809x - 0.01149$	0.99830	0.250	1.37



## 4.1.11 Determination of the Target Analyte Yield – Recovery

As described in 3.9.11, the mouse cell line NIH3T3 was used as a matrix for recovery experiments. In the literature, it is recommended to use different concentrations to determine recovery<sup>94</sup>. Therefore, either 15 fmol, 250 fmol, or 500 fmol EN<sub>s</sub> were spiked into the sample for each analyte. The formula described in chapter 3.9.11 was used to calculate the recovery. Besides, the measured EN<sub>s</sub>/IS ratios were corrected using the linear equations determined in chapter 4.1.10 before the formula was applied. Table 23 shows the results for multiplex assays 1-6 at different spike-in levels. For the results marked with a star, a high base level of the mouse matrix has already been measured. No recovery experiments were performed for the CYP 17-plex.

Table 23. Recovery of analytes out of NIH3T3 cell samples by use of three different spike-in amounts of EN<sub>s</sub> (15 fmol, 250 fmol, and 500 fmol). Recovery in percentage (%), as well as the coefficients of variation (C.V.), are shown for each spike-in level. Only multiplex 1-6 were investigated.

Multiplex	Analyte	Recovery		Recovery		Recovery	
		in % (15 fmol spike-in)	C.V. in %	in % (250 fmol spike-in)	C.V. in %	in % (500 fmol spike-in)	C.V. in %
MpCombi1	ARG1(PFSK)	80	3	74	1	80	5
	UGT1A1	107	2	108	3	113	6
	UGT1A3	60	1	80	1	94	2
MpCombi2	FASN	79	8	86	3	88	6
	LMNA	66*	12	92	4	100	2
	TNFRSF12A	71	2	82	2	100	8
MpCombi3	ALDH3A1	91	7	104	10	99	8
	UGT2B15	88	10	112	2	115	6
MpCombi4	SULT1B1	98	3	103	3	104	1
	UGT2B7	77	3	80	1	90	1
MpCombi5	ARG1(YILK)	103	5	113	9	108	5
	CYP7A1	102	2	100	2	96	3
	S100P	78	5	82	6	101	10
MpCombi6	ADH1B	70	13	81	1	85	3
	HSD11B2	101	0	99	2	102	2
	NQO1	128*	0	80	0	79	3
	PRKDC	110	5	113	4	111	2

\*= Due to high base level in the matrix, 15 fmol spike-in is within the measurement error range and, therefore, cannot be determined.

## Results

Table 23 reveals that the recoveries were between  $60.47 \pm 1.49\%$  for UGT1A3 (marked with orange) at 15 fmol EN<sub>s</sub> spike-in to  $127.60 \pm 0.42\%$  at 15 fmol EN<sub>s</sub> spike-in for NAD(P)H dehydrogenase [quinone] 1 (NQO1). The results for all analytes at each concentration level were precise and reproducible with a maximum C.V. of 13.4% for alcohol dehydrogenase 1B (ADH1B) at 15 fmol EN<sub>s</sub> spike-in.

### 4.1.12 Intra- and Interday Precision

For the assessment of intra- and interday precision, three different samples were used. First, a negative HepaRG control (DMSO-treated), second a prochloraz-treated ( $10 \mu\text{mol L}^{-1}$ ) HepaRG sample, and third a cryopreserved primary human hepatocyte sample (PHH; donor 1). Each sample was digested five times per day, and this procedure was repeated for three days. For intraday precision, the mean value for the five single determinations was used. For the interday precision, one random value was chosen for each day. Table 24 on the next two pages shows the results. Only multiplex 1 to multiplex 6 were investigated. The table shows that for both intra- and interday results, C.V.s with less than 20% could be obtained. The smallest C.V. was obtained for ARG1(PFSK) with 0.5% in the PHH sample (interday), the highest for corticosteroid 11-beta-dehydrogenase isozyme 2 (HSD11B2) with 19.6% in the negative control (intraday). CYP7A1 and S100P were only detected and quantified in the PHH sample. On the other hand, ALDH3A1, HSD11B2, NQO1, and tumor necrosis factor receptor superfamily member 12A (TNFRSF12A) were identified only in the HepaRG cells and not in the hepatocyte sample.

In summary, it can be said that the method development was completed successfully with regard to the investigated parameters for six new multiplexes containing a total of 17 peptides (representative of 16 proteins). In combination with the CYP 17-plex, the analysis of pesticide-treated HepaRG cells was performed for 34 peptides (representative of 32 proteins).

Table 24. Intra- and interday precision of multiplex assays 1-6, where intraday variance was determined with n=5 replicates and interday variance with n=3 replicates. For the assessment, a negative HepaRG cell sample (DMSO-treated), a prochloraz-treated (10 µmol L<sup>-1</sup>) HepaRG cell sample, and a cryopreserved primary human hepatocyte (PHH; donor 1) sample were used. Shown are the mean values in fmol µg<sup>-1</sup> and the respective coefficient of variation (C.V.) in percent (%).

Mp	Analyte	Intraday variance (n=5)						Interday variance (n=3)					
		Control		Prochloraz-treated		PHH.1		Control		Prochloraz-treated		PHH.1	
		mean in fmol µg <sup>-1</sup>	C.V. in %	mean in fmol µg <sup>-1</sup>	C.V. in %	mean in fmol µg <sup>-1</sup>	C.V. in %	mean in fmol µg <sup>-1</sup>	C.V. in %	mean in fmol µg <sup>-1</sup>	C.V. in %	mean in fmol µg <sup>-1</sup>	C.V. in %
1	ARG1 (PFSK)	2.5	6	1.9	5	69.8	11	2.5	6	1.7	5	66.3	1
	UGT1A1	6.8	9	5.6	6	10.9	12	6.8	12	5.4	4	9.1	15
	UGT1A3	1.1	4	0.8	9	3.0	6	1.1	3	0.8	1	3.1	10
2	FASN	18.6	10	19.0	12	4.4	6	20.3	11	23.0	16	4.0	5
	LMNA	28.4	7	6.6	7	0.3	17	29.8	3	6.5	7	0.4	9
	TNFRSF12A	0.2	11	0.2	7	n.d.	na	0.2	18	0.2	11	n.d.	na
3	ALDH3A1	15.2	8	10.1	6	n.d.	na	15.3	4	12.0	15	n.d.	na
	UGT2B15	30.6	7	27.0	15	117.1	12	34.2	12	29.0	15	121.7	17
4	SULT1B1	0.9	4	0.6	4	3.3	3	1.0	8	0.7	16	3.4	3
	UGT2B7	2.8	6	1.4	7	52.1	6	3.0	13	1.5	7	54.3	2
5	ARG1(YILK)	0.8	8	0.8	12	20.9	8	0.8	3	1.0	19	19.9	7
	CYP7A1	<LLOQ	na	n.d.	na	0.1	9	<LLOQ	na	n.d.	na	0.1	18

Mp	Analyte	Intraday variance (n=5)						Interday variance (n=3)					
		Control		Prochloraz-treated		PHH.1		Control		Prochloraz-treated		PHH.1	
		mean in fmol $\mu\text{g}^{-1}$	C.V. in %	mean in fmol $\mu\text{g}^{-1}$	C.V. in %	mean in fmol $\mu\text{g}^{-1}$	C.V. in %	mean in fmol $\mu\text{g}^{-1}$	C.V. in %	mean in fmol $\mu\text{g}^{-1}$	C.V. in %	mean in fmol $\mu\text{g}^{-1}$	C.V. in %
	S100P	<LLOQ	na	<LLOQ	na	0.1	4	<LLOQ	na	<LLOQ	na	0.1	3
6	ADH1B	58.5	12	49.4	3	172.5	7	59.8	9	52.4	13	173.4	3
	HSD11B2	0.1	20	0.1	12	n.d.	na	0.1	2	0.05	9	n.d.	na
	NQO1	0.5	7	0.4	11	n.d.	na	0.5	13	0.4	14	n.d.	na
	PRKDC	4.9	8	4.1	18	1.0	19	5.6	15	4.3	10	1.0	9

n.d.= not detected; na= not applicable; <LLOQ= below the lower limit of quantification

## 4.2 Analysis of Pesticide-Treated HepaRG Cells with Immunoaffinity-Based Mass Spectrometry

### 4.2.1 Determination of the Fold Change's Significance Levels

For the analysis of induction or repression effects, it was necessary to determine what the threshold would be to distinguish between the variations due to experimental errors and a significant change referred to the control. To address this issue, RStudio v.1.0.153 (R Consortium, Boston, USA) was used, and in cooperation with Dr. Hannes Planatscher (Signatope GmbH, Reutlingen, Germany), a script for a simulation with random fold change values (transformed to  $\log_2$  values) was written. It was considered that each pesticide treatment was measured three times, as well as the control samples. Also,  $\alpha$  was set to 0.05, which means the observed fold change is not a random product with a probability of 5%. To obtain a more accurate result, alpha was divided by the number of analytes for which the evaluation was performed (alpha was divided by 27). As a further criterion, the tested coefficient of variation (C.V.) was set to 20%, since interday variation did not exceed 20% (see Table 24).

With these parameters set, the simulation was performed with 100, 1000, 10 000, and 100 000 random fold change ( $\log_2$  transformed) values. Figure 26 shows that with an increased number of test samples, the histograms approximated a perfect Gaussian distribution. The simulation revealed that a fold change ( $\log_2$  transformed) must be less than -0.56 or higher than +0.56 to be considered as significant. This transforms into 1.5-fold and 0.7-fold in absolute values.

## Results

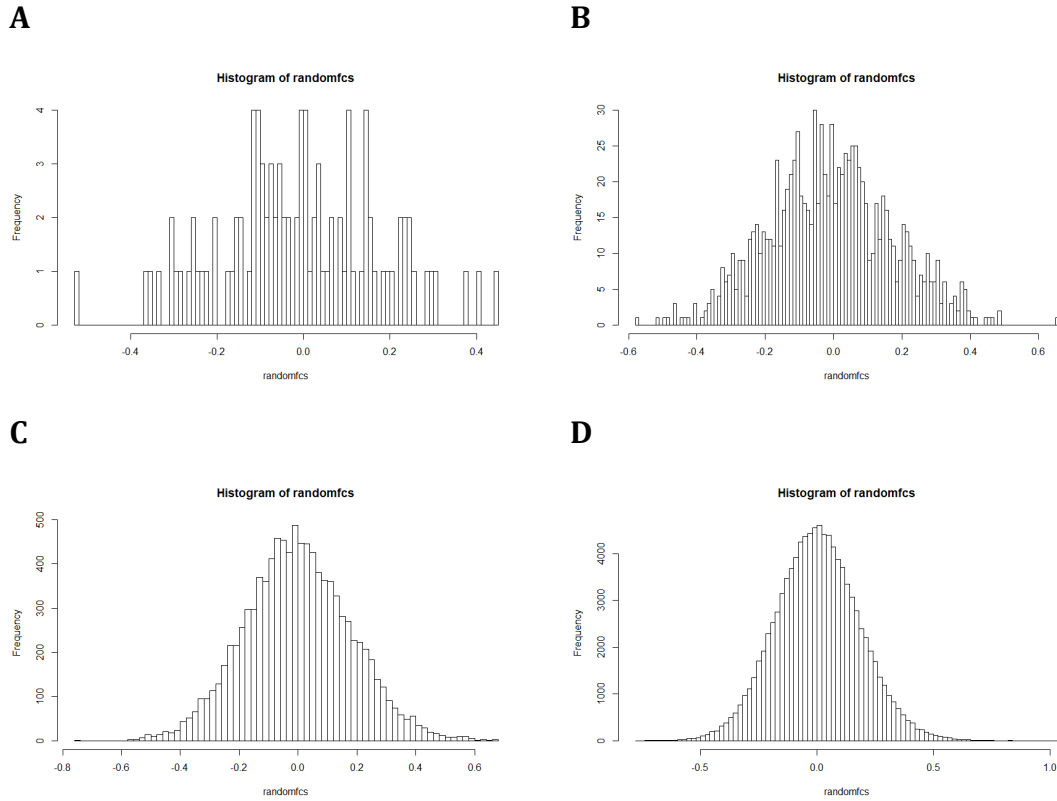


Figure 26. Histogram of randomly generated fold changes. The simulations were performed with 100 (A), 1000 (B), 10 000 (C), and 100 000 (D) randomly generated fold changes ( $\log_2$  transformed). The simulation revealed that the  $\log_2$  transformed fold changes must be less than -0.56 or greater than +0.56 to be considered as significant. The simulations were run with RStudio v.1.0.153.

Since the effects of pesticide treatments on toxicologically relevant proteins in HepaRG cells were determined using fold changes, quadratic error propagation was used to calculate the errors of these fold changes. The following equation shows the general formula of the quadratic error propagation law.

$$\Delta F = \sqrt{\left(\frac{\partial F}{\partial x} \cdot \Delta \bar{x}\right)^2 + \left(\frac{\partial F}{\partial y} \cdot \Delta \bar{y}\right)^2 + \dots} \quad (95)$$

This formula has been modified for the calculation of fold change errors as follows:

$$\Delta F = \left( \sqrt{\left(\frac{\sigma_{tr}}{\bar{x}_{tr}}\right)^2 + \left(\frac{\sigma_{nc}}{\bar{x}_{nc}}\right)^2} \right) \cdot \left( \frac{\bar{x}_{tr}}{\bar{x}_{nc}} \right)$$

$\sigma_{tr}$  = standard deviation of treated samples

$\bar{x}_{tr}$  = mean value of treated samples

$\sigma_{nc}$  = standard deviation of the negative control

$\bar{x}_{nc}$  = mean value of the negative control

#### 4.2.2 Analysis of HepaRG Cells Treated with Single Pesticides – Screening

Before the analysis of potential mixture effects was investigated, a screening of 30 different pesticides, comprising acaricides, fungicides, insecticides, nematicides, and plant growth regulators, was performed. Treatment of HepaRG cells was performed with each pesticide in three replicates. The concentration of the particular pesticide was the highest non-toxic concentration determined with a cell viability test performed by Dr. Dajana Lichtenstein (German Federal Institute for Risk Assessment (BfR)). After the measurement, mean values were calculated for each analyte. Fold changes were determined, and results were transformed to  $\log_2$  data. Figure 27 shows a heatmap of the results. On the y-axis, all 27 quantified peptides (7/34 peptides were either below the quantification limit or not detectable) are presented, on the x-axis all pesticide treatments. A gray field indicates that no evaluable data point has been obtained. At first glance, the heatmap shows that weak changes can be observed for most analytes across all pesticides (only 28.1% of all data points showed a significant change). The effects, however, are more towards down-regulation. Nevertheless, for a few proteins, stronger changes were observed. For example, CYP1A1 shows a strong induction effect, with a 695 or 322 fold change after treatment with cyprodinil (CDN) or fludioxinil (FDO), respectively. Strong induction effects were also observed for CYP1A1 after treatment with iprodione (IPR; 188-fold), carbendazim (CBZ; 158-fold), chlorpyrifos (CLP; 80-fold), or pyraclostrobin (PCL; 67-fold). In contrast to CYP1A1, CYP2C19 shows a partially strong down-regulation. These effects are mainly observed after the treatment of CLP (0.08-fold), azoxystrobin (AOS; 0.10-fold), ethoprophos (ETP; 0.12-fold), or thiram (TRM; 0.13). Looking at the pesticide treatments across all analytes, it can be observed that the treatment with ethoprophos (ETP) produced a significant effect (greater than 0.56 and less than -0.56 or 1.5-fold and 0.7-fold) in 18 out of 27 analytes. Significant changes were observed for 14 analytes each when treated with fludioxonil (FDO), maneb (MAN), and thiram (TRM). On the other hand, only two analytes showed a significant change after treatment with captan (CPT) and thiacloprid (THI). When treated with chlormequat (CMQ), it was even only one analyte. Table 25 summarizes the 30 pesticides used for the screening. It contains both the substance name and the abbreviation (abbrev.) used in Figure 27, as well as the treatment concentration

## Results

in  $\mu\text{mol L}^{-1}$  applied. It also displays how many significant up- or down-regulations were observed during the screening.

Table 25. Pesticides of the screening. The table shows the pesticides of the screening with the corresponding abbreviations and concentrations used. It also shows the number of significant up- or down-regulation of the respective pesticide treatment.

Substance	Abbrev.	Concentration in $\mu\text{mol L}^{-1}$	Significant up-regulation #	Significant down-regulation #
Azoxystrobin	AOS	100	0	8
Boscalid	BOS	500	2	6
Captan	CPT	50	1	1
Carbendazim	CBZ	250	5	2
Chlormequat	CMQ	1000	1	0
Chlorpyrifos	CLP	200	5	5
Cyproconazole	CC	80	4	1
Cyprodinil	CDN	100	6	3
Difenoconazole	DIF	25	2	5
Dimethomorph	DIM	500	2	5
Epoxiconazole	EPC	80	5	1
Ethoprophos	ETP	500	2	16
Fenhexamid	FHM	250	0	6
Fenpyroximate	FPX	5	2	5
Fipronil	FIP	50	4	1
Fludioxonil	FDO	250	6	8
Flusilazole	FLZ	80	6	1
Fluxapyroxad	FLP	250	2	10
Imazalil	IMZ	50	4	5
Iprodione	IPR	200	5	2
Maneb	MAN	200	2	12
Metalaxyl	MTX	1000	1	5
Myclobutanil	MCB	250	6	2
Prochloraz	PCZ	80	2	2
Propiconazole	PPC	80	9	0
Pyraclostrobin	PCL	25	3	3
Tebuconazole	TBC	80	6	1
Thiacloprid	THI	500	0	2
Thiamethoxam	TMX	1000	2	1
Thiram	TRM	100	4	10



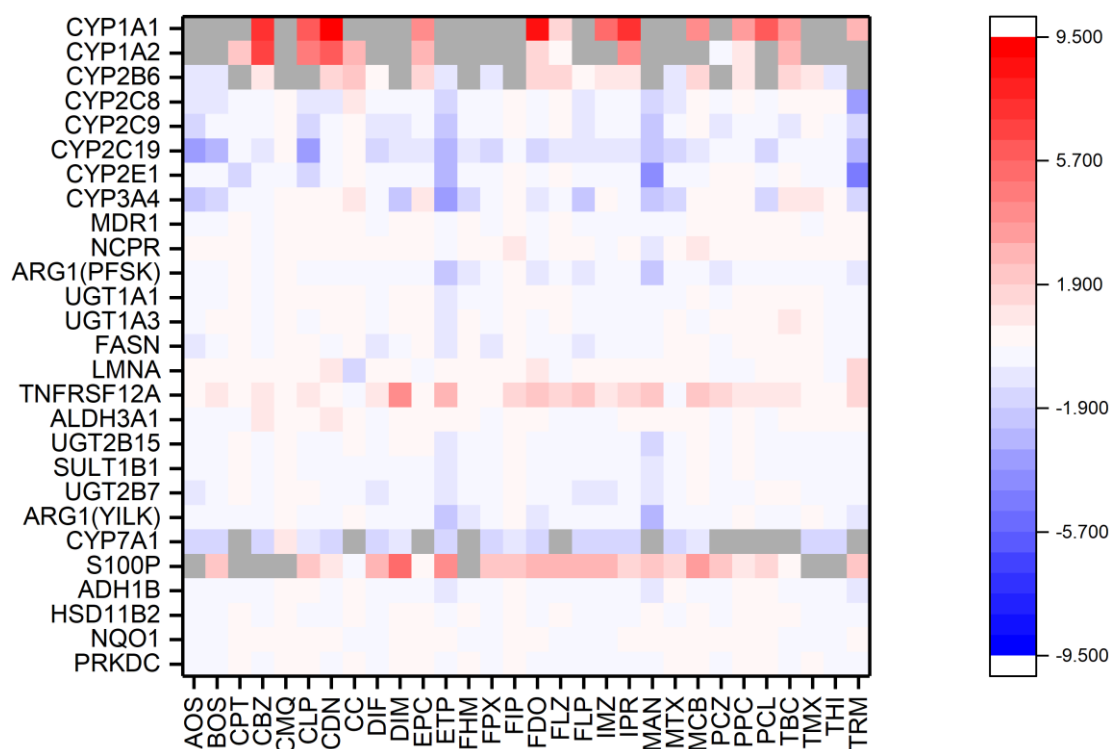


Figure 27. Heatmap of screening results. Here, data for all analytes after the treatment with 30 different single pesticides are shown. Measurement of each treatment was performed in triplicates. Abbreviations of the treatments are shown in Table 25. Gray fields indicate that no evaluable data point has been obtained.

#### 4.2.3 Time-Dependency of Effects after Varying Pesticide Incubations

Since the results of the screening showed only few significant changes at the protein level, it was decided that the time dependency on the effects of a small selection of pesticides should be re-analyzed. Hence the treatment duration was extended from 24 to 72 hours. Four different pesticides and a prototypical inducer were selected. Results of the 72-hour treatment were then compared to the already obtained data after 24 hours of treatment. HepaRG cells were treated with difenoconazole, fenpyroximate, flusilazole, and imazalil. Rifampicin was used as a prototypical inducer. Concentrations of flusilazole ( $80 \mu\text{mol L}^{-1}$ ), imazalil ( $50 \mu\text{mol L}^{-1}$ ), and rifampicin ( $5 \mu\text{mol L}^{-1}$ ) were the same for both treatment durations. Due to cytotoxicity data, the concentration of difenoconazole and fenpyroximate had to be adjusted ( $25 \mu\text{mol L}^{-1}$  to  $10 \mu\text{mol L}^{-1}$  and  $5 \mu\text{mol L}^{-1}$  to  $2.5 \mu\text{mol L}^{-1}$ , respectively). Heat maps were generated from the obtained data using mean  $\log_2$  data ( $n=3$ ; errors not displayed), and results are shown in Figure 28. The analytes were plotted on the y-axis while the four pesticides and the prototypical inducer were plotted on the x-axis. In

## Results

addition, the scales of both heat maps were set to the same values to allow a visual comparison. Gray fields indicate that no evaluable data point has been obtained since values were below the lower limit of quantification (LLOQ), or no endogenous signal was detected.

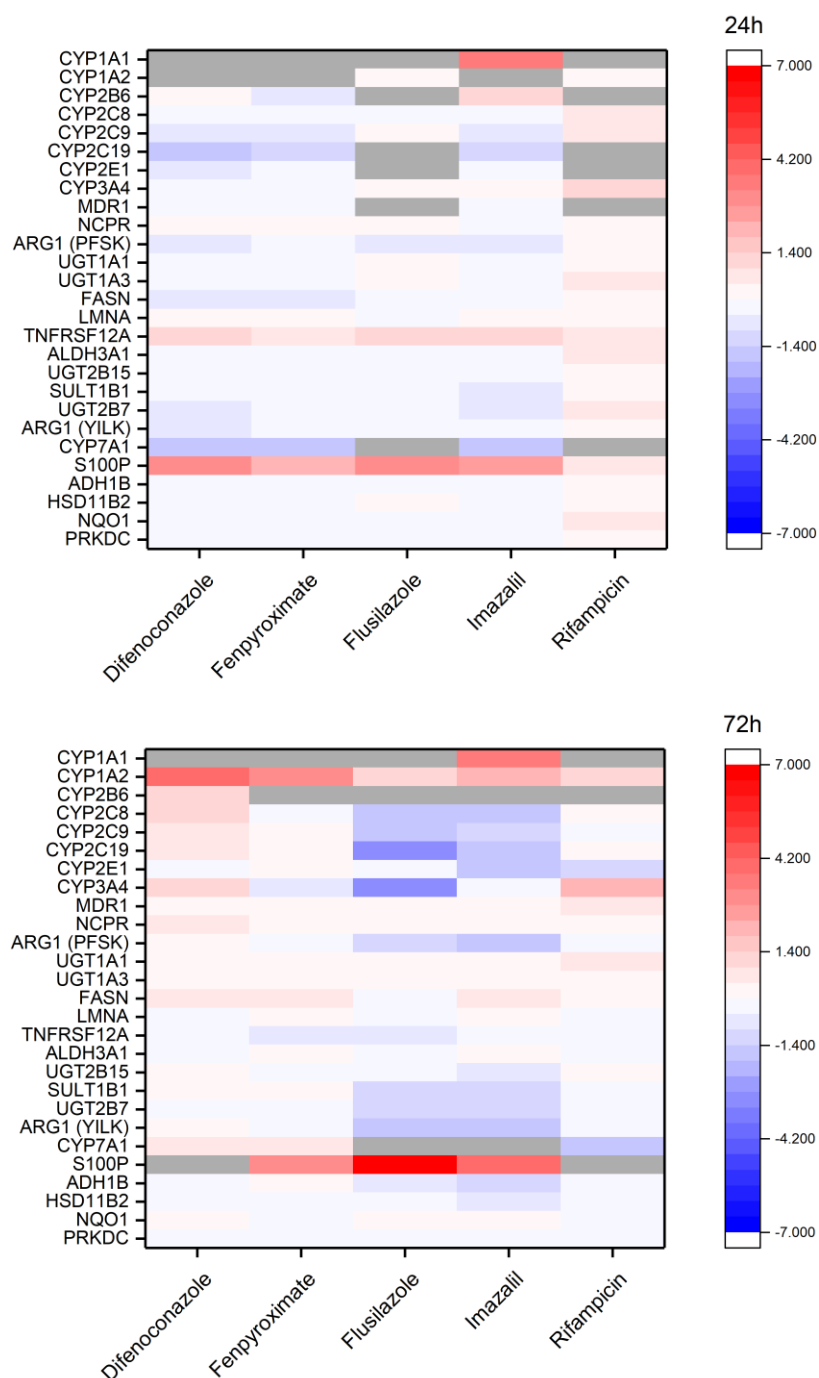


Figure 28. Heatmap comparison of 24 h and 72 h treatment. HepaRG cells were treated with difenoconazole, fenpyroximate, flusilazole, imazalil, and rifampicin for 24 h (upper graph) and 72 h (lower graph). The concentration of flusilazole, imazalil, and rifampicin ( $80 \mu\text{mol L}^{-1}$ ,  $50 \mu\text{mol L}^{-1}$ , and  $5 \mu\text{mol L}^{-1}$ , respectively) remained unaltered. Difenconazole and fenpyroximate had to be adjusted based on cytotoxicity data ( $25 \mu\text{mol L}^{-1}$  to  $10 \mu\text{mol L}^{-1}$  and  $5 \mu\text{mol L}^{-1}$  to  $2.5 \mu\text{mol L}^{-1}$ ). Each treatment was performed three times, and measurements were performed in single determinations. Mean values were then calculated; errors are not displayed. Gray fields indicate that no evaluable data point has been obtained. For visual comparison, the scales were set to the same values.

Figure 28 clearly shows differences between the results from cell cultures treated for 24 hours and 72 hours. Due to cytotoxic effects after 72 hours of treatment, the concentration for difenoconazole and fenpyroximate had to be reduced and adjusted. Therefore, a direct comparison could only be made for flusilazole, imazalil,

## Results

and rifampicin. In general, the effect of flusilazole and imazalil was more pronounced after 72 hours than after 24 hours. While 11 proteins showed a significant change (less than -0.56 or more than 0.56; or 0.7-fold and 1.5-fold) after the 24-hour treatment with flusilazole and imazalil, 25 proteins showed a significant change after 72 hours. In addition to the higher number of significant protein changes, the amplitude of some analytes also increased. S100P, for example, showed a stronger induction after 72 hours. The fold changes of S100P after treatment with flusilazole and imazalil for 24 hours were 7.5 and 6.4, respectively, whereas these protein changes were 118.6 and 17.7 after 72 hours. Moreover, CYP2C8, CYP2C9, or CYP2C19 showed stronger repression effects after 72 hours.

Interestingly, the results after 24-hour treatment with rifampicin indicate a trend towards up-regulation. Comparing the results with the 72-hour treatment, it is notable that the direction of regulation of many proteins switched towards down-regulation. Moreover, 17 protein concentrations were below LLOQ after 24 hours, while only 12 data points were below LLOQ after 72 hours of treatment (characterized by gray fields, which is particularly visible after treatment with flusilazole and rifampicin).

### 4.2.4 HepaRG Cell Viability after Treatment with Single Pesticides and Mixtures thereof

Once the screening was completed, the data were used to decide which substances should be combined to investigate potential mixing effects. The composition of the mixtures should be based on the potency of the substance and not on concentrations. One challenge was that typically, only one effect (i.e., on a specific endpoint, e.g., a single protein) is considered when calculating the potency. In this case, however, it was necessary to consider the effect on all proteins to be investigated. It was therefore decided to calculate a multiple potency factor of the individual pesticide effects on the proteins in order to obtain relative potency factors (RPFs) of the treatments by relating them to each other. This calculation was performed at the protein level and to compare the data obtained, the calculation was also performed with AdipoRed data (test for the intracellular enrichment of triacylglycerides; the measurement and calculation was performed by Dr. Dajana Lichtenstein, BfR) and at the

mRNA level (assay and calculation was performed by Dr. Almut Mentz at the Center for Biotechnology (CeBiTec)).

To calculate the RPFs at the protein level, confidence intervals for all analytes were determined respectively and normalized to the concentration used. In order to obtain RPFs, all calculated values were related to each other. The results are shown in Figure 29. The encircled values show the RPFs of the substances that were used for the generation of mixtures.

	Relative potency factors																													
	AOS	BOS	CBZ	Cc	CDN	CMQ	CLP	CPT	DIF	DIM	EPC	ETP	FDO	FHM	FIP	FLP	FLZ	FPX	IMZ	IPR	MAN	MCB	MTX	PCL	PCZ	PPC	TBC	THI	TMX	TRM
AOS	1.0	4.9	1.2	1.4	0.4	40.6	0.9	0.8	0.2	2.7	1.8	2.5	1.1	4.7	0.8	2.3	0.9	0.1	0.4	1.1	1.1	1.8	12.4	0.2	0.8	1.6	1.4	10.4	18.7	0.5
BOS	0.2	1.0	0.2	0.3	0.1	8.3	0.2	0.2	0.1	0.5	0.4	0.5	0.2	1.0	0.2	0.5	0.2	0.0	0.1	0.2	0.2	0.4	2.5	0.0	0.2	0.3	0.3	2.1	3.8	0.1
CBZ	0.8	4.0	1.0	1.2	0.3	33.3	0.8	0.6	0.2	2.2	1.5	2.0	0.9	3.8	0.6	1.8	0.7	0.1	0.3	0.9	0.9	1.5	10.2	0.1	0.7	1.3	1.2	8.5	15.3	0.4
Cc	0.7	3.5	0.9	1.0	0.3	28.8	0.7	0.5	0.2	1.9	1.3	1.8	0.8	3.3	0.5	1.6	0.6	0.0	0.3	0.8	0.8	1.3	8.8	0.1	0.6	1.2	1.0	7.4	13.2	0.4
CDN	2.8	12.7	3.2	3.6	1.0	105.1	2.4	2.0	0.6	7.0	4.7	6.4	2.9	12.1	1.9	5.8	2.3	0.2	1.1	2.9	2.9	4.7	32.1	0.4	2.1	4.2	3.7	26.9	48.3	1.3
CMQ	0.0	0.1	0.0	0.0	0.0	1.0	0.0	0.0	0.0	0.1	0.0	0.1	0.0	0.1	0.0	0.1	0.0	0.0	0.0	0.0	0.0	0.0	0.3	0.0	0.0	0.0	0.0	0.3	0.5	0.0
CLP	1.1	5.2	1.3	1.5	0.4	43.0	1.0	0.8	0.3	2.9	1.9	2.6	1.2	4.9	0.8	2.4	0.9	0.1	0.4	1.2	1.2	1.9	13.1	0.2	0.9	1.7	1.5	11.0	19.8	0.5
CPT	1.3	6.5	1.6	1.9	0.5	53.7	1.2	1.0	0.3	3.6	2.4	3.3	1.5	6.2	1.0	3.0	1.2	0.1	0.6	1.5	1.5	2.4	16.4	0.2	1.1	2.2	1.9	13.7	24.7	0.7
DIF	4.0	19.7	4.9	5.7	1.6	163.2	3.8	3.0	1.0	10.8	7.2	10.0	4.5	18.7	3.0	9.1	3.5	0.2	1.7	4.5	4.5	7.3	49.8	0.6	3.2	6.6	5.7	41.7	75.0	2.1
DIM	0.4	1.8	0.5	0.5	0.1	15.1	0.4	0.3	0.1	1.0	0.7	0.9	0.4	1.7	0.3	0.8	0.3	0.0	0.2	0.4	0.4	0.7	4.6	0.1	0.3	0.5	0.5	3.9	6.9	0.2
EPC	0.6	2.7	0.7	0.8	0.2	22.5	0.5	0.4	0.1	1.5	1.0	1.4	0.6	2.6	0.4	1.3	0.5	0.0	0.2	0.6	0.6	1.0	6.9	0.1	0.4	0.9	0.8	5.8	10.4	0.3
ETP	0.4	2.0	0.5	0.6	0.2	16.4	0.4	0.3	0.1	1.1	0.7	1.0	0.5	1.9	0.3	0.9	0.4	0.0	0.2	0.4	0.4	0.7	5.0	0.1	0.3	0.7	0.6	4.2	7.5	0.2
FDO	0.9	4.3	1.1	1.2	0.3	36.0	0.8	0.7	0.2	2.4	1.6	2.2	1.0	4.1	0.7	2.0	0.8	0.1	0.4	1.0	1.0	1.6	11.0	0.1	0.7	1.4	1.3	9.2	16.6	0.5
FHM	0.2	1.1	0.3	0.3	0.1	8.7	0.2	0.2	0.1	0.6	0.4	0.5	0.2	1.0	0.2	0.5	0.2	0.0	0.1	0.2	0.2	0.4	2.7	0.0	0.2	0.3	0.3	2.2	4.0	0.1
FIP	1.3	6.5	1.6	1.9	0.5	54.0	1.3	1.0	0.3	3.6	2.4	3.3	1.5	6.2	1.0	3.0	1.2	0.1	0.6	1.5	1.5	2.4	16.5	0.2	1.1	2.2	1.9	13.8	24.8	0.7
FLP	0.4	2.2	0.5	0.6	0.2	18.0	0.4	0.3	0.1	1.2	0.8	1.1	0.5	2.1	0.3	1.0	0.4	0.0	0.2	0.5	0.5	0.8	5.5	0.1	0.4	0.7	0.6	4.6	8.3	0.2
FLZ	1.1	5.6	1.4	1.6	0.4	46.3	1.1	0.9	0.3	3.1	2.1	2.8	1.3	5.3	0.9	2.6	1.0	0.1	0.5	1.3	1.3	2.1	14.1	0.2	0.9	1.9	1.6	11.8	21.3	0.6
FPX	16.3	80.1	20.0	23.0	6.3	663.8	15.4	12.4	4.1	44.0	29.5	40.5	18.4	76.2	12.3	36.8	14.3	1.0	6.8	18.2	18.2	29.5	202.6	2.6	13.2	26.7	23.3	169.6	305.2	8.4
IMZ	2.4	11.8	2.9	3.4	0.9	97.4	2.3	1.8	0.6	6.5	4.3	5.9	2.7	11.2	1.8	5.4	2.1	0.1	1.0	2.7	2.7	4.3	29.7	0.4	1.9	3.9	3.4	24.9	44.8	1.2
IPR	0.9	4.4	1.1	1.3	0.3	36.5	0.8	0.7	0.2	2.4	1.6	2.2	1.0	4.2	0.7	2.0	0.8	0.1	0.4	1.0	1.0	1.6	11.1	0.1	0.7	1.5	1.3	9.3	16.8	0.5
MAN	0.9	4.4	1.1	1.3	0.3	36.6	0.8	0.7	0.2	2.4	1.6	2.2	1.0	4.2	0.7	2.0	0.8	0.1	0.4	1.0	1.0	1.6	11.2	0.1	0.7	1.5	1.3	9.3	16.8	0.5
MCB	0.6	2.7	0.7	0.8	0.2	22.5	0.5	0.4	0.1	1.5	1.0	1.4	0.6	2.6	0.4	1.2	0.5	0.0	0.2	0.6	0.6	1.0	6.9	0.1	0.4	0.9	0.8	5.8	10.3	0.3
MTX	0.1	0.4	0.1	0.1	0.0	3.3	0.1	0.1	0.0	0.2	0.1	0.2	0.1	0.4	0.1	0.2	0.1	0.0	0.0	0.1	0.1	0.1	1.0	0.0	0.1	0.1	0.1	0.8	1.5	0.0
PCL	6.4	31.3	7.8	9.0	2.5	259.3	6.0	4.8	1.6	17.2	11.5	15.8	7.2	29.8	4.8	14.4	5.6	0.4	2.7	7.1	7.1	11.5	79.1	1.0	5.1	10.4	9.1	66.3	119.2	3.3
PCZ	1.2	6.1	1.5	1.7	0.5	50.4	1.2	0.9	0.3	3.3	2.2	3.1	1.4	5.8	0.9	2.8	1.1	0.1	0.5	1.4	1.4	2.2	15.4	0.2	1.0	2.0	1.8	12.9	23.2	0.6
PPC	0.6	3.0	0.7	0.9	0.2	24.9	0.6	0.5	0.2	1.7	1.1	1.5	0.7	2.9	0.5	1.4	0.5	0.0	0.3	0.7	0.7	1.1	7.6	0.1	0.5	1.0	0.9	6.4	11.4	0.3
TBC	0.7	3.4	0.9	1.0	0.3	28.6	0.7	0.5	0.2	1.9	1.3	1.7	0.8	3.3	0.5	1.6	0.6	0.0	0.3	0.8	0.8	1.3	8.7	0.1	0.6	1.1	1.0	7.3	13.1	0.4
THI	0.1	0.5	0.1	0.1	0.0	3.9	0.1	0.1	0.0	0.3	0.2	0.2	0.1	0.4	0.1	0.2	0.1	0.0	0.0	0.1	0.1	0.2	1.2	0.0	0.1	0.2	0.1	1.0	1.8	0.0
TMX	0.1	0.3	0.1	0.1	0.0	2.2	0.1	0.0	0.0	0.1	0.1	0.1	0.1	0.2	0.0	0.1	0.0	0.0	0.0	0.1	0.1	0.1	0.7	0.0	0.0	0.1	0.1	0.6	1.0	0.0
TRM	1.9	9.5	2.4	2.7	0.7	78.8	1.8	1.5	0.5	5.2	3.5	4.8	2.2	9.1	1.5	4.4	1.7	0.1	0.8	2.2	2.2	3.5	24.1	0.3	1.6	3.2	2.8	20.1	36.2	1.0

Figure 29. Relative potency factor matrix. For each substance, a multiple potency factor was calculated, which contains the effects of the respective substance on all measured analytes. For this purpose, confidence intervals were determined, which were normalized to the concentration of the respective pesticide used. In order to obtain relative potency factors (RPFs), all calculated values were related to each other. The matrix shows the calculation at the protein level. The RPFs of the substances used to generate the mixtures are encircled in black.

This matrix showed how the potency of a treatment behaved in comparison to the referenced one. In order to distinguish the similarities of the effects, a Pearson correlation was performed with the mRNA data only, since here, stronger effects were observed. The mixtures should represent four different classes: very strong, strong, moderate, and weak. The values of these classifications were:  $>0.9$ ,  $0.6-0.9$ ,  $0.3-0.6$ , and  $<0.3$ , respectively. In addition, it was investigated which of these substances are commercially available as combination products. Table 26 shows the information about the selected mixtures. The reference column shows to which particular substance the mixing partner was normalized.

Table 26. Selection of mixtures for the analysis of potential mixture effects. The mixtures were classified into four different groups based on their Pearson scores (mRNA). In addition, the RPFs were calculated using AdipoRed, mRNA, and protein data. The reference corresponds to the single substance to which the normalization was performed. The last column shows the products available on the market as mixtures.

Similarity	Pearson Score	Reference	Mixing partner	Relative potency				Product
				AdipoRed	mRNA	Protein	Applied	
Very strong	0.95	PPC	DIF	5.2	3.2	6.6	5	TASPA
Strong	0.89	AOS	DIF	5.8	6.5	4.0	5	ASKON
Moderate	0.48	THI	AOS	9.1	11.4	10.4	10	-
Weak	0.23	AOS	CC	0.3	0.6	0.7	0.5	Several

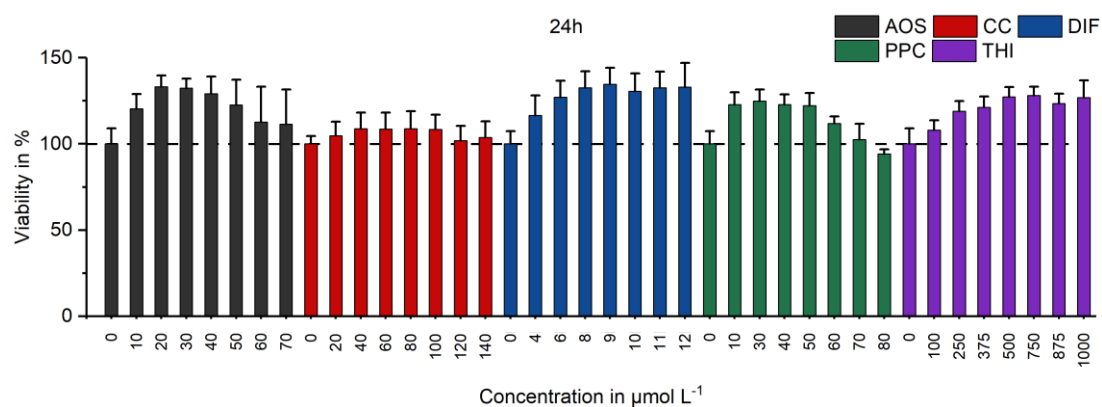
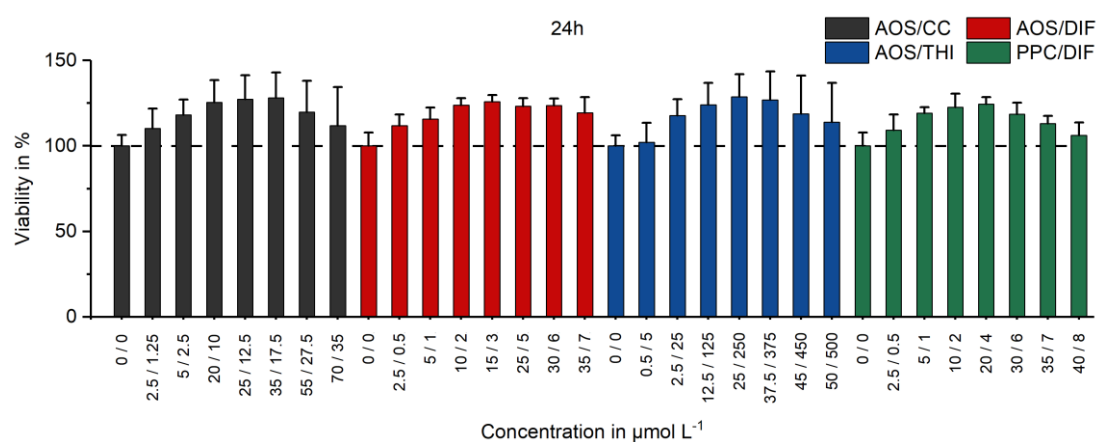
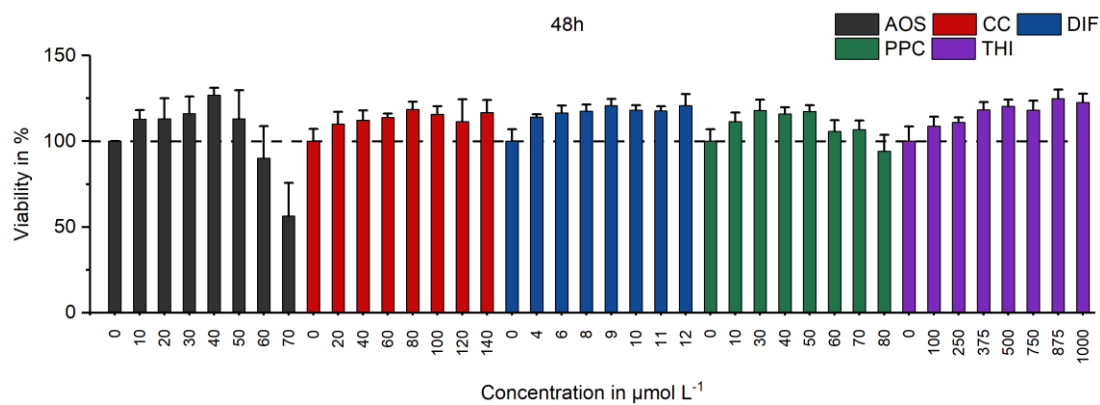
The results of the RPFs using the three different calculations with AdipoRed, mRNA, and protein data, showed slight differences. Therefore, it was decided to use the potencies closest to all three calculation paths. These are for the mixture PPC/DIF= 5; AOS/DIF= 5; THI/AOS= 10 and AOS/CC= 0.5. With these calculated values, an equi-potent ratio between the substances in the respective mixture should be obtained. Since the results of the treatment kinetics (4.2.3 Time-Dependency of Effects after Varying Pesticide Incubations) showed that after 24-hour treatment only few significant changes were observed and the number of significant changes was increased after 72 hours, it was decided that the duration of treatment to determine potential mixing effects should not only be 24 hours but additionally 48 and 72 hours. In addition, not only one concentration of the individual substance and the mixtures but concentration series should be investigated in order to determine concentration dependencies. The results of the individual treatment should be used as a reference for the mixture treatment. Hence, five different concentrations were prepared for

## Results

each substance and each mixture. The highest concentration should be the highest non-toxic concentration for the HepaRG cells.

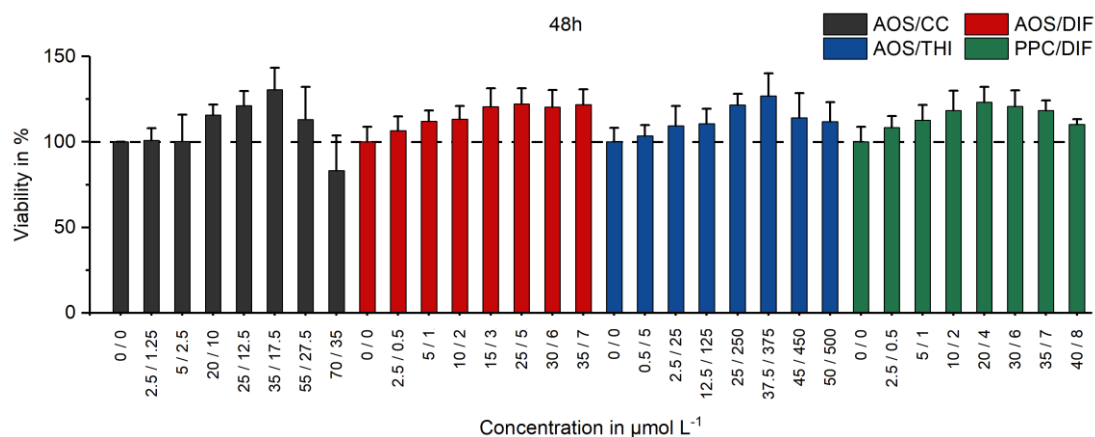
Therefore, the cytotoxicity of these individual substances, as well as in combination, were investigated. This was done, so changes in protein levels based on the cytotoxicity of the substance could be ruled out. To determine cytotoxic effects, a viability test was performed by Dr. Lichtenstein (BfR) as described in Luckert et al.<sup>96</sup> The cells were treated for either 24, 48, or 72 hours with the respective concentration series of the individual substances or mixtures. The measurements for each concentration were repeated nine times. The data were kindly provided by Dr. Lichtenstein. These data are shown in Figure 30. For the mixtures, the first concentration on the x-axis stands for the first substance in the legend.



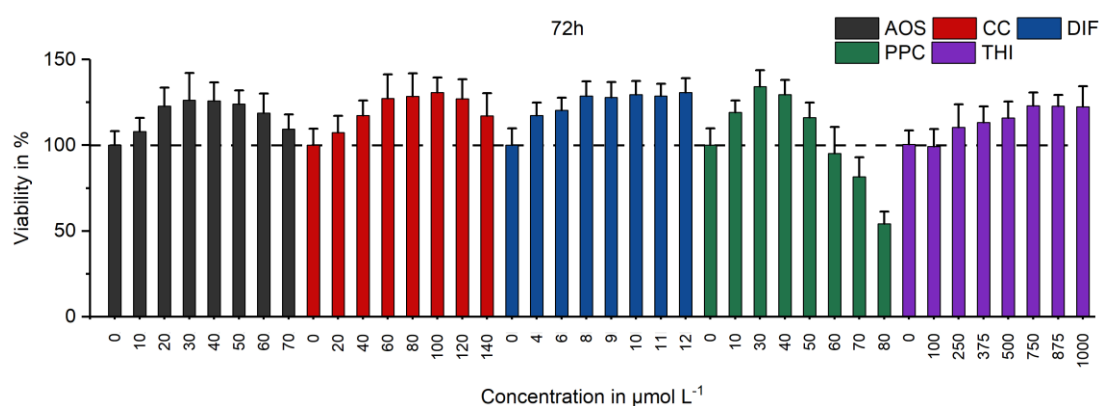
**A****B****C**

## Results

**D**



**E**



**F**

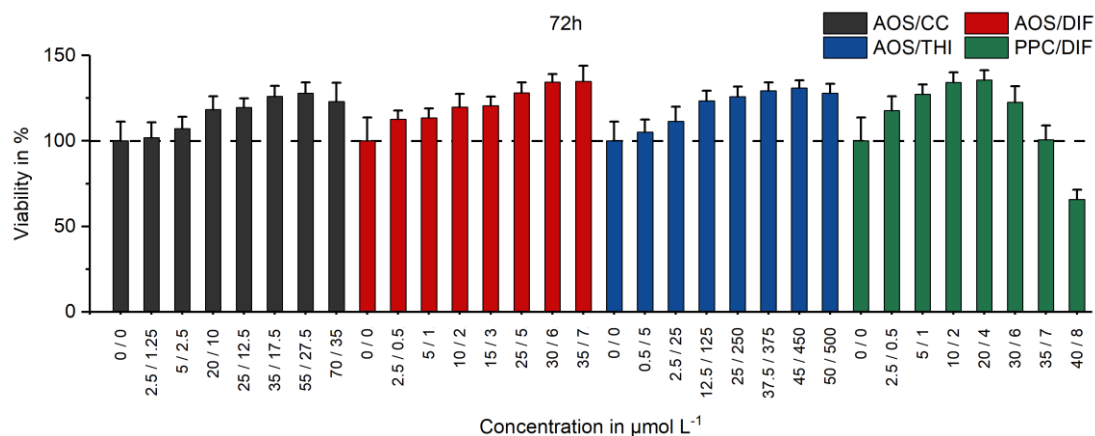


Figure 30. HepaRG cell viability after pesticide treatment. In (A), the viability after 24 hours of single treatment is shown. (B) shows the respective mixtures after 24 hours. (C) and (D) represent the 48-hour treatments and (E), (F) the 72-hour treatments. In the case of mixtures, the first concentration on the x-axis stands for the first respective substance in the legend. The dashed horizontal line indicates 100% viability, which represents the solvent control. Data were referred to the solvent control. Measurements for each treatment was performed nine times.

The data of the 24-hour treatment (A and B) showed no evidence of cytotoxic effects on the cells if 80% viability was set as threshold. This applies both to the individual

substances and to the mixtures thereof. Nevertheless, a trend towards cytotoxic effects can be observed after treatment with an increasing concentration of PPC. In contrast to the 24-hour treatment, cytotoxic effects can be observed at high concentrations after 48 hours of treatment with AOS and 72 hours of treatment with PPC and PPC/DIF. After 48 hours of treatment with  $70 \mu\text{mol L}^{-1}$  AOS, cell viability decreased to 56%. For single treatment with PPC (72 h), the viability decreased to 82% at  $70 \mu\text{mol L}^{-1}$  and to 54% at  $80 \mu\text{mol L}^{-1}$ . In the mixture PPC/DIF ( $40+8 \mu\text{mol L}^{-1}$ ), the viability decreased to 66%. Interestingly, no cytotoxic effects were observed after 72 hours of treatment with AOS.

#### 4.2.5 Analysis of HepaRG Cells Treated with Pesticide Mixtures

In Chapter 4.2.4 HepaRG Cell Viability after Treatment with Single Pesticides and Mixtures thereof, the selection of mixtures to be investigated was described. In addition to the mixtures, the individual substances were also examined with different concentrations in order to obtain reference values. Therefore, a concentration series consisting of five different concentrations were prepared for each mixture as well as for each substance, and HepaRG cells were treated for either 24, 48, or 72 hours. Experiments were independently performed three times with the respective pesticides and mixtures. As a prototypical inducer 6-(4-Chlorophenyl) imidazo [2,1-b][1,3] thiazole-5-carbaldehyde O-(3,4-dichlorobenzyl) oxime (CITCO), and as a negative control, DMSO-treated HepaRG cells were used. The total number in one replicate experiment was 141 (135 pesticide-treated samples, three CITCO-treated samples, and three negative controls). Table 9 and Table 10 (3.6 Samples) show the concentrations of the individual substances or the mixtures, respectively. Mean values were calculated from each of the three individual measured values, and then fold changes with respect to the negative control were determined. Afterward, the data were  $\log_2$  transformed. With these  $\log_2$  transformed data, four heat maps were generated as an overview for the four different mixtures with corresponding single substances covering all 27 quantified analytes. Each heat map contains all three treatment durations of 24, 48, and 72 hours and the five different concentrations, in ascending order from left to right, measured at each timepoint. The analytes were plotted on the y-axis, the treatments on the x-axis. Gray fields indicate that the values

## Results

for the respective protein were below the LLOQ, or no signal was detected. The results after 48 hours of treatment with the highest AOS concentration and the highest concentration after 72 hours of treatment with PPC and PPC/DIF showed cytotoxic effects on cell viability (viability below 80%, Figure 30). These results are shaded in gray in the following graphs.

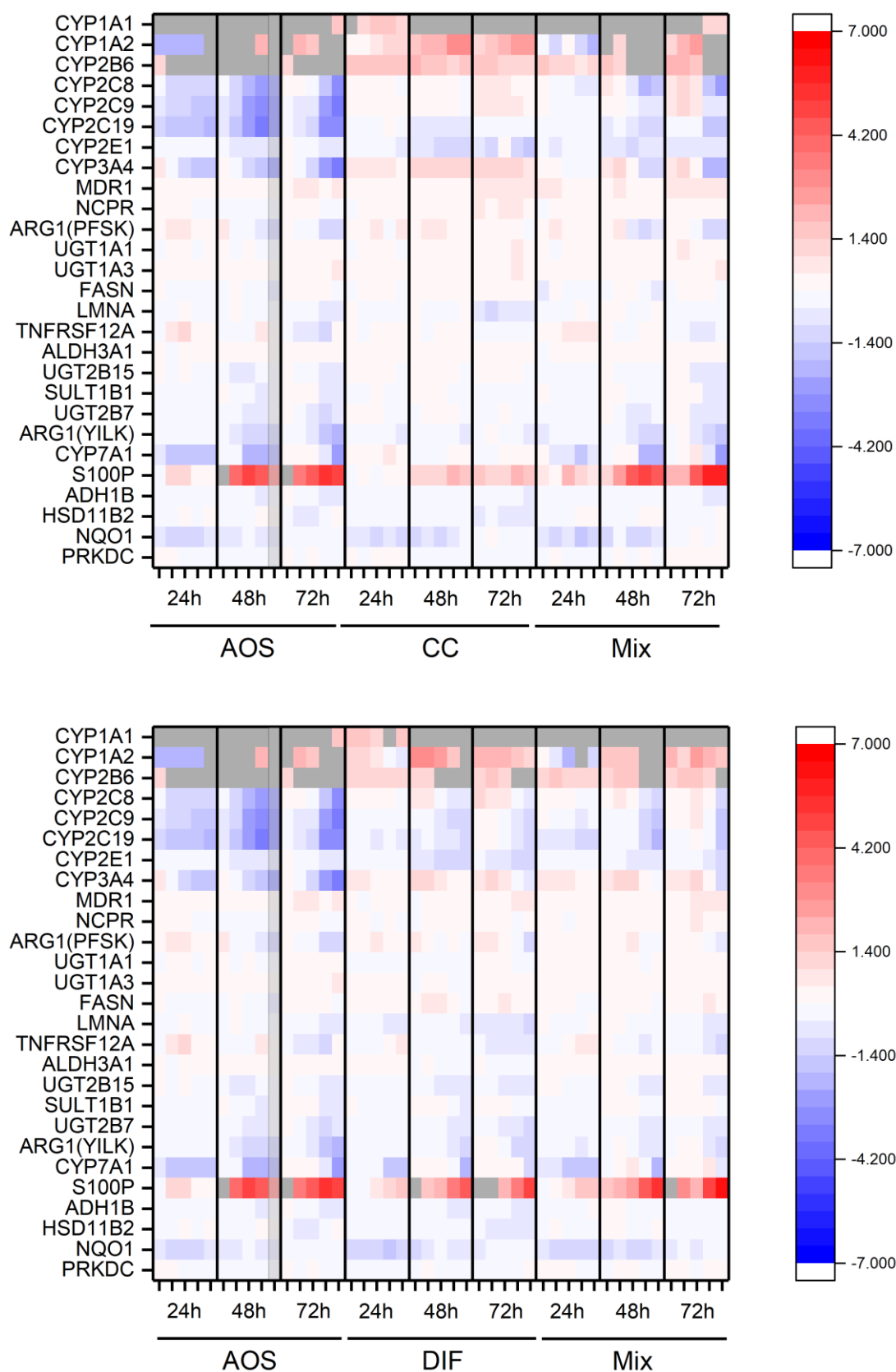


Figure 31. Protein abundance analysis in HepaRG cells treated with the mixture of AOS/CC and AOS/DIF. The upper graph shows the heatmap for the mixture of AOS/CC and respective single treatments; the lower graph the results for AOS/DIF. The concentrations at each timepoint are shown in ascending order from left to right ( $n=3$ ). Gray fields indicate that no evaluable value was obtained (either no endogenous signal or below lower limit of quantification). Shaded gray fields indicate that for this concentration, the cell viability was below 80%.

Results

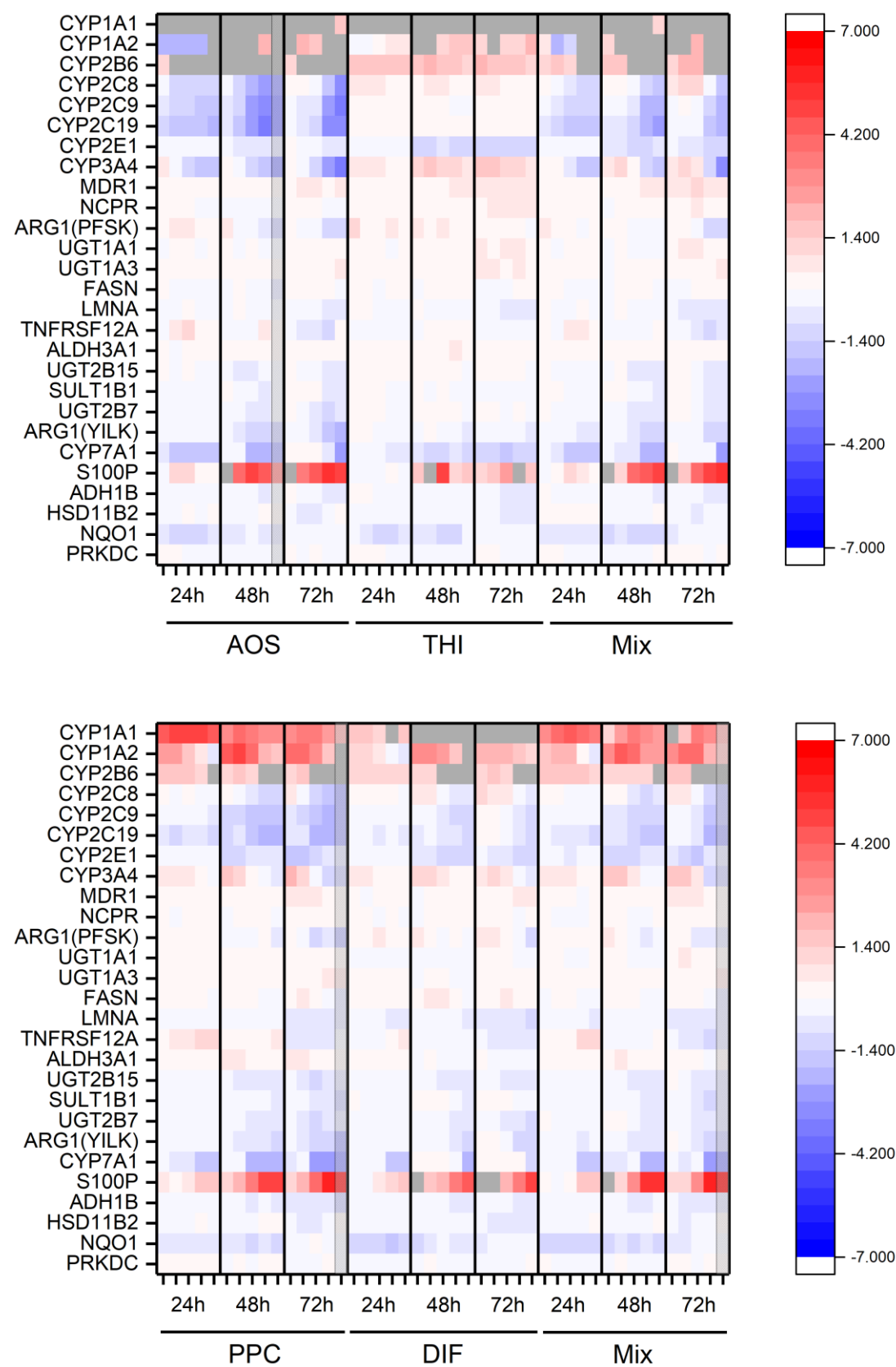


Figure 32. Protein abundance analysis in HepaRG cells treated with the mixture of AOS/THI and PPC/DIF. The upper graph shows the heatmap for the mixture of AOS/THI and respective single treatments; the lower graph the results for PPC/DIF. The concentrations at each timepoint are shown in ascending order from left to right (n=3). Gray fields indicate that no evaluable value was obtained (either no endogenous signal or below lower limit of quantification). Shaded gray fields indicate that for this concentration, the cell viability was below 80%.

Figure 31 and Figure 32 show the  $\log_2$  transformed data of the mixtures with the respective individual substances as a heatmap. The data of single substances such as azoxystrobin are the same for every heatmap. The scales were set to the same range so that a comparison could be made according to the intensity of colors. At first glance, it can be observed that the treatment with azoxystrobin generally had a stronger effect on protein abundance than the other single substances. In particular, CYPs show a stronger trend towards down-regulation. This is evident in CYP2C8, CYP2C9, CYP2C19, and CYP3A4. On closer examination of the results for CYP3A4 after treatment with AOS, it can be seen that there was a concentration dependency. With increasing pesticide concentration, the down-regulation becomes stronger. In addition, stronger repression could be observed after longer treatment times. Another interesting observation is the fact that S100P appears to be the only analyte that shows a strong trend towards up-regulation across all treatments. Treatment with AOS/CC, AOS/DIF, AOS/THI, and the respective single substances showed for CYP1A1 that only a few changes were observed. For most conditions except CC and DIF after 24 hours, no quantifiable results for CYP1A1 (marked by gray fields) were obtained. Interestingly, there was a strong induction effect after treatment with PPC and the mixture of PPC/DIF. For single treatment with PPC, the effect became weaker by increasing the duration of treatment.

Besides these four heatmaps,  $\log_2$  graphs were also generated for each analyte to provide a more in-depth insight into the regulation. The results for CYP3A4 and prelamin-A/C (LMNA) are shown in Figure 33 and Figure 34 as examples. The remaining graphs can be found in Figure 48-Figure 60 in the appendix (9 Supplementary Data). These two proteins were chosen because they clearly show time and concentration effects after pesticide treatment.

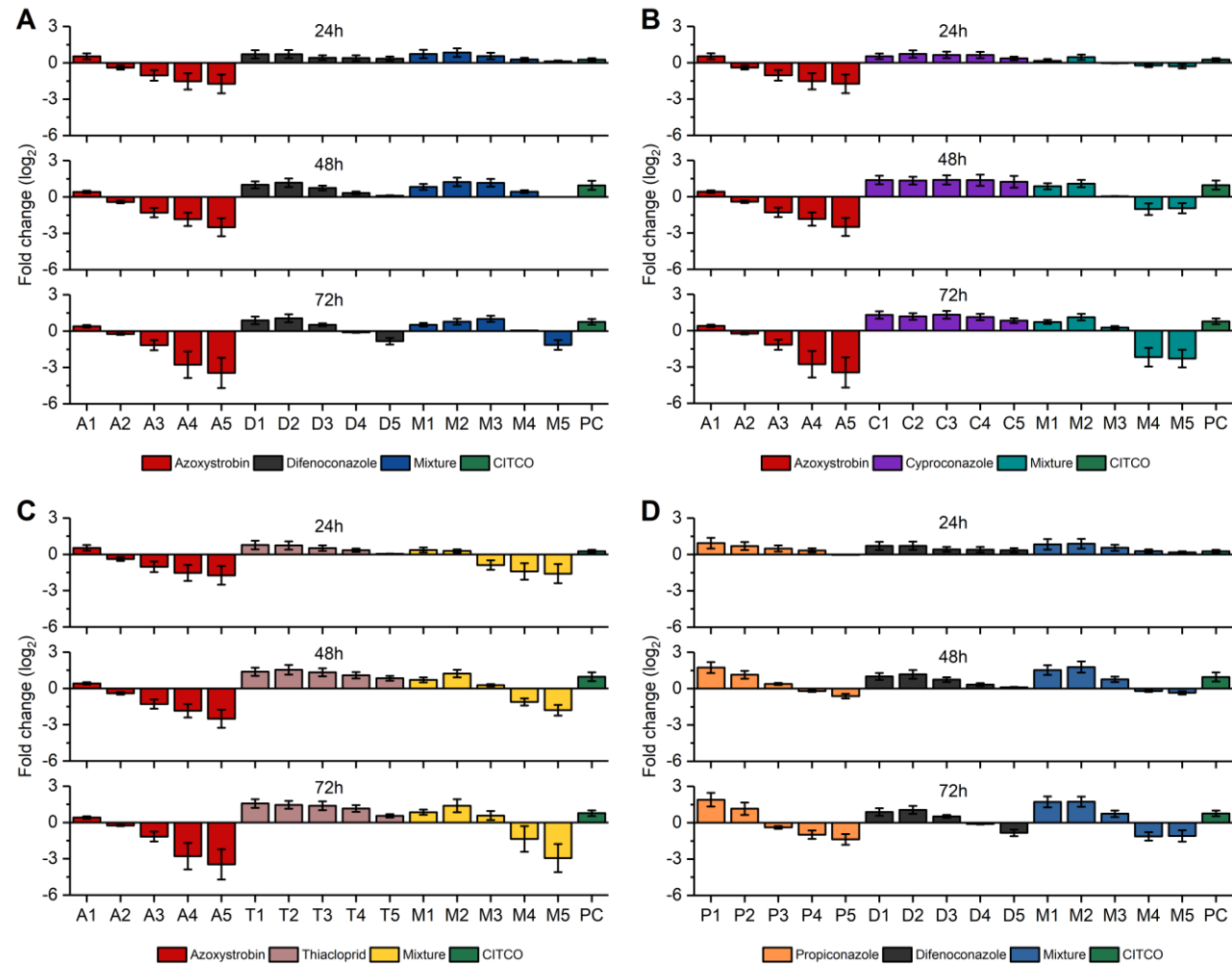


Figure 33. Results of potential mixture effects on CYP3A4 protein abundance in HepaRG cells. Log<sub>2</sub> transformed fold changes of single as well as mixture treatment with azoxystrobin and difenoconazole is shown in (A), azoxystrobin and cyproconazole in (B), azoxystrobin and thiacloprid in (C), and propiconazole and difenoconazole in (D); n=3. Concentrations of treatments can be found in Table 9 and Table 10.



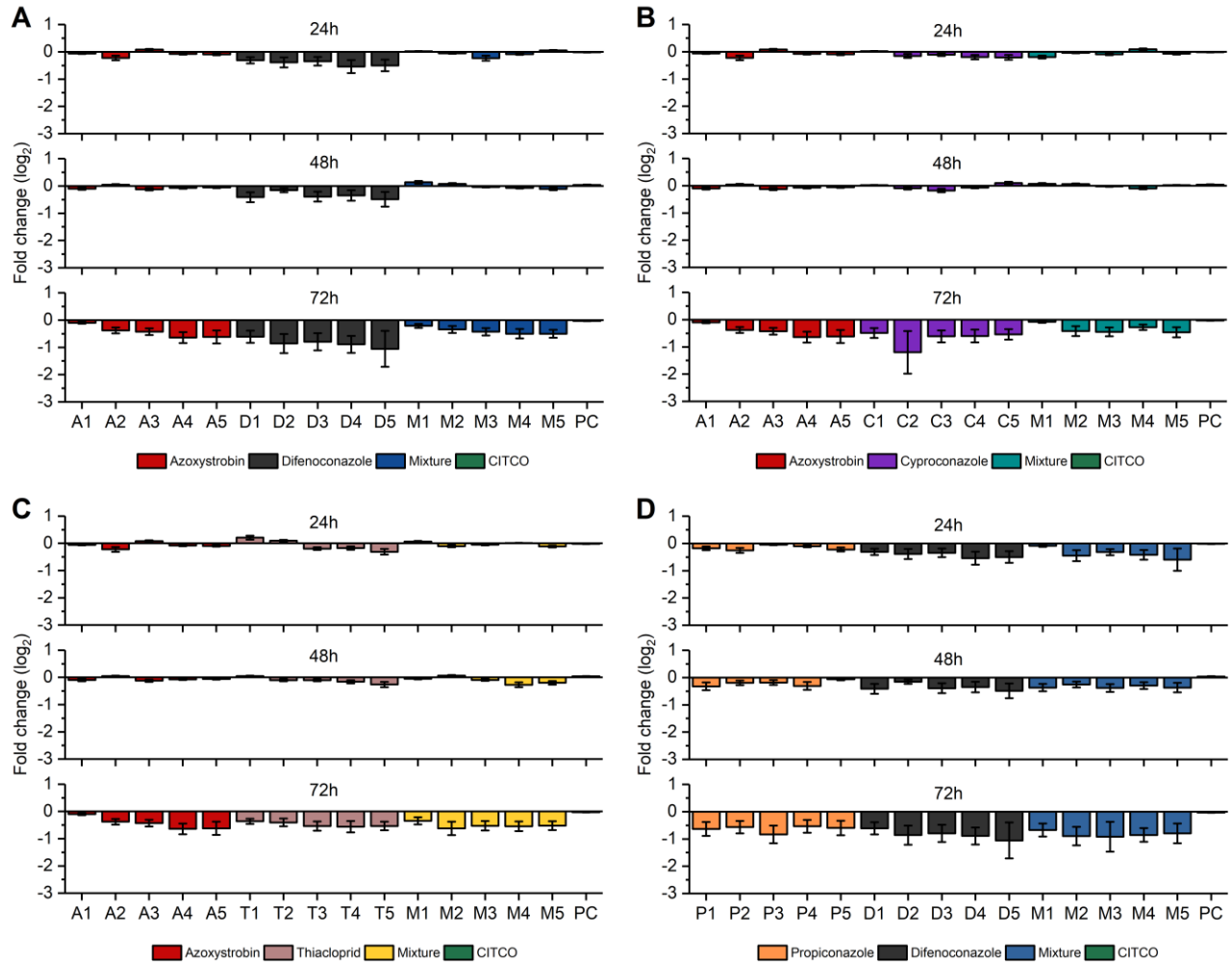


Figure 34. Results of potential mixture effects on LMNA protein abundance in HepaRG cells. Log<sub>2</sub> transformed fold changes of single as well as mixture treatment with azoxystrobin and difenoconazole is shown in (A), azoxystrobin and cyproconazole in (B), azoxystrobin and thiaploprid in (C), and propiconazole and difenoconazole in (D); n=3. Concentrations of treatments can be found in Table 9 and Table 10.

## Results

Figure 33 shows the results for CYP3A4. The concentration dependency indicated in the heatmap can also be clearly seen in this additional illustration. A concentration-dependent effect was present after the treatment with azoxystrobin (A1 lowest concentration; A5 highest concentration). The higher the concentration, the more the enzyme was down-regulated. This observation could also be made after treatment with propiconazole (P1-P5) and difenoconazole (D1-D5). In azoxystrobin- and propiconazole-treated samples, a change in the direction of regulation was detected after all treatment durations, for difenoconazole only after the 72-hour treatment. This change of effect direction could also be observed with the mixture treatment of AOS/DIF (72 h), AOS/CC, AOS/THI, and PPC/DIF (48 h; 72 h). Furthermore, the effect of different treatment durations could be observed in the treatment of azoxystrobin. The longer the treatment, the stronger was the down-regulation compared to the shorter periods. In total, the data for CYP3A4 revealed that out of 135 data points, 89 showed a significant change (less than -0.56 or greater than 0.56). In comparison, the results of LMNA show a lower concentration dependency. More notable is the effect of treatment time. After the 24-hour treatment, in most cases, hardly any effect is visible, whereas these effects become stronger with longer treatment. This can be seen particularly in Figure 34 (Part D). While 89 values for CYP3A4 indicated a significant change, only 21 values were found for LMNA. Of these 21 values, 20 were observed after 72 hours of treatment.

Both substances were chosen to show that not only the different concentrations used but also the treatment duration had an influence on protein abundance and direction of change. While significant changes in protein abundance for CYP3A4 were already observed after 24 hours of treatment, these effects could only be observed after 72 hours for LMNA. These results demonstrate that it was important not only to investigate one treatment timepoint, but several timepoints since the change in protein abundance was different for the analytes measured.

### 4.2.6 Multiple Linear Regression Analysis for the Determination of Combinatorial Effects

In order to discover whether combinatorial effects of pesticide treatments could be observed, the data obtained were used and further evaluated. Various models are used in the literature to determine whether there is a combinatorial effect, such as

antagonism, additivity, or synergism. A distinction is made between mixtures that follow the same mode of action (MOA) and mixtures that follow different MOAs. The most common and widely applied models are Loewe Additivity <sup>97</sup> (same MOA) and Bliss Independence <sup>98</sup> (dissimilar MOA), which are used in pharmacology to investigate mixing effects of drugs. The following formula describes the Loewe Additivity of a binary mixture. The effect concentration (EC<sub>x</sub>) of a mixture is determined. For the determination, the respective concentrations of substances A and B, which lead to an x% effect of the individual substances (EC<sub>xA</sub> and EC<sub>xB</sub>), are taken into account. If substance A and B are additive, the term for EC<sub>xmix</sub> becomes 1. The formula was adapted from Cedergreen <sup>99</sup>.

$$ECx_{mix} = \frac{c_A}{ECx_A} + \frac{c_B}{ECx_B} \quad (\text{adapted from Cedergreen } ^{99})$$

EC<sub>x</sub>= effect concentration of either mix, substance A or substance B causing an x% effect  
 c<sub>A</sub>= concentration of substance A  
 c<sub>B</sub>= concentration of substance B

If the substances in a mixture follow a different MOA, the Bliss Independence formula can be applied. Which is (formula adapted from Bliss <sup>98</sup>):

$$E_{mix} = E_A + E_B - E_A \cdot E_B \quad (\text{adapted from Bliss } ^{98})$$

The mixing effect (E<sub>mix</sub>) is calculated by the sum of the individual effects of substance A (E<sub>A</sub>) and B (E<sub>B</sub>) and the subtraction of the product of both effects.

However, these methods are based on the availability of dose-response curves. When determining dose-response dependencies, receptors are often explicitly targeted <sup>100</sup>. In this thesis, proteins were used as a readout for potential combinatorial effects. Compared to a specific receptor, this is a complex system that depends on different time-shifted processes: mRNA synthesis, presence of microRNA, biosynthesis of these proteins as well as protein degradation.

Due to this fact, both models are not practicable for the analytes used in this work, as the following example shows. In Figure 35, the graph for the analyte LMNA is shown after 24 hours of treatment with azoxystrobin. The mean amount in fmol µg<sup>-1</sup> was plotted against the azoxystrobin concentration used. The graph clearly shows

## Results

that after 24-hour treatment with AOS, no dose-response dependency could be observed, but that the values fluctuated around the value 30 fmol  $\mu\text{g}^{-1}$ . That means no effect concentration that causes an x% effect can be defined.

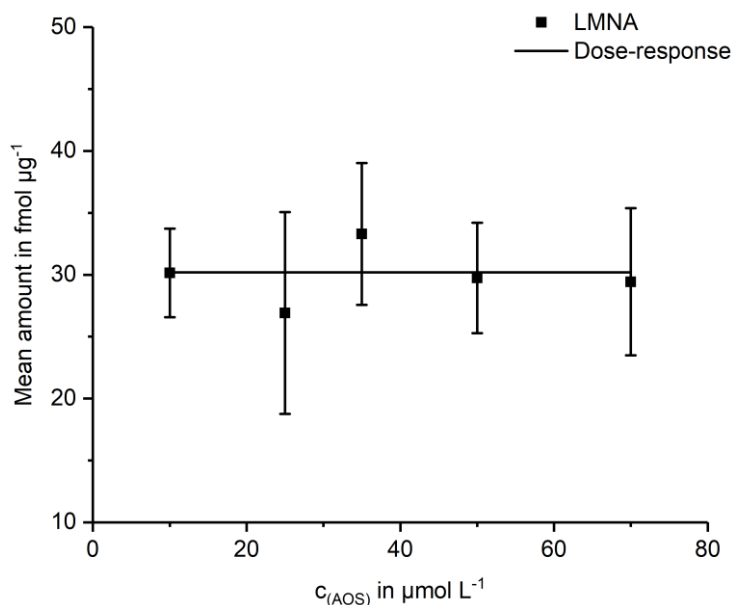


Figure 35. Dose-response plot of LMNA after 24-hour treatment with azoxystrobin. The mean amount in  $\text{fmol } \mu\text{g}^{-1}$  was plotted against the concentration in  $\mu\text{mol L}^{-1}$  of azoxystrobin (AOS) used. The treatment duration was 24 hours.

Since, in these cases, neither the Loewe Additivity nor the Bliss Independence could be applied, and because it is desirable to have an evaluation system with which all analytes can be evaluated equally, it was decided to conduct the evaluation in another way. Multiple linear regression analysis was used as the basis for this. Thus, a model prediction was made for all analytes based on the results of the individual substances, which is composed as follows:

$$y = p_1 c_{\text{(AOS)}} + p_2 c_{\text{(CC)}} + p_3 c_{\text{(DIF)}} + p_4 c_{\text{(THI)}} + p_5 c_{\text{(PPC)}} + p_6 \text{time} + \text{base level}$$

$p_{1-5}$ = coefficients for the respective treatments

$c_{\text{(substance)}}$ = applied concentration during a single treatment

base level= instrument noise consideration

time= treatment time of single substances (24, 48, or 72 hours)

If, for example, the model for the AOS/CC mixture is considered, the formula would change as follows, since the terms for  $c_{\text{(DIF)}}$ ,  $c_{\text{(THI)}}$  and  $c_{\text{(PPC)}}$  have a value of zero:

$$y = p_1 c_{\text{(AOS)}} + p_2 c_{\text{(CC)}} + p_6 \text{time} + \text{base level}$$

This model prediction was performed for each analyte using RStudio v.1.0.153. It needs to be mentioned that the highest concentrations of AOS after 48-hour treatment and PPC after 72-hour treatment were not considered for the modeling because the viability of the cells was below 80%. These multiple linear regression models were then used to compare them with the actual measured value of the mixture. This was done using the Model Deviation Ratio (MDR) described by Belden et al., where the predictive value was divided by the measured value <sup>101</sup>. For the determination of the MDR, the concentration causing a given effect (EC<sub>x</sub>) is usually used. Cedergreen applied the MDR for the evaluation of combinatorial effects and classified the MDR into the three following groups: MDR<0.5 antagonism, 0.5<MDR<2 additivity, and MDR>2 synergism <sup>99</sup>. This could not directly be transferred to our data since no EC<sub>x</sub> was determined by multiple regression analysis. However, the boundaries for the characterization of the effects were adopted. Thus, if the MDR was between 0.5 and 2, it was defined as an additive effect. Once the value was below 0.5 or above 2, it was either a synergistic or antagonistic effect. A distinction between the effects could only be made after considering the sign of the slope of the multiple regression parameters. This becomes apparent with the following schematic illustration (Figure 36).

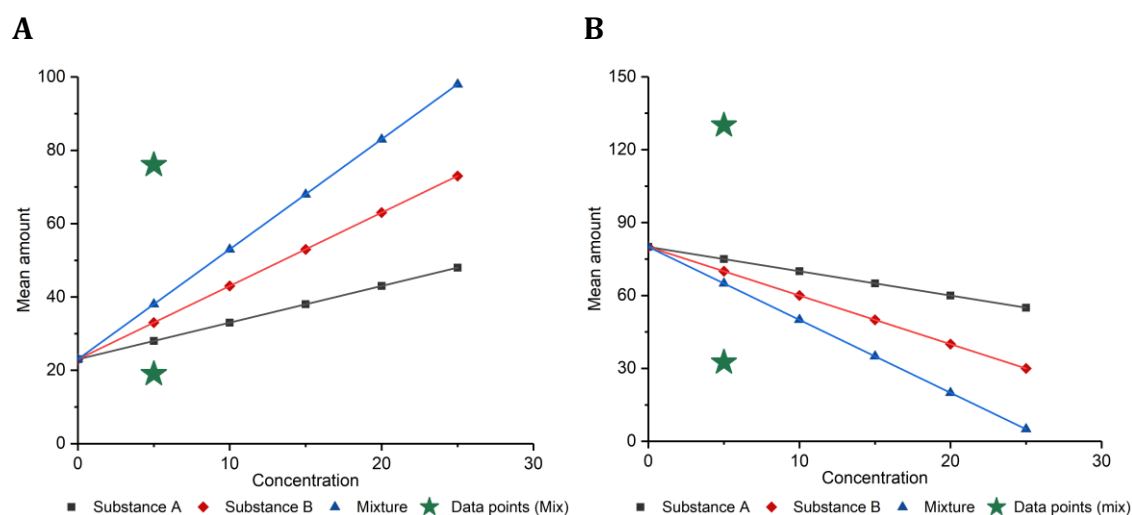


Figure 36. Two different schematic cases for determining a combinatorial effect. In the graphs, the red and black lines are the regression lines of the individual substances. The blue lines are the model predictions of the respective mixture. The green stars represent measured values after mixing treatments. In (A), all slopes are positive. This means that values smaller than 0.5 indicate a synergism. In (B), all slopes are negative, which means that values greater than 2 indicate a synergism.

## Results

In (A), the case is shown where both individual substances have a positive slope. This results in a model prediction for the mixture, which also increases with increasing concentration. The green stars represent theoretical measuring points after mixing treatment where the upper star indicates a synergism, the lower star an antagonism. Thus, if the MDR equation is used, an MDR for the upper value (synergism) of 0.5 is obtained (predicted value divided by the measured value). In example (B), the slopes of the regression lines are all negative. If the lower measured data point is considered, it also shows that there is a model deviation (synergism), but the MDR assumes a value of 2 in this case. In order to distinguish the effects of the values below 0.5 and above 2 for the respective analytes, the slopes of the regression line were taken into account. A limitation of the analysis by mixture model predictions was that some protein abundance values were below the respective LLOQ of the assays. In these cases, the value half of the LLOQ was used for the calculations. This was done for the following reasons. Firstly, this ensured that no negative MDR values were obtained, and secondly, this procedure was also applied to the evaluation of the raw data. Otherwise, MDRs across all analytes could not be obtained. The following table (Table 27) shows the slope directions of the regression lines for each analyte in the respective mixtures. Furthermore, it was entered whether a synergism or antagonism was present at values above 2 or below 0.5. In orange marked fields, the slopes have negative and positive values after single pesticide treatment. In these cases, a decision whether a synergistic or antagonistic effect was present is not applicable. It can only be said that MDR values greater than 2 or less than 0.5 indicate a significant deviation from an additive model.

Table 27. Slopes of regression lines and effects in the respective mixtures. For the ten analytes with values outside the boundaries, the directions of the regression line slopes were determined. These slopes were then used to decide which effect was present for the respective values. In orange fields, the calculated slopes for the single analytes had positive and negative values. In these cases, the decision of whether a synergistic or antagonistic effect was present is not applicable.

Analyte	AOS/CC			AOS/DIF			AOS/THI			PPC/DIF		
	Slope	Syn	Anta	Slope	Syn	Anta	Slope	Syn	Anta	Slope	Syn	Anta
ARG1(PFSK)	- / -	>2	<0.5	- / -	>2	<0.5	- / -	>2	<0.5	- / -	>2	<0.5
CYP1A1	- / -	>2	<0.5	- / -	>2	<0.5	- / -	>2	<0.5	+ / -	na	na
CYP1A2	- / -	>2	<0.5	- / -	>2	<0.5	- / -	>2	<0.5	- / -	>2	<0.5
CYP2B6	- / +	na	na	- / -	>2	<0.5	- / +	na	na	- / -	>2	<0.5
CYP2C8	- / -	>2	<0.5	- / -	>2	<0.5	- / +	na	na	- / -	>2	<0.5
CYP2C9	- / +	na	na	- / -	>2	<0.5	- / +	na	na	- / -	>2	<0.5
CYP2C19	- / -	>2	<0.5	- / -	>2	<0.5	- / +	na	na	- / -	>2	<0.5
CYP3A4	- / -	>2	<0.5	- / -	>2	<0.5	- / -	>2	<0.5	- / -	>2	<0.5
CYP7A1	- / +	na	na	- / -	>2	<0.5	- / -	>2	<0.5	- / -	>2	<0.5
S100P	+ / +	<0.5	>2	+ / +	<0.5	>2	+ / +	<0.5	>2	+ / +	<0.5	>2

Syn= Synergism; Anta= Antagonism; na= not applicable

## Results

To get a first impression of the distribution, all obtained MDRs were used to create a histogram. The class width was set to 0.1. Figure 37 depicts the histogram containing the MDRs of all measured analytes.

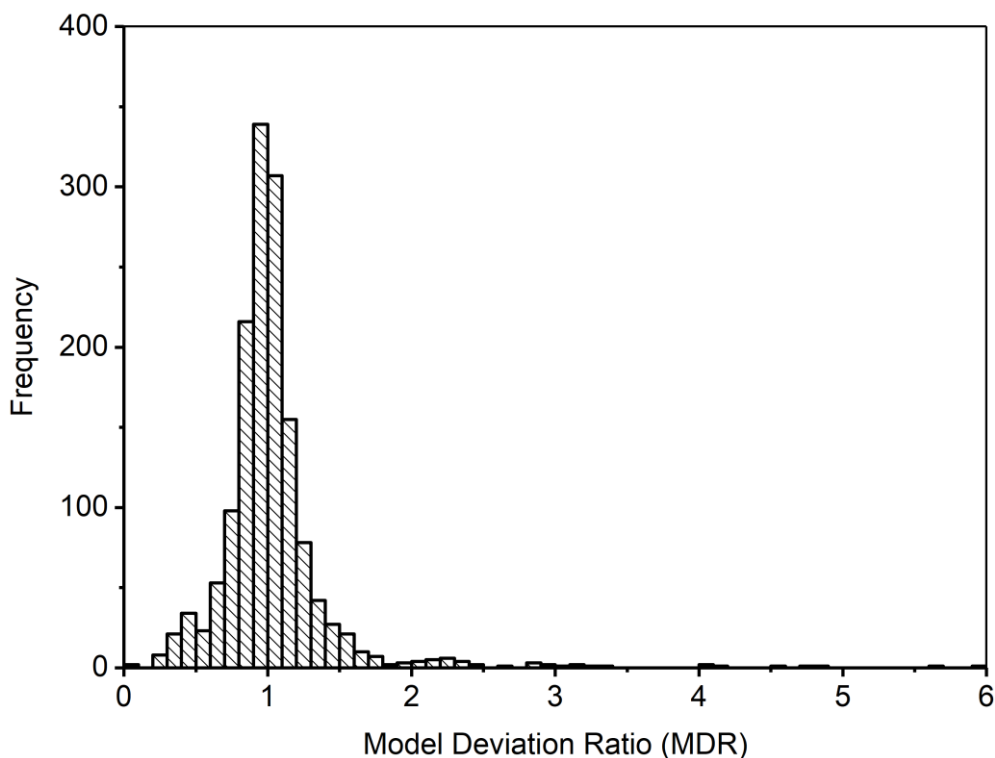


Figure 37. Histogram of Model Deviation Ratios. Predicted model values were divided by measured values of mixtures. The distribution of the determined Model Deviation Ratios (MDR) for all measured analytes are shown in this histogram. The class width was set to 0.1.

A total of 1486 data points were obtained. The results for the highest concentration after 72 hours of treatment with PPC/DIF were not considered, as viability was below 80% (Figure 30). The distribution clearly shows that most values were between 0.5 and 2, which means that most combinatorial treatments resulted in additive effects. There, most values were found between the class width of 0.9 and 1.0 (339 data points). More interesting, however, are the values observed below 0.5 and above 2. Therefore, these results were examined more closely. A total of 65 values below 0.5 and 40 values above 2 were determined. The minimum value was 0.0005 at the highest concentration of the AOS/THI mixture after 24 hours for CYP3A4. On the other hand, the highest value of 5.92 was observed at the highest concentration of AOS/THI after 24 hours for S100P. The mixture with most values outside these thresholds was AOS/DIF at the highest concentration level after 24 hours of treatment. Of these seven values, six were below 0.5. Most model deviations outside the



thresholds were obtained for S100P with 29 values, followed by CYP2B6 with 21 and CYP1A2 with 17 values. The values for S100P are distributed in approximately equal parts below and above both thresholds (16 values below 0.5; 13 values above 2).

While the values of the model deviation for CYP1A2 and CYP3A4 are also distributed above 2 and below 0.5, there are other analytes, such as CYP2B6 and CYP7A1, for which only model deviations below 0.5 were obtained (21 and 6 respectively). In total, values outside the thresholds were observed in 10 of the 27 analytes examined. Of these ten analytes, eight were from the cytochrome P450 family. The MDRs for all analytes are shown in the following matrix (Figure 38). The mixtures are shown in rows, the MDRs of the respective analytes in columns. A red-white-blue color scale was used to identify trends in the respective mixtures. Blue fields indicate trends towards values below 0.5, red fields towards values above 2. The results for the highest concentration of PPC/DIF after 72 hours of treatment were crossed out because the viability was below 80%.

		Model Deviation Ratios of analytes																										
		CYP1A1	CYP1A2	CYP2B6	CYP2C8	CYP2C9	CYP2C19	CYP2E1	CYP3A4	MDR1	NCPY	ARG1(PFSK)	UGT1A1	UGT1A3	FASN	LMNA	TNFRSF12A	ALDH3A1	UGT2B15	SULT1B1	UGT2B7	ARG1(YLK)	CYP7A1	S100P	ADH1B	HSD11B2	NQO1	PRKDC
Mixtures	PPC+DIF_24-1	1.04	0.80	0.97	1.04	1.09	1.16	1.16	0.94	0.92	1.00	1.11	0.98	0.90	1.09	1.07	0.95	1.04	1.11	1.09	1.01	1.05	1.22	0.87	1.14	1.07	1.13	0.98
	PPC+DIF_24-2	0.61	0.59	0.84	1.00	0.95	1.16	1.19	0.82	1.00	1.07	1.12	1.00	0.95	1.00	1.33	1.07	1.02	1.10	1.10	1.02	1.16	1.00	0.99	1.10	1.08	1.13	1.02
	PPC+DIF_24-3	0.46	0.57	0.29	0.98	0.89	1.04	1.15	0.84	1.01	1.19	1.14	1.03	0.92	1.01	1.12	0.88	1.01	1.00	1.05	0.97	1.02	0.35	2.34	1.00	1.03	1.07	1.03
	PPC+DIF_24-4	0.56	1.28	0.32	0.94	0.65	0.85	0.86	0.77	1.21	1.06	1.00	1.03	1.04	1.22	1.09	0.61	0.99	0.83	0.97	0.82	0.92	1.53	0.95	1.00	1.04	1.06	1.06
	PPC+DIF_24-5	0.81	2.25	0.45	0.70	0.43	0.77	0.79	0.56	1.10	0.95	0.72	0.88	0.98	1.30	1.12	0.67	0.89	0.60	0.87	0.67	0.67	2.19	0.87	0.93	1.00	1.04	1.04
	PPC+DIF_48-1	2.29	1.20	0.94	0.91	1.23	1.25	1.29	0.71	0.92	1.00	0.79	0.95	1.02	0.93	1.11	1.11	0.94	1.06	1.04	0.93	0.98	1.42	1.08	1.04	1.49	1.01	1.01
	PPC+DIF_48-2	1.04	0.50	0.86	0.85	1.17	1.10	1.31	0.55	0.93	1.00	1.15	0.96	1.01	0.80	0.99	1.13	0.86	0.97	1.00	0.84	0.89	1.16	2.64	1.03	1.07	1.04	0.96
	PPC+DIF_48-3	0.67	0.55	0.42	1.31	1.22	1.19	1.36	0.92	1.01	1.08	1.14	1.04	1.05	0.94	0.99	1.23	0.88	1.12	1.21	1.05	1.18	0.77	1.55	1.23	1.15	1.39	1.08
	PPC+DIF_48-4	0.88	1.22	0.49	1.65	1.14	1.42	0.90	1.45	1.09	1.07	1.44	1.00	0.98	1.33	0.84	1.26	1.01	0.89	1.35	0.96	1.13	0.45	1.11	1.09	1.00	1.06	1.06
	PPC+DIF_48-5	1.26	0.69	0.73	1.07	0.74	1.18	0.70	1.20	1.12	1.00	1.13	0.98	1.00	1.46	0.79	1.19	0.91	0.65	1.11	0.80	0.79	0.55	0.90	0.87	1.22	0.97	0.97
	PPC+DIF_72-1	1.24	0.73	0.73	1.05	1.07	1.13	0.60	0.90	1.03	0.79	0.92	0.92	0.84	1.25	0.80	0.89	0.89	0.97	0.90	0.80	1.03	3.22	0.90	0.81	1.32	0.94	0.94
	PPC+DIF_72-2	1.28	0.53	0.37	0.83	1.11	1.08	1.54	0.55	0.89	0.93	0.74	0.85	0.91	0.80	1.39	1.10	1.00	0.94	0.98	0.89	0.82	1.14	4.05	1.06	1.04	1.16	0.95
	PPC+DIF_72-3	0.43	0.35	0.35	1.32	1.23	1.08	1.80	0.94	0.92	1.12	1.31	1.06	1.03	0.82	1.29	1.10	0.89	1.27	1.16	1.22	1.28	0.78	1.96	1.31	1.00	1.04	1.03
	PPC+DIF_72-4	0.58	0.81	0.35	2.26	2.03	2.14	0.83	2.86	1.23	1.07	1.50	0.97	0.94	1.51	1.10	1.53	1.11	1.01	1.68	1.18	1.36	0.36	1.09	1.00	1.02	0.90	0.90
	PPC+DIF_72-5	1.30	0.80	0.35	2.12	1.29	1.66	0.63	2.23	1.19	1.14	1.25	0.91	0.77	1.66	0.94	1.39	0.88	0.65	1.29	0.82	1.07	0.31	0.96	0.85	0.91	0.87	0.87
	AOS+DIF_24-1	2.19	0.98	0.97	0.97	1.28	1.12	1.12	0.95	0.98	0.94	1.17	0.96	0.98	0.95	1.00	1.06	1.04	1.04	1.06	1.17	1.15	1.23	0.42	1.08	1.03	1.07	0.96
	AOS+DIF_24-2	3.01	0.77	0.94	0.95	1.25	1.09	0.79	0.79	0.92	0.99	1.11	0.96	0.97	0.89	1.02	1.23	1.08	1.02	1.02	1.15	1.06	1.09	1.03	0.97	0.93	1.36	0.99
	AOS+DIF_24-3	0.41	0.88	0.92	1.13	1.09	1.13	0.71	0.87	1.02	1.09	0.92	0.96	0.96	1.11	1.07	1.07	1.07	1.04	1.08	1.17	1.11	1.44	1.07	1.07	1.11	0.94	1.03
	AOS+DIF_24-4	0.40	0.75	0.68	1.04	1.00	1.00	0.45	0.91	0.94	0.83	0.94	0.96	1.14	0.92	0.67	0.96	0.93	1.00	1.04	0.95	1.39	0.96	1.01	1.34	1.01	1.04	0.93
	AOS+DIF_24-5	0.47	0.42	0.42	0.32	0.45	0.90	0.03	1.08	0.85	0.75	0.85	0.96	1.18	0.77	0.65	0.90	0.69	0.92	0.83	0.66	2.23	0.80	1.01	1.16	0.99	1.01	0.99
	AOS+DIF_48-1	3.35	0.93	0.87	0.87	0.91	0.77	1.08	1.05	0.90	1.08	0.92	0.95	1.00	0.79	1.02	1.08	0.88	0.95	0.99	0.87	0.95	1.20	0.89	0.87	1.41	1.03	1.03
	AOS+DIF_48-2	1.98	0.34	0.56	0.67	0.76	0.77	0.70	0.84	0.80	0.91	0.92	1.00	0.85	0.79	1.10	1.03	0.79	0.85	0.97	0.72	0.63	1.44	0.88	0.90	1.17	0.90	0.90
	AOS+DIF_48-3	1.81	0.38	0.65	0.61	0.70	0.93	0.61	0.89	0.84	0.76	0.92	0.98	0.80	0.82	1.27	1.01	0.95	0.77	1.03	0.75	0.50	1.62	0.88	1.04	1.53	0.93	0.93
	AOS+DIF_48-4			1.01	0.81	0.90	1.14	0.62	0.87	0.80	1.03	0.97	1.03	0.81	0.77	1.57	1.00	1.04	0.94	1.14	1.06	0.63	0.66	0.98	1.02	1.59	1.01	1.01
	AOS+DIF_48-5			0.78	0.59	0.97	0.93	0.30	0.86	0.82	0.94	0.91	1.00	1.10	0.72	1.27	0.92	0.76	1.01	0.98	0.82	0.82	0.43	0.91	0.90	1.16	0.97	0.97
	AOS+DIF_72-1	1.78	0.87	0.93	1.00	0.92	0.79	1.31	1.11	0.99	0.82	1.08	1.01	1.08	0.91	0.91	0.81	1.18	0.98	0.89	0.96	0.90	0.86	0.84	0.85	1.48	0.92	0.92
	AOS+DIF_72-2	2.05	0.36	0.82	0.88	0.93	0.77	0.96	1.14	1.06	0.76	0.98	0.97	0.97	0.96	0.86	1.16	0.89	0.73	0.96	0.72	0.71	1.09	0.81	0.89	1.14	0.90	0.90
	AOS+DIF_72-3	0.47	0.38	0.60	0.55	0.53	0.64	0.70	0.95	0.81	0.65	0.87	0.93	0.79	0.97	0.91	1.09	0.83	0.70	0.83	0.65	0.54	2.43	0.77	0.98	1.18	0.95	0.95
	AOS+DIF_72-4	0.23	0.46	0.69	0.59	0.60	0.79	0.93	0.99	0.83	0.88	0.91	0.99	0.70	0.93	1.27	0.93	1.06	0.71	0.96	0.92	0.41	0.65	0.76	0.96	1.06	0.87	0.87
	AOS+DIF_72-5	0.36		1.27	0.81	0.93	1.05	1.09	0.92	0.88	1.23	0.87	1.03	0.85	0.84	1.52	0.94	0.94	0.89	1.02	1.16	0.74	0.32	0.90	0.86	0.95	0.82	0.82
	AOS+THI_24-1	1.83	1.00	1.11	1.14	1.33	1.04	1.34	0.82	0.88	0.98	0.97	0.98	0.97	1.00	0.94	1.02	1.04	0.87	0.99	1.14	1.13	0.42	0.91	0.85	0.92	0.91	0.91
	AOS+THI_24-2		0.84	1.27	1.31	1.55	1.08	1.11	0.91	0.99	0.99	1.06	1.02	0.95	1.09	1.23	1.06	1.16	0.96	1.13	1.22	1.20	0.74	1.08	0.93	1.05	0.96	0.96
AOS+THI_24-3	1.68	0.49	1.40	1.41	2.05	1.10	1.63	0.94	0.93	1.05	0.98	0.96	1.11	1.01	0.74	1.03	1.17	0.94	1.10	1.02	1.09	1.06	0.97	0.93	1.05	1.05	1.05	
AOS+THI_24-4			1.13	1.20	1.77	0.94	1.09	1.06	1.02	0.99	0.97	1.08	1.08	0.98	0.96	0.75	0.95	1.07	0.96	1.05	0.88	2.96	0.87	0.84	1.00	1.05	1.05	
AOS+THI_24-5			0.67	0.58	1.19	0.83	0.00	1.08	1.04	0.78	1.01	1.06	1.05	0.96	1.04	0.91	0.94	0.80	0.92	0.66	5.92	0.84	0.95	0.91	1.02	1.02	1.02	
AOS+THI_48-1	4.16	0.96	1.05	1.02	1.12	0.92	1.29	1.07	1.07	1.18	1.10	1.09	1.13	0.93	1.06	1.16	1.07	0.93	0.98	1.01	1.11	0.95	0.96	0.96	1.50	1.03	1.03	
AOS+THI_48-2		0.72	0.78	0.84	1.01	0.90	0.72	0.86	0.88	1.10	1.03	1.10	1.01	0.83	1.28	1.02	0.93	0.89	0.94	0.93	1.01	2.31	0.96	0.99	1.17	1.00	1.00	
AOS+THI_48-3			0.85	0.91	1.37	1.24	1.00	0.86	1.04	1.43	1.07	1.11	0.89	0.89	1.61	1.02	1.32	1.03	1.18	1.14	0.73	0.80	1.05	1.17	1.39	0.98	0.98	
AOS+THI_48-4			1.39	1.52	2.22	1.14	1.52	0.90	1.03	1.07	1.07	1.14	0.84	0.96	1.45	1.00	1.20	1.13	1.22	1.10	0.65	1.09	1.06	1.40	1.00	1.00	1.00	
AOS+THI_48-5	0.44		1.19	1.15	2.27	0.86	0.71	0.95	1.09	1.11	1.06	1.10	1.11	0.88	0.97	1.07	1.13	1.13	1.16	0.87	0.66	1.06	0.95	1.24	0.95	0.95	0.95	
AOS+THI_72-1			1.01	0.87	1.28	0.97	0.85	1.13	0.85	1.07	0.83	1.01	0.93	1.18	1.03	0.70	1.06	0.93	0.88	0.92	0.97	0.85	0.83	0.83	1.21	0.80	0.80	
AOS+THI_72-2		0.27	0.56	0.89	0.86	0.96	0.65	0.82	0.99	0.84	0.86																	

Additionally, graphs for CYP3A4 and S100P are shown exemplarily as dot plots. The MDRs were plotted against the concentrations at the respective timepoint of treatment. Thereby is one the lowest and five the highest concentration. The upper graph shows the results for CYP3A4, the lower graph for S100P.

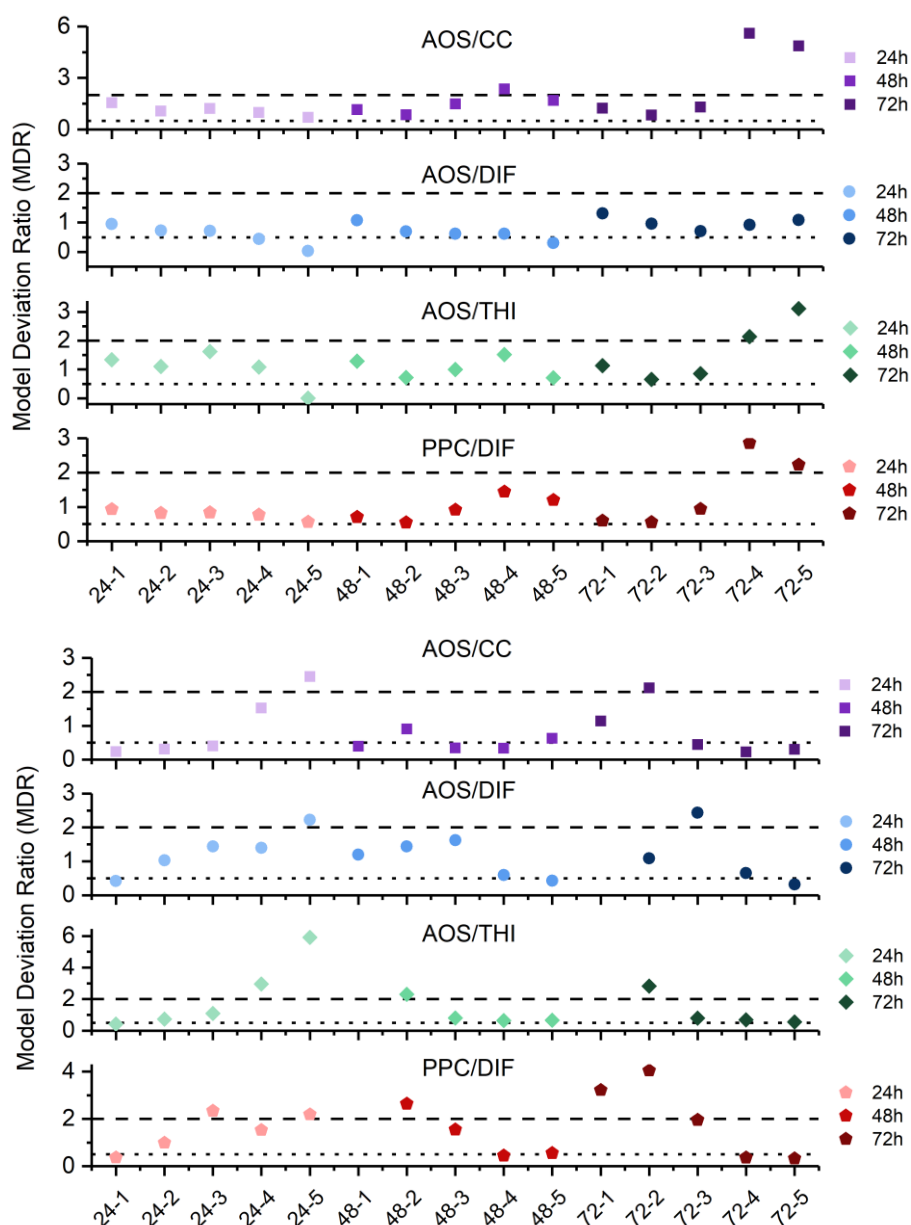


Figure 39. Model Deviation Ratios for CYP3A4 and S100P. The upper graph shows the results for CYP3A4, the lower graph for S100P. Model Deviation Ratios (MDRs) are plotted against the respective concentration at each timepoint of treatment. Values above the dashed horizontal line and values below the dotted line indicate either synergistic or antagonistic effects. Values between both thresholds show an additive effect. The data for the highest concentration after 72-hour treatment with PPC/DIF are shown but are not reliable as the viability was below 80%.

These two analytes were selected as examples since, in both cases, the change in the MDRs over the different concentrations, as well as after different treatment times,

is clearly visible. Here it can be observed that combinatorial effects, such as synergism and antagonism, can be concentration-dependent, and therefore it was necessary to investigate several concentrations. Looking at the upper graph (CYP3A4), it can be seen that most values are between 0.5 and 2. These values indicate additivity between the two substances in the mixture. In addition, it can be observed that concentration dependencies exist. This can especially be seen in all mixtures after 24-hour treatment. The higher the concentration, the lower the MDR. It can also be seen that the MDRs for the mixtures AOS/CC, AOS/THI, and PPC/DIF increase sharply at concentrations four and five, and are above the threshold of two. Considering the table of slopes (Table 27), it can be noted that values above 2 indicate synergistic effects, and values below 0.5 indicate antagonistic effects. This means that, after 24 hours of treatment, with increasing concentrations, the trend is towards antagonism, while apparent synergistic effects can be seen at high concentrations after 72 hours of treatment.

Considering the lower graph (S100P), the concentration dependency after 24 hours of treatment is also recognizable. In this case, however, the direction of the MDRs is reversed. With increasing concentration, the values move in the upward direction. After 48 and 72 hours of treatment, this effect is reversed again. After longer treatment times, the MDR decreases with the increasing concentration. Referring again to Table 27, it can be said that for all mixtures, all values above 2 indicate an antagonism, all values below 0.5 a synergism. This means that after 24 hours of treatment in the low concentrations, synergistic effects can be observed, which move towards antagonism with increasing concentration. However, this changes after 48-hour and 72-hour treatment. After these treatment periods, the trend is towards synergism with increasing concentration, as observed for CYP3A4.



## 5 Discussion

### 5.1 Development of Immunoaffinity-Based Mass Spectrometry Assays

Before the analysis and quantification of toxicologically relevant liver proteins using immunoaffinity-based mass spectrometry assays, it was necessary to investigate method parameters to ensure the reliability of these assays. This includes, for example, determination of the dynamic ranges, optimal proteolysis time, or the optimization of the antibody-protein ratio. For the discovery of new biomarkers in proteomics approaches, shotgun experiments are usually performed <sup>74</sup>. However, in this thesis, the selection of potential markers has already been made by the German Federal Institute for Risk Assessment (BfR) based on mRNA results discovered previously (e.g., in Seeger et al.<sup>39</sup>). Since some of these analytes, such as HULC <sup>102</sup> or NEAT1 <sup>103</sup>, which are non-protein-coding genes and therefore unsuitable for mass spectrometric analysis of toxicologically relevant liver proteins, this selection of analytes was modified. The modified list of analytes is shown in Table 14.

This list was used as a starting point for a detailed database search for suitable peptides. Prior to the search, criteria were established that the peptides should meet in order to be considered reliable. The first criterion was that the peptide should be proteotypic, meaning that this peptide only exists in one protein and no other. The uniqueness of the peptide is essential to make reliable statements about the quantification. The sequence should also not contain methionine (prone to oxidation) <sup>104</sup>, N-terminal glutamic acid (prone to cyclization) <sup>105</sup>, and, if possible, cysteine (prone to oxidation) <sup>106</sup>. The presence of modifications or natural variants within the sequence was also investigated. Another characteristic that was considered was the hydrophobicity factor. It was decided that only analytes with a factor less than 2.8, if possible, should be used to minimize or prevent potential problems within chromatographic separation. Krokhin et al. determined retention coefficients for individual amino acids of tryptic peptides <sup>107</sup>. Based on these results, hydrophobicity factors were calculated for each peptide. After all these parameters had been investigated, it was additionally checked whether the peptide had already been detected in other liquid chromatography-mass spectrometry (LC-MS) experiments. This was

done with the help of proteomicsDB, a database developed by a working group of the Technical University of Munich (TUM) <sup>87</sup>.

For the entire database search, UniProt <sup>90</sup>, a TXP-tool (internal bioinformatics tool of Dr. Hannes Planatscher, Signatope GmbH, Germany; used for the investigation of peptide proteotypicity) and the proteomics database (proteomicsDB <sup>87</sup>) were used. In order to test whether these analytes were directly measurable from HepaRG cells, in-gel digestion was performed, and the samples were measured with a full-scan method (Full-MS / ddMS<sup>2</sup>). Untreated and prochloraz-treated HepaRG cells were used as samples. The results in Table 19 show that in this experiment, between 2570 and 2907 proteins and between 11705 and 13125 peptides could be identified using Proteome Discoverer 2.1 (Thermo Fisher Scientific, Waltham, USA). The number of identified proteins or peptides depends strongly on the sample to be examined, sample preparation, as well as on the mass spectrometers used and the parameters set. In an experiment by Tascher et al., a secretome analysis with HepaRG cells was performed. This enabled the identification of 4394 intracellular proteins <sup>108</sup>. However, the analysis was preceded by an additional albumin depletion, and the analysis was performed on a different instrument, making direct comparison difficult. Nevertheless, there were overlaps in the proteins identified by Tascher et al. and in this thesis. These include, for example, aldehyde dehydrogenase, dimeric NADP-preferring (ALDH3A1), several cytochrome P450 enzymes like CYP2E1, CYP2C9, CYP2C19, sulfotransferase family cytosolic 1B member 1 (SULT1B1), or UDP-glucuronosyltransferase 2B7 (UGT2B7).

After analysis, the protein and peptide lists derived from Proteome Discoverer 2.1 were used to investigate whether the target analytes could be identified directly after in-gel digestion. It was found that only 15 of the new 36 proteins (without CYP 17-plex) and even only 8 of the 37 target peptides (two for arginase-1; ARG1) could be found. In addition, the identification of peptides for the already developed CYP 17-plex assay was also investigated. This showed that only 5 out of 17 target peptides representing 16 proteins (two for CYP3A5) could be detected. In summary, only a small part (13 of 54 initial peptides) of these analytes were found directly by LC-MS in the HepaRG cell samples, although the detection compatibility experiment (4.1.2) showed that all selected peptides could be detected in the mass spectrometer. This may, for example, be due to the fact that low abundant proteins are overlaid

by high-abundant proteins. Kim et al. have already described and compared different enrichment strategies in their review, with which it is possible to analyze also low-abundant proteins by mass spectrometry <sup>60</sup>. In order to increase the yield of the analytes for the measurement, it was therefore decided that antibodies (AB) should be generated and that immune precipitation should be used as an additional sample preparation step. Furthermore, since the analytes to be investigated were already known, it was decided to use a targeted MS method instead of the full-scan method to increase the sensitivity additionally <sup>80</sup>.

In order to decide which targeted method, targeted selected ion monitoring (tSIM) or parallel reaction monitoring (PRM), was more suitable for this purpose, prochloraz-treated HepaRG cells were analyzed with the already developed CYP 17-plex. Figure 18 clearly shows that the analysis using the tSIM method was influenced by interferences. Since this measurement method is based on the detection of precursor ions only, the probability that peptides with the same mass can be present in a complex sample is very high and thus interfere with unambiguous identification and quantification. In a study by Gallien et al., targeted mass spectrometric approaches were investigated, and they found that some peptides were affected by interferences in SIM mode, which influenced the limit of quantification (LOQ), while the LOQ remained constant when measured with the PRM method <sup>109</sup>. The additional fragmentation in PRM and the associated evaluation at the MS2 level increases the specificity, which leads to more specific results <sup>52,82</sup>. By combining immune precipitation and PRM as a targeted measurement mode, the number of detectable CYP peptides could be increased from initially 5/17 after in-gel digestion and full-scan (Full-MS) measurement to 14/17 in HepaRG cells. Of these 14 peptides, ten peptides were quantifiable. Only for the analytes CYP2D6, CYP2F1, and CYP3A43, no endogenous signals could be observed.

As described in chapter 1.3.4, no sequence-specific but tag-specific antibodies were generated. These enable the enrichment of whole peptide groups with the same C-terminal tag. This has not only the advantage that the number of animals to be immunized can be drastically reduced but also reduces the costs for the antibodies to be generated. Since polyclonal antibodies (pABs) usually consist of a heterogeneous mixture, their functionality was determined first. The aim was to determine whether they were able to recognize the target epitope against which they were gen-



erated and whether they were able to enrich the target peptide from a complex matrix. Two antibodies were tested for each tag. The results showed that for each analyte at least one of the two antibodies recognized the target from a tryptically digested human cell mixture consisting of human embryonic kidney (HEK), human colon tumor (HCT), and hepatoma G2 (HepG2) in a ratio of 1:1:1 (w:w:w). A total of 72 antibodies were tested for the 37 peptides (for fatty acid synthase (FASN) with the LEVR-tag and acyl-CoA desaturase (SCD) with the PTYK-tag one animal each died during the 4-month immunization). Of these 72 antibodies tested, 69 epitope binding motifs were generated (protocol of Weiss et al. was used and modified <sup>86</sup>). This showed that the immunization was successful for 96% of all antibodies.

Nevertheless, it had to be investigated further whether the antibodies could enrich not only the appropriate tag but also the target peptide from a complex matrix. In a second experiment, the standard non-labeled synthetic (EN<sub>s</sub>) peptide was spiked into the human cell mixture, and the samples were measured in PRM. It was shown that each antibody that was able to enrich the appropriate epitope motif also enriched the spiked target peptide.

Due to the varying performance of the antibodies and endogenous amounts of the respective analytes, the least optimal ratio between antibody and lysate used, which is required for reliable quantification, was determined in the next step. For this purpose, prochloraz-treated (10  $\mu\text{mol L}^{-1}$ ) HepaRG cells were used. The different antibody amounts of either 1, 2, or 5 micrograms were tested with either 10, 20, or 40 micrograms lysate. The amounts used were based on previous experiments. Nine different combinations were tested for each antibody. Considering the high number of measurements, only one replicate each was measured, and the decision which antibody-protein ratio was used for further method development was made via the mass spectrometric fragment pattern. The optimization for two antibodies is illustrated in Figure 40.

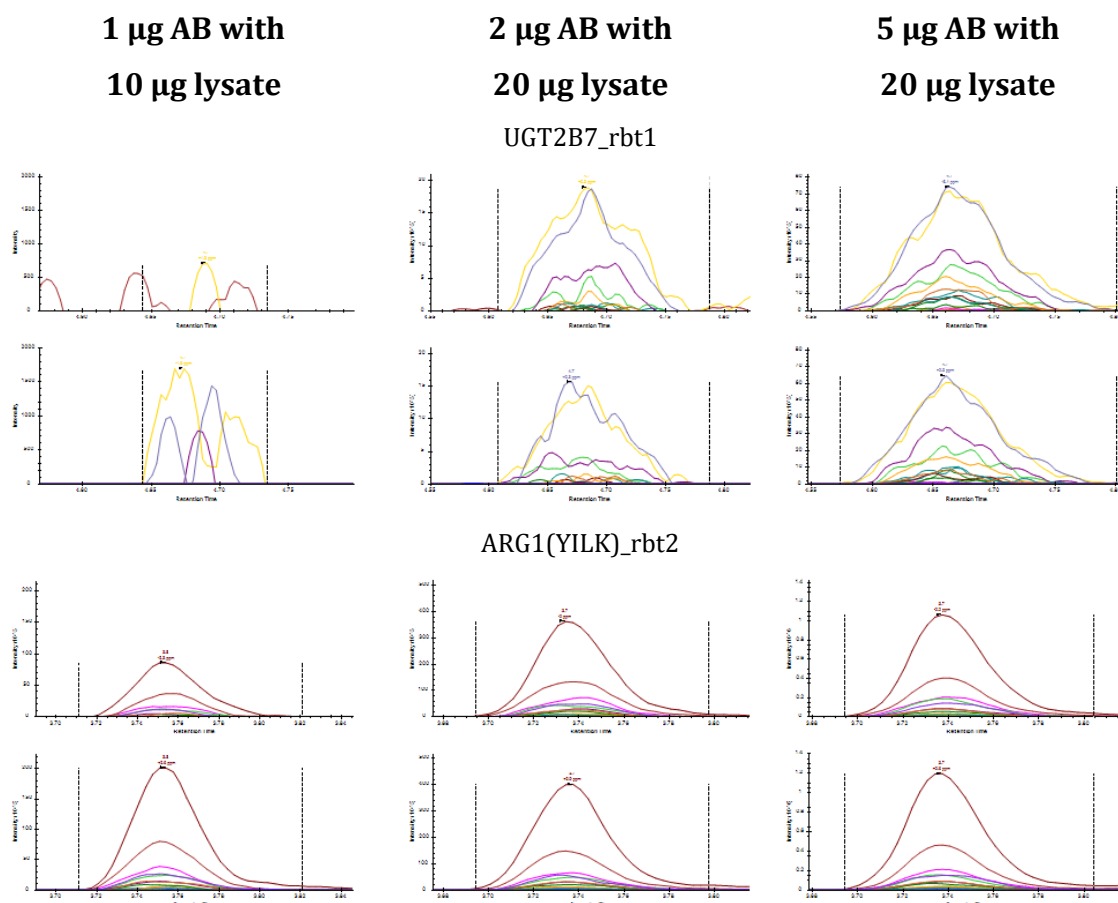


Figure 40. Antibody-lysate amount optimization for ARG1 and UGT2B7. In each graph, the upper chromatogram displays the endogenous signal (EN), the lower the internal isotopically labeled standard (IS) signal. Three of the nine different combinations are shown for UGT2B7\_rbt1 (upper graphs) and ARG1(YILK)\_rbt2 (lower graphs). The analysis was done in a single measurement per combination. For UGT2B7, the signal for EN and IS increases by increasing the antibody (AB) and lysate amount. To enable reliable and stable results, 5 µg AB and 20 µg lysate are at least needed. For ARG1(YILK), EN and IS signal also increases by increasing AB and lysate amount, but quantification shows that the combination of 1 µg AB and 10 µg lysate already led to reliable and stable results.

Three of the nine measured combinations for UDP-glucuronosyltransferase 2B7 (UGT2B7; upper graphs) and ARG1(YILK; lower graphs) are shown. For UGT2B7, the combination of 1 µg AB with 10 µg lysate shows neither an endogenous signal (EN) nor a signal from the internal isotopically labeled standard (IS) peptide. In each graph, the upper chromatogram shows the signal of the EN peptide and the lower one the signal of the IS peptide. The signals become better for 2 µg AB with 20 µg lysate, but the peak shape and the signal intensity obtained are not yet stable. At 5 µg AB and 20 µg lysate, not only the shape of the peak but also the intensity improves by a five-fold factor. In contrast, the result of the second AB for ARG1(YILK) is shown. Here, an increase of the endogenous as well as of the standard signal can be seen with an increase of AB and lysate amount, but the results deliver almost similar values (approx. 2 fmol µg<sup>-1</sup> in each case). Furthermore, the graph already

shows a clear fragment pattern and a signal height of the EN peptide of  $2.0 \cdot 10^5$  for the combination of 1  $\mu\text{g}$  AB with 10  $\mu\text{g}$  lysate. During this investigation, many assays failed, and analytes had to be excluded from further method development since either no endogenous signal or in some cases, even no isotopically labeled standard peptide signal was obtained. Antibodies that did not enrich either endogenous or standard peptide were excluded. Antibodies only enriching the standard were additionally tested whether an endogenous signal could be obtained from cryopreserved primary human hepatocytes (PHH). It was found that 3 of the 18 analytes investigated could be detected in PHHs. Due to a lack of primary hepatocyte samples and the fact that the pesticide-treated samples to be examined later were HepaRG cells, the method development for these three analytes: Peroxisomal acyl-coenzyme A oxidase 2 (ACOX2), granzyme B (GZMB), and histidine-rich glycoprotein (HRG), detected only in primary human hepatocytes, was not further pursued. In total, the method development was continued with 17 of the initial 37 peptides.

Another essential aspect that can influence detection and quantification is digestion time. There are several reasons why digestion time varies between proteins. Proteins have different properties due to their amino acid sequence. These include, for example, the folding due to intramolecular interactions, solubility, presence, and the number of disulfide bonds, et cetera. The localization of the target peptide within the protein sequence may also play a role. For this reason, it is not surprising that the use of different detergents or concentrations can also significantly influence proteolysis what has already been shown by Proc et al. in a study in which they examined and compared different digestion protocols <sup>93</sup>.

Given the results from Figure 20, where the normalized peptide release in percent over time is shown, it can be said that for most analytes, an increase with increasing digestion time was observed at first, which then decreased to a greater or lesser extent over time. Exceptions are the results for ARG1(PFSK), UGT1A1, and UGT1A3. There the maximum was already reached after two hours of digestion. For these three analytes, it was therefore decided to perform two-hour digestion before the analysis. For the remaining analytes, the maximum value was reached between 6 and 24 hours of digestion. In order to decide which digestion time should be used, a minimum percentage of 80% was set as a threshold for all analytes. For the 6- and 16-hour digestion, all analytes were above 80%. As the digestion kinetics for the

CYP 17-plex had already been investigated, the digestion time of the new assays was set to the same digestion time of 16 hours.

Since the LC-MS detection system enables multiplexing <sup>110</sup>, i.e., the simultaneous detection of several analytes, multiplex assays have been compiled. The results of the antibody-protein ratio, as well as the digestion kinetics, were taken into account. It was also considered that the total antibody amount of 7 µg within one multiplex must not be exceeded. The use of microspheres during the immunoprecipitation is limited due to the transfer efficiency of the KingFisher device. To increase the amount of microspheres, 3-[(3-Cholamidopropyl) dimethylammonio] -1-propane-sulfonate (CHAPS) is used, which reduces the surface tension. However, CHAPS is a known mass spectrometric impurity (spreadsheet from supplementary data) <sup>111</sup>, and therefore only small amounts can be used. Experience has shown that the maximum antibody limit per multiplex is 7 µg. After taking these factors into account, a total of six multiplex assays were established to minimize the amount of sample to be used and to shorten the analysis time.

In order to increase the number of data points per analyte and to avoid possible interferences between the target analytes to be measured, it was necessary to consider the chromatographic separation. It is desirable to achieve an optimal separation within a multiplex. However, it must be considered that the ionization capacity of the respective analytes changes with different solvent compositions <sup>112</sup>. In order to investigate the optimal chromatographic separation, where reproducible and reliable results could be obtained, different gradients were tested. Each gradient was measured three times, mean values of the intensities were calculated, and then normalized to the highest respective intensity obtained. Figure 23 shows the results. When looking at the graph for multiplex 1 (A and B), an evident influence of the different gradients, i.e., the different solvent compositions during ionization, can be seen. Comparing the gradient of 10-40% eluent B with the gradient of 10-20% B, the signals for ARG1(PFSK) and UGT1A3 decreased sharply. The normalized signal decreased from 82% to 27% and from 100% to 50%, respectively. The signal from UGT1A1 was reversed. The signal increased from 68% to 100%. Since the analytes were influenced differently, the decision which gradient should be used for each multiplex was based on a combined consideration of retention times, normalized intensities of the analytes, and the coefficient of variation (C.V.) of the triplicate determination.

The criteria to be met in the study of linearity were that the accuracy for each concentration level should be between 80-120% and the precision below 20%. The results of the linearity test showed that the developed assays have a wide dynamic range. This is particularly advantageous because, for example, the protein profile of cytochrome P450 enzymes (CYPs) can vary between different sample types such as tissue or cells and between different species <sup>38</sup>. Most of the analytes showed a dynamic range over several orders of magnitude. The least lower limit of quantification (LLOQ) was obtained for CYP3A4, with 50 amol. The linear range of this analyte was over five orders of magnitude. On the other hand, an upper limit of quantification (ULOQ) for alcohol dehydrogenase 1B (ADH1B) of 3 pmol was determined. After pesticide treatment of HepaRG cells, partly strong repression and induction effects could be observed. Therefore, broad dynamic ranges were necessary to determine the target analytes quantitatively. From 34 peptides representative for 32 proteins (two peptides for ARG1 and CYP3A5), 27 peptides could be quantified during the analysis of the effects of pesticides and pesticide mixtures in HepaRG cells. The concentrations of the analytes in the samples ranged from the attomolar range for CYP1A1 to the picomolar range for (ADH1B).

According to the U.S. Food and Drug Administration (FDA) guidelines <sup>94</sup>, three different concentrations in the assumed concentration range are to be tested each in five replicates for precision analysis by determining the intra- and interday variance. Since the amount of the different analytes measured so far in method development differs considerably, it was difficult to find samples with low, medium, and high concentrations. In order to come close to the criteria of the FDA guidelines, it was therefore decided to use three different samples for the analysis. Firstly, untreated HepaRG cells (dimethyl sulfoxide (DMSO)-treated), secondly prochloraz-treated HepaRG cells (10  $\mu\text{mol L}^{-1}$ ), and thirdly a cryopreserved primary human hepatocyte sample (PHH; donor 1). Intraday variation was determined by calculating the mean value of the five individual measurements per day. The measurement was repeated on two further days, and for determining the interday variance, one random value was selected from each day ( $n=3$ ). This was done because, in the later analysis of pesticide-treated HepaRG cells, only one single determination was to be measured of each treatment per substance set. The results in Table 24 clearly show that partly very different amounts were obtained for the analytes. Although three

different samples were examined instead of three different concentrations, the results showed that both the intraday and interday values were precise. Coefficients of variation below 20% were obtained for all analytes. For CYP7A1 and protein S100-P (S100P), no quantifiable results were obtained in the HepaRG cells. The values for S100P were all below LLOQ. No endogenous signals were obtained for CYP7A1 in prochloraz-treated HepaRG samples. However, since the results in the cryopreserved human hepatocyte sample met the criteria and the difficulty of using a sample suitable for all analytes, it was decided that the test was successful for these analytes.

To investigate the recovery, the mouse cell line NIH3T3 was used as a matrix for spike-in experiments. The selection of this cell line, instead of HepaRG cells, was made because the target analytes should preferably not be present in the matrix. The spike-in experiments were performed according to the FDA guidelines<sup>94</sup>. There it is suggested that three different spike-in concentrations should be used. In addition, unspiked samples were analyzed, and the experiment was performed three times. Since the measurements were performed in a different sample matrix and endogenous signals were already measured for some analytes in the blanks, the EN<sub>s</sub>/IS ratios obtained were corrected with the linear equations determined in the linearity experiment. The FDA guidelines of bioanalytical method validation state that the recovery of analytes does not have to be 100%, but the recoveries of analyte and internal standard should be consistent, precise, and reproducible<sup>94</sup>. Table 23 shows that the results were precise within each spike-in level. The coefficients of variation were between 0.3% for NAD(P)H dehydrogenase [quinone] 1 (NQO1; 250 fmol spike-in) and 13.4% for ADH1B (15 fmol spike-in). Recovery ranged from 60% (UGT1A3; 15 fmol spike-in) to 128% (NQO1; 15 fmol spike-in). As mentioned before, for some analytes, signals were already obtained in the blank sample. The measured blank signal for prelamin-A/C (LMNA) was 253 fmol and 74 fmol for NQO1. The literature search using UniProt<sup>90</sup> revealed that the peptide sequences for LMNA and NQO1 were identical for human and mouse. Therefore, a high base level for these analytes was measured in the NIH3T3 mouse cell line. Since the spike-in of 15 fmol synthetic non-labeled standard peptide is in the range of the measurement error, no accuracy determination was possible in these cases. On the other hand, sulfotransferase family cytosolic 1B member 1 (SULT1B1), for example, in which no endogenous blank signal was obtained, showed a very similar recovery

in all three spike-in concentrations between 98-104%. It can be concluded that the results for all analytes are precise and accurate, which is in concordance with the criteria set by the FDA <sup>94</sup>.

## 5.2 HepaRG Cells as a Suitable Model for the Analysis of Potential Mixture Effects after Pesticide Treatment

The use of primary hepatocytes is limited due to their availability. Therefore, HepG2 cell lines have often been used for *in vitro* toxicity studies. However, this cell line shows differences compared to human hepatocytes in both enzyme quantity and activity.<sup>113,114</sup>

Therefore, the number of experiments using HepaRG cells has increased in recent years. For example, in a recent study by Yokohama et al., the activities of CYP1A2, CYP2B6, CYP2C9, CYP2C19, CYP2D6, CYP3A4, UGTs, and SULTs were measured and compared in human hepatocytes, HepG2 cells, and HepaRG cells. They found that the activities of these CYPs in HepaRG cells were comparable to those in human hepatocytes while activities in HepG2 were much lower.<sup>115</sup>

In order to get a first impression of whether the HepaRG cells were useful for the analysis of the analytes to be investigated in this work, measurements of three human donors (cryopreserved primary human hepatocytes; in the following abbreviated with PHH.1; PHH.2; PHH.3) were performed. Results were compared with data from HepaRG cells after 24-hour DMSO treatment (results of the sample set from the mixture experiment). The obtained mean amounts in fmol  $\mu\text{g}^{-1}$  were corrected with the linear equations determined (4.1.10) since no fold changes were investigated here. The results are displayed in Figure 41.

## Discussion

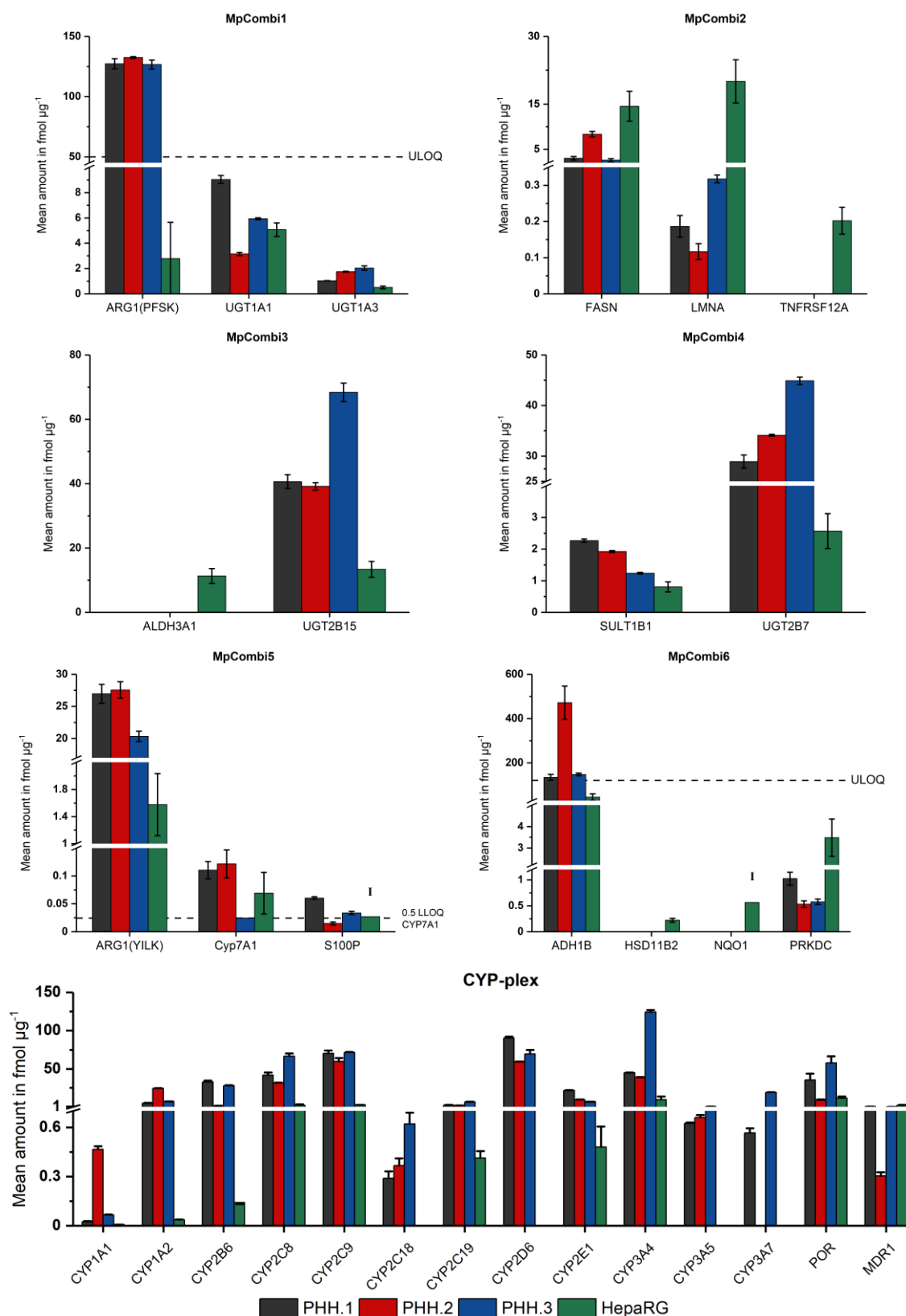


Figure 41. Comparison of cryopreserved human hepatocytes with HepaRG cells. Three human donors (PHH.1, PHH.2, and PHH.3) and the results obtained in HepaRG cells are presented. For the HepaRG cell results, the values from the mixture experiment after 24-hour DMSO treatment were used. Each sample was digested three times. Mean values were calculated and corrected with linear equations determined in (4.1.10). The dashed horizontal line in the MpCombi1 and MpCombi6 graphs indicates that the values for ARG1(PFSK) and ADH1B were above the upper limit of quantification (ULOQ). In the graph for MpCombi5, the dashed horizontal line indicates half the lower limit of quantification (0.5·LLOQ) for CYP7A1. For S100P and NQO1, only one value was obtained in the HepaRG cells (marked with I). For CYP3A5, only the results for the LPNK peptide are shown.



The graphs show that the measured protein amounts differ considerably in most cases. This also applies to the quantities obtained in the different donors (e.g., LMNA; MpCombi2 or UGT1A1 MpCombi1). For analytes such as UGT2B7 and UGT2B15, the amount obtained in the HepaRG cells is comparatively low. On the other hand, aldehyde dehydrogenase, dimeric NADP-preferring (ALDH3A1), corticosteroid 11-beta-dehydrogenase isozyme 2 (HSD11B2), tumor necrosis factor receptor superfamily member 12A (TNFRSF12A), and NQO1 could only be detected in the HepaRG cells and in none of the three donors. The results for ARG1 in the donors indicate discrepancies. However, since the ULOQ was exceeded in the case of ARG1(PFSK), and the results are not in the linear range, no reliable statement can be made here. Looking at the results of the CYP multiplex assay, it can be observed that the amount of CYP450 proteins (in fmol  $\mu\text{g}^{-1}$ ) in the HepaRG cells was lower than in the primary hepatocytes, except for multidrug resistance protein 1 (MDR1). Besides, some CYP450 proteins show that the amounts differed depending on the donor (particular visible for CYP1A1 or CYP3A4). Since the analytes CYP2F1 and CYP3A43 were not detected in any of the samples, they were not included in the graph. The results of the HepaRG cells show that 10 of the 14 analytes were quantifiable. For the analytes CYP2C18, CYP2D6, CYP3A5, and CYP3A7, the measured values were below the LLOQ.

It can be summarized that although differences to cryopreserved primary human hepatocytes have been observed, the HepaRG cell model is suitable to investigate the potential mixture effect of pesticides on toxicologically relevant liver proteins for the following reasons. On the one hand, 32 of 34 peptides (two peptides for ARG1 and two peptides for CYP3A5) were detected, of which 27 could be quantified in HepaRG cells and, on the other hand, the focus when studying the mixture effects is to determine the change in the respective treatment compared to the negative control (fold changes).

### 5.3 Comparison of mRNA and Protein Data

Although some pesticide studies with HepaRG cells have been published, only little data on the effect at protein level can be found in literature because most analyses

are performed at the mRNA level, or using enzyme activity tests <sup>116-118</sup>. In addition, the pesticides used, and the concentrations applied differ strongly from these used in this study, which makes a comparison difficult. However, a comparison of mRNA data with protein data was performed. With the marker genes identified in the study of Seeger et al. <sup>39</sup>, which indicate liver toxicity, the screening of the 30 pesticides was also carried out at the mRNA level by Dr. Almut Mentz (Center for Biotechnology (CeBiTec), Bielefeld). The cells were also treated with individual pesticides for 24 hours. The 17 analytes that were quantified both at mRNA and protein level are shown in the heatmap in Figure 42, whereby the upper graph shows the mRNA results, and the lower graph shows the protein data. Gray fields indicate that no data point was obtained (not detected or below LLOQ).



changes of a total of 510 data points were obtained at the protein level. In percentage terms, this means that 75.1% of the mRNA data showed significant changes, whereas, at the protein level, it was only 25.7% (almost thrice as many values). This could, for example, be explained with the fact that the biosynthesis of protein and mRNA occurs with a time-delay. Moreover, protein and mRNA half-lives differ most probably, too.<sup>119,120</sup> In addition to that, also effects of microRNA regulation might play a role.

In order to investigate the effects of the time delay between mRNA and protein results, it was decided that four pesticides and a prototypical inducer should be investigated at an additional timepoint. HepaRG cells were treated for 72 hours and analyzed at the protein level. Afterward, the results of the 24-hour and 72-hour treatment were compared. It was found that the treatment time had an influence on the regulatory strength and even the direction of regulation. The results are shown in Figure 28. A direct comparison was only possible for flusilazole, imazalil, and rifampicin treatment, as the concentration of difenoconazole and fenpyroximate had to be changed due to cytotoxic effects. If these three substances are considered, 16 significant changes were observed after 24-hour treatment, and 29 after 72-hour treatment (factor 1.8). For the analyte S100P, the inductive effect after 72 hours was 2.4 times stronger for flusilazole and 1.5 times stronger for imazalil compared to the 24-hour value. Based on these data, it was decided that further experiments should be performed with 24-, 48- and 72-hour treatment durations to study time dependencies.

### **5.4 Combinatorial Effects of Pesticide Mixtures on Protein Profiles in HepaRG Cells**

There is a lack of data regarding potential mixture effects, since to date, the toxicological properties of pesticides are only investigated on an individual basis during the authorization procedure. Mixture effects can either be antagonistic, additive, or even synergistic. The primary goal of this thesis was to develop immunoaffinity-based mass spectrometry assays to investigate whether combinatorial effects can be observed at protein level after pesticide mixture treatment of HepaRG cell

cultures. The conventional methods of determining combinatorial effects, such as Loewe Additivity or Bliss Independence, were unsuitable for modeling such effects at the protein level. In general, both methods require the determination of the EC<sub>50</sub> (EC<sub>50</sub>; the concentration at which a half-maximum effect is achieved), and hence, if analytes showed no dose-dependency, they could not be included in the analysis. The example in Figure 35 makes this clear. The mean amount in fmol  $\mu\text{g}^{-1}$  of LMNA after 24-hour treatment with azoxystrobin is shown. The values fluctuate around 30 fmol  $\mu\text{g}^{-1}$ , and no dose-dependency can be observed. It was, therefore, necessary to establish an alternative evaluation method. We applied multiple linear regression analysis to determine potential combinatorial effects. The workflow of multiple linear regression analysis is illustrated in Figure 43 below.

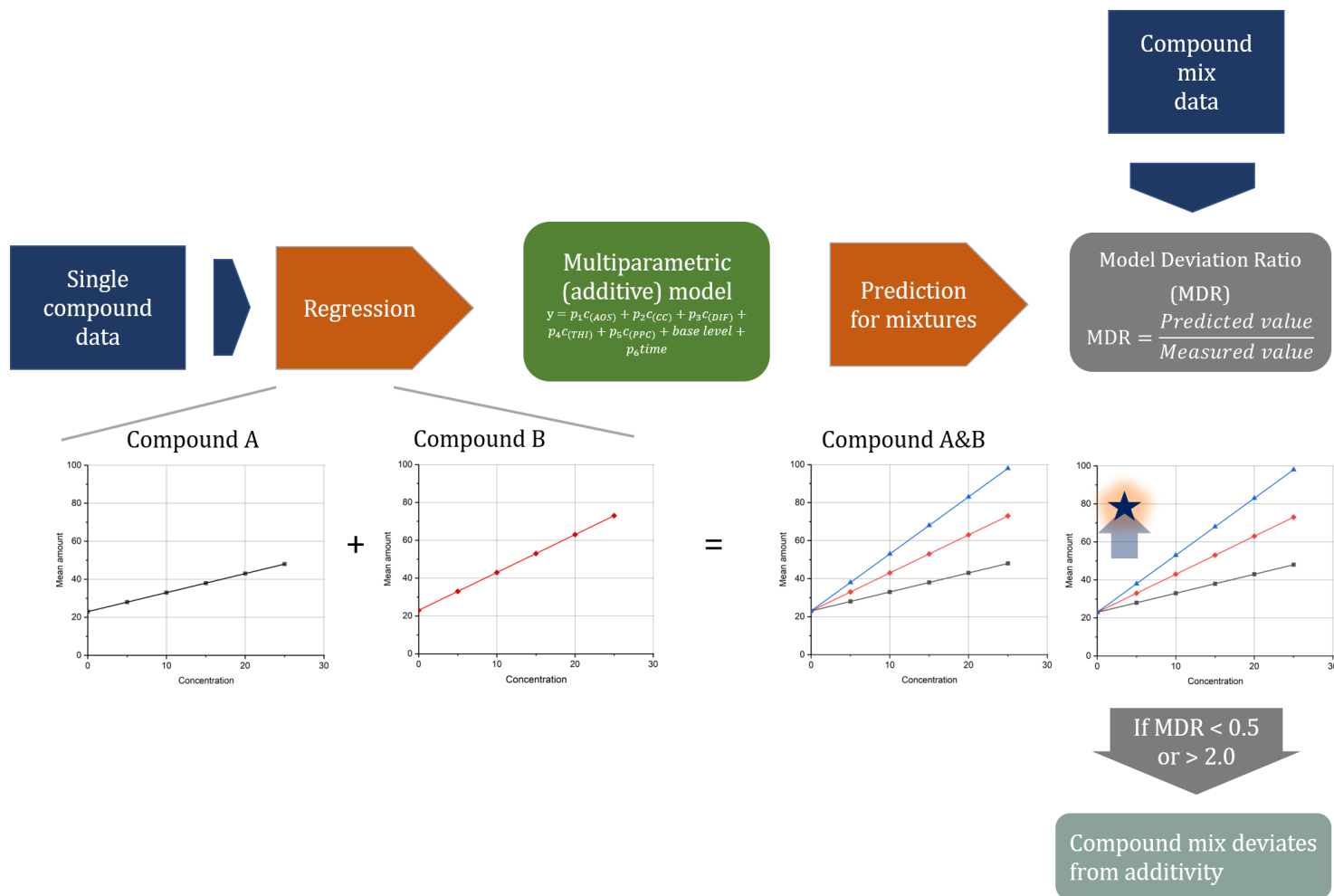


Figure 43. Workflow multiple linear regression analysis. This scheme shows the procedure of multiple linear regression. The results of the individual substances are used to obtain linear regressions of the respective substance (black and red fit). With these regressions, a predictive mixture model is generated (blue fit). If the measured value deviates from the prediction model, a non-additive effect can be assumed. Via the Model Deviation Ratio, where the predicted value is divided by the measured value, MDR scores are obtained. Values below 0.5 and above 2 are considered as a significant deviation from the additive model. Using the linear regression slopes, it can be determined as to whether it is an antagonistic or synergistic effect.

With RStudio v.1.0.153, linear regression equations were calculated using the individual results of pesticide treatments for each analyte. A model prediction was then calculated for the two functions of a binary mixture. This model prediction indicates an additive effect of the two substances in the mixture. The experimentally determined values were then compared with those of the model prediction. This was done using the Model Deviation Ratio (MDR), where the predicted value was divided by the measured value. Based on the thresholds described in Cedergreen, it was decided that values less than 0.5 and greater than 2 indicate a significant deviation from the additive model, and thus a combinatorial effect, such as synergism or antagonism<sup>99</sup>. In addition, it was specified in R that half of the LLOQ was used for values below the respective LLOQ in the mixture model predictions. This was done for the following reasons. Firstly, this ensured that no negative MDR values were obtained, and secondly, this procedure was also applied to the evaluation of the raw data. Thus, reasonable and consistent applicability across all analytes could be obtained.

Considering the histogram in Figure 37, it was found that most values were between the boundaries 0.5 and 2, which means that mostly additive effects of the test substances were observed according to the MDR model. A total of 1486 MDRs were obtained, of which 105 indicate a significant deviation from the additive model. This corresponds to about 7.1%. Of these 105 values, 39 synergistic, 50 antagonistic, and 16 further, not definable significant deviations from the additive model were identified with the defined criteria. Most of these values were obtained for cytochrome P450 enzymes (visible in Figure 38 Matrix of Model Deviation Ratios). The following Table 28 gives an overview of the number of antagonistic, synergistic, and the not definable significant changes from the additive model. Apart from ARG1(PFSK) and S100P, deviations from the additive model were only found for CYPs. It shows that most of the significant changes were found for S100P with 29 values, followed by CYP2B6 with 21 values and CYP1A2 with 17 values.

## Discussion

Table 28. Number of significant changes from the additive model. Here, all analytes are shown for which values outside the boundaries of 0.5 and 2 were found. It is also defined whether these effects were antagonistic, synergistic, or not definable.

Analyte	Antagonism	Synergism	Not definable	$\Sigma$
ARG1(PFSK)	0	1	0	1
CYP1A1	3	0	3	6
CYP1A2	7	10	0	17
CYP2B6	14	0	7	21
CYP2C8	1	4	1	6
CYP2C9	2	1	0	3
CYP2C19	2	1	3	6
CYP3A4	4	6	0	10
CYP7A1	4	0	2	6
S100P	13	16	0	29

Since cytochrome P450 enzymes play an essential role in the biotransformation of endogenous as well as xenobiotic substances, the results of this family are discussed in more detail. It has to be mentioned first that the CYPs can be regulated not only by one but by several receptors<sup>121-123</sup>. These receptors include, for example, the aryl hydrocarbon receptor (AhR), the constitutive androstane receptor (CAR), or the pregnane X receptor (PXR). In parallel to the screening experiment, prototypical inducers were also used for treating the cell cultures. These inducers consisted of benz[a]pyrene, 6-(4-Chlorophenyl) imidazo[2,1-b][1,3] thiazole-5-carbaldehyde O-(3,4-dichlorobenzyl) oxime (CITCO), and rifampicin (concentration of each substance was 5  $\mu\text{mol L}^{-1}$ ). In the literature, it can be found that benz[a]pyrene is an agonist for AhR, CITCO for CAR, and rifampicin for PXR. The following graph shows the fold change of eight CYPs after treatment with the particular substance, related to the negative control (DMSO-treated).



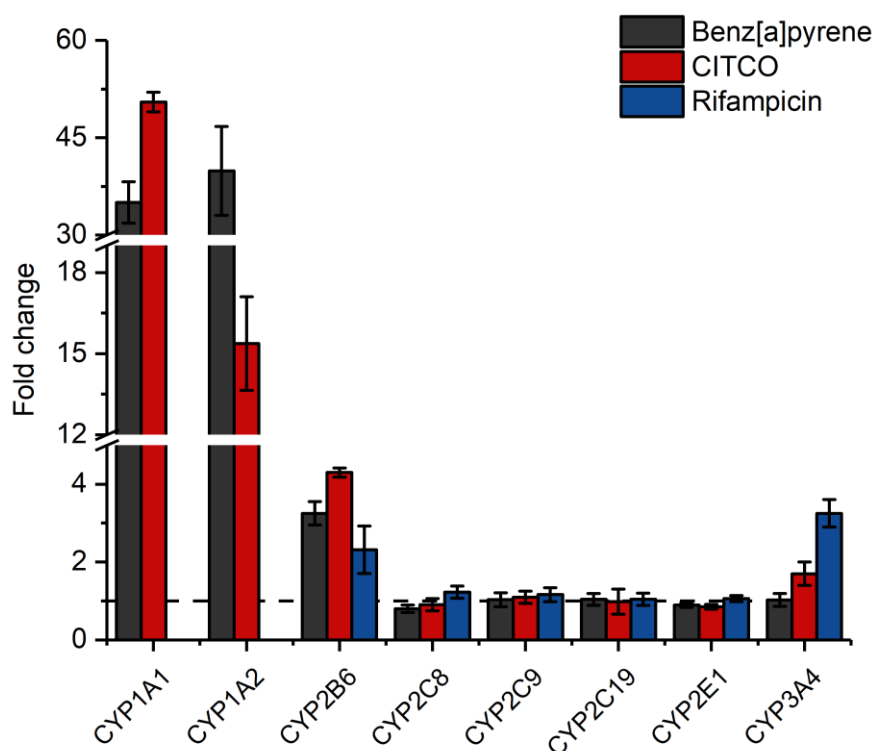


Figure 44. Fold change of CYPs after prototypical inducer treatment. Shown is the fold change of each respective prototypical inducer (benz[a]pyrene, CITCO, and rifampicin; each  $5 \mu\text{mol L}^{-1}$ ) related to the negative control (DMSO-treated). HepaRG cell culture and treatment were done in triplicates; mean values and standard deviations were calculated. The dashed horizontal line indicates the control value of 1.

Rifampicin is described in the literature as an agonist of the PXR, which can primarily induce CYP3A4<sup>124</sup>. The data confirms this and shows an induction of CYP3A4 by a factor of 3.2. CITCO is often used as CAR agonist, and the induction of CYP2B6 is observed<sup>125</sup>. This can also be confirmed. In addition, CYP2B6 is induced by rifampicin, as well as by benz[a]pyrene, suggesting regulation of this enzyme via CAR, as well as via AhR and PXR. The regulation of CYP1A1 and CYP1A2 is mainly associated with AhR<sup>126</sup>. Results show a strong induction of these two enzymes after treatment with the AhR agonist benz[a]pyrene (fold change of 35.0 and 39.9, respectively). In addition, the two enzymes also show a strong induction by CITCO, which indicates regulation via CAR as well. However, it should be mentioned that no values for CYP1A1 and 1A2 could be obtained for the negative control in both cases, and thus, values were referenced to half of the lower limit of quantification (LLOQ). For the other CYPs, no significant changes could be observed after treatment with these three prototypical inducers, suggesting regulation by different routes. Looking at the results for CYP1A1, CYP1A2, CYP2B6, and CYP3A4, it can be concluded that the regulation system of the tested substances benz[a]pyrene, CITCO, and rifampicin worked as positive controls in HepaRG cells.

The results after propiconazole (PPC) treatment are consistent with the results of the positive controls. Knebel et al. showed that propiconazole acts not only as an agonist for CAR and PXR but also as an activator of AhR <sup>127</sup>. Considering the results shown in Figure 32, this result can be confirmed. Not only CYP2B6 and CYP3A4, which are mainly regulated by CAR and PXR but also CYP1A1 and CYP1A2, show an induction after PPC treatment. However, the observed effects of CYP1A1/1A2 are more pronounced. In addition, it can be observed that CYP1A2, CYP2B6, and CYP3A4 show concentration-dependent changes. With increasing concentration, the effect of induction switches to down-regulation. With CYP3A4, a repression effect can already be observed after 48 and 72 hours at high concentrations.

Furthermore, it can be observed that the concentration of these proteins is also time-dependent. With more prolonged treatment, the observed inductive effects are weaker with CYP1A1 and CYP2B6. These observations could be explained by the cytotoxicity of PPC. Figure 30 shows that the viability after PPC treatment decreases sharply at high concentrations (after 72 hours). Also, a slight trend towards a decrease in viability at high concentrations can already be observed after 24 and 48 hours of treatment. After the 72-hour treatment, the value at the highest concentration is only 54%. Rose et al. came to similar conclusions <sup>125</sup>. Propiconazole showed cytotoxicity at high concentrations ( $100\text{ }\mu\text{mol L}^{-1}$ ) after 24 and 72 hours. They also showed that CYP1A1/1A2, CYP2B6, and CYP3A4 were induced after PPC treatment. However, the effect was more pronounced in that study with CYP2B6 and CYP3A4. The analysis was performed in a human micropatterned coculture model (MPCC) with cryopreserved human hepatocytes, which may explain these differences compared to the analyses performed here in HepaRG cells.

The results for CYP2C8, 2C9, and 2C19 in Figure 44 show no significant effects after treatment with the prototypical inducers. After 24 hours of treatment with PPC, also no significant changes (less than -0.56 and greater than 0.56) were observed for CYP2C8 and 2C9. After 48 and 72 hours, a down-regulation can be observed, which could also be explained by cytotoxicity at high concentrations. Since the trend of these three enzymes is towards down-regulation and no significant changes could be observed after treatment with the prototypical inducers for AhR, CAR, and PXR, it could be assumed that these enzymes follow a different regulatory pathway in HepaRG cells.

Difenoconazole (DIF), also from the triazole group, shows a similar regulatory picture to PPC. However, the effects are less intense than in PPC.

Cyproconazole (CC; triazole), was investigated by Luckert et al. with regard to receptor regulation in HepG2 and HEK-293 cells, as well as protein levels in HepaRG cells <sup>96</sup>. They showed that cyproconazole activated only one of the three receptors described so far, namely the PXR, but neither AhR nor CAR. Part of the protein data in HepaRG cells after 72 hours of treatment are shown as fold change ( $\log_2$ ) in Table 29 and are compared with the results of this thesis.

Table 29. Comparison of cyproconazole protein data. Fold change ( $\log_2$ ) protein values of cyproconazole-treatment (72h) were taken from table S5 <sup>96</sup>.

	Analyte	Cyproconazole (72h) in $\mu\text{mol L}^{-1}$			Cyproconazole (72h) in $\mu\text{mol L}^{-1}$ (Luckert et al. <sup>96</sup> )		
		35	55	110	25	50	100
Fold change ( $\log_2$ )	CYP2E1	-0.74	-1.10	-1.21	-0.16	-0.38	-0.76
	CYP3A4	1.30	1.17	1.13	1.9	2.04	2.21
	FASN	0.01	0.06	0.25	-0.1	-0.23	-0.78
	LMNA	-0.49	-1.20	-0.60	0.04	0.02	-0.04
	NCPR/POR	0.55	0.35	0.53	0.29	0.25	0.14
	NQO1	-0.32	0.10	-0.30	-0.07	0.22	0.41
	SULT1B1	-0.19	-0.19	-0.13	-1.65	-1.28	-0.45
	UGT2B7	-0.05	-0.09	-0.03	-0.2	-0.4	-0.94

Green field= significant up-regulation; blue field= significant down-regulation

First of all, it should be mentioned that different concentrations were used in both studies. Nevertheless, results for the most similar concentrations applied are compared in Table 29. Besides, the significance was determined in different ways. In this work, a simulation with 100 000 random fold changes ( $\log_2$ ) was run by RStudio with  $\alpha=0.05$ . Luckert et al. used an unpaired t-test with  $p<0.05$  <sup>96</sup>. Comparing the data measured in both studies, it is notable that the total number of significant changes in this thesis was higher (8/24 vs. 4/24 fold changes) than in Luckert et al. Comparing the data where no significant change occurred, it can partly be observed that concentration dependencies were observed in both studies. This can be seen, for example, for CYP2E1 or SULT1B1. The values obtained decrease with increasing cyproconazole concentration. A concentration dependency is also recognizable for FASN, whereby the regulation direction is different. In this work, the value increased

with increasing concentration, whereas the values decreased in the other study. In both cases, CYP3A4 showed a significant inductive effect for all concentrations, which supports the findings that cyproconazole acts as a PXR activator.

After thorough literature research, no data were found on thiacloprid metabolism regulated by these three receptors. Since CYP2B6 and CYP3A4 showed inductive effects, it can be assumed that thiacloprid could act via CAR or PXR or even both receptors. In order to verify this, further investigations would have to be conducted using gene reporter assays.

In a study by Zahn et al., the individual substances azoxystrobin (AOS) and cyproconazole, as well as the mixture of these substances and a plant protection product already available on the market consisting of these two substances, were investigated<sup>128</sup>. Gene reporter assays in HepG2 cells and protein quantity changes after 24-hour treatment of HepaRG cells were examined. They were able to show that both the product and the self-produced mixture (to a lesser extent than the product) induced the AhR. Furthermore, it was shown that after azoxystrobin treatment, concentration-dependent inhibition of CAR was present. This inhibition was also maintained after treatment with the mix and the product. On the other hand, CAR was induced by cyproconazole, whereby this effect became weaker with increasing concentration. No significant difference was observed at the highest concentration ( $13.7 \mu\text{mol L}^{-1}$ ). PXR was strongly induced by increasing AOS concentration, as well as the mixture and the product. Interestingly, the results show no induction after CC treatment. It must be mentioned that the concentrations chosen and used were much lower than in the work presented here. While the highest concentration for CC was  $13.7 \mu\text{mol L}^{-1}$  and for AOS  $3.97 \mu\text{mol L}^{-1}$ , the lowest concentrations in this study were  $35 \mu\text{mol L}^{-1}$  and  $10 \mu\text{mol L}^{-1}$ , respectively. Since the concentration differences are substantial, it is difficult to compare the results directly to this work. However, with increasing concentration of AOS, all CYPs observed in this study have been down-regulated. For CYP2B6, for example, only the lowest AOS concentration (after 24 h or 72 h) was detectable. All other values were already below the LLOQ. A concentration-dependent down-regulation was also observed for CYP3A4, 2C8, 2C9, and 2C19. Since Zahn et al. discovered strongly induced PXR gene targets but strongly repressed CAR gene targets after AOS treatment with increasing concentration, it could be assumed that the regulations in different directions balance each other out, and thus the regulated enzymes show only minor changes<sup>128</sup>. However,

this is not the case. In order to find out what the transactivation of receptors actually looks like at the concentrations used, additional reporter gene assays would have to be performed to explain the regulatory mechanism. Moreover, only the transactivation after 24-hour treatment is usually investigated. It would be interesting to conduct a time-dependent experiment to find out whether the transactivation changes with more prolonged treatment periods and, thus, the enzyme regulation.

Besides, Zahn et al. showed that differences between the mixtures they produced themselves, and the plant protection products were obtained <sup>128</sup>. This suggests that the co-formulants and excipients in the products could have an additional effect.

As a result, it is necessary to test not only the individual substances but also the mixtures and products available on the market. So far, only binary mixtures have been investigated in this thesis. However, since it is possible to get into contact with a variety of different pesticide residues at the same time, a further step would be to produce a multi-mixture of several individual substances below the no observed adverse effect level (NOAEL) and to test whether the combination of this variety produces an adverse effect. At this point, it should be mentioned that the concentrations used so far are much higher than the residue concentrations on food with which the consumer comes into contact. The concentrations used were chosen in such a way that it was possible to investigate and define mode of actions or mixture effects, but not yet so high that cytotoxic effects could be observed. Also of interest is the analysis of primary human hepatocytes after pesticide treatment. Therefore a further step would be the treatment of primary hepatocytes with pesticides and pesticide mixtures in order to compare the results with those of HepaRG cells.

In summary, an applicable test system for the analysis of pesticide mixtures in HepaRG cells has been developed. New immunoaffinity-based mass spectrometry assays were developed for 16 analytes. In total, the influence of pesticides and pesticide mixtures on 32 different marker proteins in HepaRG cells was tested. It could be shown that the cell model was suitable for these investigations and that the CYPs and S100P stood out in the analyses with regard to the Model Deviation Ratios (as shown in Table 28). Although results were obtained with all 32 proteins, S100P and the CYPs, especially CYP1A2 and CYP2B6, appear to be most sensitive to pesticide treatments and are therefore most suitable for future mixing studies. A total of 105 significant combinatorial effects deviating from the additive model were identified using multiple linear regression analysis. As a result of this, the question arises on

how relevant a synergistic effect found in a mixture is and whether such a mixture may require additional regulation for use in pest control. Since not only one concentration but a series was investigated in this work, the results of the other concentrations should also be taken into account in the case of synergisms. If a synergistic effect is consistent across the investigated concentration range, consideration should be given to further studying this particular mixture. This includes, for example, analyses that are necessary to understand the mechanisms behind the regulation of the respective analytes, such as gene reporter assays, in order to investigate the transactivation of receptors that play an essential role in the metabolism of xenobiotics.

However, not only the synergistic or antagonistic but also the additive effects are very interesting. It can partly be observed that the effects cancel each other out or that the direction of regulation can change with increasing concentration. This shows that it was necessary to investigate not only at a single concentration but at a series of concentrations. It was also shown that the results at the protein level were dependent on the duration of treatment.

It needs to be mentioned that the assays developed here do not replace the mandatory animal tests for the market release of new active substances, but they represent an alternative to animal testing in the context of possible combinatorial effects after exposure to several pesticide residues. Nevertheless, a direct transfer to the *in vivo* situation is difficult with these developed *in vitro* tests. However, there is an immense number of possible mixtures (in Europe alone, more than 450 individual substances are approved) that cannot be covered by animal testing alone. The developed *in vitro* tests can be used to prioritize mixtures that may cause synergistic effects, which can then be further investigated using animal models or other appropriate test systems. The results of *in vitro* studies can also be used to classify pesticides into cumulative assessment groups in order to predict whether it might be a critical mixture that needs further investigation. Thus, the present work can help to reduce the number of animal experiments to a minimum.



## 6 Summary

Pesticides are used worldwide to protect plants and fields as it is a necessity to provide sufficient and safe food. When these substances shall be approved, their toxicological effects must be investigated first. However, as today, not only individual pesticides but also pesticide mixtures are widely applied, consumers come into contact with a variety of pesticide residues. Therefore, it is essential to investigate potential mixture effects. If all potential mixtures were tested with the standard, mandatory toxicological tests that must be carried out for approval, the number of animal tests would increase dramatically. Hence, this work aimed to develop an *in vitro* test system to investigate the influence of potential mixing effects on toxicologically relevant liver proteins. Method development was initially started for 36 proteins. A total of six multiplex assays with 16 different proteins were successfully developed. In addition, a CYP 17-plex assay method already developed in targeted selected ion monitoring (tSIM) was transferred to the parallel reaction monitoring (PRM) like the six other multiplex assays. This resulted in the total number of 32 proteins used for the analysis of potential mixing effects in HepaRG cells. During method development, it was shown that immune precipitation and the use of targeted mass spectrometric methods could significantly increase the number of analytes detected (especially for the CYPs from 5/17 to 14/17) compared to full-scan analysis. These assays were used to investigate the effect of 30 individual pesticides on 32 proteins in HepaRG cells. These pesticides were also investigated at the mRNA level by a collaboration partner. Similarities have been observed between the two molecule species, but the effect was more pronounced at the mRNA level after 24 hours of treatment. By a similarity analysis using Pearson correlation, the pesticides were classified into four groups, and then four mixtures of five single substances were prepared. Based on the mRNA/protein expression result comparison, it was additionally decided that the treatment periods should be extended to 24, 48, and 72 hours. A novel mathematical model was developed to determine whether combinatorial effects such as antagonism, additivity, or synergism were observed after mixture treatment. For the very first time, multiple linear regression analysis was used to identify combinatorial effects after pesticide treatment. The results of the individual treatments were used to obtain theoretical model values of the respective mixture. These proposed



values were then compared with the measured values from the mixture experiments. According to this model, the results showed that most mixtures had an additive effect on the different proteins analyzed. However, in some cases, synergistic or antagonistic effects were observed. Most model deviations that indicate synergistic/antagonistic effects were obtained for the three analytes S100P, followed by CYP2B6, and CYP1A2, suggesting them as the most sensitive sensors for detecting these effects.

## 7 Zusammenfassung

Pestizide werden weltweit zum Schutz von Pflanzen und Feldern eingesetzt, da eine ausreichende und sichere Versorgung mit Lebensmitteln unerlässlich ist. Bei der Zulassung dieser Stoffe müssen zunächst ihre toxikologischen Auswirkungen untersucht werden. Da heutzutage jedoch nicht nur einzelne Pestizide, sondern auch Pestizidmischungen eingesetzt werden, können Verbraucher mit einer Vielzahl von Pestizidrückständen in Berührung kommen. Daher ist es unerlässlich, diese potenziellen Mischeffekte ebenfalls zu untersuchen. Würden alle potenziellen Mischungen mit den üblichen, obligatorischen toxikologischen Untersuchungen, die zur Zulassung durchgeführt werden müssen, getestet, würde sich die Zahl der Tierversuche drastisch erhöhen. Daher zielte diese Arbeit darauf ab, ein *in vitro* Testsystem zu entwickeln, um den Einfluss möglicher Mischungseffekte auf toxikologisch relevante Leberproteine zu untersuchen. Die Methodenentwicklung wurde zunächst für 36 Proteine begonnen. Insgesamt wurden sechs Multiplex-Assays für 16 verschiedene Proteine erfolgreich entwickelt. Darüber hinaus wurde der bereits im targeted selected ion monitoring (tSIM) entwickelte CYP 17-plex Assay zum parallel reaction monitoring (PRM) Modus transferiert, um ihn gleich wie die sechs Multiplex-Assays messen zu können. Daraus ergab sich die Gesamtzahl von 32 Proteinen, die für die Analyse möglicher Mischeffekte in HepaRG Zellen verwendet wurden. Bei der Methodenentwicklung konnte gezeigt werden, dass durch die Immunpräzipitation und den Einsatz gezielter massenspektrometrischer Methoden die Anzahl der detektierten Analyten, im Vergleich zur Full-Scan Analyse, deutlich erhöht werden konnte (insbesondere für die CYPs von 5/17 zu 14/17 Peptiden). Mit diesen Assays wurde die Wirkung von 30 einzelnen Pestiziden auf 32 Proteine in HepaRG-Zellen untersucht. Diese Pestizide wurden von einem Kooperationspartner auch auf mRNA-Ebene untersucht. Es wurden Ähnlichkeiten zwischen den beiden Molekülspezies beobachtet, wobei der Effekt nach 24-stündiger Behandlung auf mRNA-Ebene stärker ausgeprägt war. Durch eine Ähnlichkeitsanalyse mittels Pearson-Korrelation wurden die Pestizide in vier Gruppen eingeteilt und anschließend vier Mischungen aus fünf Einzelsubstanzen hergestellt. Basierend auf dem mRNA/Protein-Vergleich wurde zusätzlich entschieden, dass die Behandlungszeiten auf 24, 48 und 72 Stun-

den erweitert werden sollten. Ein neuartiges mathematisches Modell wurde entwickelt, um festzustellen, ob kombinatorische Effekte wie Antagonismus, Additivität oder Synergismus nach Mischungsbehandlung beobachtet werden konnten. Zum ersten Mal wurde die multiple lineare Regression verwendet, um kombinatorische Effekte nach der Pestizidbehandlung zu identifizieren. Die Ergebnisse der einzelnen Behandlungen wurden dabei genutzt, um theoretische Modellwerte der jeweiligen Mischung zu erhalten. Diese Vorhersagewerte wurden dann mit den Messwerten aus den Mischungsversuchen verglichen. Laut diesem Modell zeigten die Ergebnisse, dass die meisten Mischungen einen additiven Effekt auf die verschiedenen analysierten Proteine hervorriefen. In einigen Fällen wurden jedoch synergistische oder antagonistische Effekte beobachtet.

Die meisten Modellabweichungen, die synergistische/antagonistische Effekte anzeigten, wurden für die drei Analyten S100P, gefolgt von CYP2B6 und CYP1A2 ermittelt, was nahelegt, dass sie die empfindlichsten Sensoren zur Erkennung dieser Effekte sind.

## 8 References

- (1) Munoz-Pineiro, M. A.; Robouch, P. "Fipronil in eggs: Factsheet – December 2017," 2018.
- (2) Matthews, Graham *Pesticides: Health, Safety and the Environment. Second Edition 2015*; John Wiley & Sons, Ltd, 2015.
- (3) Bishopp, F. C. Insect Problems in World War II with Special References to the Insecticide DDT. *American journal of public health and the nation's health* **1945**, 35 (4), 373.
- (4) Raju, Tonse N. K. The Nobel Chronicles. *The Lancet* **1999**, 353 (9159), 1196.
- (5) Aktar, M. W.; Sengupta, D.; Chowdhury, A. Impact of pesticides use in agriculture: their benefits and hazards. *Interdisciplinary Toxicology* **2009**, 2 (1), 1.
- (6) Food and Agriculture Organization of the United Nations, Food and agriculture data, <http://www.fao.org/faostat/en/#home>, (last access: June 13<sup>th</sup> 2019)
- (7) United Nations, Department of Economic and Social Affairs, Population Division. World Population Prospects: The 2017 Revision, Key Findings and Advance Tables. **2017**, *Working Paper No. ESA/P/WP/248*.
- (8) Kim, K. H.; Kabir, E.; Jahan, S. A. Exposure to pesticides and the associated human health effects. *Sci Total Environ* **2017**, 575, 525.
- (9) Koutros, S.; Silverman, D. T.; Alavanja, M. C.; Andreotti, G.; Lerro, C. C.; Heltse, S.; Lynch, C. F.; Sandler, D. P.; Blair, A.; Beane Freeman, L. E. Occupational exposure to pesticides and bladder cancer risk. *Int J Epidemiol* **2016**, 45 (3), 792.
- (10) Henneberger, P. K.; Liang, X.; London, S. J.; Umbach, D. M.; Sandler, D. P.; Hoppin, J. A. Exacerbation of symptoms in agricultural pesticide applicators with asthma. *Int Arch Occup Environ Health* **2014**, 87 (4), 423.
- (11) Van Maele-Fabry, G.; Gamet-Payrastre, L.; Lison, D. Household exposure to pesticides and risk of leukemia in children and adolescents: Updated systematic review and meta-analysis. *Int J Hyg Environ Health* **2019**, 222 (1), 49.
- (12) Requena, M.; Parron, T.; Navarro, A.; Garcia, J.; Ventura, M. I.; Hernandez, A. F.; Alarcon, R. Association between environmental exposure to pesticides and epilepsy. *Neurotoxicology* **2018**, 68, 13.
- (13) Brouwer, M.; Koeman, T.; Van Den Brandt, P. A.; Kromhout, H.; Schouten, L. J.; Peters, S.; Huss, A.; Vermeulen, R. Occupational exposures and Parkinson's disease mortality in a prospective Dutch cohort. *Occup Environ Med* **2015**, 72 (6), 448.
- (14) Hansen, M. R.; Jors, E.; Lander, F.; Condarco, G.; Schlunssen, V. Is cumulated pyrethroid exposure associated with prediabetes? A cross-sectional study. *J Agromedicine* **2014**, 19 (4), 417.
- (15) Harner, Tom; Shoeib, Mahiba; Diamond, Miriam; Stern, Gary; Rosenberg, Bruno. Using Passive Air Samplers To Assess Urban–Rural Trends for Persistent Organic Pollutants. 1. Polychlorinated Biphenyls and Organochlorine Pesticides. *Environmental Science & Technology* **2004**, 38 (17), 4474.
- (16) Dirinck, E.; Jorens, P. G.; Covaci, A.; Geens, T.; Roosens, L.; Neels, H.; Mertens, I.; Van Gaal, L. Obesity and persistent organic pollutants:

- possible obesogenic effect of organochlorine pesticides and polychlorinated biphenyls. *Obesity (Silver Spring)* **2011**, 19 (4), 709.
- (17) World Health Organization, Persistent organic pollutants (POPs), [https://www.who.int/foodsafety/areas\\_work/chemical-risks/pops/en/](https://www.who.int/foodsafety/areas_work/chemical-risks/pops/en/), (last access: July 1<sup>st</sup> 2019)
  - (18) Pang, Guo-Fang *Analytical methods for food safety by mass spectrometry*; Elsevier Inc., 2018.
  - (19) Garcia, F. P.; Ascencio, S. Y. C.; Gaytán-Oyarzún, Juan; Ceruelohernandez, A.; Alavarado, P. V. *Pesticides: classification, uses and toxicity. Measures of exposure and genotoxic risks*, 2012.
  - (20) World Health Organization *The WHO Recommended Classification of Pesticides by Hazard and guidelines to classification: 2009*, 2009.
  - (21) Regulation (EC) 1107/2009/EC of the European Parliament and the Council of 21 October 2009 concerning the placing of plant protection products on the market and repealing Council Directives 79/117/EEC and 91/414/EEC. **2009**.
  - (22) Federal Institute for Risk Assessment. Gesetzliche Verfahren im Bereich Pflanzenschutz. **2015**.
  - (23) Storck, V.; Karpouzas, D. G.; Martin-Laurent, F. Towards a better pesticide policy for the European Union. *Sci Total Environ* **2017**, 575, 1027.
  - (24) Commission Regulation (EU) No 283/2013 of 1 March 2013 setting out the data requirements for active substances, in accordance with Regulation (EC) No 1107/2009 of the European Parliament and of the Council concerning the placing of plant protection products on the market. **2013**.
  - (25) Commission Regulation (EU) No 284/2013 of 1 March 2013 setting out the data requirements for plant protection products, in accordance with Regulation (EC) No 1107/2009 of the European Parliament and of the Council concerning the placing of plant protection products on the market. **2013**.
  - (26) Strazzullo, M.; Matarazzo, M. R. Epigenetic Effects of Environmental Chemicals on Reproductive Biology. *Curr Drug Targets* **2017**, 18 (10), 1116.
  - (27) Hahn, T.; Schenk, K.; Schulz, R. Environmental chemicals with known endocrine potential affect yolk protein content in the aquatic insect *Chironomus riparius*. *Environ Pollut* **2002**, 120 (3), 525.
  - (28) De Barros, A. L. C.; Schmidt, F. F.; De Aquino, S. F.; Afonso, Rjcf. Determination of nine pharmaceutical active compounds in surface waters from Paraopeba River Basin in Brazil by LTPE-HPLC-ESI-MS/MS. *Environmental science and pollution research international* **2018**, 25 (20), 19962.
  - (29) Meyer, U. A. Overview of enzymes of drug metabolism. *J Pharmacokinet Biopharm* **1996**, 24 (5), 449.
  - (30) Koepsell, H.; Endou, H. The SLC22 drug transporter family. *Pflugers Arch* **2004**, 447 (5), 666.
  - (31) Doring, B.; Petzinger, E. Phase 0 and phase III transport in various organs: combined concept of phases in xenobiotic transport and metabolism. *Drug Metab Rev* **2014**, 46 (3), 261.
  - (32) Xu, C.; Li, C. Y.; Kong, A. N. Induction of phase I, II and III drug metabolism/transport by xenobiotics. *Arch Pharm Res* **2005**, 28 (3), 249.
  - (33) Jancova, Petra; Anzenbacher, Pavel; Anzenbacherova, Eva. Phase II Drug Metabolizing Enzymes. *Biomedical Papers* **2010**, 154 (2), 103.

## References

- (34) Mullican, S. E.; Dispirito, J. R.; Lazar, M. A. The orphan nuclear receptors at their 25-year reunion. *J Mol Endocrinol* **2013**, *51* (3), T115.
- (35) Hahn, M. E. Aryl hydrocarbon receptors: diversity and evolution. *Chem Biol Interact* **2002**, *141* (1-2), 131.
- (36) Sever, R.; Glass, C. K. Signaling by nuclear receptors. *Cold Spring Harb Perspect Biol* **2013**, *5* (3), a016709.
- (37) Glass, C. K.; Rosenfeld, M. G. The coregulator exchange in transcriptional functions of nuclear receptors. *Genes Dev* **2000**, *14* (2), 121.
- (38) Martignoni, M.; Groothuis, G. M.; De Kanter, R. Species differences between mouse, rat, dog, monkey and human CYP-mediated drug metabolism, inhibition and induction. *Expert opinion on drug metabolism & toxicology* **2006**, *2* (6), 875.
- (39) Seeger, B.; Mentz, A.; Knebel, C.; Schmidt, F.; Bednarz, H.; Niehaus, K.; Albaum, S.; Kalinowski, J.; Noll, T.; Steinberg, P.; Marx-Stoelting, P.; Heise, T. Assessment of mixture toxicity of (tri)azoles and their hepatotoxic effects in vitro by means of omics technologies. *Archives of toxicology* **2019**.
- (40) Twyman, R.M. *Principles of Proteomics*; 2nd ed.; Garland Science, 2013.
- (41) Lottspeich, F.; Engels, J.W. *Bioanalytik*; 3rd ed.; Springer Spektrum, 2012.
- (42) Graves, P. R.; Haystead, T. A. J. Molecular Biologist's Guide to Proteomics. *Microbiology and Molecular Biology Reviews* **2002**, *66* (1), 39.
- (43) Tyers, Mike; Mann, Matthias. From genomics to proteomics. *Nature* **2003**, *422* (6928), 193.
- (44) Yates, J. R., 3rd. Mass spectral analysis in proteomics. *Annu Rev Biophys Biomol Struct* **2004**, *33*, 297.
- (45) Aebersold, Ruedi; Mann, Matthias. Mass spectrometry-based proteomics. *Nature* **2003**, *422* (6928), 198.
- (46) Walther, T. C.; Mann, M. Mass spectrometry-based proteomics in cell biology. *The Journal of cell biology* **2010**, *190* (4), 491.
- (47) Gregorich, Z. R.; Chang, Y. H.; Ge, Y. Proteomics in heart failure: top-down or bottom-up? *Pflugers Arch* **2014**, *466* (6), 1199.
- (48) Rabilloud, T. Solubilization of proteins for electrophoretic analyses. *Electrophoresis* **1996**, *17* (5), 813.
- (49) Krueve, A.; Kaupmees, K.; Liigand, J.; Oss, M.; Leito, I. Sodium adduct formation efficiency in ESI source. *J Mass Spectrom* **2013**, *48* (6), 695.
- (50) Uchida, Y.; Tachikawa, M.; Obuchi, W.; Hoshi, Y.; Tomioka, Y.; Ohtsuki, S.; Terasaki, T. A study protocol for quantitative targeted absolute proteomics (QTAP) by LC-MS/MS: application for inter-strain differences in protein expression levels of transporters, receptors, claudin-5, and marker proteins at the blood-brain barrier in ddY, FVB, and C57BL/6J mice. *Fluids Barriers CNS* **2013**, *10* (1), 21.
- (51) Gerber, S. A.; Rush, J.; Stemman, O.; Kirschner, M. W.; Gygi, S. P. Absolute quantification of proteins and phosphoproteins from cell lysates by tandem MS. *Proceedings of the National Academy of Sciences of the United States of America* **2003**, *100* (12), 6940.
- (52) Peterson, A. C.; Russell, J. D.; Bailey, D. J.; Westphall, M. S.; Coon, J. J. Parallel reaction monitoring for high resolution and high mass accuracy quantitative, targeted proteomics. *Molecular & cellular proteomics : MCP* **2012**, *11* (11), 1475.

- (53) Kuzyk, M. A.; Parker, C. E.; Domanski, D.; Borchers, C. H. Development of MRM-based assays for the absolute quantitation of plasma proteins. *Methods in molecular biology* **2013**, 1023, 53.
- (54) Moser, A. C.; Hage, D. S. Immunoaffinity chromatography: an introduction to applications and recent developments. *Bioanalysis* **2010**, 2 (4), 769.
- (55) Bonifacino, J. S.; Dell'angelica, E. C.; Springer, T. A. Immunoprecipitation. *Curr Protoc Protein Sci* **2001**, Chapter 9, Unit 9 8.
- (56) Anderson, N. Leigh; Anderson, Norman G.; Haines, Lee R.; Hardie, Darryl B.; Olafson, Robert W.; Pearson, Terry W. Mass Spectrometric Quantitation of Peptides and Proteins Using Stable Isotope Standards and Capture by Anti-Peptide Antibodies (SISCAPA). *Journal of proteome research* **2004**, 3 (2), 235.
- (57) Annesley, T. M. Ion suppression in mass spectrometry. *Clinical chemistry* **2003**, 49 (7), 1041.
- (58) Gu, Hongbo; Ren, Jian Min; Jia, Xiaoying; Levy, Tyler; Rikova, Klarisa; Yang, Vicky; Lee, Kimberly A.; Stokes, Matthew P.; Silva, Jeffrey C. Quantitative Profiling of Post-translational Modifications by Immunoaffinity Enrichment and LC-MS/MS in Cancer Serum without Immunodepletion. *Molecular & Cellular Proteomics* **2016**, 15 (2), 692.
- (59) Steinhilber, A. E.; Schmidt, F. F.; Naboulsi, W.; Planatscher, H.; Niedzwiecka, A.; Zagon, J.; Braeuning, A.; Lampen, A.; Joos, T. O.; Poetz, O. Mass Spectrometry-Based Immunoassay for the Quantification of Banned Ruminant Processed Animal Proteins in Vegetal Feeds. *Analytical chemistry* **2018**.
- (60) Kim, B.; Araujo, R.; Howard, M.; Magni, R.; Liotta, L. A.; Luchini, A. Affinity enrichment for mass spectrometry: improving the yield of low abundance biomarkers. *Expert Rev Proteomics* **2018**, 15 (4), 353.
- (61) Hoofnagle, A. N.; Wener, M. H. The fundamental flaws of immunoassays and potential solutions using tandem mass spectrometry. *J Immunol Methods* **2009**, 347 (1-2), 3.
- (62) Zhao, Y.; Gu, H.; Zeng, J. Opportunities and challenges for hybrid immunoaffinity LC-MS approach for quantitative analysis of protein biomarkers. *Future Science OA* **2018**, 4 (3).
- (63) Whiteaker, J. R.; Zhao, L.; Lin, C.; Yan, P.; Wang, P.; Paulovich, A. G. Sequential multiplexed analyte quantification using peptide immunoaffinity enrichment coupled to mass spectrometry. *Molecular & cellular proteomics : MCP* **2012**, 11 (6), M111 015347.
- (64) Rosting, C.; Tran, E. V.; Gjellstad, A.; Halvorsen, T. G. Determination of the low-abundant protein biomarker hCG from dried matrix spots using immunocapture and nano liquid chromatography mass spectrometry. *Journal of chromatography. B, Analytical technologies in the biomedical and life sciences* **2018**, 1077-1078, 44.
- (65) Schneck, N. A.; Phinney, K. W.; Lee, S. B.; Lowenthal, M. S. Quantification of cardiac troponin I in human plasma by immunoaffinity enrichment and targeted mass spectrometry. *Anal Bioanal Chem* **2018**, 410 (11), 2805.
- (66) Schumacher, J. A.; Crockett, D. K.; Elenitoba-Johnson, K. S.; Lim, M. S. Evaluation of enrichment techniques for mass spectrometry: identification of tyrosine phosphoproteins in cancer cells. *J Mol Diagn* **2007**, 9 (2), 169.
- (67) Nishikaze, T.; Kawabata, S.; Iwamoto, S.; Tanaka, K. Reversible hydrazide chemistry-based enrichment for O-GlcNAc-modified peptides

- and glycopeptides having non-reducing GlcNAc residues. *Analyst* **2013**, 138 (23), 7224.
- (68) Porath, J. Immobilized metal ion affinity chromatography. *Protein Expr Purif* **1992**, 3 (4), 263.
- (69) Becker, J. O.; Hoofnagle, A. N. Replacing immunoassays with tryptic digestion-peptide immunoaffinity enrichment and LC-MS/MS. *Bioanalysis* **2012**, 4 (3), 281.
- (70) Wingren, Christer; James, Peter; Borrebaeck, Carl A. K. Strategy for surveying the proteome using affinity proteomics and mass spectrometry. *Proteomics* **2009**, 9 (6), 1511.
- (71) Poetz, O.; Hoeppe, S.; Templin, M. F.; Stoll, D.; Joos, T. O. Proteome wide screening using peptide affinity capture. *Proteomics* **2009**, 9 (6), 1518.
- (72) Hoeppe, S.; Schreiber, T. D.; Planatscher, H.; Zell, A.; Templin, M. F.; Stoll, D.; Joos, T. O.; Poetz, O. Targeting peptide termini, a novel immunoaffinity approach to reduce complexity in mass spectrometric protein identification. *Molecular & cellular proteomics : MCP* **2011**, 10 (2), M110 002857.
- (73) Chen, E. I.; Cociorva, D.; Norris, J. L.; Yates, J. R., 3rd. Optimization of mass spectrometry-compatible surfactants for shotgun proteomics. *Journal of proteome research* **2007**, 6 (7), 2529.
- (74) Liao, L.; McClatchy, D. B.; Yates, J. R. Shotgun proteomics in neuroscience. *Neuron* **2009**, 63 (1), 12.
- (75) Verberkmoes, Nathan C.; Bundy, Jonathan L.; Hauser, Loren; Asano, Keiji G.; Razumovskaya, Jane; Larimer, Frank; Hettich, Robert L.; Stephenson, James L. Integrating "Top-Down" and "Bottom-Up" Mass Spectrometric Approaches for Proteomic Analysis of *Shewanella oneidensis*. *Journal of proteome research* **2002**, 1 (3), 239.
- (76) Schuhmann, K.; Herzog, R.; Schwudke, D.; Metelmann-Strupat, W.; Bornstein, S. R.; Shevchenko, A. Bottom-up shotgun lipidomics by higher energy collisional dissociation on LTQ Orbitrap mass spectrometers. *Analytical chemistry* **2011**, 83 (14), 5480.
- (77) Molina, Henrik; Horn, David M.; Tang, Ning; Mathivanan, Suresh; Pandey, Akhilesh. Global proteomic profiling of phosphopeptides using electron transfer dissociation tandem mass spectrometry. *Proceedings of the National Academy of Sciences* **2007**, 104 (7), 2199.
- (78) Waldron, R. T.; Lugea, A.; Gulla, A.; Pandol, S. J. Proteomic Identification of Novel Plasma Biomarkers and Pathobiologic Pathways in Alcoholic Acute Pancreatitis. *Front Physiol* **2018**, 9, 1215.
- (79) Duijvesz, D.; Burnum-Johnson, K. E.; Gritsenko, M. A.; Hoogland, A. M.; Vredenburg-Van Den Berg, M. S.; Willemsen, R.; Luider, T.; Pasa-Tolic, L.; Jenster, G. Proteomic profiling of exosomes leads to the identification of novel biomarkers for prostate cancer. *PLoS One* **2013**, 8 (12), e82589.
- (80) Boja, E. S.; Rodriguez, H. Mass spectrometry-based targeted quantitative proteomics: achieving sensitive and reproducible detection of proteins. *Proteomics* **2012**, 12 (8), 1093.
- (81) Michalski, A.; Damoc, E.; Hauschild, J. P.; Lange, O.; Wieghaus, A.; Makarov, A.; Nagaraj, N.; Cox, J.; Mann, M.; Horning, S. Mass spectrometry-based proteomics using Q Exactive, a high-performance benchtop quadrupole Orbitrap mass spectrometer. *Molecular & cellular proteomics : MCP* **2011**, 10 (9), M111 011015.



- (82) Ronsein, G. E.; Pamir, N.; Von Haller, P. D.; Kim, D. S.; Oda, M. N.; Jarvik, G. P.; Vaisar, T.; Heinecke, J. W. Parallel reaction monitoring (PRM) and selected reaction monitoring (SRM) exhibit comparable linearity, dynamic range and precision for targeted quantitative HDL proteomics. *Journal of proteomics* **2015**, *113*, 388.
- (83) Lewis, K.A.; Tzilivakis, J.; Warner, D.; Green, A. An international database for pesticide risk assessments and management. *Human and Ecological Risk Assessment: An International Journal* **2016**, *22* (4), 1050.
- (84) European Union, EU Pesticides database, <http://ec.europa.eu/food/plant/pesticides/eu-pesticides-database/public/?event=homepage&language=EN>, 1995-2019. (last access: March 19<sup>th</sup> 2019)
- (85) Thermo Fisher Scientific Inc. TECH TIP #6. Extinction Coefficients.
- (86) Weiss, F.; Hammer, H. S.; Klein, K.; Planatscher, H.; Zanger, U. M.; Noren, A.; Wegler, C.; Artursson, P.; Joos, T. O.; Poetz, O. Direct Quantification of Cytochromes P450 and Drug Transporters-A Rapid, Targeted Mass Spectrometry-Based Immunoassay Panel for Tissues and Cell Culture Lysates. *Drug metabolism and disposition: the biological fate of chemicals* **2018**, *46* (4), 387.
- (87) Schmidt, T.; Samaras, P.; Frejno, M.; Gessulat, S.; Barnert, M.; Kienegger, H.; Krcmar, H.; Schlegl, J.; Ehrlich, H. C.; Aiche, S.; Kuster, B.; Wilhelm, M. ProteomicsDB. *Nucleic Acids Res* **2018**, *46* (D1), D1271.
- (88) Shevchenko, A.; Tomas, H.; Havlis, J.; Olsen, J. V.; Mann, M. In-gel digestion for mass spectrometric characterization of proteins and proteomes. *Nat Protoc* **2006**, *1* (6), 2856.
- (89) Thermo Fisher Scientific Inc. Protein A280 Thermo Scientific NanoDrop Spectrophotometers. **2010**.
- (90) Uniprot Consortium. UniProt: a worldwide hub of protein knowledge. *Nucleic Acids Res* **2019**, *47* (D1), D506.
- (91) Mani, D. R.; Abbatiello, S. E.; Carr, S. A. Statistical characterization of multiple-reaction monitoring mass spectrometry (MRM-MS) assays for quantitative proteomics. *BMC bioinformatics* **2012**, *13 Suppl 16*, S9.
- (92) Magnusson, B.; Örnemark, U. Eurachem Guide: The Fitness for Purpose of Analytical Methods – A Laboratory Guide to Method Validation and Related Topics. **2014**, *2nd ed.* .
- (93) Proc, J. L.; Kuzyk, M. A.; Hardie, D. B.; Yang, J.; Smith, D. S.; Jackson, A. M.; Parker, C. E.; Borchers, C. H. A quantitative study of the effects of chaotropic agents, surfactants, and solvents on the digestion efficiency of human plasma proteins by trypsin. *Journal of proteome research* **2010**, *9* (10), 5422.
- (94) U.S. Department of Health and Human Services Food and Drug Administration. Guidance for Industry Bioanalytical Method Validation. **2013**.
- (95) Kuchling, Horst *Taschenbuch der Physik*; Fachbuchverl. Leipzig im Carl-Hanser-Verlag, 2010.
- (96) Luckert, C.; Braeuning, A.; De Sousa, G.; Durinck, S.; Katsanou, E. S.; Konstantinidou, P.; Machera, K.; Milani, E. S.; Peijnenburg, Aacm; Rahmani, R.; Rajkovic, A.; Rijkers, D.; Spyropoulou, A.; Stamou, M.; Stoop, G.; Sturla, S.; Wollscheid, B.; Zucchini-Pascal, N.; Lampen, A. Adverse Outcome Pathway-Driven Analysis of Liver Steatosis in Vitro: A

- Case Study with Cyproconazole. *Chemical research in toxicology* **2018**, 31 (8), 784.
- (97) Loewe, S.; Muischnek, H. Über Kombinationswirkungen. *Archiv für Experimentelle Pathologie und Pharmakologie* **1926**, 114 (5-6), 313.
- (98) Bliss, C. I. The Toxicity of Poisons Applied Jointly1. *Annals of Applied Biology* **1939**, 26 (3), 585.
- (99) Cedergreen, N. Quantifying synergy: a systematic review of mixture toxicity studies within environmental toxicology. *PLoS One* **2014**, 9 (5), e96580.
- (100) Lambert, D. G. Drugs and receptors. *Continuing Education in Anaesthesia Critical Care & Pain* **2004**, 4 (6), 181.
- (101) Belden, J. B.; Lydy, M. J. Joint toxicity of chlorpyrifos and esfenvalerate to fathead minnows and midge larvae. *Environ Toxicol Chem* **2006**, 25 (2), 623.
- (102) Yu, X.; Zheng, H.; Chan, M. T.; Wu, W. K. HULC: an oncogenic long non-coding RNA in human cancer. *J Cell Mol Med* **2017**, 21 (2), 410.
- (103) Dong, P.; Xiong, Y.; Yue, J.; Hanley, S. J. B.; Kobayashi, N.; Todo, Y.; Watari, H. Long Non-coding RNA NEAT1: A Novel Target for Diagnosis and Therapy in Human Tumors. *Front Genet* **2018**, 9, 471.
- (104) Kim, G.; Weiss, S. J.; Levine, R. L. Methionine oxidation and reduction in proteins. *Biochimica et biophysica acta* **2014**, 1840 (2), 901.
- (105) Godugu, B.; Neta, P.; Simon-Manso, Y.; Stein, S. E. Effect of N-terminal glutamic acid and glutamine on fragmentation of peptide ions. *J Am Soc Mass Spectrom* **2010**, 21 (7), 1169.
- (106) Miki, H.; Funato, Y. Regulation of intracellular signalling through cysteine oxidation by reactive oxygen species. *J Biochem* **2012**, 151 (3), 255.
- (107) Krokhin, O. V.; Craig, R.; Spicer, V.; Ens, W.; Standing, K. G.; Beavis, R. C.; Wilkins, J. A. An improved model for prediction of retention times of tryptic peptides in ion pair reversed-phase HPLC: its application to protein peptide mapping by off-line HPLC-MALDI MS. *Molecular & cellular proteomics : MCP* **2004**, 3 (9), 908.
- (108) Tascher, G.; Burban, A.; Camus, S.; Plumel, M.; Chanon, S.; Le Guevel, R.; Shevchenko, V.; Van Dorsselaer, A.; Lefai, E.; Guguen-Guillouzo, C.; Bertile, F. In-Depth Proteome Analysis Highlights HepaRG Cells as a Versatile Cell System Surrogate for Primary Human Hepatocytes. *Cells* **2019**, 8 (2).
- (109) Gallien, S.; Duriez, E.; Crone, C.; Kellmann, M.; Moehring, T.; Domon, B. Targeted proteomic quantification on quadrupole-orbitrap mass spectrometer. *Molecular & cellular proteomics : MCP* **2012**, 11 (12), 1709.
- (110) Cross, Timothy G.; Hornshaw, Martin P. Can LC and LC-MS ever replace immunoassays? *Journal of Applied Bioanalysis* **2016**, 2 (4), 108.
- (111) Keller, B. O.; Sui, J.; Young, A. B.; Whittall, R. M. Interferences and contaminants encountered in modern mass spectrometry. *Analytica chimica acta* **2008**, 627 (1), 71.
- (112) Kostianen, R.; Kauppila, T. J. Effect of eluent on the ionization process in liquid chromatography-mass spectrometry. *Journal of chromatography. A* **2009**, 1216 (4), 685.
- (113) Westerink, W. M.; Schoonen, W. G. Cytochrome P450 enzyme levels in HepG2 cells and cryopreserved primary human hepatocytes and their induction in HepG2 cells. *Toxicol In Vitro* **2007**, 21 (8), 1581.

- (114) Guillouzo, A.; Corlu, A.; Aninat, C.; Glaise, D.; Morel, F.; Guguen-Guillouzo, C. The human hepatoma HepaRG cells: a highly differentiated model for studies of liver metabolism and toxicity of xenobiotics. *Chem Biol Interact* **2007**, 168 (1), 66.
- (115) Yokoyama, Y.; Sasaki, Y.; Terasaki, N.; Kawataki, T.; Takekawa, K.; Iwase, Y.; Shimizu, T.; Sanoh, S.; Ohta, S. Comparison of Drug Metabolism and Its Related Hepatotoxic Effects in HepaRG, Cryopreserved Human Hepatocytes, and HepG2 Cell Cultures. *Biol Pharm Bull* **2018**, 41 (5), 722.
- (116) Kanebratt, K. P.; Andersson, T. B. HepaRG cells as an in vitro model for evaluation of cytochrome P450 induction in humans. *Drug metabolism and disposition: the biological fate of chemicals* **2008**, 36 (1), 137.
- (117) Antherieu, S.; Chesne, C.; Li, R.; Camus, S.; Lahoz, A.; Picazo, L.; Turpeinen, M.; Tolonen, A.; Uusitalo, J.; Guguen-Guillouzo, C.; Guillouzo, A. Stable expression, activity, and inducibility of cytochromes P450 in differentiated HepaRG cells. *Drug metabolism and disposition: the biological fate of chemicals* **2010**, 38 (3), 516.
- (118) Klein, M.; Thomas, M.; Hofmann, U.; Seehofer, D.; Damm, G.; Zanger, U. M. A systematic comparison of the impact of inflammatory signaling on absorption, distribution, metabolism, and excretion gene expression and activity in primary human hepatocytes and HepaRG cells. *Drug metabolism and disposition: the biological fate of chemicals* **2015**, 43 (2), 273.
- (119) Liu, Y.; Beyer, A.; Aebersold, R. On the Dependency of Cellular Protein Levels on mRNA Abundance. *Cell* **2016**, 165 (3), 535.
- (120) Gedeon, T.; Bokes, P. Delayed protein synthesis reduces the correlation between mRNA and protein fluctuations. *Biophys J* **2012**, 103 (3), 377.
- (121) Wei, P.; Zhang, J.; Dowhan, D. H.; Han, Y.; Moore, D. D. Specific and overlapping functions of the nuclear hormone receptors CAR and PXR in xenobiotic response. *Pharmacogenomics J* **2002**, 2 (2), 117.
- (122) Tolson, A. H.; Wang, H. Regulation of drug-metabolizing enzymes by xenobiotic receptors: PXR and CAR. *Adv Drug Deliv Rev* **2010**, 62 (13), 1238.
- (123) Wang, Y. M.; Ong, S. S.; Chai, S. C.; Chen, T. Role of CAR and PXR in xenobiotic sensing and metabolism. *Expert opinion on drug metabolism & toxicology* **2012**, 8 (7), 803.
- (124) Yamashita, F.; Sasa, Y.; Yoshida, S.; Hisaka, A.; Asai, Y.; Kitano, H.; Hashida, M.; Suzuki, H. Modeling of rifampicin-induced CYP3A4 activation dynamics for the prediction of clinical drug-drug interactions from in vitro data. *PLoS One* **2013**, 8 (9), e70330.
- (125) Rose, Kelly; Wolf, Kristina K.; Ukairo, Okechukwu; Moore, Amanda; Gaffney, Jeannemarie; Bradford, Blair U.; Wetmore, Barbara A.; Andersen, Melvin E.; Lecluyse, Edward L. Nuclear Receptor-Mediated Gene Expression Changes in a Human Hepatic Micropatterned Coculture Model After Treatment with Hepatotoxic Compounds. *Applied In Vitro Toxicology* **2016**, 2 (1), 8.
- (126) Nebert, D. W.; Dalton, T. P.; Okey, A. B.; Gonzalez, F. J. Role of aryl hydrocarbon receptor-mediated induction of the CYP1 enzymes in environmental toxicity and cancer. *The Journal of biological chemistry* **2004**, 279 (23), 23847.

## References

- (127) Knebel, C.; Kebben, J.; Eberini, I.; Palazzolo, L.; Hammer, H. S.; Sussmuth, R. D.; Heise, T.; Hessel-Pras, S.; Lampen, A.; Braeuning, A.; Marx-Stoelting, P. Propiconazole is an activator of AHR and causes concentration additive effects with an established AHR ligand. *Archives of toxicology* **2018**, 92 (12), 3471.
- (128) Zahn, E.; Wolfrum, J.; Knebel, C.; Heise, T.; Weiss, F.; Poetz, O.; Marx-Stoelting, P.; Rieke, S. Mixture effects of two plant protection products in liver cell lines. *Food and chemical toxicology : an international journal published for the British Industrial Biological Research Association* **2018**, 112, 299.

## 9 Supplementary Data

### A. Analytes Covered in this Thesis

Table 30. Abbreviation of analytes covered in this work. Here all analytes that were initially used are defined with their abbreviation, their UniProtID, and the respective protein name after UniProt.<sup>90</sup>

Abbreviation	UniProtID <sup>90</sup>	Name according to UniProt <sup>90</sup>
ACOX2	Q99424	Peroxisomal acyl-coenzyme A oxidase 2
ADH1B	P00325	Alcohol dehydrogenase 1B
ALDH3A1	P30838	Aldehyde dehydrogenase, dimeric NADP-preferring
ANXA10	Q9UJ72	Annexin A10
ARG1	P05089	Arginase-1
CCL20	P78556	C-C motif chemokine 20
CD36	P16671	Platelet glycoprotein 4
CES2	O00748	Cocaine esterase
CGA	P01215	Glycoprotein hormones alpha chain
COX1	P00395	Cytochrome c oxidase subunit 1
CYP1A1	P04798	Cytochrome P450 1A1
CYP1A2	P05177	Cytochrome P450 1A2
CYP2B6	P20813	Cytochrome P450 2B6
CYP2C8	P10632	Cytochrome P450 2C8
CYP2C9	P11712	Cytochrome P450 2C9
CYP2C18	P33260	Cytochrome P450 2C18
CYP2C19	P33261	Cytochrome P450 2C19
CYP2D6	P10635	Cytochrome P450 2D6
CYP2E1	P05181	Cytochrome P450 2E1
CYP2F1	P24903	Cytochrome P450 2F1
CYP3A4	P08684	Cytochrome P450 3A4
CYP3A5	P20815	Cytochrome P450 3A5
CYP3A7	P24462	Cytochrome P450 3A7
CYP3A43	Q9HB55	Cytochrome P450 3A43
CYP7A1	P22680	Cholesterol 7-alpha-monooxygenase
FASN	P49327	Fatty acid synthase
G6PC	P35575	Glucose-6-phosphatase
GAPDH	P04406	Glyceraldehyde-3-phosphate dehydrogenase
GZMB	P10144	Granzyme B
HRG	P04196	Histidine-rich glycoprotein
HSD11B2	P80365	Corticosteroid 11-beta-dehydrogenase isozyme 2
IL6	P05231	Interleukin-6

## Supplementary Data

Abbreviation	UniProtID <sup>90</sup>	Name according to UniProt <sup>90</sup>
INSIG1	O15503	Insulin-induced gene 1 protein
LMNA	P02545	Prelamin-A/C
LY6D	Q14210	Lymphocyte antigen 6D
MDR1	P08183	Multidrug resistance protein 1
MLXIP	Q9HAP2	MLX-interacting protein
NCPR	P16435	NADPH-cytochrome P450 reductase
NQO1	P15559	NAD(P)H dehydrogenase [quinone] 1
NR1I3	Q14994	Nuclear receptor subfamily 1 group I member 3
PRKDC	P78527	DNA-dependent protein kinase catalytic subunit
S100P	P25815	Protein S100-P
SCARA3	Q6AZY7	Scavenger receptor class A member 3
SCD	O00767	Acyl-CoA desaturase
SREBF1	P36956	Sterol regulatory element-binding protein 1
SULT1B1	O43704	Sulfotransferase family cytosolic 1B member 1
SYT1	P21579	Synaptotagmin-1
TNFRSF12A	Q9NP84	Tumor necrosis factor receptor superfamily member 12A
UGT1A1	P22309	UDP-glucuronosyltransferase 1-1
UGT1A3	P35503	UDP-glucuronosyltransferase 1-3
UGT2B7	P16662	UDP-glucuronosyltransferase 2B7
UGT2B15	P54855	UDP-glucuronosyltransferase 2B15

## B. Results of Comprehensive Database Search

Table 31. Results of the database search for potential target peptides. In this table, the proteins with their respective UniProt ID <sup>90</sup>, the chosen peptide with its parameters like proteotypicity, length, natural variants, or modifications within the sequence and the hydrophobicity factor are shown. Besides, it was checked whether already an antibody existed and if these particular peptides have already been found in other mass spectrometric projects.

Protein	UniProt ID <sup>90</sup>	Peptide	Antibody available	Proteotypic	Length (amino acids)	Natural Variant/Modification	Hydrophobicity factor	Entry in ProteomicsDB <sup>87</sup>
ACOX2	Q99424	LENEPAIQVLK	N	Y	12	N/N	2.4	Y
		FAQVLPDGTYYK	N	Y	12	N/N	2.6	Y
ADH1B	P00325	GAVYGGFK	N	Y	8	N/N	2.0	Y
		-	-	-	-	-	-	-
ALDH3A1	P30838	ISEAVK	Y	Y	6	N/N	1.9	Y
		IQQLEALQR	N	Y	9	N/N	2.7	Y
ANXA10	Q9UJ72	LYSAIHDFGFHNK	N	Y	13	N/N	2.8	Y
		NFASGHYK	N	Y	8	N/N	1.2	Y
ARG1	P05089	DVDPGEHYILK	N	Y	11	N/N	2.0	Y
		TIGHIGAPFSK	Y	Y	11	Y/Y	3.0	Y
CCL20	P78556	LSVCANPK	N	Y	8	N/N	1.4	Y
		-	-	-	-	-	-	-
CD36	P16671	LQVNLLVKPSEK	N	Y	12	N/N	2.7	Y
		-	-	-	-	-	-	-
CES2	O00748	IQELEEPEER	Y	Y	10	N/N	1.6	Y
		TTHTGQVLGSLVHVK	N	Y	15	N/N	1.8	Y
CGA	P01215	AYPTPLR	N	Y	7	N/N	2.0	Y

Protein	UniProt ID <sup>90</sup>	Peptide	Antibody available	Proteotypic	Length (amino acids)	Natural Variant/Modification	Hydrophobicity factor	Entry in ProteomicsDB <sup>87</sup>
		-	-	-	-	-	-	-
COX1	P00395	DIGTLYLLFGAWAGVLG-TALSLLIR	N	Y	25	N/N	4.5	Y
		-	-	-	-	-	-	-
CYP7A1	P22680	TLENAGQK	N	Y	8	N/N	0.7	Y
		LSSASLNIR	N	Y	9	N/N	2.6	Y
FASN	P49327	TGTVSLEVR	Y	Y	9	N/N	1.9	Y
		VVEVLAGHGHLYSR	N	Y	14	N/N	2.3	Y
G6PC	P35575	YFLITFFLFSFAIGFYLLK	N	Y	20	Y/N	6.7	N
		GLGVDLLWTLEK	N	Y	12	Y/N	4.2	N
GAPDH	P04406	AGAHLQGGAK	N	Y	10	N/N	0.5	Y
		QASEGPLK	N	Y	8	N/N	0.8	Y
GZMB	P10144	VSSFVHWIK	N	Y	9	N/N	3.9	Y
		HSHTLQEVK	N	Y	9	N/N	1.0	Y
HRG	P04196	EENDDFASFR	N	Y	10	N/N	1.8	Y
		HPNVFGFCR	Y	Y	9	N/N	2.3	Y
HSD11B2	P80365	VSIIQPGCFK	N	Y	10	N/N	2.7	Y
		-	-	-	-	-	-	-
IL6	P05231	FESSEEQAR	N	Y	9	N/N	0.8	Y
		-	-	-	-	-	-	-
INSIG1	O15503	LHDHFWSCSCAHSAR	N	Y	15	N/N	1.5	Y
		-	-	-	-	-	-	-



Protein	UniProt ID <sup>90</sup>	Peptide	Antibody available	Proteotypic	Length (amino acids)	Natural Variant/Modification	Hydrophobicity factor	Entry in ProteomicsDB <sup>87</sup>
LMNA	P02545	LEAALGEAK	N	Y	9	N/N	2.1	Y
		DLEDGLAR	N	Y	8	N/N	2.1	Y
LY6D	Q14210	HSVVCASSR	N	Y	10	N/N	0.5	Y
		TTNTVEPLR	N	Y	9	N/N	1.5	Y
MLXIP	Q9HAP2	LTSHAITLQK	N	Y	10	N/N	2.4	Y
		GYDFDTVNK	N	Y	9	N/N	1.7	Y
NQO1	P15559	FGLSVGHHLGK	N	Y	11	N/N	2.4	Y
		DPANFQYPAESVLAYK	N	Y	16	N/N	1.9	Y
NR1I3	Q14994	AQQTPVQLSK	N	Y	10	N/N	1.1	Y
		-	-	-	-	-	-	-
PRKDC	P78527	VTELALTASDR	N	Y	11	N/N	2.2	Y
		LGLPGDEVNKK	N	Y	11	N/N	1.7	Y
S100P	P25815	ELPGFLQSGK	N	Y	10	N/N	2.5	Y
		YSGSEGSTQTLTK	N	Y	13	N/N	0.6	Y
SCARA3	Q6AZY7	AVDTQHGEILR	N	Y	11	N/N	1.8	Y
		NLQGLDPK	N	Y	8	N/N	1.8	Y
SCD	O00767	VLQNGGDK	N	Y	8	N/N	1.0	Y
		DDIYDPTYK	N	Y	9	N/N	1.5	Y
SREBF1	P36956	VFLHEATAR	N	Y	9	N/N	2.7	Y
		FLQHSNQK	N	Y	8	N/N	1.6	Y
SULT1B1	O43704	TSGIEQLEK	N	Y	9	N/N	1.5	Y
		NYFTVAQNEK	N	Y	10	N/N	1.6	Y

Protein	UniProt ID <sup>90</sup>	Peptide	Antibody available	Proteotypic	Length (amino acids)	Natural Variant/Modification	Hydrophobicity factor	Entry in ProteomicsDB <sup>87</sup>
SYT1	P21579	VFVGYNSTGAELR	N	Y	13	N/N	2.3	Y
		HDIIGEFGK	N	Y	8	N/N	2.8	N
TNFRSF12A	Q9NP84	GSSWSADLDK	N	Y	10	N/N	1.5	Y
		-	-	-	-	-	-	-
UGT1A1	P22309	TYPVPFQR	N	Y	8	Y/N	2.3	Y
		-	-	-	-	-	-	-
UGT1A3	P35503	YLSIPTVFFLR	N	Y	11	N/N	5.1	Y
		-	-	-	-	-	-	-
UGT2B7	P16662	ANVIASALAQIPQK	N	Y	14	N/N	2.1	Y
		IEIYPTSLTK	N	Y	10	N/N	2.9	Y
UGT2B15	P54855	SVINDPVYK	N	Y	9	N/N	2.0	Y
		-	-	-	-	-	-	-

## C. Results of the Mass Spectrometric Detection Compatibility

Table 32. Results of mass spectrometric detection compatibility. Analytes with determined precursor ions, charge state, quantifiers, and normalized collision energies (NCEs) are shown.

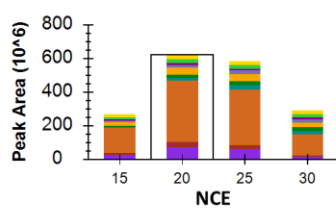
Analyte	Peptide sequence	Precursor m/z	Quantifier m/z	NCE
ACOX2	LENPAIQQVLK	691.3879++	896.5564+, y8	20
ADH1B	GAVYGGFK	399.7109++	571.2875+, y5	25
ALDH3A1	IQQLEALQR	549.8169++	857.4839+, y7	20
ANXA10	LYSAIHDFGFHNK	516.9246+++	864.3999+, y7	25
ARG1(PFSK)	TIGHGAPFSK	552.3266++	889.5142+, y9	25
ARG1(YILK)	DVDPGEHYILK	643.3248++	478.7636++, y8	25
CCL20	LSVCANPK	444.7340++	688.3447+, y6	20
CD36	LQVNLLVKPSEK	456.6134+++	460.2402+, y4	25
CES2	IQELEEPEER	636.3093++	530.2569+, y4	25
CGA	AYPTPLR	409.2320++	583.3562+, y5	20
COX1	DIGTLYLLFGAWAGV LGTALSLLR	878.5070+++	943.5935+, y9	20
CYP1A1	GFYIPK	362.7051++	520.3130+, y4	15
CYP1A2	DTTLNGFYIPK	634.8297++	838.4458+, y7	20
CYP2B6	AEAFSGR	369.1825++	537.2780+, y5	15
CYP2C8	EALIDNGEEFSGR	718.8362++	1010.4174+, y9	25
CYP2C9	GIFPLAER	451.7584++	585.3355+, y5	25
CYP2C18	EALIDHGEEFSGR	730.3442++	781.3475+, y7	30
CYP2C19	GHFPLAER	463.7458++	585.3355+, y5	25
CYP2D6	GTTLITNLSSVLK	673.8981++	861.5040+, y8	20
CYP2E1	DEFSGR	355.6588++	466.2409+, y4	15
CYP2F1	EALVDQGEFSGR	718.8362++	1024.4330+, y9	25
CYP3A4	LQEEIDAVLPNK	684.8721++	1127.5943+, y10	20
CYP3A5(FIPK)	DVEINGVFIPK	615.8401++	774.4509+, y7	20
CYP3A5(LPNK)	EIDAVLPNK	499.7795++	471.2926+, y4	20
CYP3A7	EIDTVLPNK	514.7848++	358.2085+, y3	20
CYP3A43	DIEINGVFIPK	622.8479++	1016.5775+, y9	20
CYP7A1	LSSASLNIR	480.7773++	760.4312+, y7	20
FASN	TGTVSLEVR	481.2693++	603.3461+, y5	25
G6PC	GLGVDLLWTLEK	672.3821++	1017.5615+, y8	20
GAPDH	AGAHLQGGAK	455.2487++	573.3355+, y6	25
GZMB	VSSFVHWIK	551.8058++	916.5039+, y7	20

## Supplementary Data

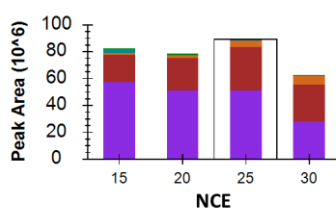
Analyte	Peptide sequence	Precursor m/z	Quantifier m/z	NCE
HRG	HPNVFGFCR	567.2691++	996.4720+, y8	25
HSD11B2	VSHIQPGCFK	574.8103++	608.2861+, y5	25
IL6	FESSEEQAR	541.7411++	806.3639+, y7	25
INSIG1	LHDHFWSCSCAHSAR	624.2669+++	1035.4095+, y9	30
LMNA	LEAALGEAK	451.2531++	659.3723+, y7	20
LY6D	TTNTVEPLR	515.7800++	828.4574+, y7	20
MDR1	EANIHAFIESLPNK	791.9148++	358.2085+, y3	25
MLXIP	GYDFDTVNK	529.7431++	838.3941+, y7	20
NCPR	ESSFVEK	413.2031++	375.2238+, y3	25
NQO1	FGLSVGHHLGK	384.5489+++	417.7327++, y8	25
NR1I3	AQQTPVQLSK	550.3089++	900.5149+, y8	20
PRKDC	LGLPGDEVNDK	578.7959++	437.2011++, y8	20
S100P	ELPGFLQSGK	538.2928++	417.2294++, y8	20
SCARA3	NLQGLDPK	442.7454++	657.3566+, y6	20
SCD	DDIYDPTYK	565.2560++	786.3668+, y6	20
SREBF1	VFLHEATAR	522.2853++	684.3424+, y6	25
SULT1B1	TSGIEQLEK	502.7666++	816.4462+, y7	20
SYT1	HDIIGEFK	479.7533++	480.2453+, y4	20
TNFRSF12A	GSSWSADLDK	533.2460++	648.3199+, y6	25
UGT1A1	TYPVPFQR	504.2691++	547.2987+, y4	25
UGT1A3	YLSIPTVFFLR	678.3897++	879.5087+, y7	20
UGT2B7	ANVIASALAQIPQK	475.2804+++	684.4039+, y6	20
UGT2B15	SVINDPVYK	517.7795++	848.4512+, y7	20

In Figure 45 on the next pages, the results for the optimized normalized collision energies (NCEs) are shown.

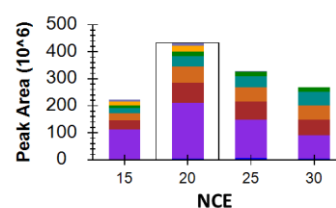
ACOX2



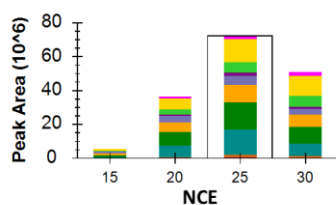
ADH1B



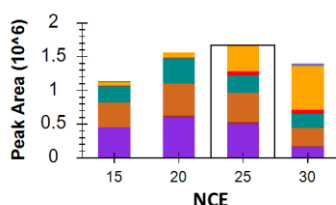
ALDH3A1



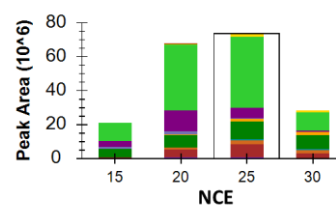
ANXA10



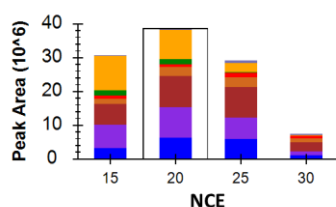
ARG1 (PFSK)



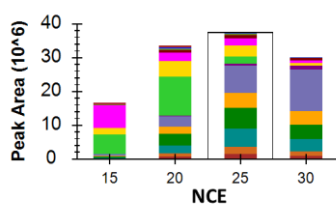
ARG1 (YILK)



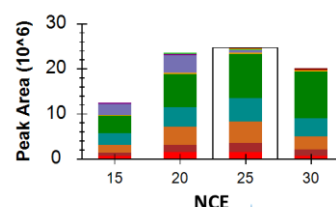
CCL20



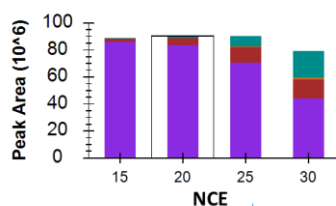
CD36



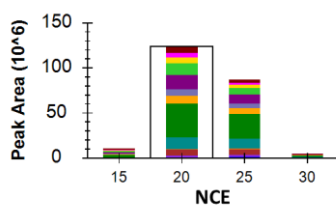
CES2



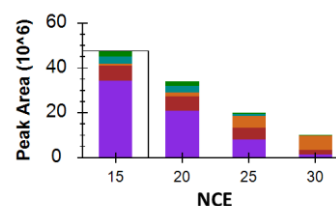
CGA



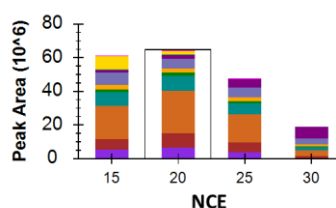
COX1



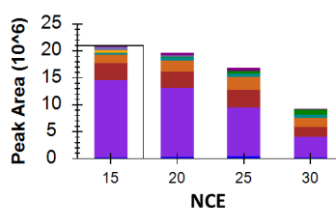
CYP1A1



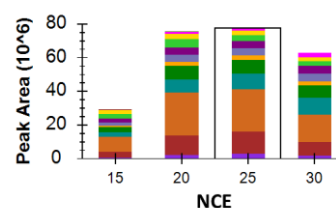
CYP1A2



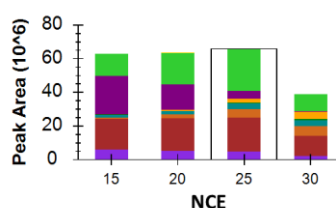
CYP2B6



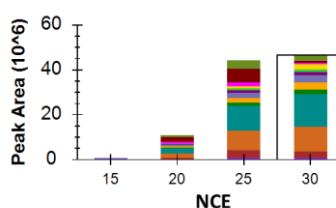
CYP2C8



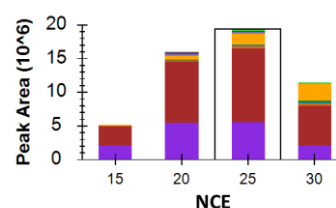
CYP2C9



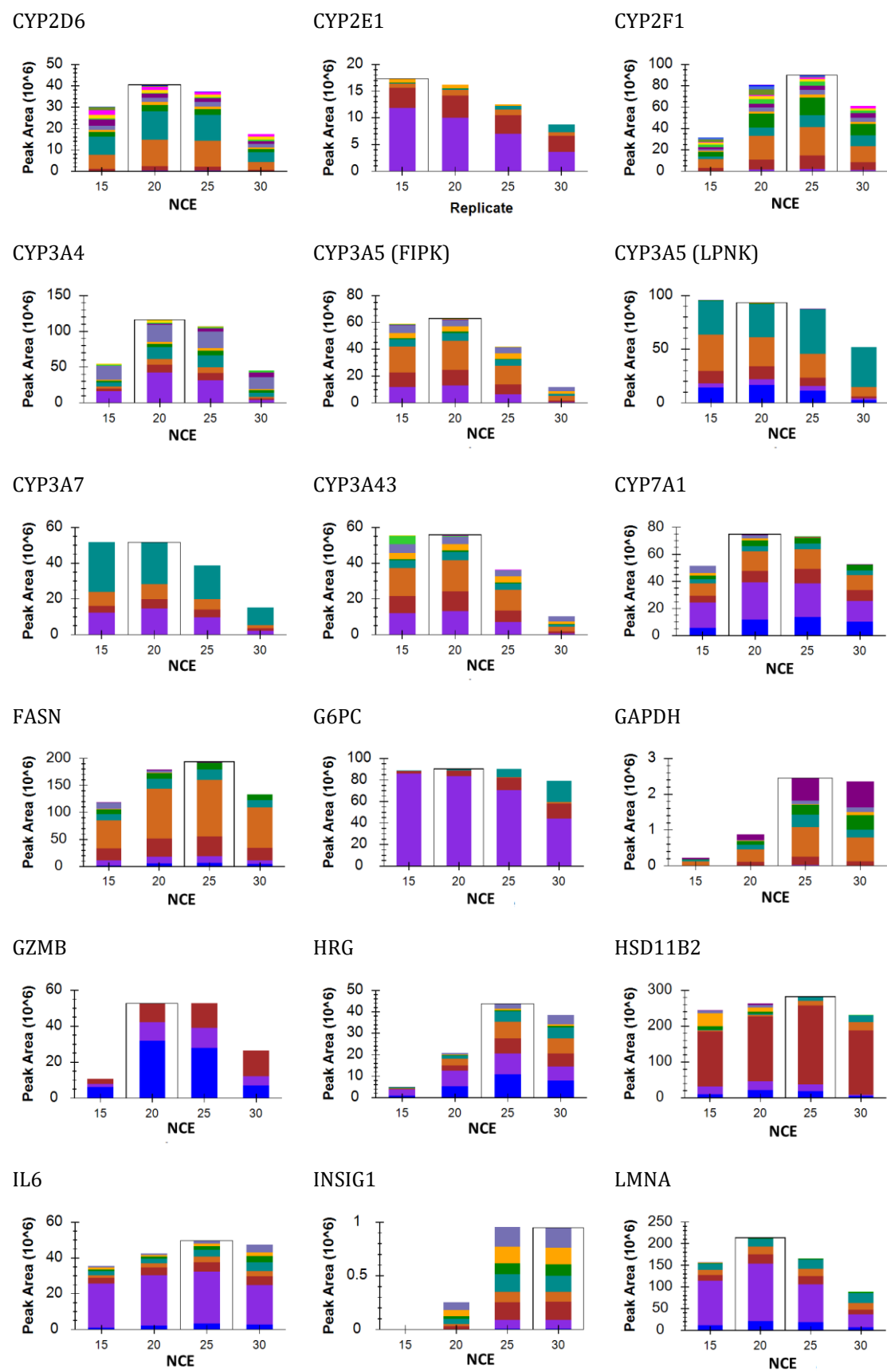
CYP2C18



CYP2C19



Supplementary Data



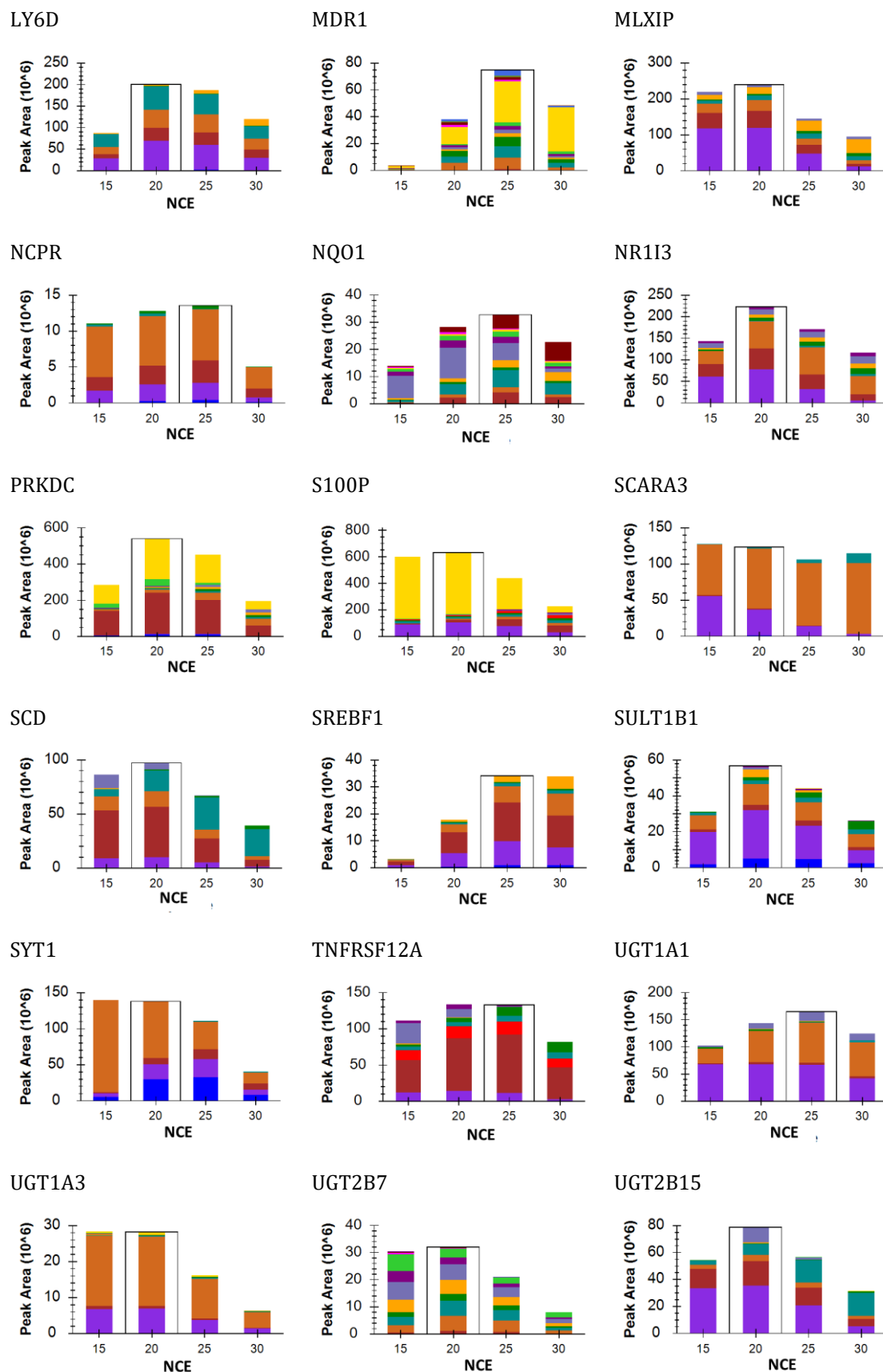


Figure 45. Summary of normalized collision energy optimization. The x-axis shows the four different normalized collision energies (NCEs) examined, and the y-axis shows the respective peak areas. The ideal NCE is marked with a black frame.

## D. Results of the Proteome Discoverer Screening after In-Gel Digest and Full-Scan (Full-MS) Measurement

Table 33. Results of Proteome Discoverer screening for analytes of interest. Here the analyte is displayed with its sequence, UniProtID <sup>90</sup>, and whether it was found after Proteome Discoverer processing. If not only the protein but also the peptide of interest was found, the retention time is also displayed.

Analyte	Peptide Sequence	UniProtID <sup>90</sup>	Protein found	Peptide found	Retention time in min
ACOX2	LENEPAIQVVLK	Q99424	N	N	-
ADH1B	GAVYGGFK	P00325	Y	Y	53.10
ALDH3A1	IQQLEALQR	P30838	Y	Y	69.69
ANXA10	LYSAIHDFGFHNK	Q9UJ72	N	N	-
ARG1	TIGHIGAPFSK	P05089	Y	Y	106.02
ARG1	DVDPGEHYILK	P05089	Y	Y	73.24
CCL20	LSVCANPK	P78556	N	N	-
CD36	LQVNLLVKPSEK	P16671	N	N	-
CES2	IQELEEPEER	O00748	Y	N	-
CGA	AYPTPLR	P01215	N	N	-
COX1	DIGTLYLLFGAWAGVLG-TALSLLIR	P00395	Y	N	-
CYP7A1	LSSASLNIR	P22680	N	N	-
FASN	TGTVSLEVR	P49327	Y	Y	63.69
G6PC	GLGVDLLWTLEK	P35575	N	N	-
GAPDH	AGAHLQGGAK	P04406	Y	N	-
GZMB	VSSFVHWIK	P10144	N	N	-
HRG	HPNVFGFCR	P04196	N	N	-
HSD11B2	VSIIQPGCFK	P80365	N	N	-
IL6	FESSEEQAR	P05231	N	N	-
INSIG1	LHDHFWSCSAHSAR	O15503	N	N	-
LMNA	LEAALGEAK	P02545	Y	Y	53.75
LY6D	TTNTVEPLR	Q14210	N	N	-
MLXIP	GYDFDTVNK	Q9HAP2	N	N	-
NQO1	FGLSVGHHLGK	P15559	N	N	-
NR1I3	AQQTPVQLSK	Q14994	N	N	-
PRKDC	LGLPGDEVDNK	P78527	Y	N	-
S100P	ELPGFLQSGK	P25815	N	N	-
SCARA3	NLQGLDPK	Q6AZY7	Y	N	-
SCD	DDIYDPTYK	O00767	N	N	-
SREBF1	VFLHEATAR	P36956	N	N	-



Analyte	Peptide Sequence	UniProtID <sup>90</sup>	Protein found	Peptide found	Retention time in min
SULT1B1	TSGIEQLEK	O43704	N	N	-
SYT1	HDIIGEFK	P21579	N	N	-
TNFRSF12A	GSSWSADLDK	Q9NP84	N	N	-
UGT1A1	TYPVPFQR	P22309	Y	N	-
UGT1A3	YLSIPTVFFLR	P35503	Y	N	-
UGT2B7	ANVIASALAQIPQK	P16662	Y	Y	111.82
UGT2B15	SVINDPVYK	P54855	Y	Y	66.73

Y= Protein/peptide was found; N= Protein/peptide was not found

## E. Results of EN<sub>s</sub> Enrichment from a Complex Matrix

Table 34. Target EN<sub>s</sub> enrichment from a complex matrix. A human blend sample in the ratio 1:1:1 (HEK, HCT, and HepG2) was used as a matrix, and by two antibodies that were generated for each respective TXP tag, EN<sub>s</sub> peptide enrichment was investigated. Measurements were done in triplicates, and coefficients of variation (C.V.s) were determined.

Analyte	TXP-tag	Area (animal 1)	C.V. in %	Area (animal 2)	C.V. in %
ACOX2	QVLK	2.60E+07	10.4	1.05E+07	20.8
ADH1B	GGFK	4.73E+06	16.4	9.97E+06	18.6
ALDH3A1	ALQR	3.82E+06	15.7	n.d.	na
ANXA10	FHNK	4.03E+07	21.7	4.42E+07	9.9
ARG1	YILK	2.58E+08	13.4	1.79E+08	3.2
ARG1	PFSK	5.97E+08	5.5	2.94E+08	3.1
CCL20	ANPK	3.93E+07	21.6	4.50E+07	11.7
CD36	PSEK	6.21E+04	28.0	2.37E+06	5.2
CES2	PEER	3.60E+06	25.9	n.d.	na
CGA	TPLR	4.36E+06	17.6	4.59E+06	20.3
COX1	LLIR	3.07E+05	36.2	3.96E+05	13.8
CYP7A1	LNIR	1.23E+08	8.4	1.13E+08	1.8
FASN	LEVR	n.d.	na	1.16E+07	18.8
G6PC	TLEK	1.91E+07	8.0	1.76E+06	33.2
GAPDH	GGAK	2.85E+05	49.0	9.59E+05	44.4
GZMB	HWIK	1.29E+07	11.3	9.50E+06	7.7
HRG	GFCR	1.40E+08	0.2	4.70E+07	5.7
HSD11B2	GCFK	1.27E+08	16.2	1.37E+08	12.9
IL6	EAQR	7.97E+05	54.3	4.44E+06	18.6
INSIG1	HSAR	2.50E+05	12.0	1.20E+05	18.2
LMNA	GEAK	1.83E+07	4.7	1.74E+07	8.9

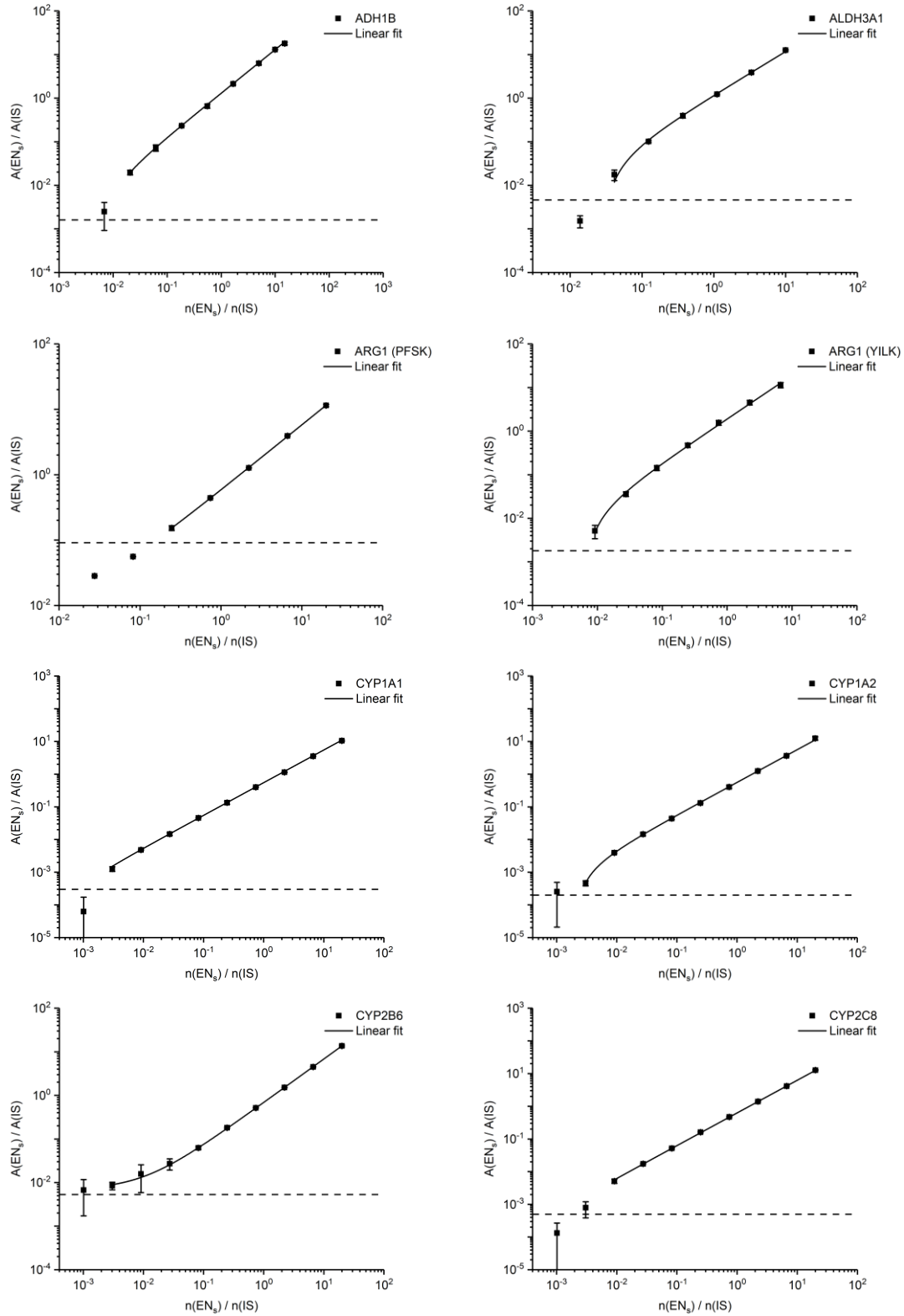
## Supplementary Data

Analyte	TXP-tag	Area (animal 1)	C.V. in %	Area (animal 2)	C.V. in %
LY6D	EPLR	2.85E+05	34.9	4.30E+05	6.7
MLXIP	TVNK	1.44E+06	10.1	3.81E+05	47.3
NQO1	HLGK	1.46E+08	11.1	1.53E+08	14.2
NR1I3	QLSK	1.98E+07	24.8	1.09E+07	28.5
PRKDC	VDNK	9.39E+07	20.5	6.52E+07	13.0
S100P	QSGK	1.30E+08	13.8	4.28E+08	7.4
SCARA3	LDPK	3.99E+06	62.1	3.43E+06	50.0
SCD	PTYK	7.24E+04	13.6	n.d.	na
SREBF1	ATAR	2.11E+06	9.5	1.67E+04	39.2
SULT1B1	QLEK	9.07E+07	7.7	2.15E+08	11.6
SYT1	GEFK	1.22E+06	13.4	6.59E+04	21.3
TNFRSF12A	DLDK	5.06E+07	11.2	6.34E+07	20.0
UGT1A1	PFQR	3.31E+05	10.5	3.35E+07	14.8
UGT1A3	FFLR	3.87E+05	7.7	4.45E+08	14.4
UGT2B7	IPQK	4.64E+07	7.2	1.36E+07	3.2
UGT2B15	PVYK	9.60E+06	17.6	7.16E+06	7.8

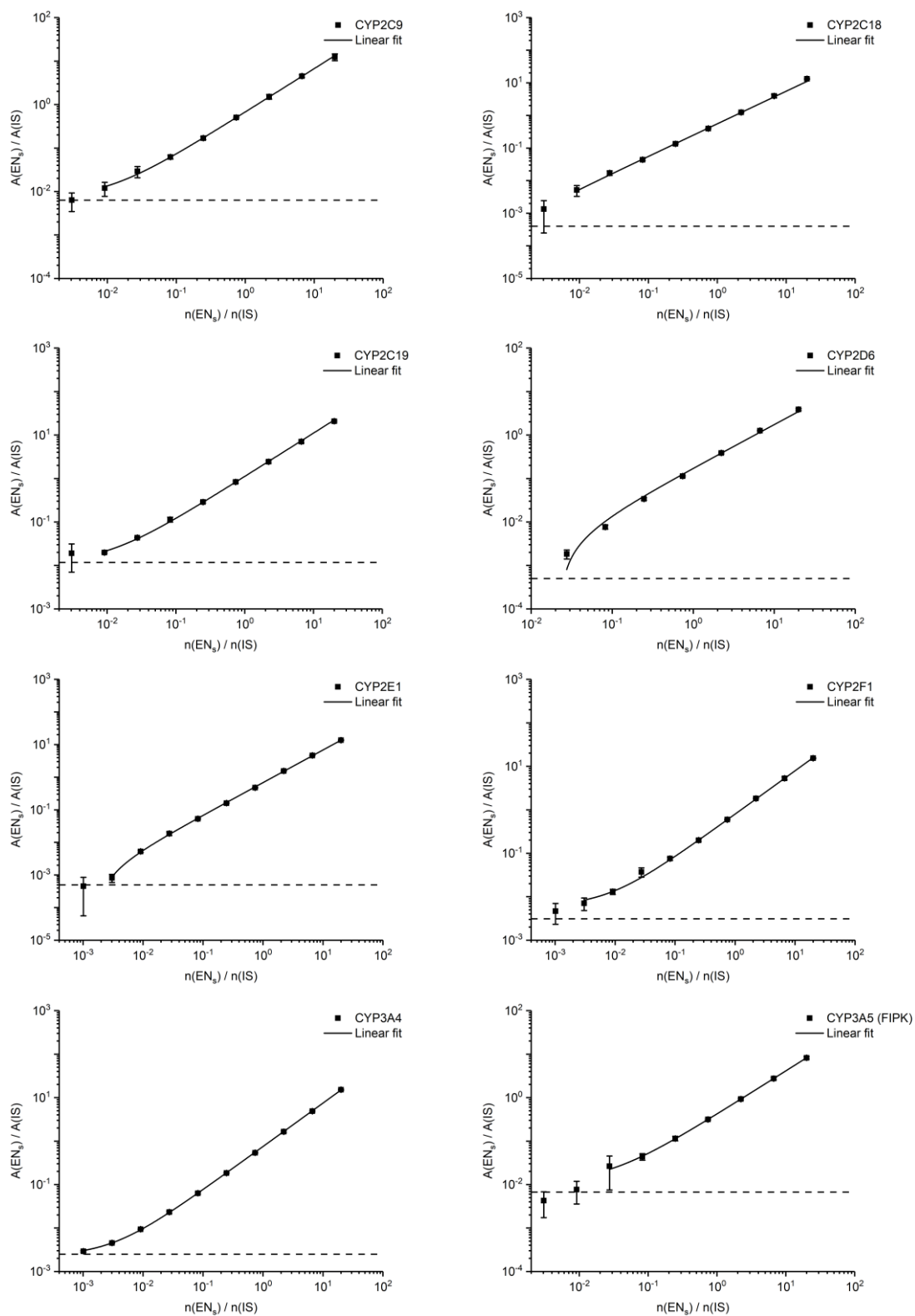
n.d.= not detected; na= not applicable

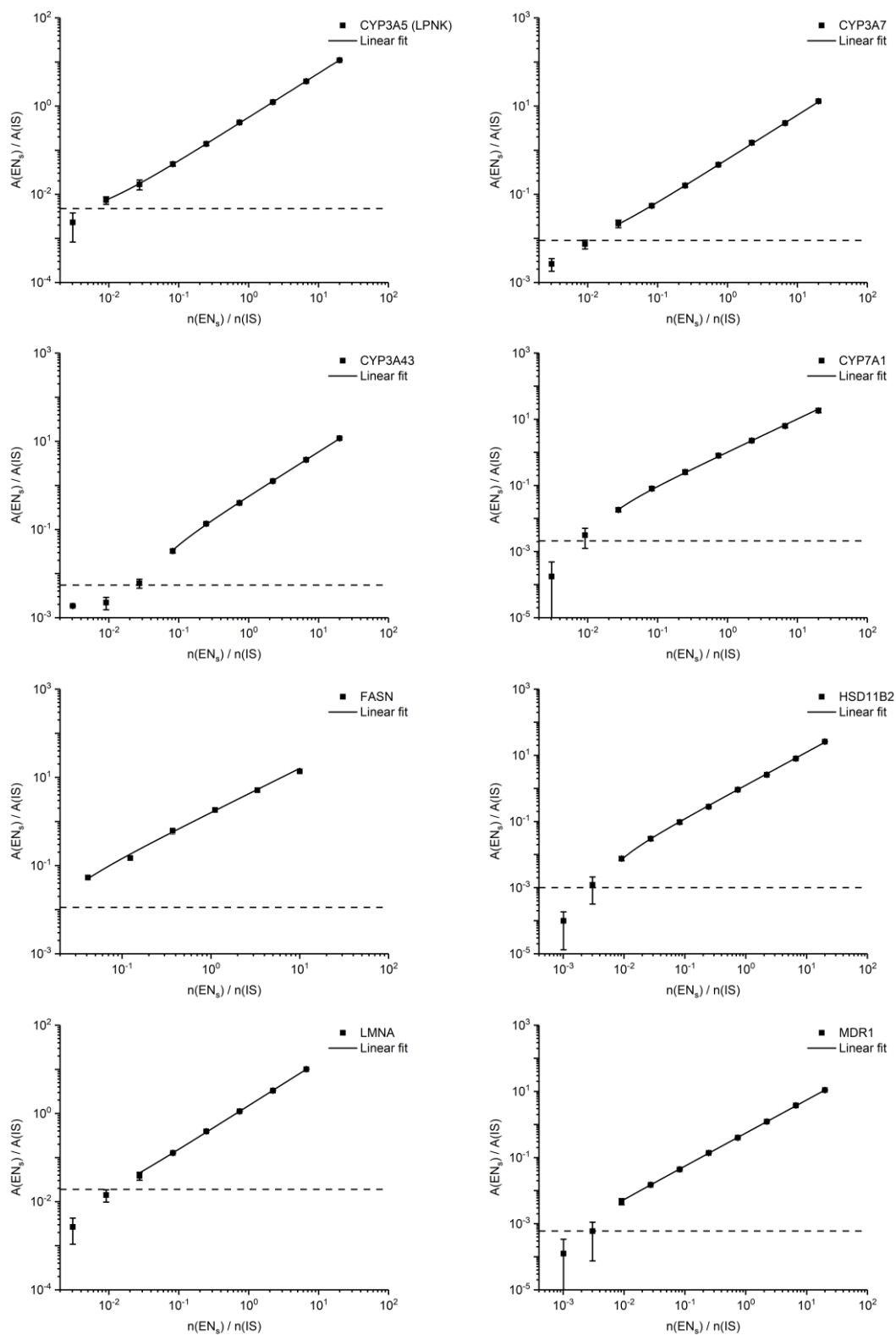
## F. Linearity and Accuracy Plots

In Figure 46, the linearity plots are shown for multiplex 1-6, as well as the CYP 17-plex.

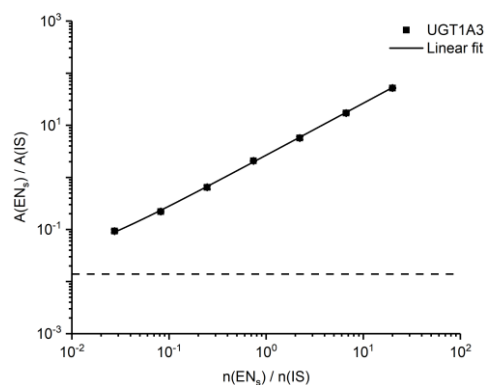
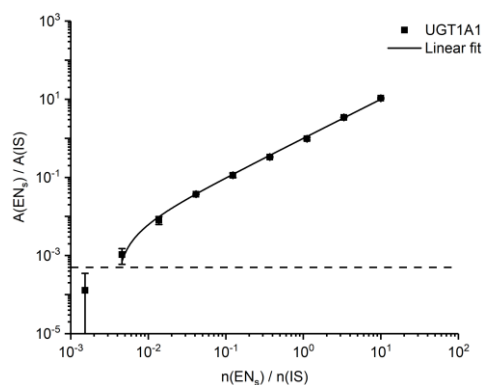
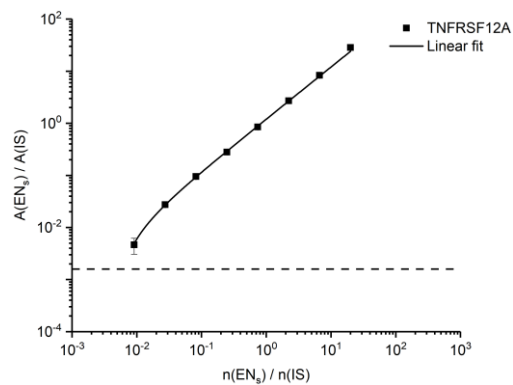
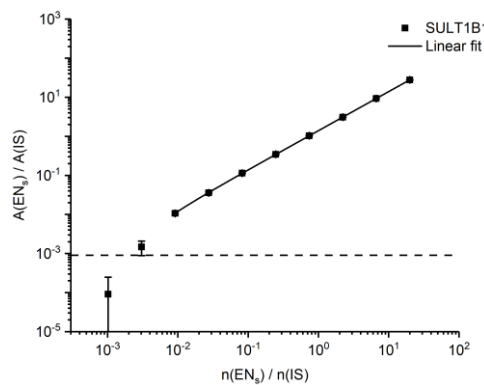
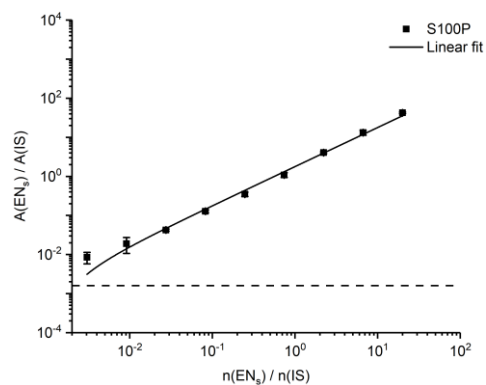
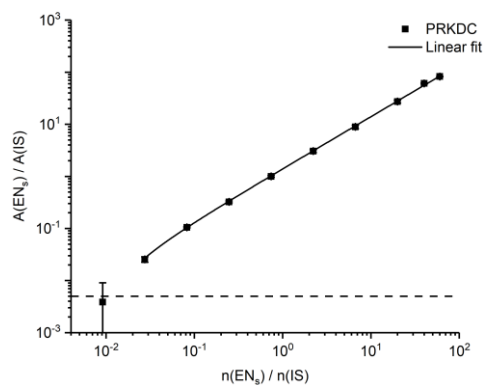
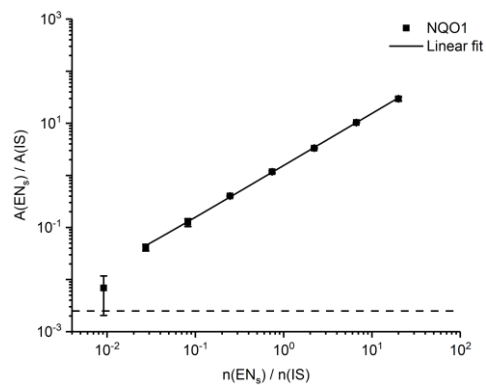
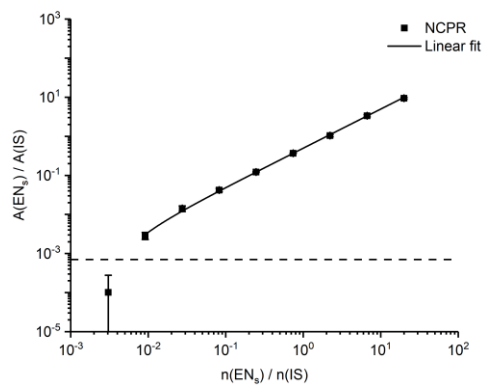


# Supplementary Data





# Supplementary Data



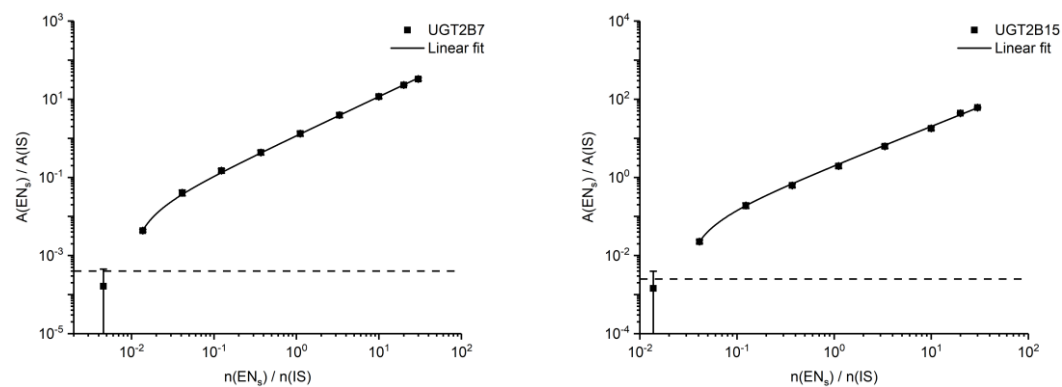
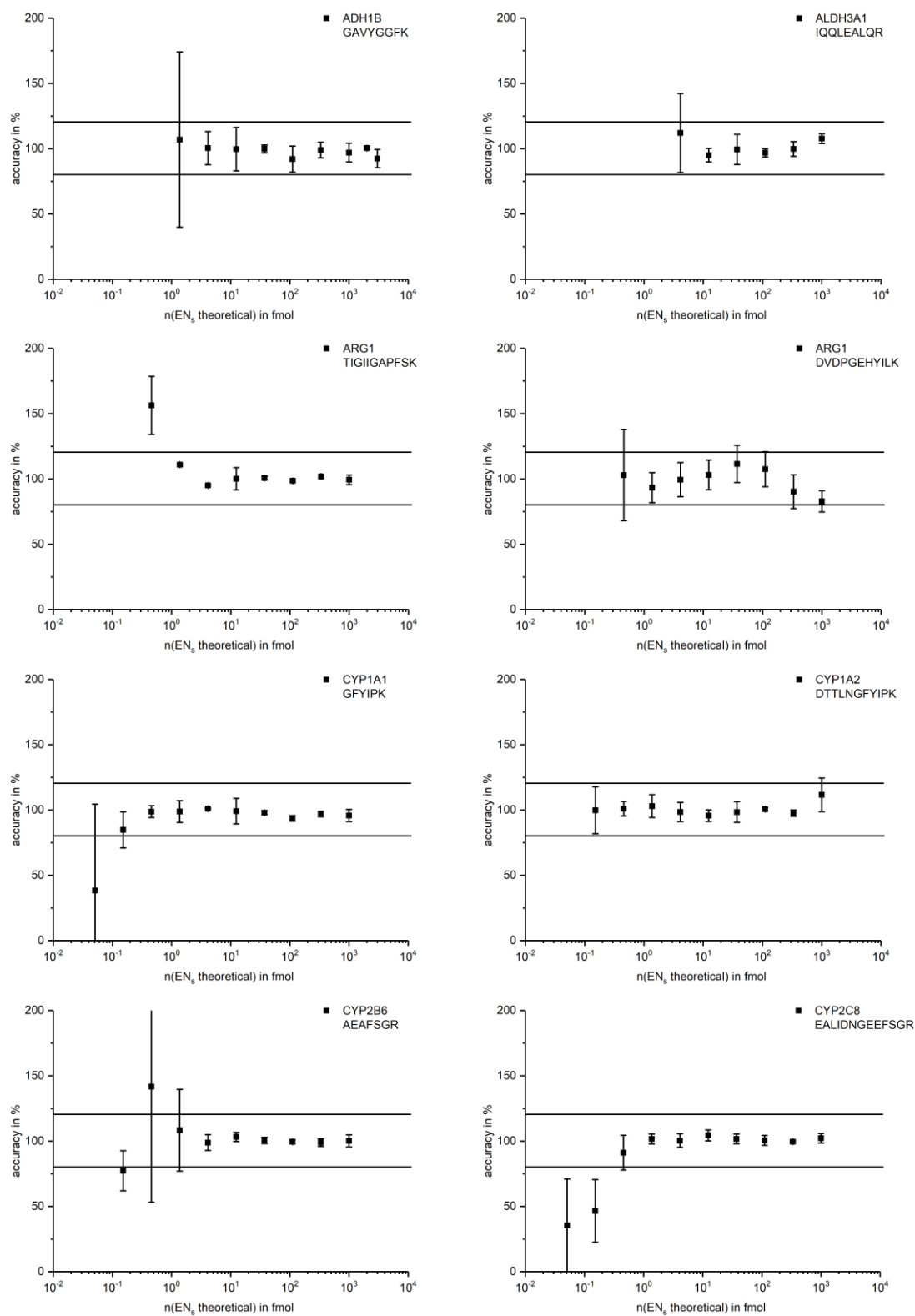


Figure 46. Linearity results of multiplex assays in PBSC. The ratio of the non-labeled synthetic peptide and the internal isotopically labeled standard peptide ( $EN_s/IS$ ) area is plotted against the amount of substance of the  $EN_s/IS$  ratio. Measurements were performed in parallel reaction monitoring (PRM) for multiplex assays 1-6 as well as for the CYP 17-plex. Dilutions were performed in triplicates. The dashed horizontal line in each graph indicates the limit of detection (LOD).

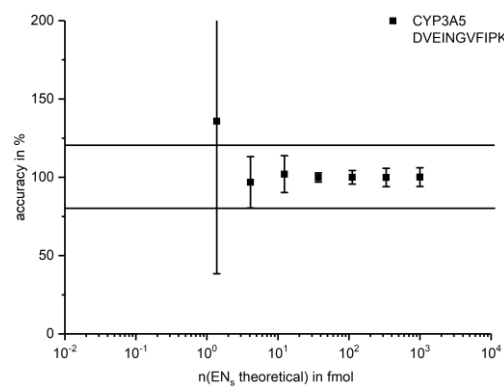
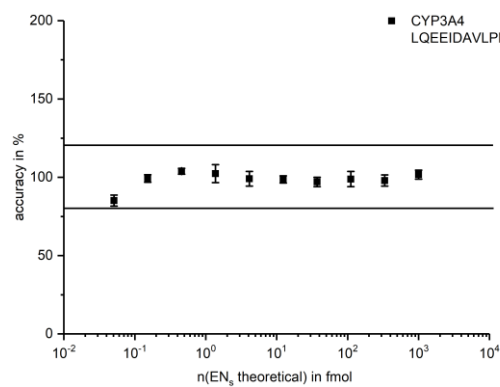
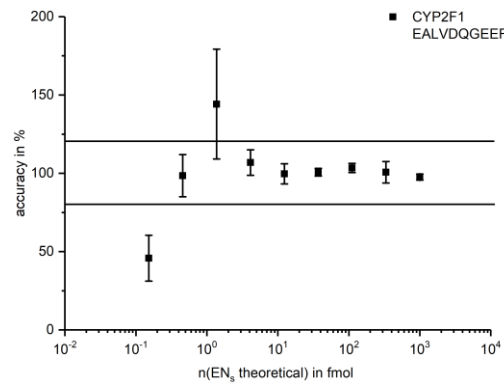
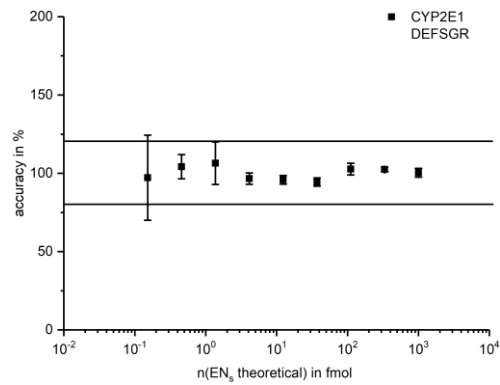
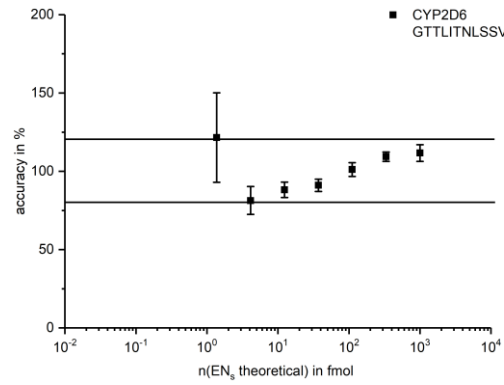
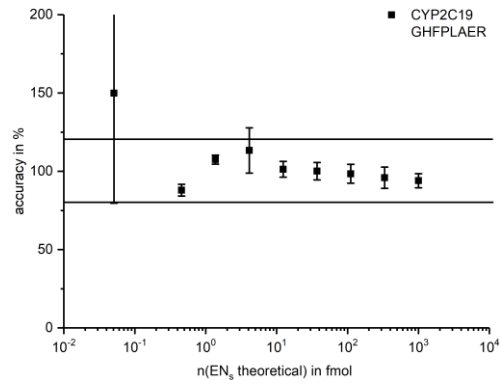
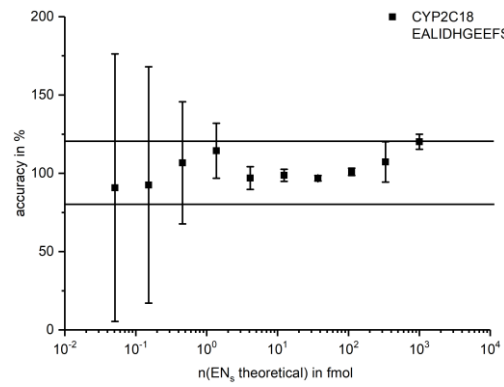
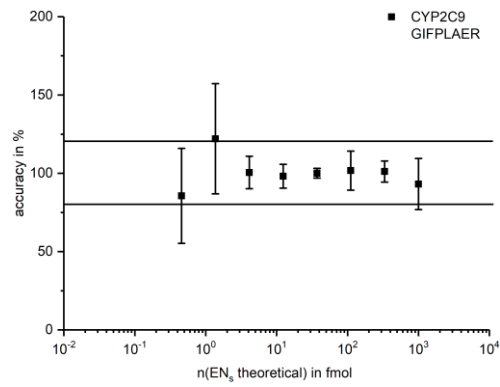
## Supplementary Data

In Figure 47, the accuracy plots are shown for multiplex 1-6, as well as the CYP 17-plex.

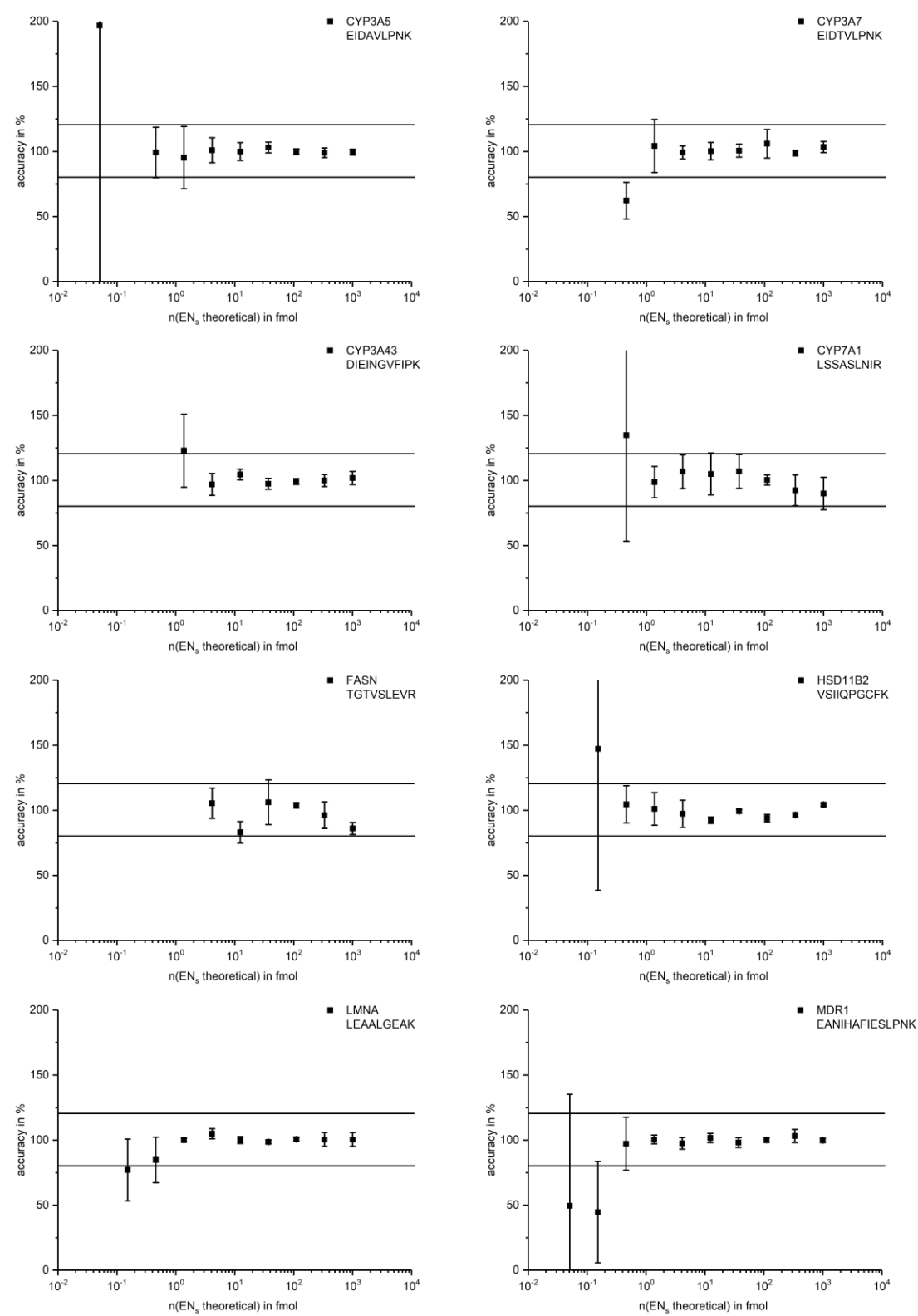




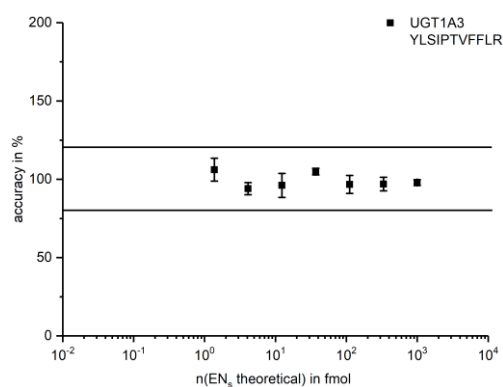
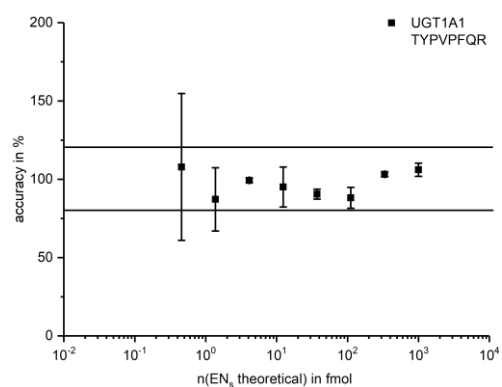
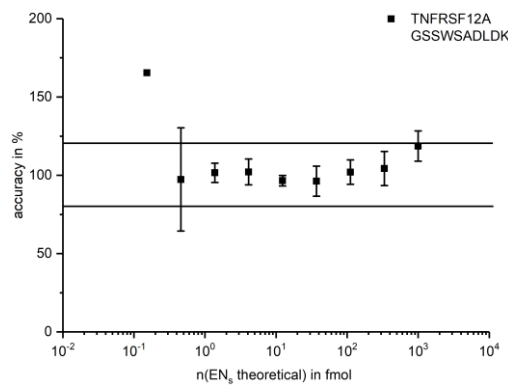
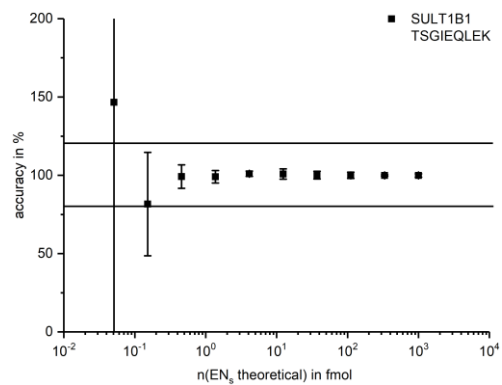
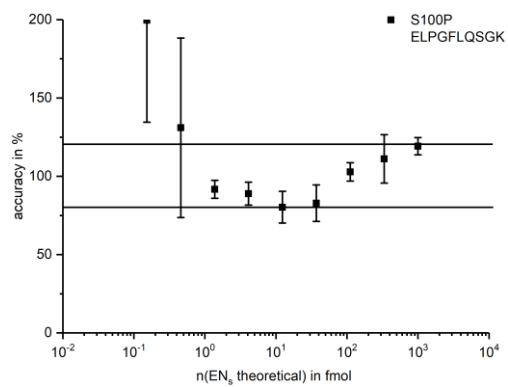
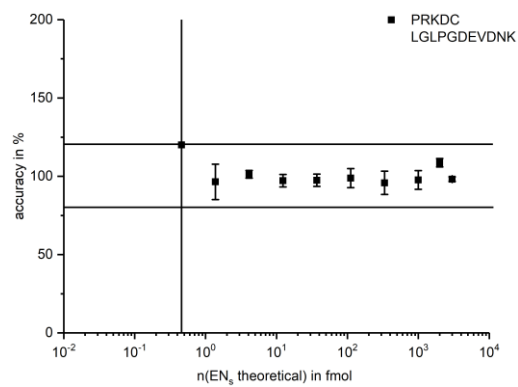
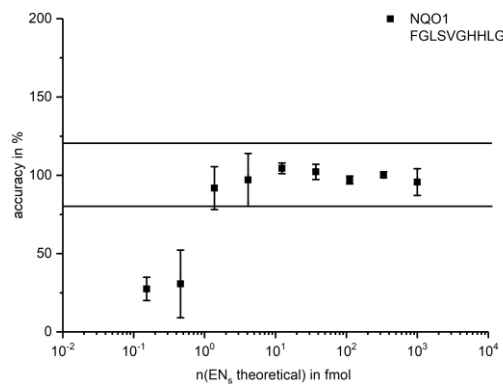
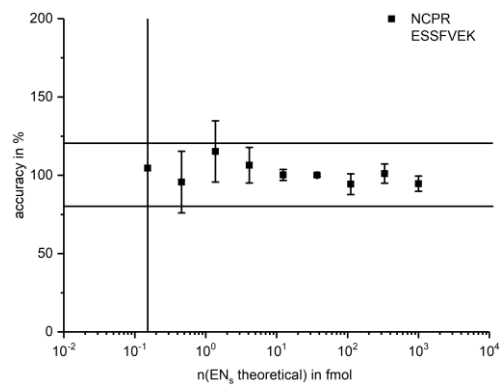
# Supplementary Data



Supplementary Data



## Supplementary Data



## Supplementary Data

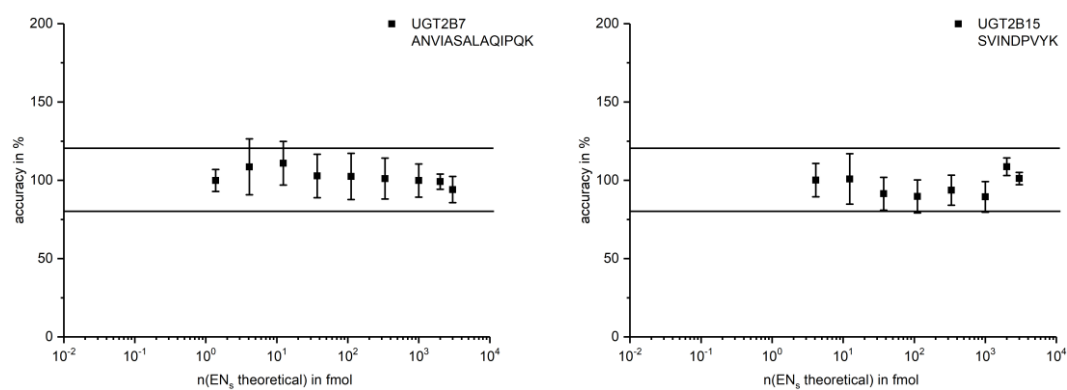


Figure 47. Accuracy plots for analytes in PBSC. The accuracy in percentage is plotted against the theoretical amount of substance of the non-labeled synthetic peptide (EN<sub>s</sub>) in fmol. The dilution was done in triplicates. Accuracy criteria were met, when a data point was between 80 and 120%, and when the deviation between the replicate measurement was  $\leq 20\%$ . Measurements were performed in parallel reaction monitoring (PRM) for multiplex assays 1-6 as well as for the CYP 17-plex.

## G. Results of Potential Mixture Effects (Log<sub>2</sub> Graphs)

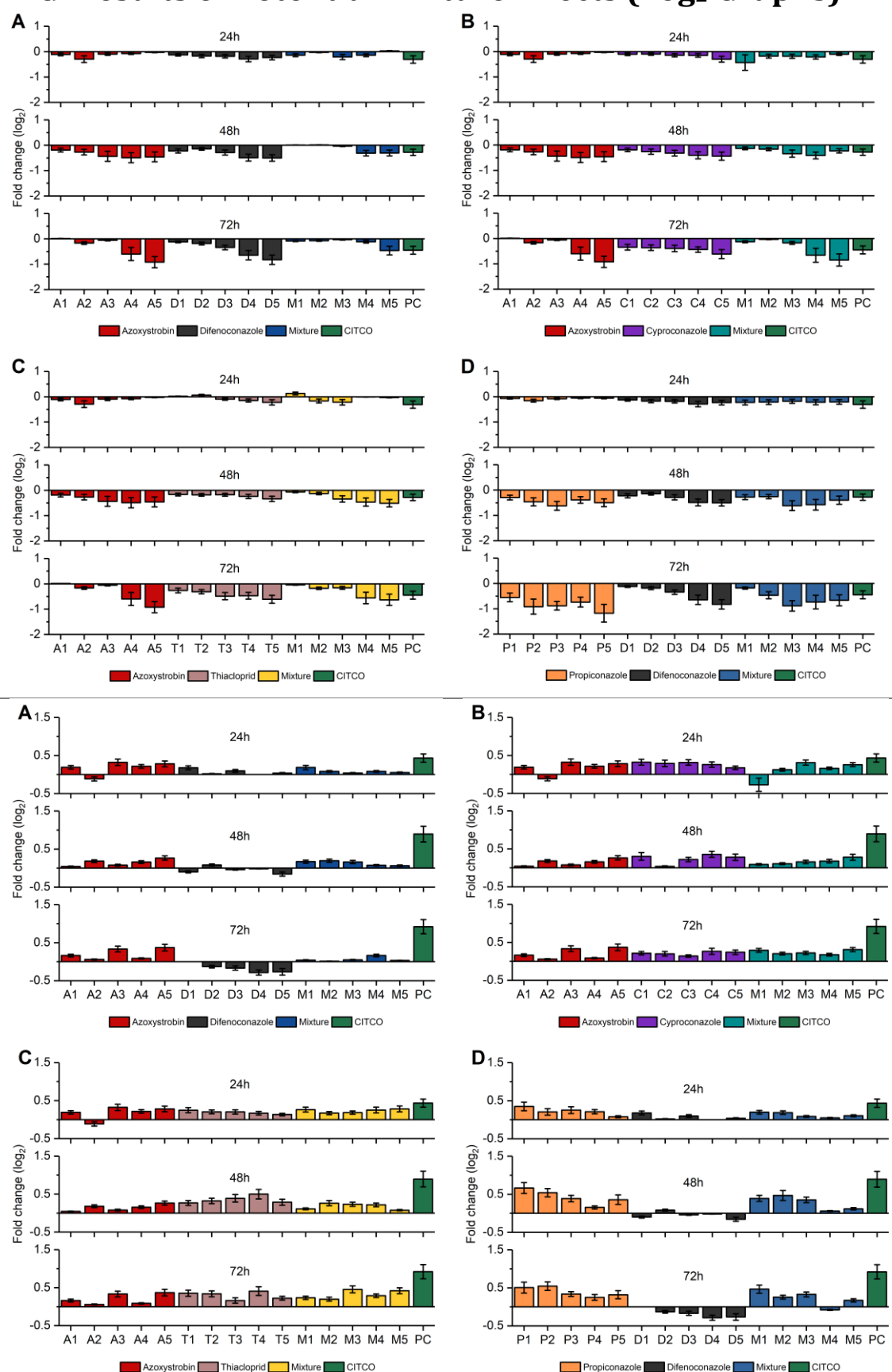


Figure 48. Results of potential mixture effects on ADH1B and ALDH3A1. The upper part shows ADH1B; the lower part shows ALDH3A1. AOS/DIF is shown in (A); AOS/CC in (B); AOS/THI in (C) and PPC/DIF in (D);  $n=3$ . Abbreviations for analytes and pesticides can be found in Table 30 and Table 25, concentrations used in Table 9 and Table 10.

Supplementary Data

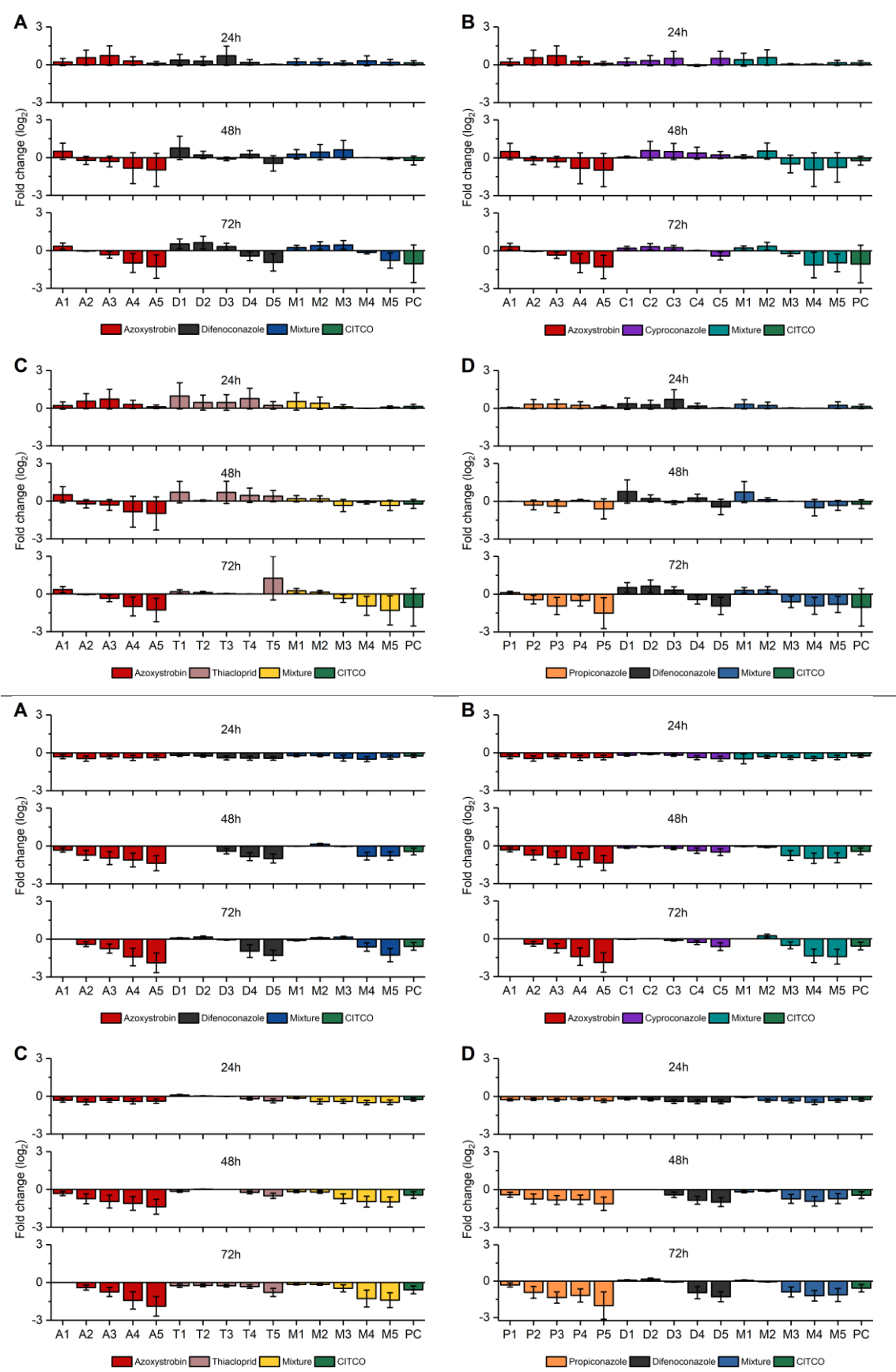


Figure 49. Results of potential mixture effects on ARG1 (PFSK) and (YILK). The upper part shows TIGIIGAPFSK; the lower part shows DVDPGEHYILK. AOS/DIF is shown in (A); AOS/CC in (B); AOS/THI in (C) and PPC/DIF in (D); n=3. Abbreviations for analytes and pesticides can be found in Table 30 and Table 25, concentrations used in Table 9 and Table 10.

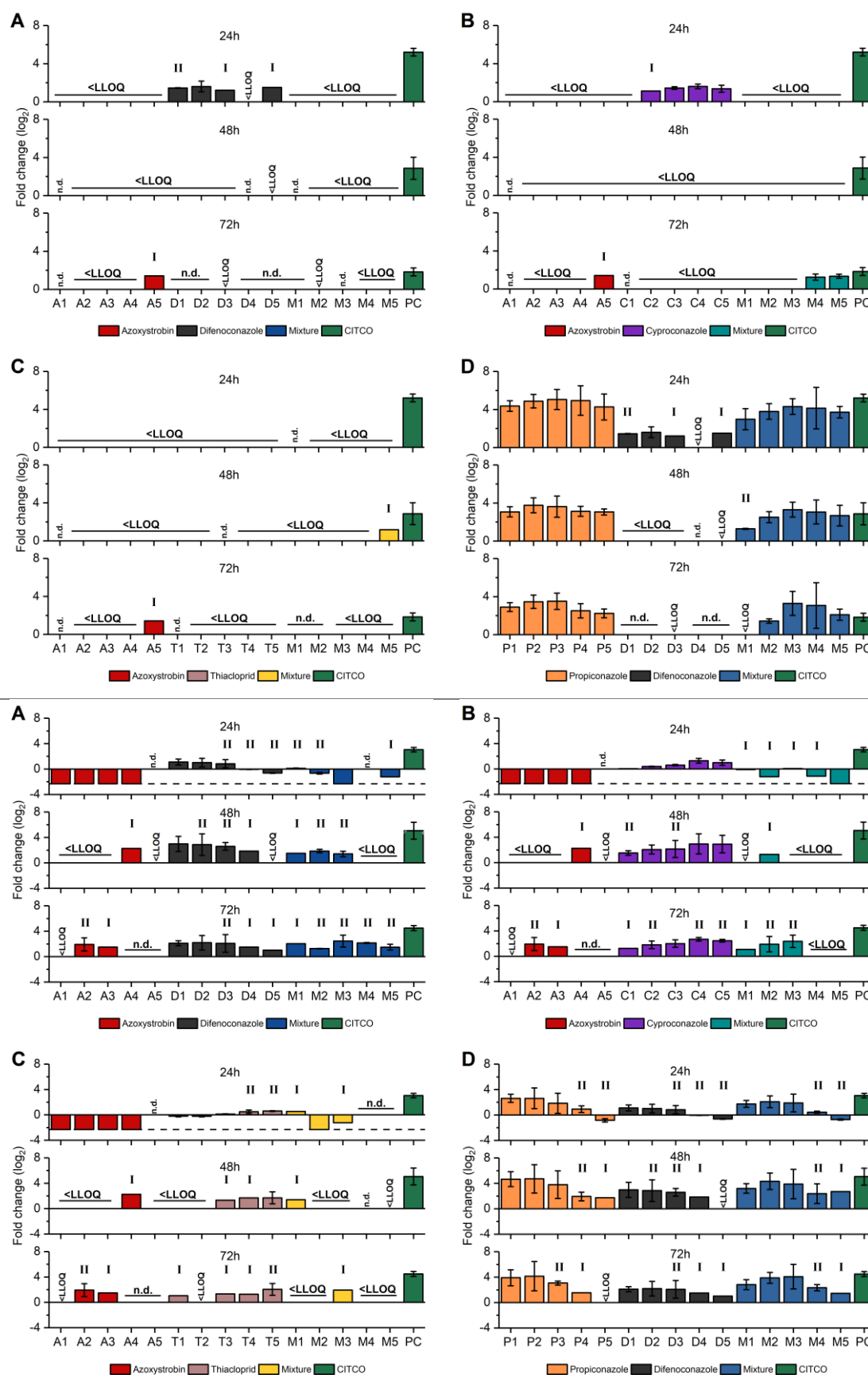


Figure 50. Results of potential mixture effects on CYP1A1 and CYP1A2. The upper part shows CYP1A1; the lower part shows CYP1A2. AOS/DIF is shown in (A); AOS/CC in (B); AOS/THI in (C) and PPC/DIF in (D); n=3. For some treatments, only two (II) or even only one replicate (I) was measurable. The dashed horizontal line indicates 0.5·LLOQ; n.d.= not detected; <LLOQ= below the lower limit of quantification. Abbreviations for analytes and pesticides can be found in Table 30 and Table 25, concentrations used in Table 9 and Table 10.

## Supplementary Data

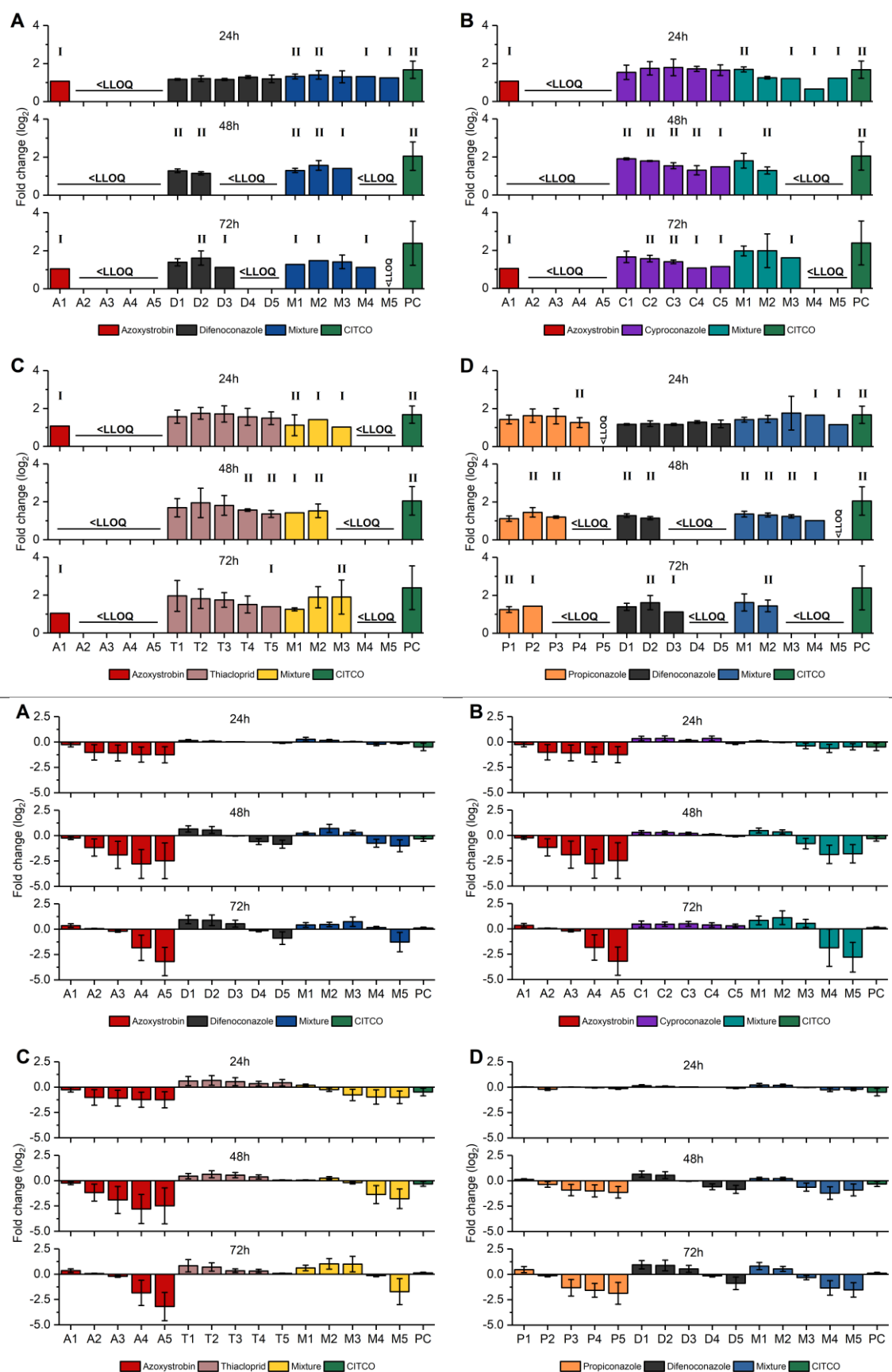


Figure 51. Results of potential mixture effects on CYP2B6 and CYP2C8. The upper part shows CYP2B6; the lower part shows CYP2C8. AOS/DIF is shown in (A); AOS/CC in (B); AOS/THI in (C) and PPC/DIF in (D); n=3. For some treatments, only two (II) or even only one replicate (I) was measurable (<LLOQ= below the lower limit of quantification). Abbreviations for analytes and pesticides can be found in Table 30 and Table 25, concentrations used in Table 9 and Table 10.



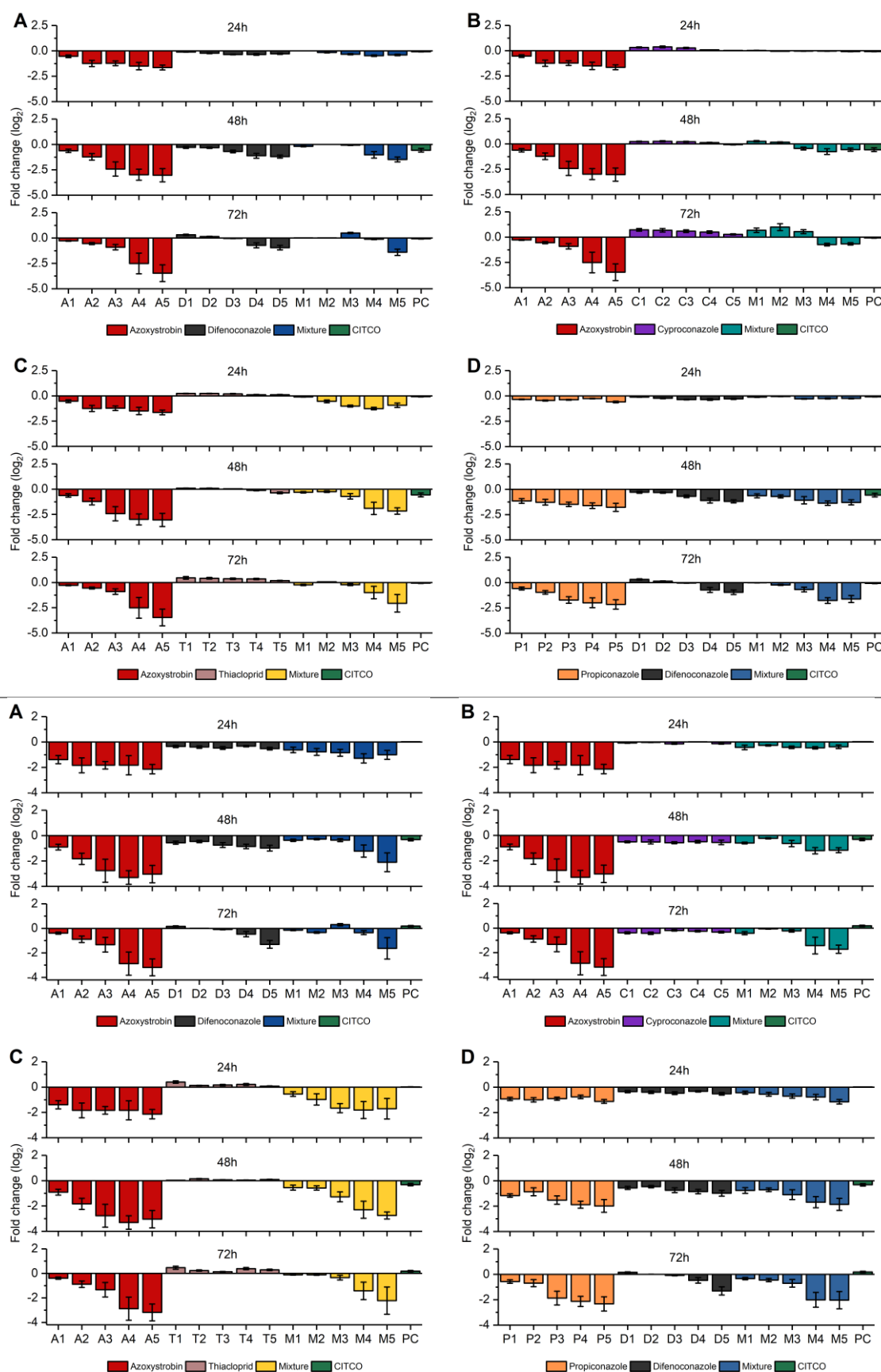


Figure 52. Results of potential mixture effects on CYP2C9 and CYP2C19. The upper part shows CYP2C9; the lower part shows CYP2C19. AOS/DIF is shown in (A); AOS/CC in (B); AOS/THI in (C) and PPC/DIF in (D);  $n=3$ . Abbreviations for analytes and pesticides can be found in Table 30 and Table 25, concentrations used in Table 9 and Table 10.

## Supplementary Data

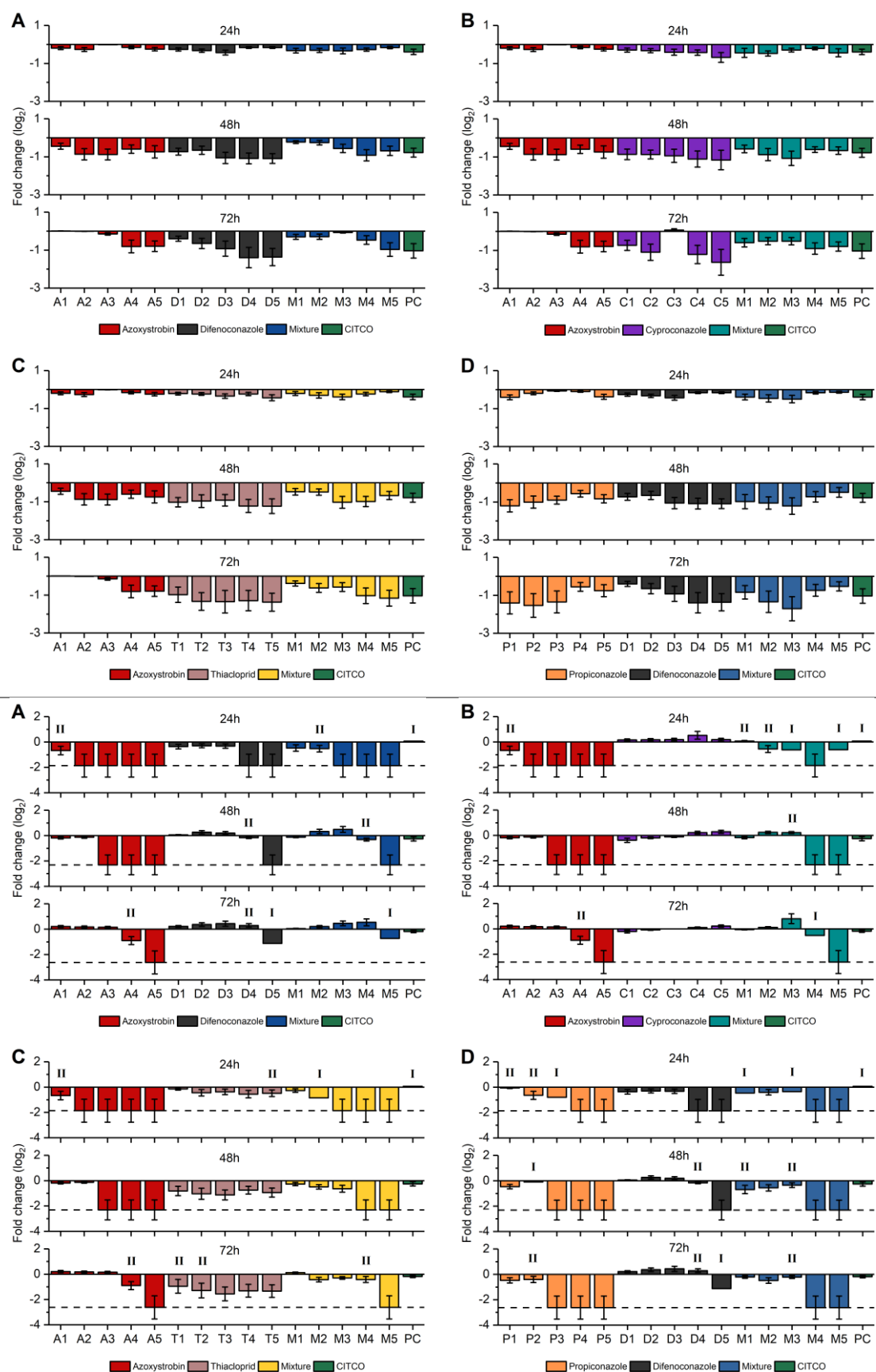


Figure 53. Results of potential mixture effects on CYP2E1 and CYP7A1. The upper part shows CYP2E1; the lower part shows CYP7A1. AOS/DIF is shown in (A); AOS/CC in (B); AOS/THI in (C) and PPC/DIF in (D);  $n=3$ . For some treatments, only two (II) or even only one replicate (I) was measurable. The dashed horizontal line indicates 0.5·LLOQ. Abbreviations for analytes and pesticides can be found in Table 30 and Table 25, concentrations used in Table 9 and Table 10.

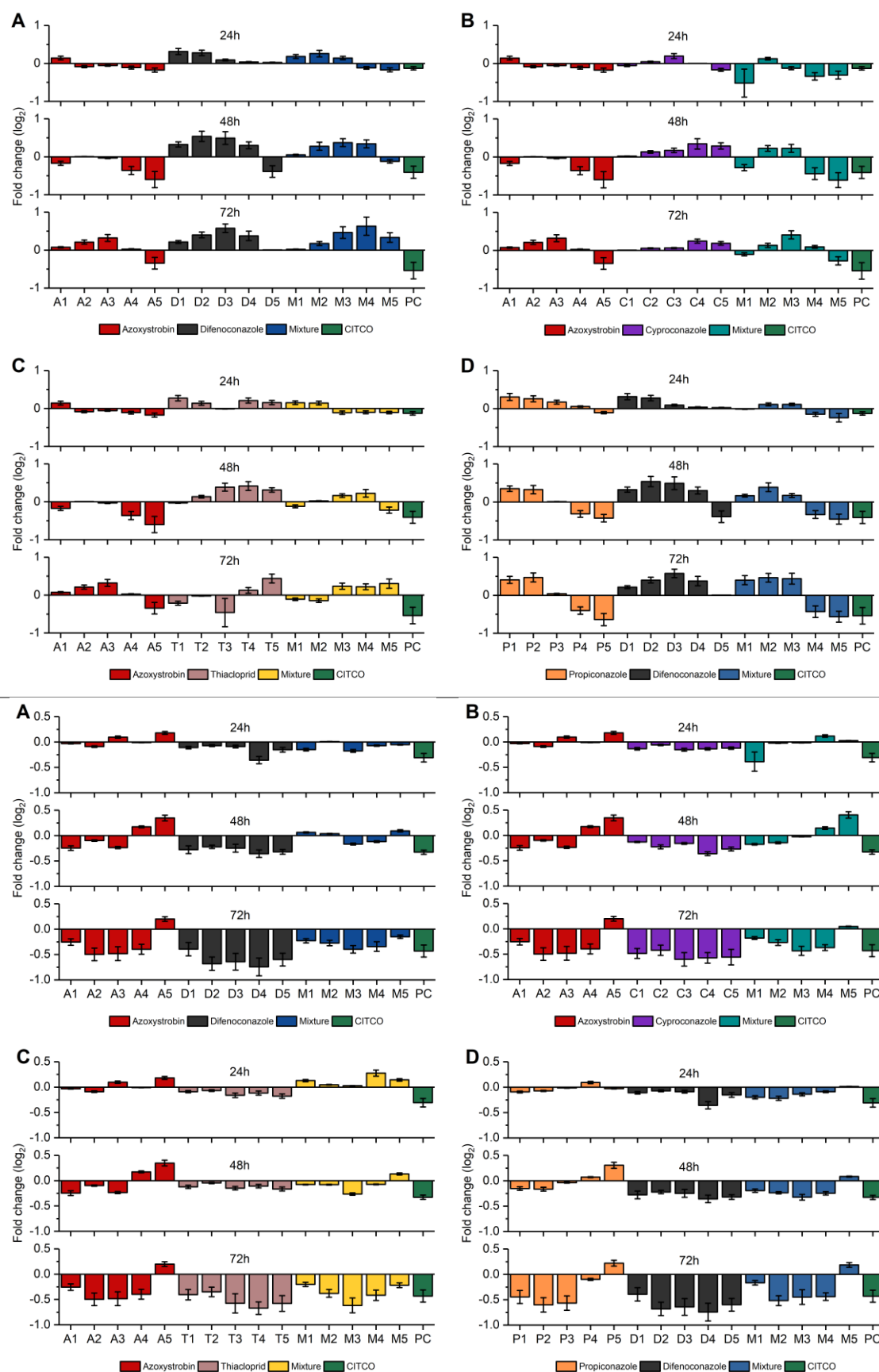


Figure 54. Results of potential mixture effects on FASN and HSD11B2. The upper part shows FASN; the lower part shows HSD11B2. AOS/DIF is shown in (A); AOS/CC in (B); AOS/THI in (C) and PPC/DIF in (D); n=3. Abbreviations for analytes and pesticides can be found in Table 30 and Table 25, concentrations used in Table 9 and Table 10.

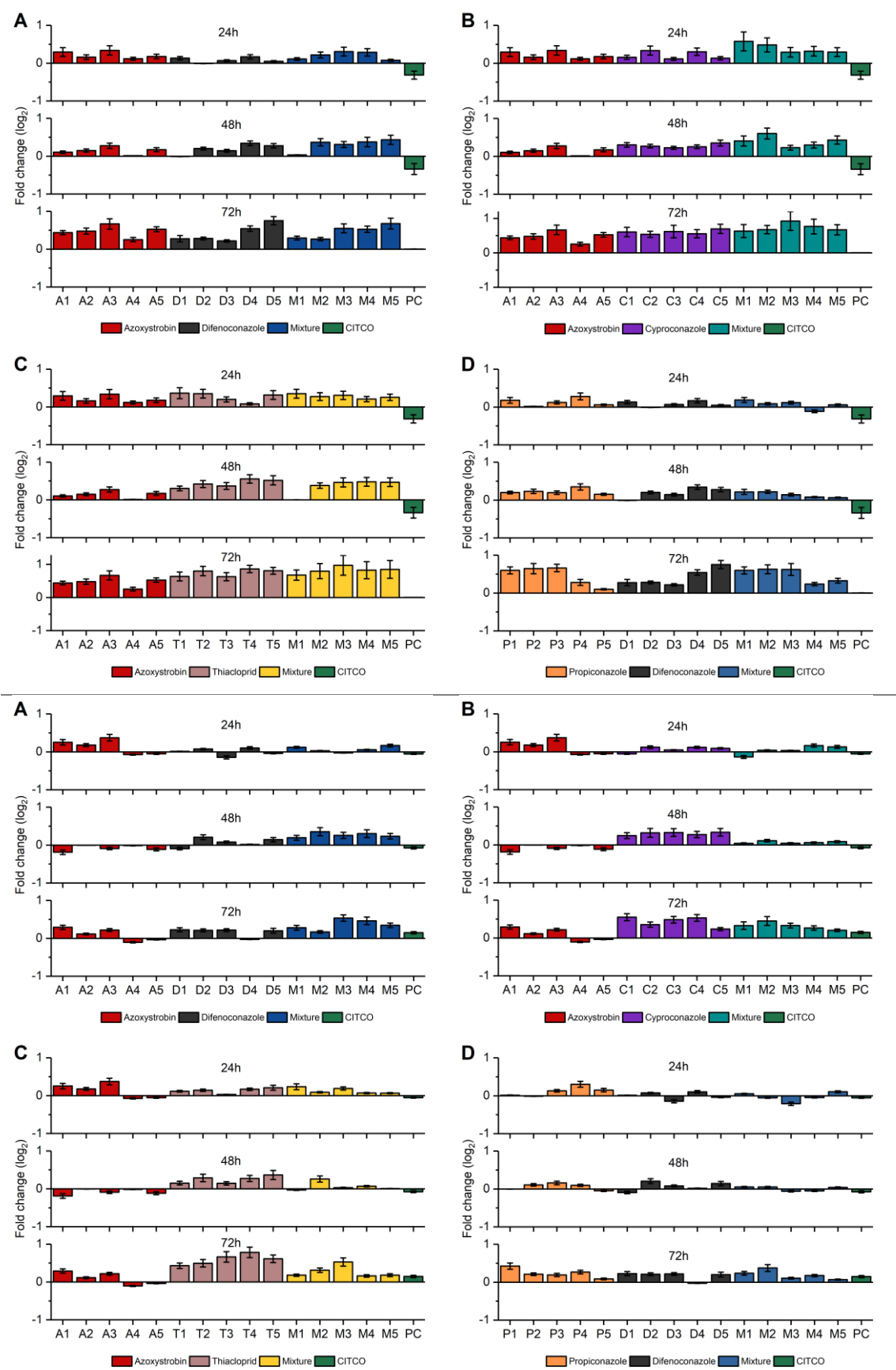


Figure 55. Results of potential mixture effects on MDR1 and NCPR. The upper part shows MDR1; the lower part shows NCPR. AOS/DIF is shown in (A); AOS/CC in (B); AOS/THI in (C) and PPC/DIF in (D); n=3. Abbreviations for analytes and pesticides can be found in Table 30 and Table 25, concentrations used in Table 9 and Table 10.

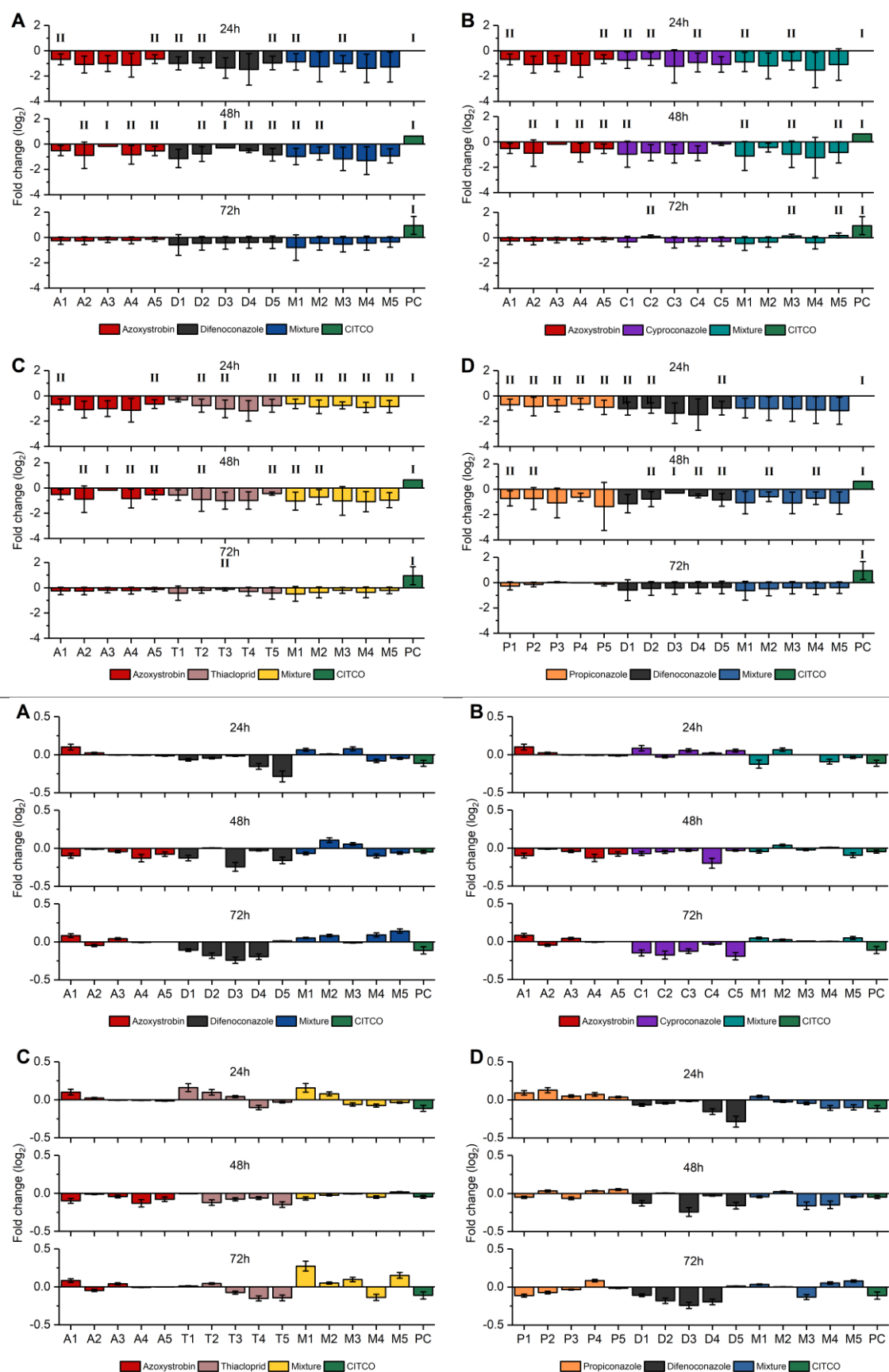


Figure 56. Results of potential mixture effects on NQO1 and PRKDC. The upper part shows NQO1; the lower part shows PRKDC. AOS/DIF is shown in (A); AOS/CC in (B); AOS/THI in (C) and PPC/DIF in (D); n=3. For some treatments, only two (II) or even only one replicate (I) was measurable. Abbreviations for analytes and pesticides can be found in Table 30 and Table 25, concentrations used in Table 9 and Table 10.

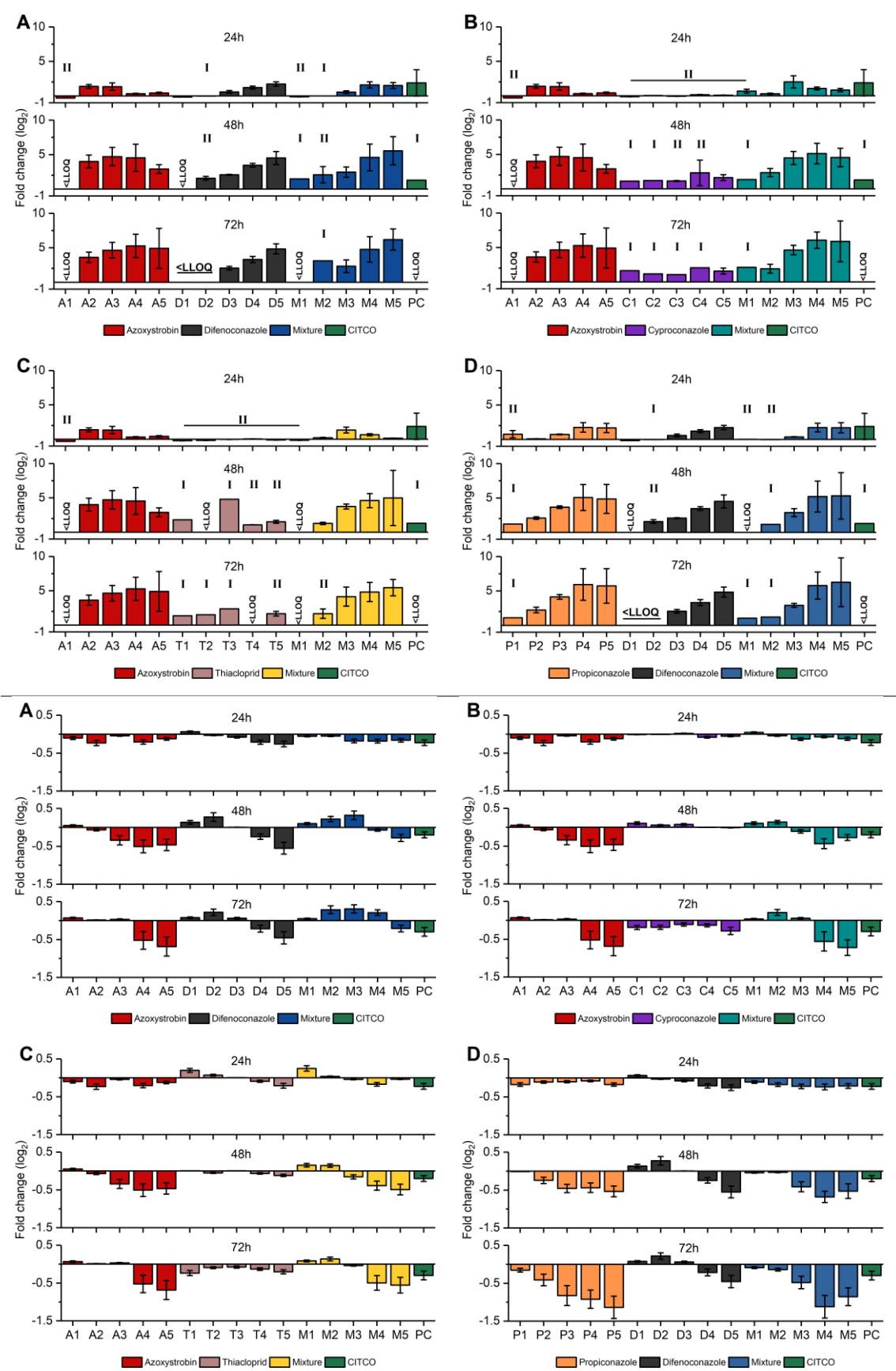


Figure 57. Results of potential mixture effects on S100P and SULT1B1. The upper part shows S100P; the lower part shows SULT1B1. AOS/DIF is shown in (A); AOS/CC in (B); AOS/THI in (C) and PPC/DIF in (D); n=3. For some treatments, only two (II) or even only one replicate (I) was measurable (<LLOQ= below the lower limit of quantification). Abbreviations for analytes and pesticides can be found in Table 30 and Table 25, concentrations used in Table 9 and Table 10.

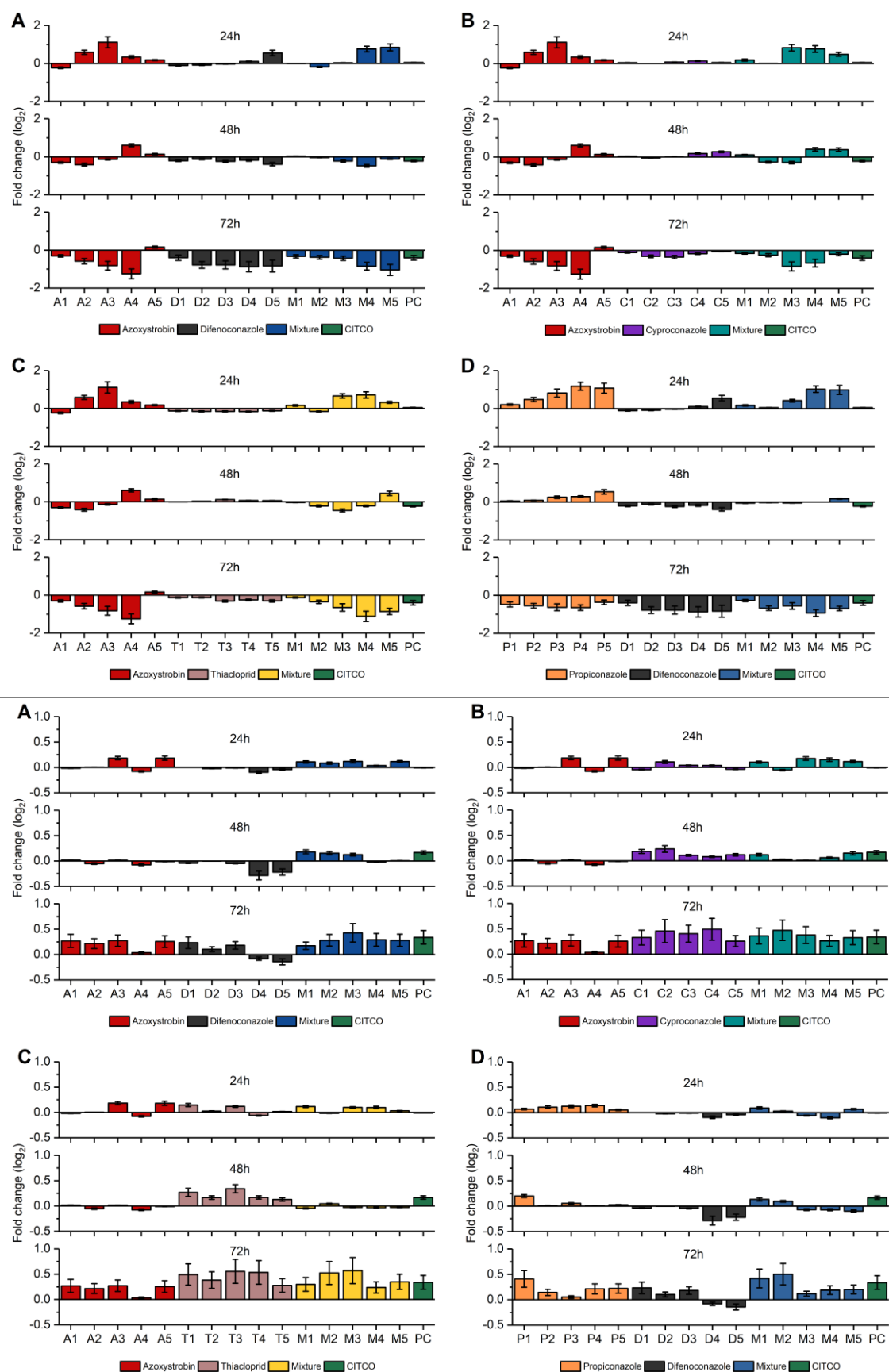


Figure 58. Results of potential mixture effects on TNFRSF12A and UGT1A1. The upper part shows TNFRSF12A; the lower part shows UGT1A1. AOS/DIF is shown in (A); AOS/CC in (B); AOS/THI in (C) and PPC/DIF in (D); n=3. Abbreviations for analytes and pesticides can be found in Table 30 and Table 25, concentrations used in Table 9 and Table 10.

Supplementary Data

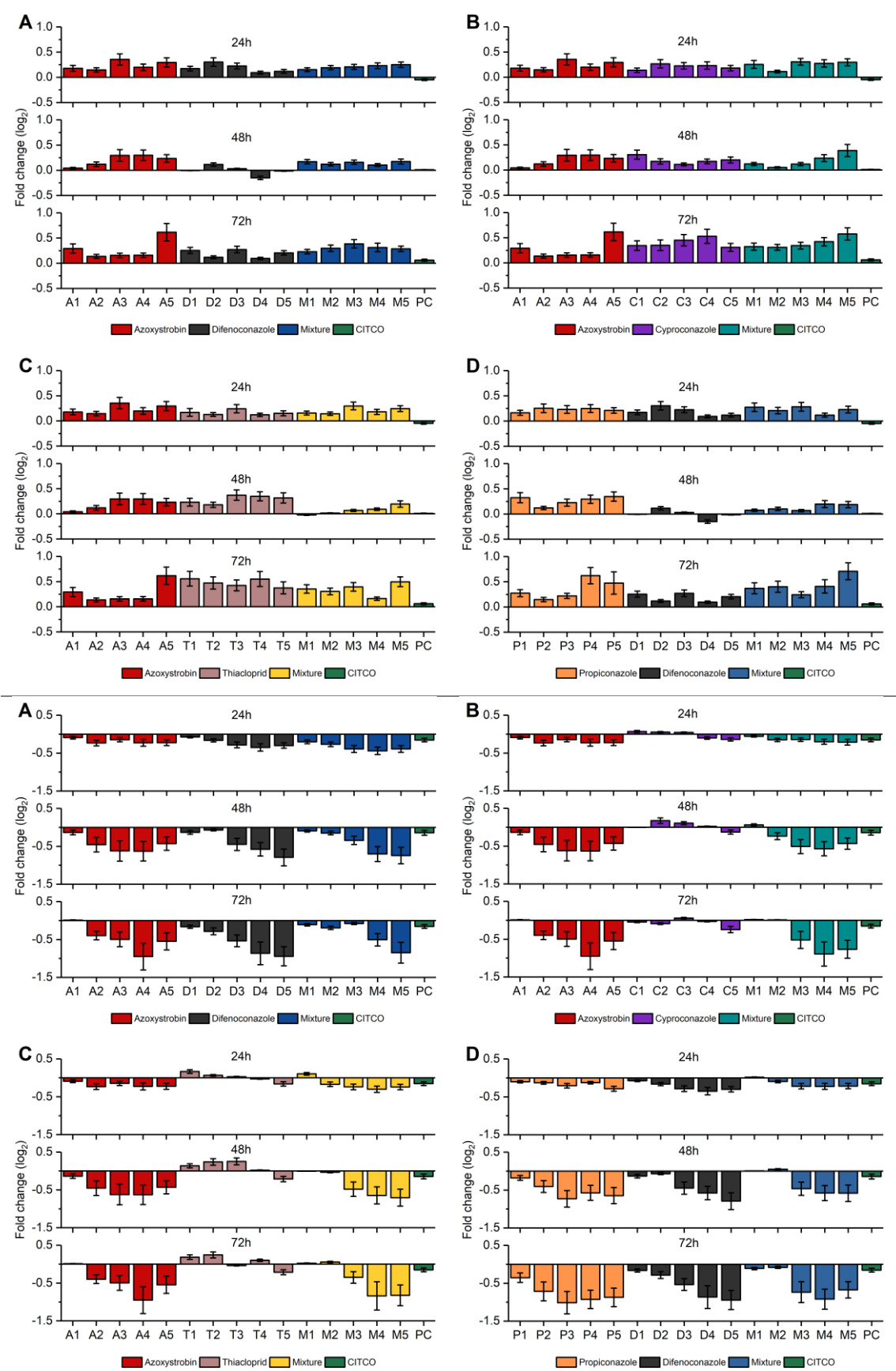


Figure 59. Results of potential mixture effects on UGT1A3 and UGT2B7. The upper part shows UGT1A3; the lower part shows UGT2B7. AOS/DIF is shown in (A); AOS/CC in (B); AOS/THI in (C) and PPC/DIF in (D); n=3. Abbreviations for analytes and pesticides can be found in Table 30 and Table 25, concentrations used in Table 9 and Table 10.



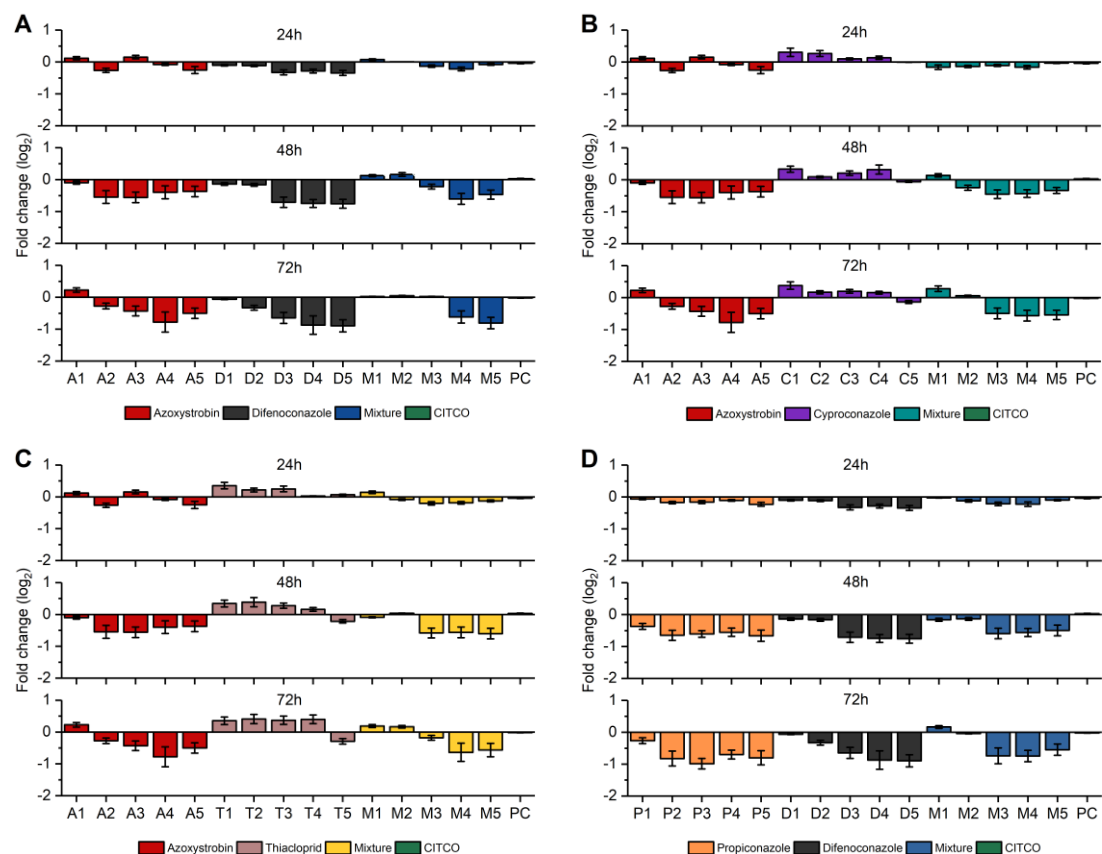


Figure 60. Results of potential mixture effects on UGT2B15. AOS/DIF is shown in (A); AOS/CC in (B); AOS/THI in (C) and PPC/DIF in (D);  $n=3$ . Abbreviations for analytes and pesticides can be found in Table 30 and Table 25, concentrations used in Table 9 and Table 10.

## 10 Curriculum Vitae

### Felix Florian Schmidt

born on July 13<sup>th</sup>, 1992 in Miltenberg

10/2016 – 07/2019	Doctoral dissertation at the Natural and Medical Sciences Institute at the University of Tübingen <i>Title: Immunoaffinity-Based Mass Spectrometry – a Method for the Analysis of Combinatorial Pesticide Effects on Liver Proteins in HepaRG Cells</i>
03/2016 – 09/2016	Master thesis at the Natural and Medical Sciences Institute at the University of Tübingen (1.0) <i>Title: Development of MS-based immunoassays and quantification of cytochrome P450 enzymes in mice</i>
09/2014 – 09/2016	Study of Analytical Chemistry with Quality Assurance (M.Sc.) at Bonn-Rhein-Sieg University of Applied Sciences (1.3)
03/2014 – 08/2014	Study abroad with Bachelor thesis at the Universidade Federal de Ouro Preto (UFOP), Ouro Preto, Brazil (1.3) <i>Title: Analysis of micropollutants with liquid/liquid extraction at low temperature partition and LC-MS/MS in Brazilian waters</i>
09/2011 – 08/2014	Study of Applied Chemistry (B.Sc.) at Reutlingen University of Applied Sciences (1.7)
06/2011	Abitur at Heinrich-Heine-Gymnasium, Ostfildern (2.7)